Development of New Transition-Metal-Catalyzed C–C and C–O Bond Activation Reactions

A DISSERTATION

SUBMITTED TO THE FACULTY OF

THE UNIVERSITY OF MINNESOTA

BY

Constance B. Anderson

IN PARTIAL FULFILLMENT OF THE

REQUIREMENTS FOR THE DEGREE OF

DOCTOR OF PHILOSOPHY

Advisor: Christopher J. Douglas

June 2021

Acknowledgements

First off, to my advisor, Chris Douglas, thank you for all your guidance through the years. Learning from your experience, both in and out of chemistry, has made me a better scientist and teacher. Your support and understanding have truly been invaluable.

I want to thank everyone in the Douglas group. You made me look forward to coming to work. Our conversations, ranging from scientific to downright ridiculous, always brightened my day. To Steve Underwood, thank you for being my friend and going through every stage of the last five and a half years with me. To Steve, Casey Carpenter, and Margaret Clapham, thank you for reading and editing this whole dissertation and for being a constant source of support during the challenges we have faced as a group over the last year. I hope I have been there for you as much as you have for me.

Thank you to Meghan McGreal. As my roommate for most of graduate school, you were the most constant presence in my life. Even writing a dissertation was more enjoyable with you by my side. I don't know how I would have gotten through the challenges of earning a Ph.D. without you.

To Taysir Bader, thank you for always being here and believing in me. I can't wait to see what the future has in store for us. Also, thank you for keeping me sane and fed while I was writing this whole thing.

Thank you to all my other friends at the University of Minnesota, especially Matt Porter, Beth Dewing, and David Goldfeld. Our conversations and adventures have made graduate school infinitely more enjoyable.

Thank you to all the professors who have helped me get to this point. To my professors at Minnesota State University Moorhead, especially Jeffrey Bodwin, who first inspired me to become a chemist and go to grad school, I would not be here without your influence and advice.

Lastly, I want to acknowledge and thank my family. Thank you to my parents for always supporting and encouraging me. I would not be a scientist if you didn't teach me to be curious and love science and learning from an early age. Thank you to my siblings Cassie, Kelly, and Phil for hanging out with me and being a source of stress relief when I needed it most. To Cassie, in particular, for listening and giving me advice when research and school were especially challenging. Thank you to my nieces and nephews, Milo, Addison, Rowan, and Aleece, for making me want to be someone to look up to. I love you all.

Dedication

For all the female scientists. To those who came before me, thank you for paving the way. To all those who come after, I can't wait to see what you accomplish.

"Life is not easy for any of us. But what of that? We must have perseverance and above all confidence in ourselves. We must believe that we are gifted for something, and that this thing, at whatever cost, must be attained."

- Dr. Marie Curie

Table of Contents

List of Tables

List of Figures

List of Schemes

Abbreviations

Ar	aryl group
ATR	attenuated total reflectance
bpy	2,2’-bipyridine
br	broad
BrettPhos	2-(dicyclohexylphosphino)3,6-dimethoxy-2′,4′,6′-triisopropyl-1,1′-biphenyl
calcd	calculated
COD	cyclooctadiene
COE	cyclooctene
CMD	concerted metalation deprotonation
Cy	cyclohexyl
d	doublet
DavePhos	2-dicyclohexylphosphino-2′-(*N*,*N*-dimethylamino)biphenyl
DCE	1,2-dichloroethane
DFT	density functional theory
DMAP	4-dimethylaminopyridine
DMB	dimethoxybenzene
dppe	1,2-diphenylphosphinoethane
dppp	1,3-diphenylphosphinopropane
EAS	electrophilic aromatic substitution
EDG	electron donating group

ESI	electrospray ionization
Et	ethyl
EtOAC	ethyl acetate
Et_2O	diethyl ether
equiv	equivalent
EWG	electronwithdrawing group
FT	fourier-transform
GC	gas chromatography
h	heptet
Hex	hexane
HRMS	high resolution mass spectrometry
ind	indene
JohnPhos	2-(di-tert-butylphosphino)biphenyl
KIE	kinetic isotope effect
m	multiplet
Me	methyl
MePhos	2-dicyclohexylphosphino-2′-methylbiphenyl
MOP	2-(diphenylphosphino)-2’-methoxy-1,1’-binaphthyl
mp	melting point
MS	mass spectrometry
NHC	*N*-heterocyclic carbene
NMR	nuclear magnetic resonance spectroscopy

OAc	acetate
Ph	phenyl
pin	pinacol
PTFE	polytetrafluoroethylene
q	quartet
qNMR	quantitative nuclear magnetic resonance spectroscopy
rt	room temperature
RuPhos	2-dicyclohexylphosphino-2′,6′-diisopropoxybiphenyl
s	singlet
SBM	sigma-bond metathesis
S-Phos	2-dicyclohexylphosphino-2′,6′-dimethoxybiphenyl
t	triplet
TLC	thin layer chromatography
TrixiePhos	*rac*-2-(di-*tert*-butylphosphino)-1,1’-binaphthyl
XPhos	2-dicyclohexylphosphino-2′,4′,6′-triisopropylbiphenyl

Chapter 1. Activation of Traditionally Inert Bonds

1.1 Introduction

As organic chemistry is often considered the chemistry of carbon, one major focus of organic chemists is developing new methods to make and break carbon bonds. The ability to use these methods to synthesize complex and novel organic molecules have revolutionized the world through fields like medicine and agriculture. In the last 50 years, homogenous organometallic catalysis has become a powerful new tool to form C–C bonds, even being the subject of the 2010 Nobel Prize in Chemistry.[1] While early work in this field focused on activating weaker C–X (X = Cl, Br, I, OTf) bonds,[2] a growing area of organic and organometallic chemistry is metal-catalyzed activation of more prevalent bonds in organic molecules, including C–H, C–C, C–O, and C–N bonds. This chapter will cover C–C and C–O bond activation processes and their application in synthetic reactions.

1.2 Traditional Cross-Coupling Methods

Early cross-coupling reactions fell into two general categories. The first reaction type couples organic halides with organometallic reagents. A general mechanism of these reactions begins with oxidative addition to the C–X bond of a preformed organohalide followed by transmetalation with the organometallic species (Scheme 1.1). Reductive elimination forms a new C–C bond. Examples of this type of coupling include Suzuki,[3,4] Negishi,[5,6] Stille,[7,8] and Kumada[9] couplings among many others.[10,11] There has been wide application of cross coupling reactions and they have been used in many syntheses.[12–19]

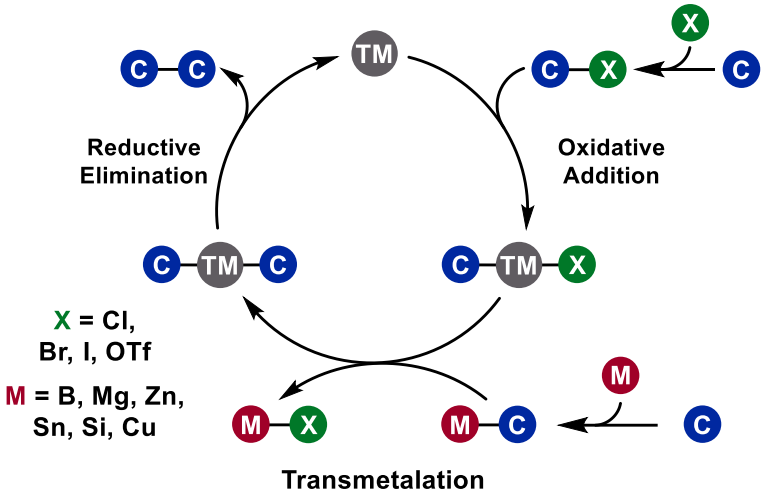

Scheme 1.1 General mechanism of transition-metal catalyzed cross coupling

The other general method for C–C bond forming reactions are π-bond insertions like the Heck reaction (Scheme 1.2).[20] These reactions also start with oxidative addition of a preformed organohalide species. Alkene association to the metal catalyst and 1,2-insertion into a M–C bond creates a new C–C bond. Next, β-hydride elimination reforms the alkene and dissociation from the newly formed π-complex releases the product. An equivalent of base is used to promote reductive elimination and regenerate the catalyst.

A major drawback of these coupling processes is the need for prefunctionalization. Halogenation and metalation of the starting materials require extra synthetic steps. Additionally, a full equivalent of metal and/or halogen waste is generated in the reaction which can be environmentally damaging. The Heck reaction eliminates the need for organometallic reagents, replacing these with alkenes which are incorporated into the product with high atom economy, losing only a hydrogen atom. This process still requires a preformed organohalide and a stoichiometric amount of base. These result in a full equivalent of base and halogenated waste being generated during the reaction. Selective

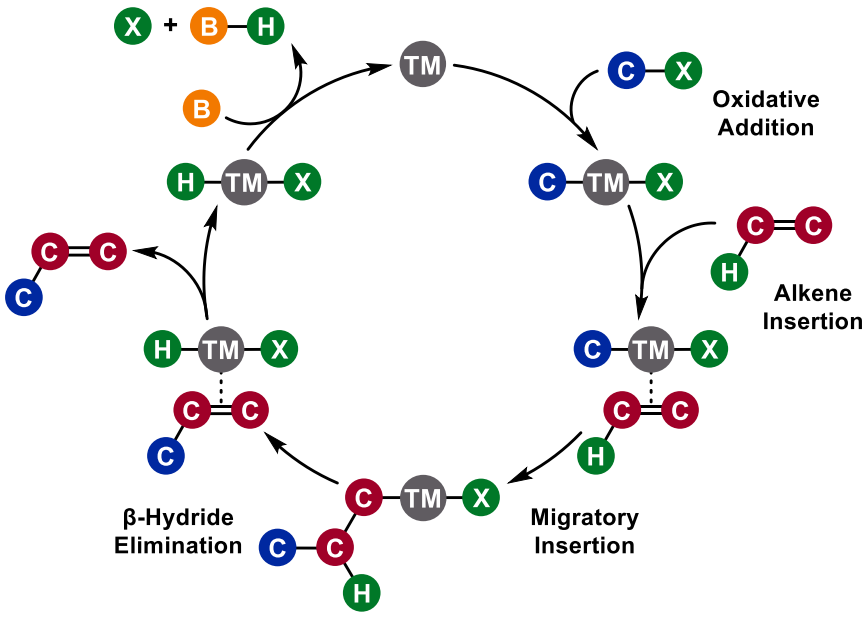

Scheme 1.2 General Heck-type coupling reaction

activation of C–C and C–O bonds for coupling reactions would allow us to avoid halogenation or metalation potentially resulting in shorter syntheses with better atom economy and less toxic waste.

1.3 Transition-Metal Catalyzed C–C Bond Activation

Carbon-carbon σ-bonds are some of the least reactive bonds in nature making them difficult targets for bond activation. Both thermodynamic and kinetic barriers must be overcome for selective activation of C–C σ-bonds. Oxidative addition of a C–C σ-bond is typically an endergonic process, trading one strong C–C bond for two weaker M–C bonds (Scheme 1.3a).[21] Formation of MR_2 through oxidative addition is estimated to be 25 kcal/mol uphill.[22] The thermodynamic barrier can vary significantly depending on metal and R-group identity so some oxidative addition to C–C bonds may be exergonic. The

kinetic barrier to oxidative addition is high due to the linear directionality of C–C σ-bonds. The bond is made of two overlapping sp^3 orbitals so both orbitals must rotate to form bonds from either the C–C σ-bonding or σ-antibonding orbitals (Scheme 1.3c) . C–C bonds are also difficult to access sterically. Steric strain occurs from the metal approaching the C–C bond and between the two R groups following bond activation (Scheme 1.3c). Selectivity of bond activation is a challenge as C–H bonds activation is typically more thermodynamically favored (Scheme 1.3b) and more sterically accessible. As C–H bonds are formed from the overlap of C(sp^3) and H(s) orbitals, less bond rotation and rearrangement energy is required for activation (Scheme 1.3d). Due to these factors, many conditions that would activate C–C bonds will also activate C–H bonds.

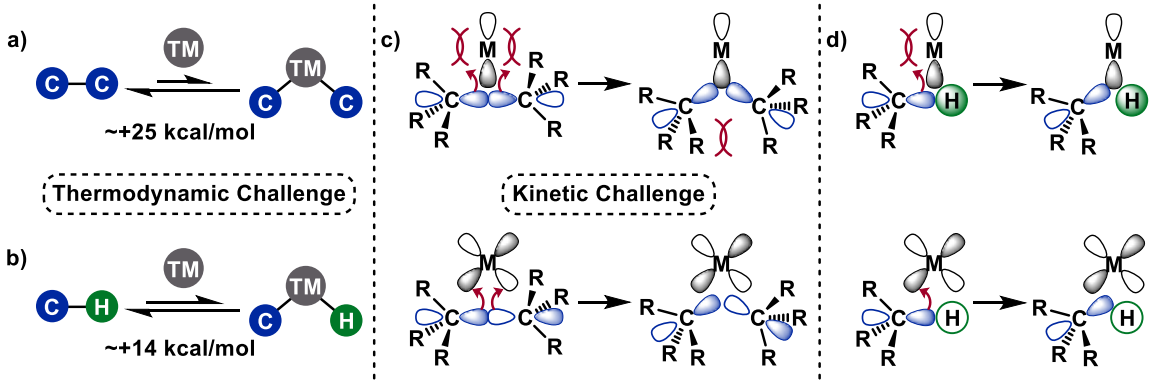

Scheme 1.3 Thermal barriers to a) C–C bond activation, b) C–H bond activation; Orbital rotation considerations from metal orbital interaction with c) C–C σ-bonding orbital and σ-antibonding orbital, e) C–H σ-bonding orbital and σ-antibonding orbital

Strategies for driving C–C bond activation work by lowering the thermodynamic or kinetic barriers. For example, more polar C–C bonds are easier to activate. Decreasing the hybridization of the carbon atoms lowers the steric strain before and after bond activation and makes the transformation more thermodynamically favored as the resulting

M–C(sp^2) or M–C(sp) bonds are more stable than their C(sp^3) counterparts. The combination of increased polarity and decreased hybridization makes bond activation of bonds adjacent to ketones, especially aryl ketones, a promising target. M–C bonds formed from lower transition-metals (Os, Ir, and Pt) are typically stronger, making C–C bond activation using these metals more thermodynamically favorable.[21]

1.3.1 Strain-Driven C–C Bond Activation

Seminal work on C–C bond activation was done using strained rings. Coupling bond activation to energy releasing processes like expansion of strained rings helps drive bond activation. Tipper[23] reported the addition of Pt(II) to the C–C bond of cyclopropane forming expanded 4-membered metallocycle **1.01**, which was subsequently trapped by pyridine forming **1.02** (Scheme 1.4).[24]

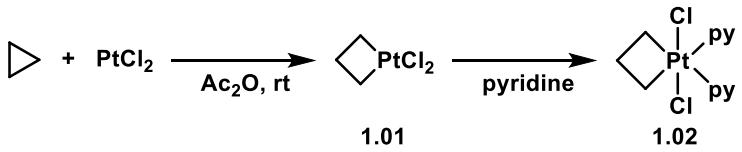

Scheme 1.4 C–C bond activation of cyclopropane

Strain energy of small rings is dependent on ring size, hybridization, and substitution (Figure 1.1). Decreasing ring size or carbon-hybridization in the ring both increase ring strain making bond activation easier.[25] Substitutions on the ring slightly decrease ring strain.

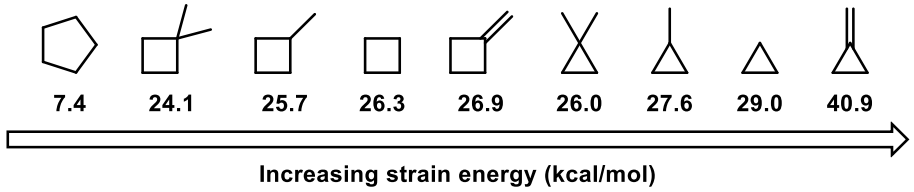

Figure 1.1 Strain energy of small rings

Undirected C–C bond activation of substituted cyclopropyl rings occurs at the distal C–C bond (Scheme 1.5a). Directing groups including alkenes,[26,27] ketones,[28–30] imines,[31–33] and amines[34] have been used to direct metal catalysts to activate proximal C–C bonds (Scheme 1.5b). Activation of alkylidenecyclopropanes **1.07** occurs at the distal C(sp^3)–C(sp^3) bond forming metallocycle **1.08**, followed by isomerization to **1.10** through trimethylenemethane intermediate **1.09** (Scheme 1.5c).

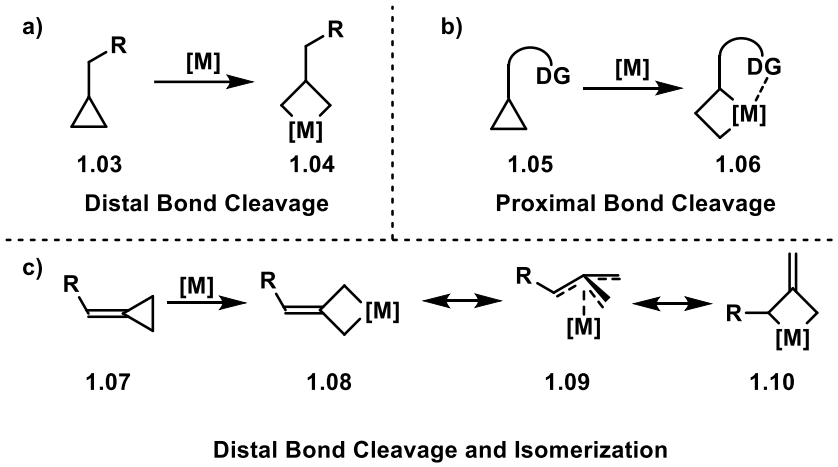

Scheme 1.5 Selectivity of 3-membered ring C–C bond activation

C–C bond activation of 3-membered rings is often coupled with π-bond insertion processes which help make the overall transformation energetically downhill, most commonly, they are used as C-3-synthons in metal-catalyzed cycloadditions to form ring

expanded products (Scheme 1.6).[35–37] Vinyl cyclopropanes, where the vinyl-group is used to direct bond activation to the proximal C–C bond have also been used as C-5-synthons in cycloaddition reactions to form medium sized rings.[38–46] Cyclopropane C–C bond activation and cycloaddition have been utilized in the synthesis of many natural products.[27,38–53]

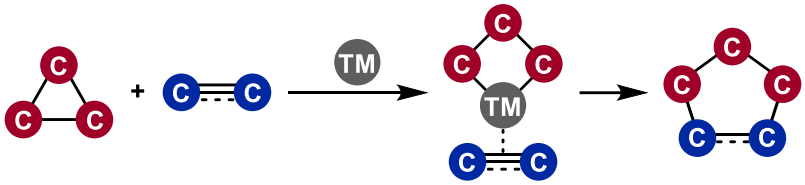

Scheme 1.6 General transition-metal-catalyzed activation of cyclopropane rings followed by ring expansion

Other early work into C–C bond activation included the Rh-catalyzed valence isomerization of cubanes **1.11** to substituted cyclooctatetraenes **1.12** (Scheme 1.7a).[54–57] More recently, Dong and coworkers developed the Rh-catalyzed C–C bond activation of benzocyclobutenones **1.13** (Scheme 1.7b).[58–60] Bond activation forming intermediate **1.14** was coupled with migratory insertion of pendent alkenes or oximes to form fused tricyclics **1.15**. A similar transformation was developed coupling bond activation to ketone migratory insertion (Scheme 1.7c). The resulting lactones **1.17** underwent spontaneous elimination driven by aromatization to form benzofurans **1.18**. Benzocyclobutenone C–C bond activation has been used as they key step in the synthesis of many natural products.[61–65] Strategies for activating various other kinds of 4-membered rings have been reported including cyclobutanones[66,67] and biphenylene.[68–72]

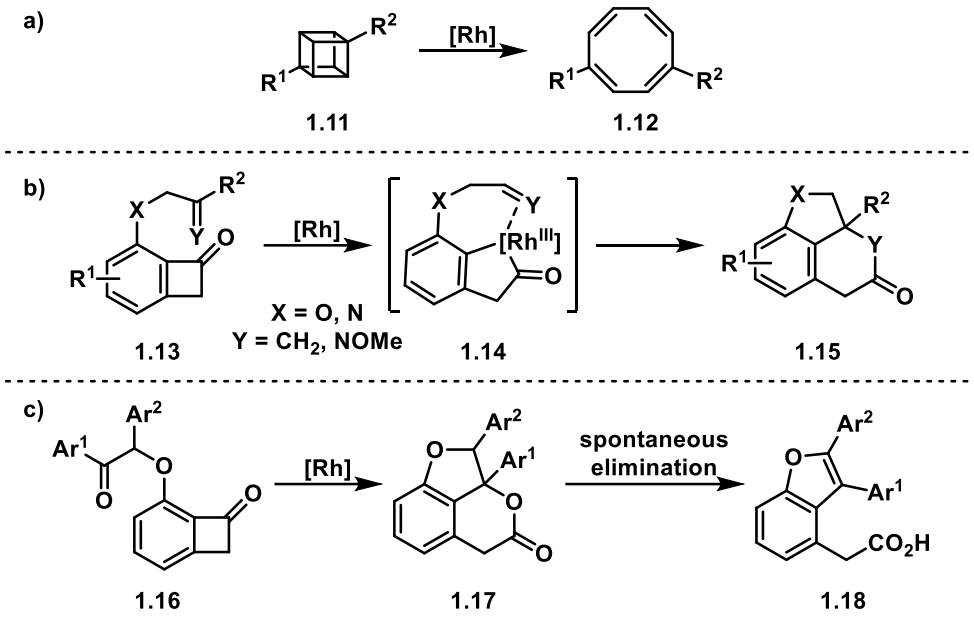

Scheme 1.7 Examples of C–C bond activation of strained 4-membered rings

1.3.2 Chelation-Directed C–C Bond Activation

Based on strategies used in the field of C–H bond activation,[73,74] Suggs and coworkers reported the Rh-catalyzed C–C bond activation of 8-acylquinolinyl ketones (Scheme 1.8).[75,76] They achieved selective C–C bond activation through two methods. First, the two bonds adjacent to the carbonyl in ketone **1.19** are polarized and sp^2 hybridized, allowing for easier bond activation. Additionally, the quinolinyl group can precoordinate to the Rh-center, bringing it in close proximity to the C_{acyl}–C bonds. The distal C_{acyl}–C bond is selectively activated due to the kinetic preference for forming 5-membered rings. Chelation in the resulting intermediates **1.20** and **1.21** also prevent α-elimination of CO, a process commonly seen in metal-acyl species, as elimination would form a highly strained 4-membered metallocycle.

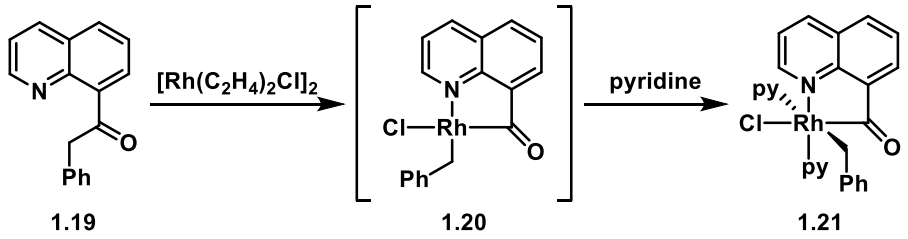

1.19 1.20 1.21

Scheme 1.8 8-Acylquinoline directed C–C bond activation

Inspired by the work of Suggs, Douglas and Dreis[77] developed quinoline-directed carboacylation of alkenes **1.22** to form cyclized dihydrobenzofurans **1.23** (Scheme 1.9a). The mechanism was elucidated by Johnson and coworkers[78,79] (Scheme 1.9b). The reaction begins with Rh coordination to the Lewis-basic nitrogen of **1.22** forming intermediate **1.24**, the resting state of the catalytic cycle. This coordination brings the Rh-center close to the C–C bond, initiating oxidative addition, the turnover-limiting step of the reaction. Migratory insertion of the pendent alkene forms the dihydrobenzofuran ring of **1.26**. Reductive elimination forms the second new C–C bond and Rh-dissociation releases product **1.23**, completing the catalytic cycle.

Coupling alkene insertions with C–C bond activation through Heck-type reaction mechanisms is a powerful method of synthesis, quickly building up molecular complexity and forming new rings in a single step. Carboacylation of 1,2-disubstituted alkenes forms quaternary carbon centers, a typically challenging task.[80–82]

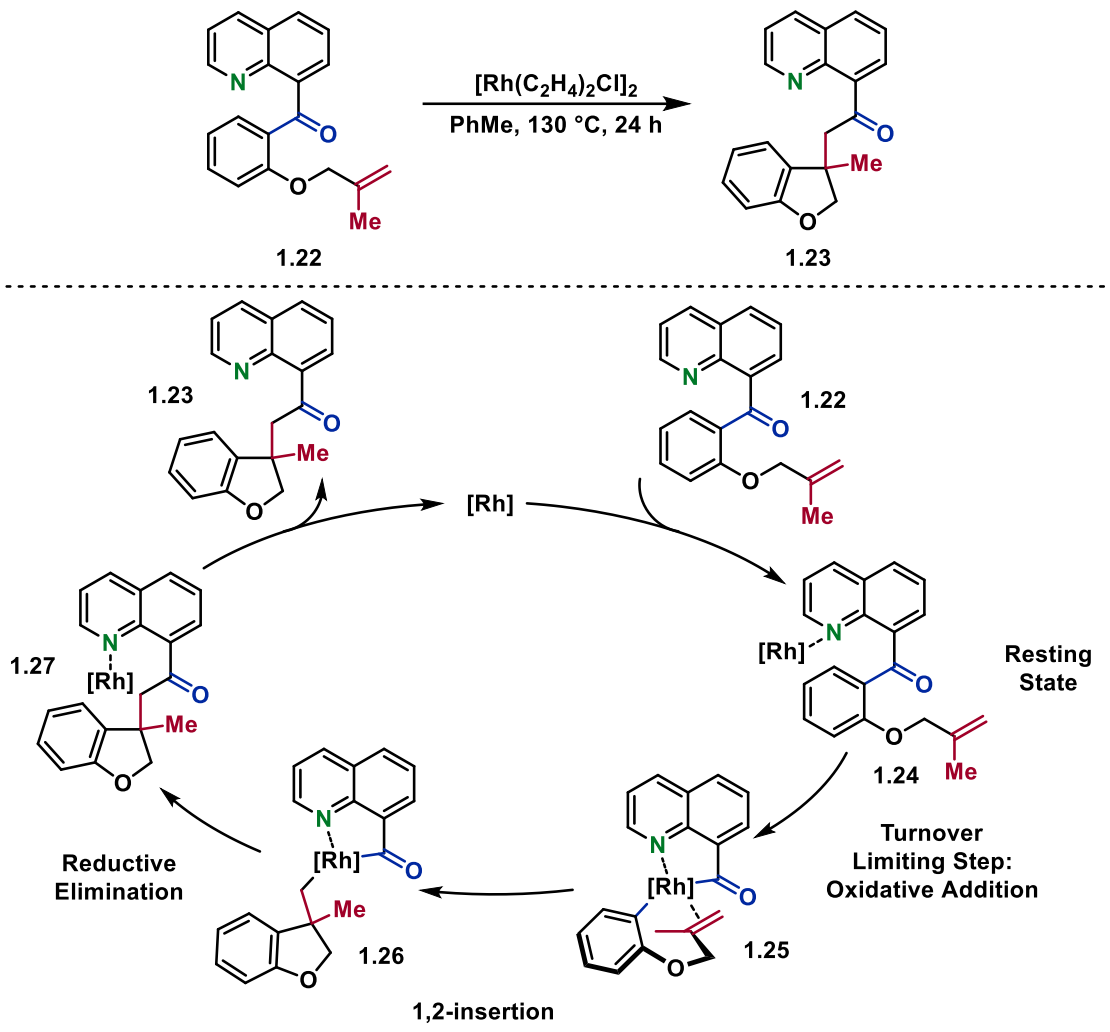

Scheme 1.9 Quinoline-directed carboacylation of alkenes via C–C bond activation

Wang et al.[83] reported a Rh-catalyzed, quinoline-directed C–C bond activation of methyl or aryl ketones **1.28** for Suzuki-type cross coupling with electron-rich aryl boronic acids (Scheme 1.10). This method was extended by Johnson et al.[84] to include coupling with electron-deficient aryl boronic acids.

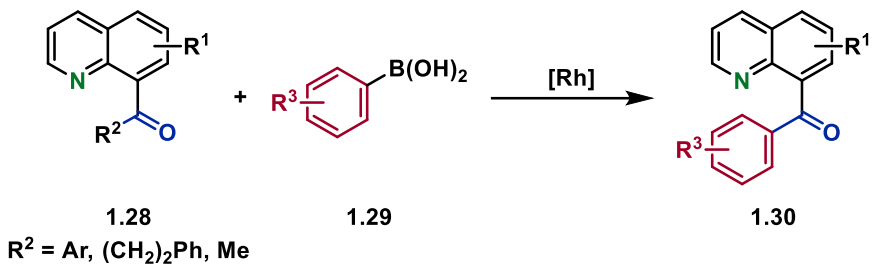

1.28
R^2 = Ar, $(CH_2)_2$Ph, Me

1.29

1.30

Scheme 1.10 Suzuki-type coupling via quinoline-directed C–C bond activation

Other nitrogen containing heterocycles, including pyridine,[85,86] pyrroline,[87] pyrimidine[88] and oxazoles[87] as well as N-oxides[89] have been used as permanent chelating directing groups for C–C bond activation. One drawback of quinoline, pyridyl, and other permanent heterocycles used for directed bond activation is that there is currently no method to remove the group after the desired reaction has taken place.

To circumvent this issue, Jun and Lee[90] developed a method to install a temporary directing group allowing for metal-organic cooperative catalysis (Scheme 1.11). By including a catalytic amount of 2-amino-3-picoline **1.35**, they form pyridylimines **1.36** from ketones **1.31** *in situ*. The pyridyl group then coordinates to the Rh-center, directing C–C bond cleavage though oxidative addition forming **1.37**. β-Hydride elimination of styrene **1.34** and insertion of alkene **1.32** forms **1.39**. Reductive elimination and *in situ* hydrolysis of the imine form product **1.33**. This strategy of metal-organic cooperative catalysis installing temporary directing groups has been applied to both Suzuki-type cross-coupling[91] and other Heck-type insertion processes.[92–94] Dong and coworkers used this transient directing group strategy to initiate C–C bond activation in the key steps of their synthesis of sesquiterpenoid[95] natural products and estrone analogues.[91]

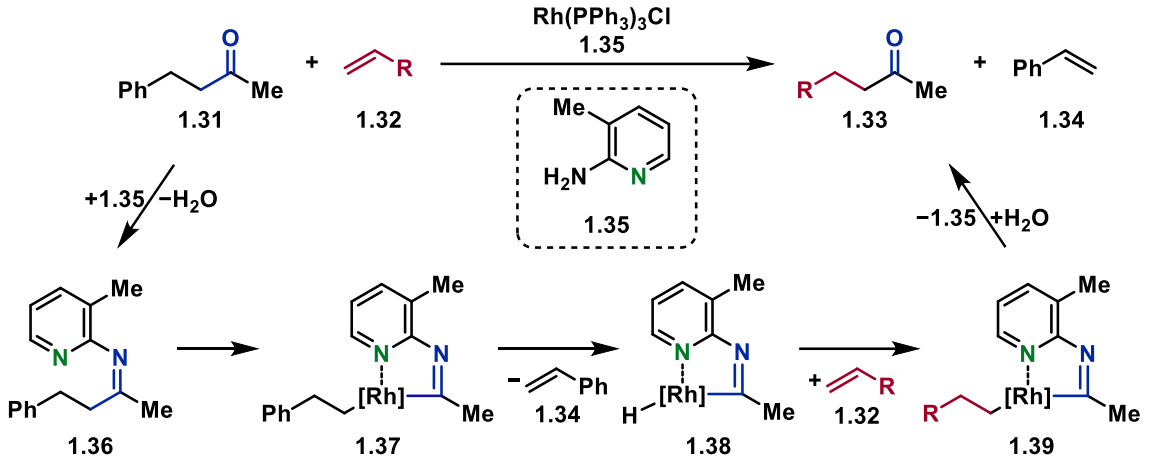

Scheme 1.11 Chelation directed C–C bond activation through *in situ* imine formation

1.3.3 Summary

Although there are significant thermal and kinetic challenges to C–C bond activation, numerous methods have been developed to overcome these barriers. By using strategies such as coupling strain-release to bond activation, increasing the polarity or decreasing the hybridization of the target bonds, or using permanent or temporary chelating directing groups we can achieve selective C–C bond activation. By coupling these bond activation processes to other elementary steps like transmetalation and alkene insertions, we can form new C–C bonds, making this a powerful strategy for the synthesis of complex molecules.

1.4 Ester C–O σ-Bond Activation

While C–Y (Y= C, H, O, N) bond activation reactions are a current focus of organic method development there are relatively few examples of C–O bond activation methods for esters. Esters are a desirable starting material for cross-coupling reactions as they are stable and abundant. Following C_{acyl}–O bond activation of esters, the acyl and alkoxide

moieties of intermediates **1.41** can be used in cross-coupling reactions with organic halides or boronic acids to form ketones **1.42**, in Heck-type insertion processes with alkenes or alkynes to form products **1.43**, or in domino Heck/Suzuki processes to form **1.44** with high atom economy (Scheme 1.12). Challenges to using ester C–O bond activation in synthetic processes forming ketones include the selectivity of bond activation and preventing decarbonylation.

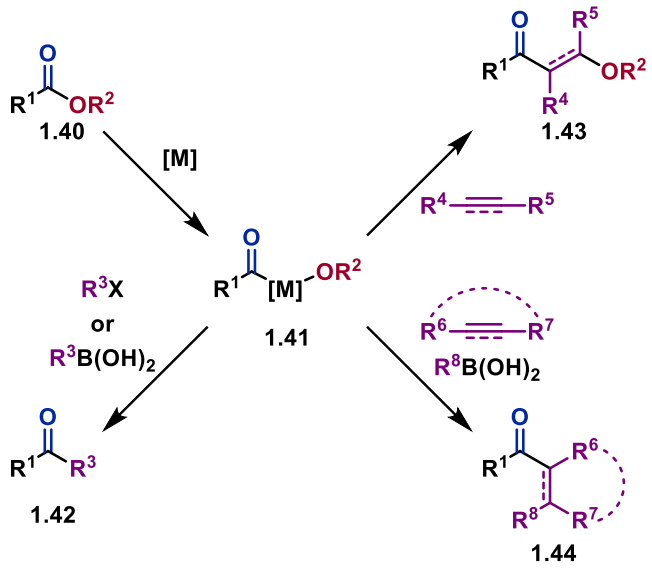

Scheme 1.12 Reaction pathways following C–O bond activation of esters

Oxidative addition of a transition metal into an ester C–O bond can occur by one of two pathways, addition into the C_{acyl}–O bond (Scheme 1.13, path 1), or addition into the O–C_{aryl} bond (path 2). Li and coworkers[96] reported a DFT study on the selectivity of C–O bond activation of aryl esters (Scheme 1.13). While the C_{acyl}–O bond has a significantly lower bond dissociation energy (80 kcal/mol vs 106 kcal/mol), only the products from O–C_{aryl} bond activation were observed experimentally. Li et al. showed that the barrier to form **1.46** through C_{acyl}–O bond activation of **1.45** was also significantly lower than that of C_{aryl}–

O bond activation to form **1.47** (+14.2 kcal/mol vs. +22.9 kcal/mol). Despite the apparent energy preference for C_{acyl}–O bond activation, both pathways are observed experimentally. Although C_{acyl}–O bond activation is more facile, it is also reversible, while C_{aryl}–O bond activation is slower and typically irreversible. To use C–O bond activation of esters in organic transformations, we must control the regioselectivity of this bond activation.

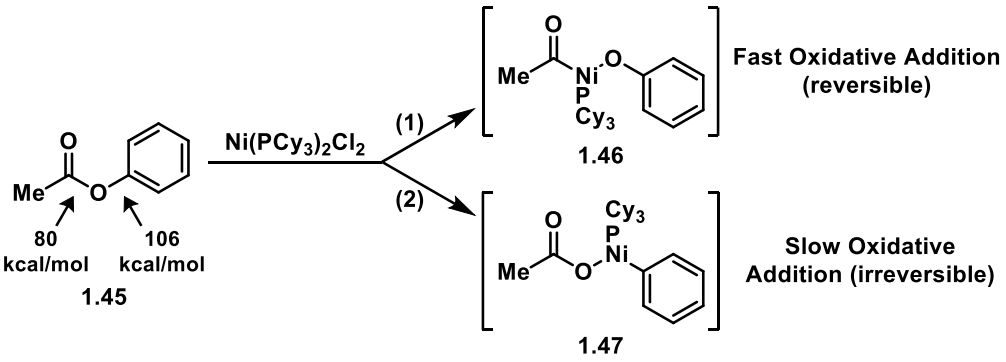

Scheme 1.13 Selectivity model for oxidative addition of ester C–O bonds

The first example of C_{acyl}–O bond activation was reported by Yamamoto et al.[97] (Scheme 1.14). Phenyl propionate **1.48** was activated by $Ni(cod)_2$ forming **1.49** which underwent decarbonylation via α-elimination of CO forming phenol, ethylene, and nickel carbonyl species **1.51**. This demonstrates how metal-acyl species are prone to decarbonylation. Catalytic transformations, including cross coupling reactions, using decarbonylation as a productive step have been reported[87,98–102] but will not be discussed here.

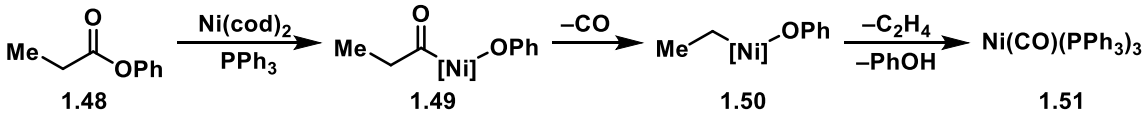

Scheme 1.14 Seminal report of ester C–O bond activation of phenyl propionate by Yamamoto et al.

We aim to develop transformations that retain the carbonyl functional group, to achieve this, we must prevent decarbonylation. Methods to avoid decarbonylation of acyl-metal species include altering the electronic properties of the metal and carbonyl species, the stabilizing intermediates with chelating directing groups, and using bulky ligands.

1.4.1 Cross-Coupling Methods

In early work on palladium catalyzed activation of esters, elevated temperatures were required to drive C–O bond activation due to the lower electron density of Pd(0) complexes relative to Ni(0) complexes.[103] Yamamoto et al. used electron deficient trifluoroacetates **1.52** to achieve C–O oxidative addition at room temperature. The resulting trifluoroacetyl-metal species did not undergo decarbonylation. Using this strategy, they developed the first reported C–C bond forming process using C_{acyl}–O bond activation followed by coupling with boronic acids to form trifluoromethyl ketones **1.53** (Scheme 1.15a).[104]

Wang et al.[105] developed a cross-coupling with aryl boronic acids using a quinoline-directed C–O bond activation of **1.54** (Scheme 1.15b). As in C–C bond activation, the chelating quinoline group worked to direct bond activation and prevent decarbonylation to form ketones **1.55**. Chatani and coworkers developed Suzuki-type cross coupling reactions via C–O bond activation using two types of pyridyl directing groups bound through the alkoxide moiety of esters **1.56** and **1.59** (Scheme 1.15c and d).[101,106] Both chelating directing groups worked to direct C–O bond activation. These directing groups may have prevented decarbonylation by stabilizing the resulting catalytic intermediates **1.57** and **1.60**, but decarbonylation was likely avoided due to fast transmetalation and reductive

elimination of ketones **1.58**. Shi et al.[107] and Halima et al.[108] independently developed cross couplings of phenyl esters **1.61** with aryl or heteroaryl boronic acids through undirected C–O bond activation (Scheme 1.15e). Decarbonylation was prevented by using bulky *N*-heterocyclic carbene (NHC) ligands.

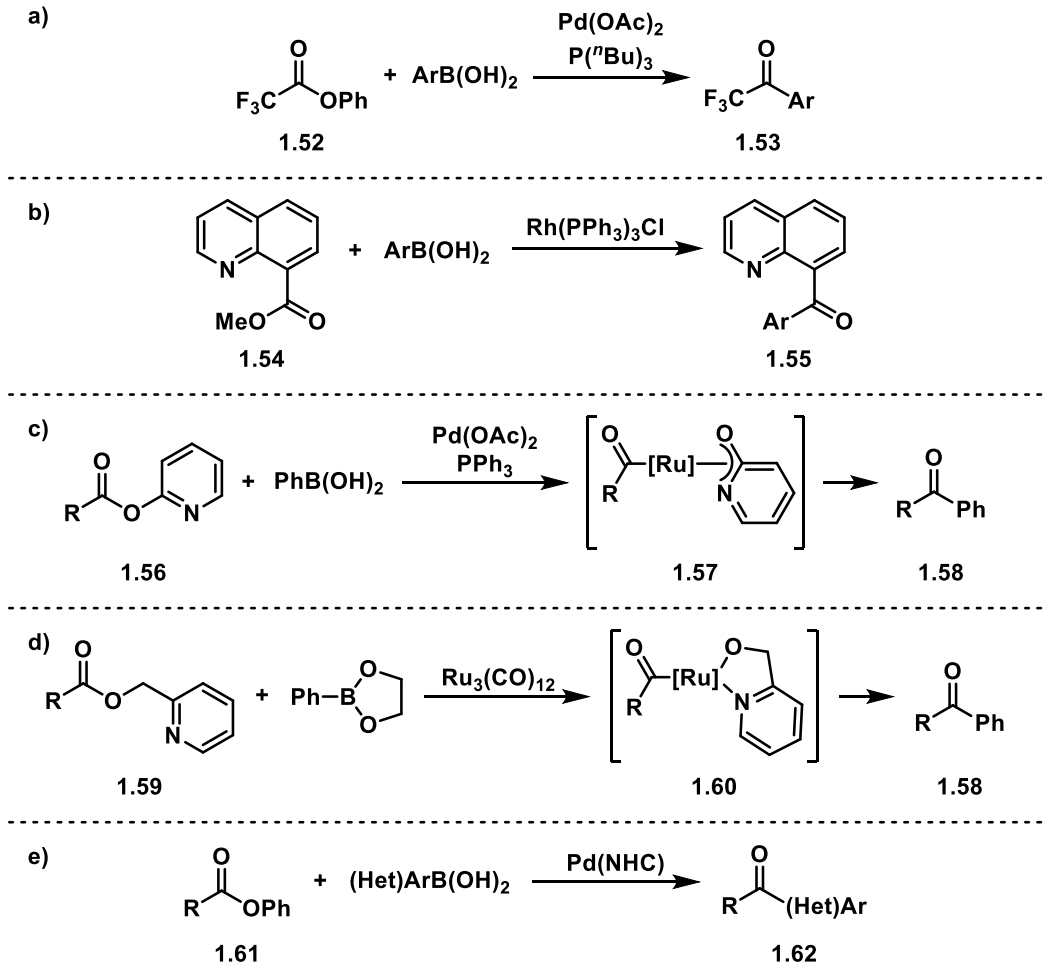

Scheme 1.15 Suzuki-type cross-coupling reaction using C–O bond activation

C–O bond activation has also been used in cross coupling reactions with amines to form amides. This was first reported by Hie et al.[109] using C–O bond activation of methyl esters **1.63** followed by coupling with aromatic secondary amines **1.64** to form tertiary amides **1.65** (Scheme 1.16a). The Lewis acid additive is proposed to bind to the carbonyl

oxygen, computations indicate that this assists the reaction in multiple ways. Lewis acid coordination lowers the energy barriers to oxidative addition, ligand exchange of methoxide for the amine, and reductive elimination and makes the overall reaction more thermodynamically favorable. Buchspies et al.[110] later developed methods cross coupling phenyl benzoate **1.66** with aniline **1.67** forming secondary amide **1.68** (Scheme 1.16b). Both methods used Ni-catalysis with bulky NHC ligands which likely worked to prevent decarbonylation.

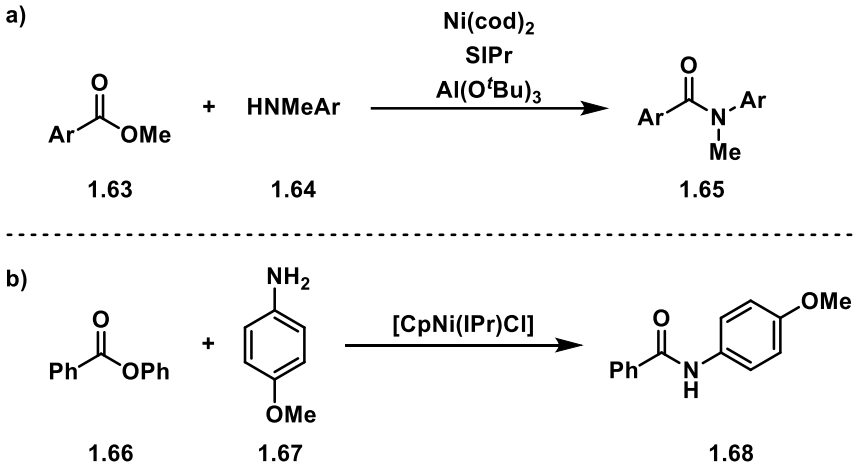

Scheme 1.16 Cross coupling with amides via C–O bond activation

1.4.2 Insertion Reactions

Cross-coupling reactions involving esters incorporate the acyl fragment, or the corresponding decarbonylated fragment, into their products, leaving the alkoxide fragment as a byproduct that is discarded or recycled for further substrate synthesis. A "cut-and-sew" insertion process activates the C_{acyl}–O bond and adds both the acyl and alkoxide fragments across the π-bond. Both fragments are incorporated into the final product giving the reaction a high atom economy.

In 2009, Murai et al.[111] reported the oxyacylation of nitriles. Various carboxylates of 2-(cyanomethyl)phenyl esters **1.69** were used in the Pd(0) catalyzed reaction to form 2-aminobenzofurans **1.70** (Scheme 1.17). Crossover reactions suggest the cycloisomerization is entirely intramolecular.

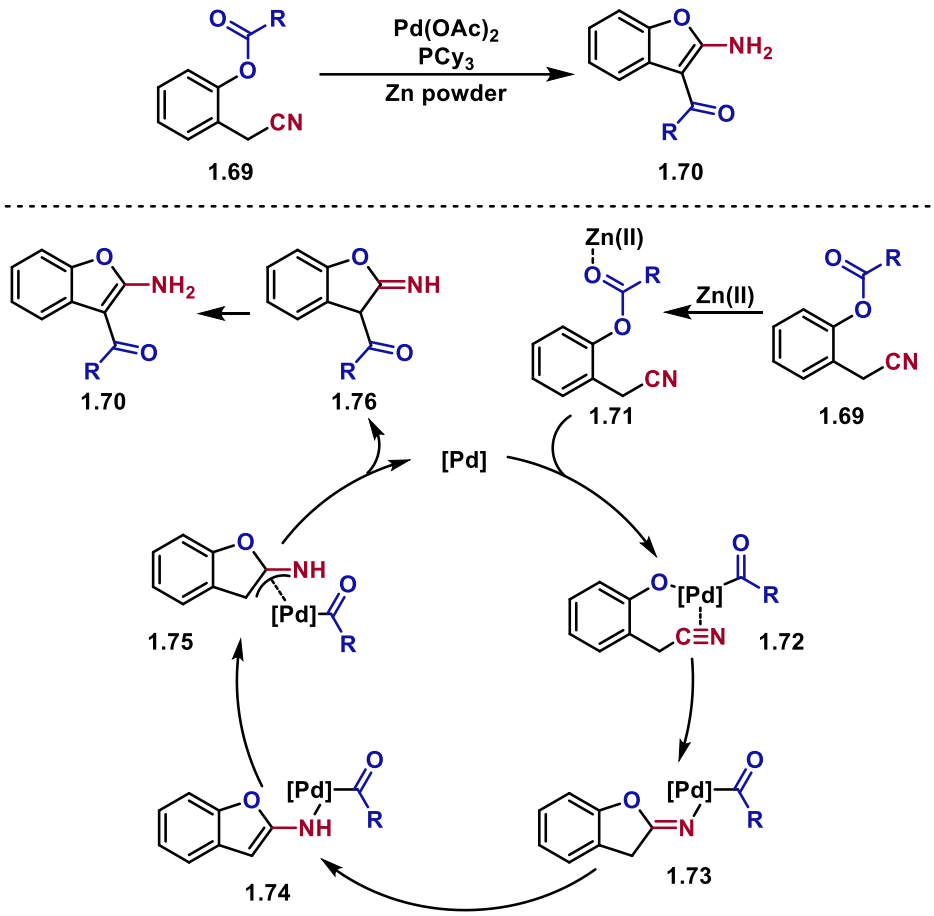

Scheme 1.17 Oxyacylation of nitriles

Lewis acid $Zn(OAc)_2$, formed *in situ*, activates the carbonyl through coordination and accelerates oxidative addition of Pd(0) to ester **1.71**. After oxidative addition, the palladium center coordinates to a π-bond of the nitrile forming **1.72** and migratory insertion

across the nitrile generates intermediate **1.73** (Scheme 1.17). Prototropic isomerization of intermediate **1.73** forms **1.74**. The azaallyl-palladium species **1.74** undergoes σ-π isomerization followed by reductive elimination. Subsequent isomerization driven by aromatization forms the final product 2-aminobenzofuran **1.70**.

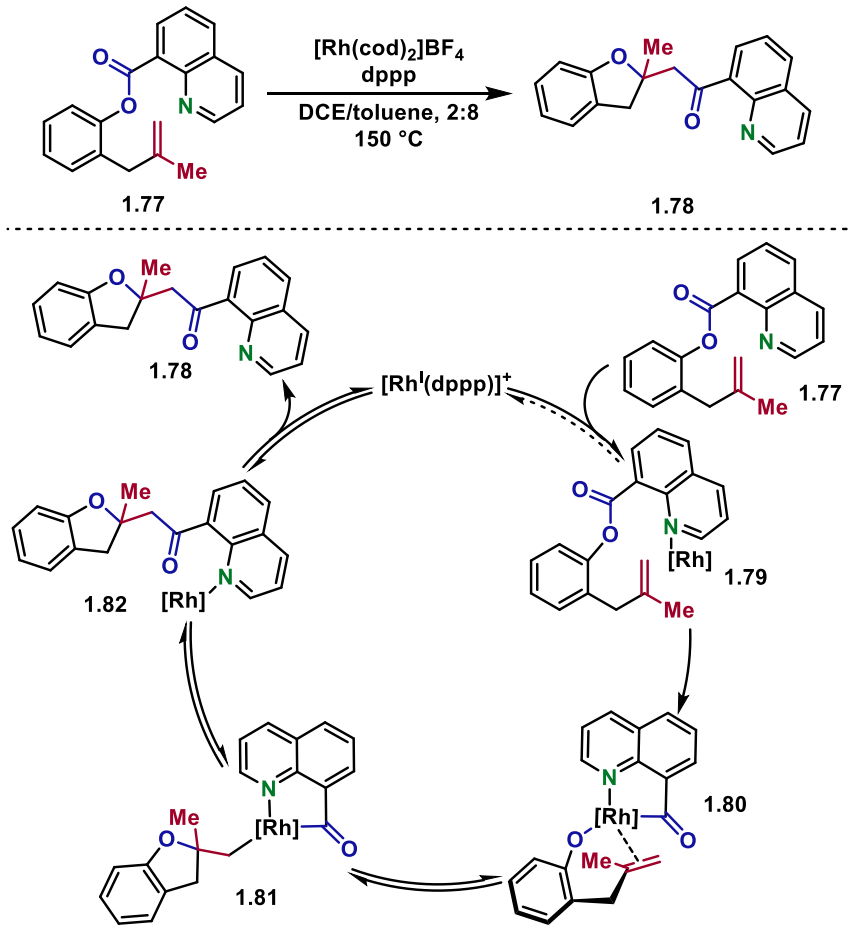

Scheme 1.18 Reaction conditions and mechanism of the quinoline-directed oxyacylation reaction

In 2009, the Douglas group reported the rhodium-catalyzed oxyacylation of alkenes (Scheme 1.18).[112] They use a quinoline directing group to direct bond activation and prevent decarbonylation by forming the stable 5-membered chelate ring seen in

intermediates **1.80** and **1.81**. Migratory insertion across the alkene gives **1.82** and reductive elimination forms the product ketone **1.78** (Scheme 1.18). We published a follow up report detailing the development, optimization, and scope of this reaction.[113] I validated this chemistry on a preparatory scale.

Uson et al.[114] showed that phenol could displace alkoxide groups on Ir(cod)(OR) (R = Me, Et) species in the presence of bulky, basic phosphine ligands. Inspired by this work, Douglas et al. used a hydroxyl directing group to facilitate iridium(I) oxidative addition into the ester C_{acyl}–O bond of **1.83** in alkene oxyacylation to form ketone **1.84** (Scheme 1.19).[115] This transformation goes through the same mechanism as quinoline-directed alkene oxyacylation.

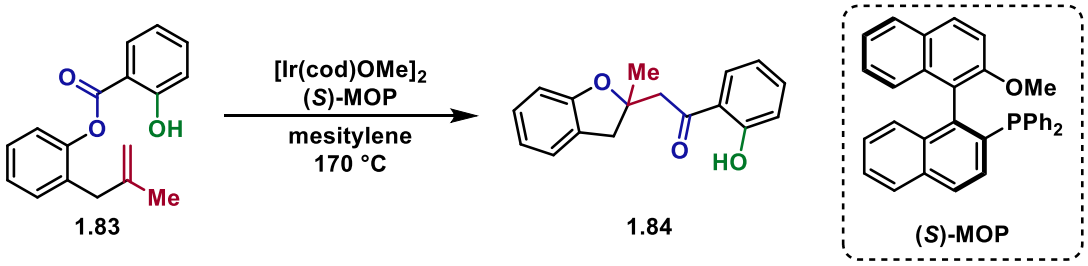

Scheme 1.19 Hydroxyl-directed oxyacylation of alkenes

1.4.3 Domino Insertion and Coupling Reactions

Recently, methods integrating alkene insertions with nucleophile additions have been developed. Iyori and Chatani[116] developed an alkyne oxyacylation reaction using ester C–O bond activation of methyl salicylates **1.85** (Scheme 1.20). The *ortho*-hydroxyl group of salicylate **1.85** works to direct C–O bond formation and prevent decarbonylation before alkyne migratory insertion forming intermediate **1.86.** The hydroxyl group then acts as an internal nucleophile for chromone **1.87** formation through reductive elimination.

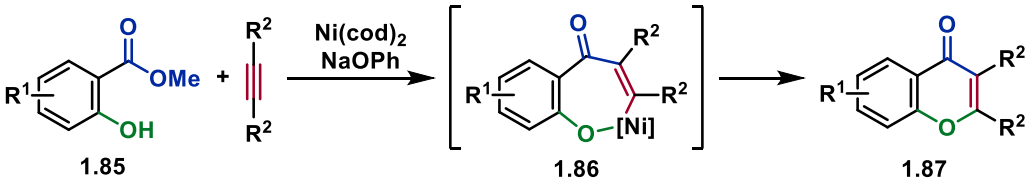

Scheme 1.20 Intermolecular oxyacylation of alkynes

Zheng and Newman reported an alkene carboacylation reaction through a domino Heck/Suzuki coupling of methyl esters **1.88** and aryl boronic acids (Scheme 1.21a). The Ni(NHC) catalyst is proposed to undergo oxidative addition to the C–O bond, followed by migratory insertion of the tethered alkene to form the benzocyclopentanone ring. Subsequent transmetalation of the boronic acid and reductive elimination form **1.89**.

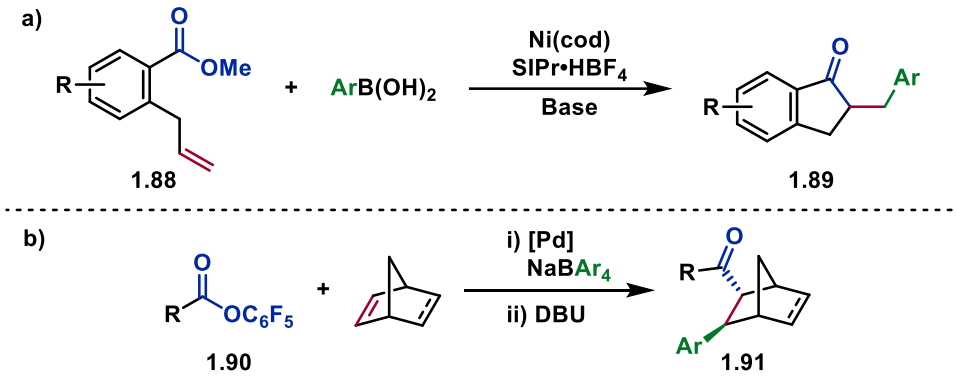

Scheme 1.21 Domino Heck/Suzuki-type coupling reactions

Banovetz et al.[117] reported a fully intermolecular, three-component coupling carboacylation reaction using privileged alkenes norbornene or norbornadiene (Scheme 1.21b). Electron-deficient pentafluorophenyl benzoate **1.90** was required for C–O bond activation. Reactions with methyl, benzyl, or other aryl benzoates in the same conditions did not result in any conversion of the starting ester. This transformation initially forms *cis*-**1.91** but this product is partially isomerized by pentafluorophenoxide generated in the

reaction. By adding additional base at the end of the reaction, they are able to fully isomerize the product to the thermodynamically favored *trans*-**1.91**.

1.4.4 Summary

To use ester C–O bond activation in synthesis, we must control the regioselectivity of bond activation and prevent side reactions like decarbonylation. Early strategies of control include chelating directing groups, activation of electron-poor esters like trifluoroacetates **1.51**, and coupling bond activation to mechanistic steps that occur at a faster rate than decarbonylation, like transmetalation with boronic acids and esters. The addition of Lewis acids or bulky ancillary ligands, like NHCs, also work to prevent decarbonylation allowing the formation of ketones. Lower row transition-metal catalysts (Ru, Rh, Ir, Pd) and electron-rich Ni catalysts have been most successful in C–O bond activation processes.

Chapter 2. Steric-Controlled Arene Acylation via Sequential C–O/C–H Bond Activation

2.1 Introduction

During our development of hydroxyl-directed alkene oxyacylation via Ir-catalyzed C_{acyl}–O bond activation of salicylate esters **2.1**, T.G. Hoang identified ketone side products **2.3aa1** and **2.3aa2** formed by the acylation of solvent *m*-xylene (Scheme 2.1a). The intramolecular oxyacylation product **2.2** was favored but, interestingly, the major isomer of *m*-xylene acylation was the *meta*-acylated 1,3,5-substituted product **2.3aa1**. Electronic-controlled regioselectivity would predict 1,2,4-substituted **2.3aa2** as the major product. The 10:1 ratio of **2.3aa1**:**2.3aa2** is indicative of a mechanism distinct from classical electrophilic aromatic substitution (EAS) reactions like Friedel-Crafts acylation. Using phenyl salicylate **2.4a** as the ester component without an alkenyl side chain made **2.3aa1** the major product (Scheme 2.1b). Control experiments showed iridium was required for the reaction. The need for iridium and interesting regioselectivity observed indicated that a mechanism involving integrated ester C–O and arene C–H bond activation was plausible.

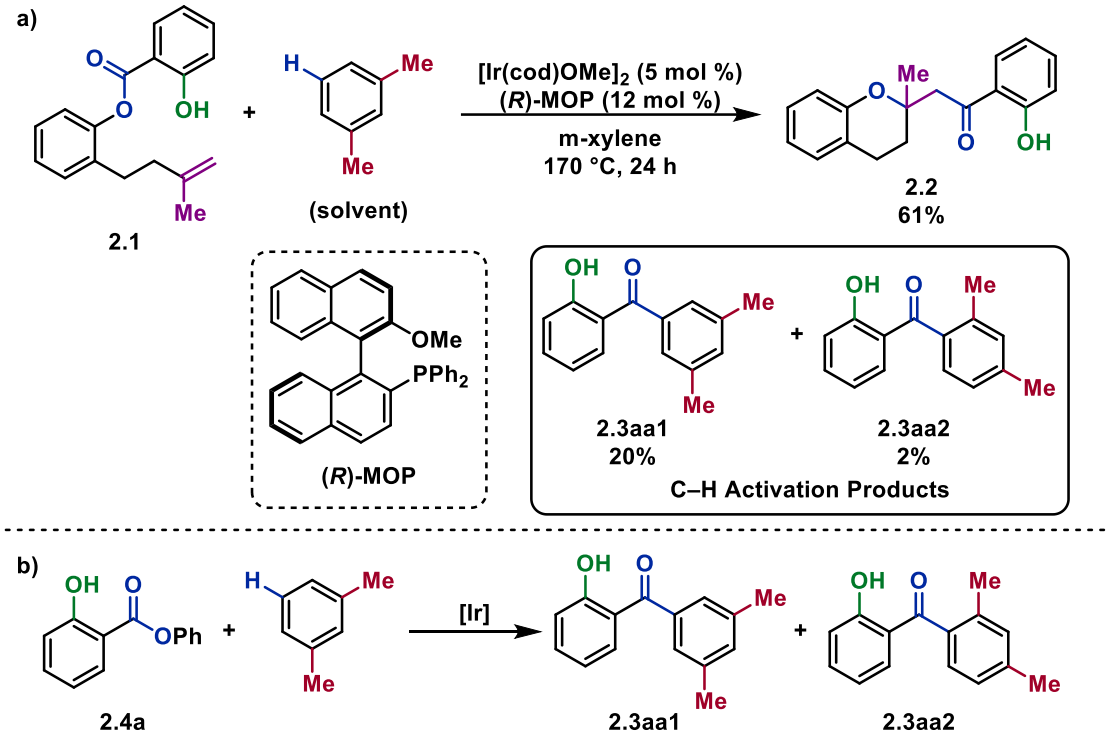

Scheme 2.1 a) Oxyacylation of a salicylate ester with (*R*)-MOP; b) acylation of *m*-xylene

Chapter 2 will begin with an introduction to steric-controlled C–H bond activation and dual bond activation methods followed by our investigation into the optimized reaction conditions, mechanism, and scope of the steric-controlled arene acylation via Ir-catalyzed sequential C–O/C–H dual bond activation.[a]

[a] Figures and text adapted with permission from Serratore, N. A.; Anderson, C. B.; Frost, G. B.; Hoang, T.-G.; Underwood, S. J.; Gemmel, P. M.; Hardy, M. A.; Douglas, C. J. Integrating Metal-Catalyzed C–H and C–O Functionalization To Achieve Sterically Controlled Regioselectivity in Arene Acylation. *J. Am. Chem. Soc.* **2018**, *140* (31), 10025–10033. Copyright 2018 American Chemical Society.

2.2 Late Transition-Metal-Catalyzed, Steric-Controlled C–H bond Activation of Arenes

2.2.1 Electrophilic Aromatic Substitution

The most common method of C–C bond formation through direct functionalization of C_{aryl}–H bonds is EAS. The regioselectivity of these transformations is dictated by electronics, resulting in substitution in the *ortho*- and *para*- positions relative to electron-donating groups (EDG) or *meta*- to electron-withdrawing groups (EWG)[118] (Figure 2.1). The selectivity of EAS can be rationalized by the mechanism. The high-energy tetrahedral arenium ion intermediate is stabilized by the presence of EDG *ortho* and *para* to the charged carbon or by the *meta* EWG. The Lewis acid catalyst is used to increase the electrophilicity of the electrophile and is typically a metal that does not undergo redox changes over the course of the reaction.

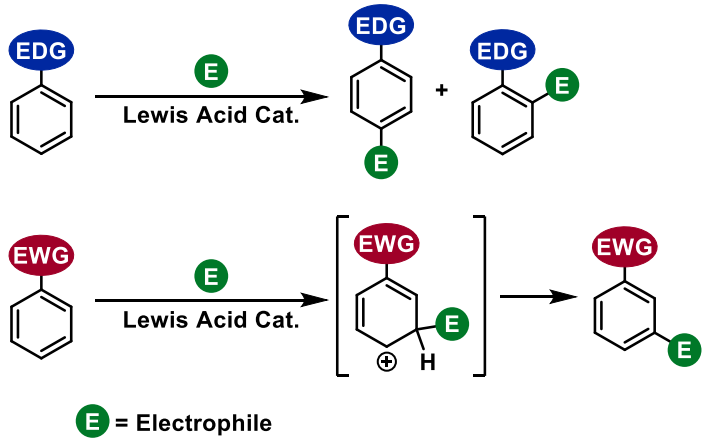

Figure 2.1 Regiocontrol of EAS reactions

The aluminum catalyzed Friedel-Crafts acylation of *m*-xylene by benzoyl chloride **2.5** gave the 1,2,4 substituted arene **2.6** in 92% yield and the 1,2,6-substituted arene **2.7** in

only 8% yield (Scheme 2.2).[119] This selectivity is in sharp contrast to the regioselectivity observed in the acylation of *m*-xylene where 1,3,5-substituted product **2.3aa1** is preferentially formed along with **2.3aa2**, and the 1,2,6-substituted product is not observed (Scheme 2.1). The difference in regioselectivity observed supports the hypothesis that **2.3aa1** is forming through an alternate mechanism to EAS.

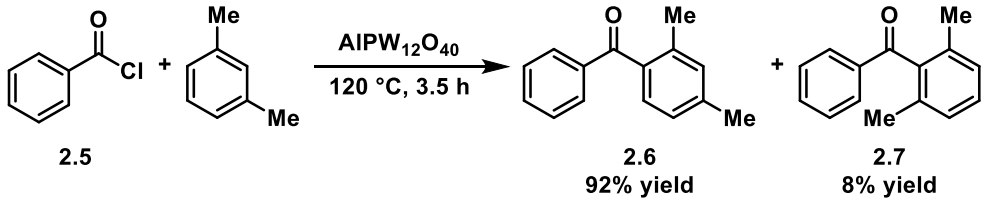

Scheme 2.2 Friedel-Crafts acylation of *m*-xylene by benzoyl chloride

2.2.2 Steric-Controlled C–H Activation of Arenes

In 2002, Smith et al.[120] published an Ir-catalyzed borylation of arenes by HBpin (Scheme 2.3a). At the same time, Hartwig et al.[121] reported the Ir-catalyzed direct borylation of arenes with B_2pin_2 (Scheme 2.3b). These reactions activate aryl C–H bonds with steric control of regiochemistry instead of the electronic control. By coupling these borylations with Suzuki-Miyaura couplings, C–C bonds can be formed at the least sterically hindered positions.

Hartwig and coworkers published two initial reports on the direct borylation of arenes and heteroarenes via C–H bond activation reaction in 2002.[121,122] Initial results showed that for monosubstituted arenes, substitution occurred at the *meta*- and *para*-positions in a statistical ratio (2:1 *meta*:*para*). Borylation of 1,3-disubstituted arenes exclusively led to substitution at the common *meta*- position. Screenings of ligands

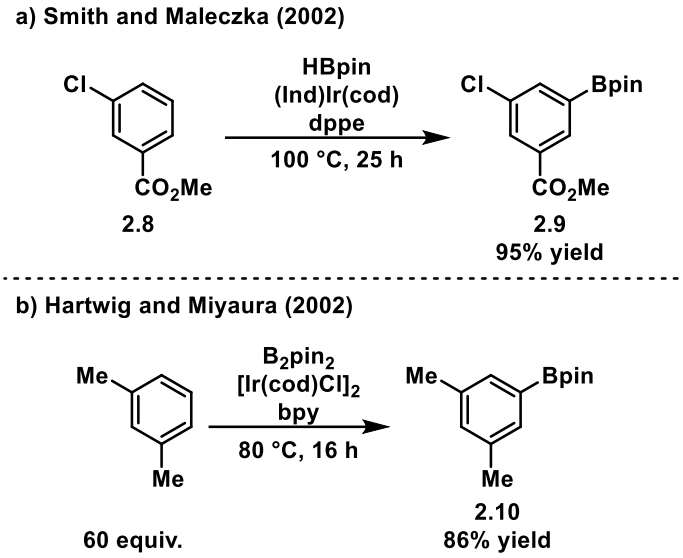

Scheme 2.3 Steric-controlled borylation of arenes

demonstrated the importance of the bipyridine ligand for successful reaction. The initial reaction was optimized using a $[Ir(cod)Cl]_2$ and 2,2'-bipyridine (bpy) catalyst system at 80 °C (Scheme 2.3b). Changing the precatalyst to $[Ir(cod)OMe]_2$ and the ligand to 4,4'-di-*tert*-butyl-2,2'-bipyridine (dtbpy) gave significant improvement (Scheme 2.4), removing the need for elevated temperatures, shortening the reaction time, and lowering the concentration of arene from neat to 0.33 M. This is the first reported example of C–H borylation at room temperature.

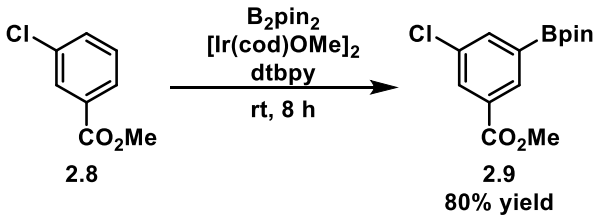

Scheme 2.4 Improved conditions for steric-controlled borylation at room temperature

During a stoichiometric catalyst study in mesitylene, complex **2.11** was isolated (Scheme 2.5).[121] Dissolving **2.11** in deuterated-benzene yielded the borylation product **2.12** in minutes. Reaction of **2.11** with other arenes yielded similar results. These results suggested that complex **2.11** is a catalytic intermediate or can quickly convert to a catalytic intermediate. Computations supported these results, indicating that the C–H activation reaction occurred at a trisboryl transition metal complex.[123] Kinetic isotope effect (KIE) data obtained from a competition reaction between benzene and d_6-benzene with **2.11** indicated that C–H bond activation is the rate-limiting step.[124]

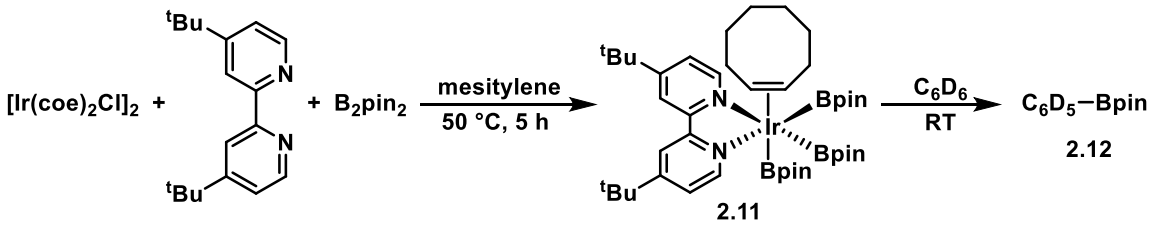

Scheme 2.5 Stoichiometric studies of arene borylation

The authors also observed an inverse dependence on cyclooctene (COE). Unexpectedly, the reaction was found to occur faster with electron-poor phenyl arenes than with electron-rich phenyl arenes in a one-pot competition reaction. Conversely, electron-rich heterocycles reacted faster than electron-neutral arenes. The authors proposed that the arene that forms the more stable η^2-arene complex before oxidative addition results in the faster reaction.

Based on these observations, they proposed the following mechanism for borylation (Scheme 2.6). The catalytic cycle is entered through the dissociation of COE from **2.11**. Next complex **2.13** activates the C–H bond of the arene. From the data, the authors could not determine if the mechanism of the C–H activation step is oxidative

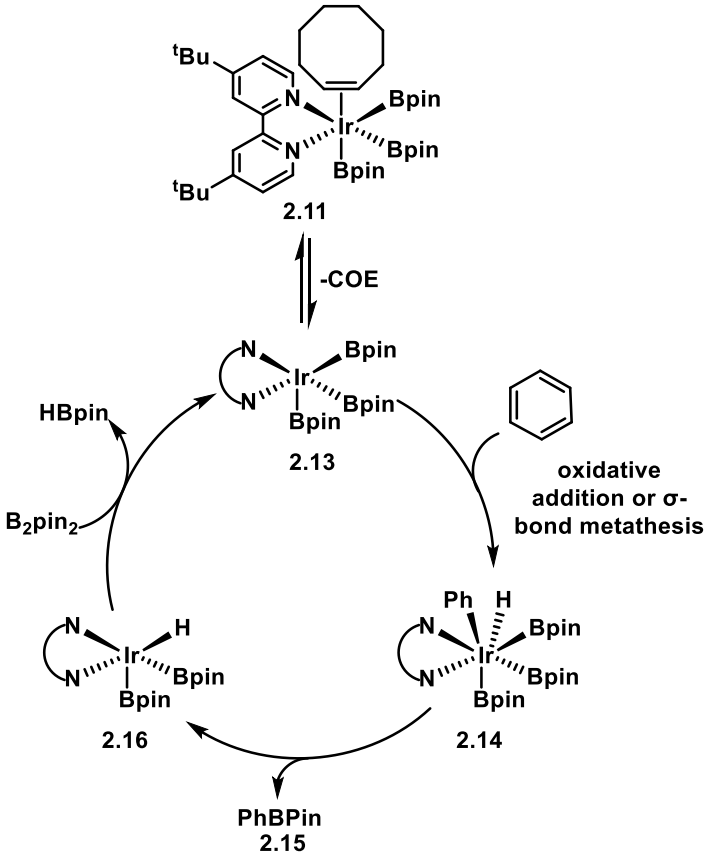

Scheme 2.6 Mechanism of iridium-catalyzed steric-controlled C–H borylation

addition or σ-bond metathesis (SBM). Computations suggest oxidative addition through formal Ir(V) intermediate **2.14** is a lower energy pathway compared to SBM.[123] Complex **2.14** then reductively eliminates borylated arene **2.15**, forming **2.16**. Exchange of a hydride for Bpin closes the catalytic cycle. Hartwig and colleagues later reported the steric controlled silylation of arenes[125–127] which was found to proceed through a similar mechanism.[128]

2.2.3 Aryl C–H Bond Activation Mechanisms

Several mechanisms of transition-metal mediated aryl C–H bond activations are known, including SBM and concerted metalation deprotonation (CMD). The overall transformations of these SBM and CMD are similar, but the mechanisms are distinct. SBM involves concerted M–R and Ar–H bond breakage and M–Ar and R–H bond formation via a four-center, four-electron transition state (Scheme 2.7a).[129] CMD requires an X-type ligand, Y, that has at least one lone pair (Y = alkoxide, amido, hydroxide, imido, or oxo). The lone pair on Y acts as an internal base, deprotonating the C–H σ-adduct at the same time as the M–Ar bond is forming, resulting in a six-electron, four-center transition state (Scheme 2.7b).

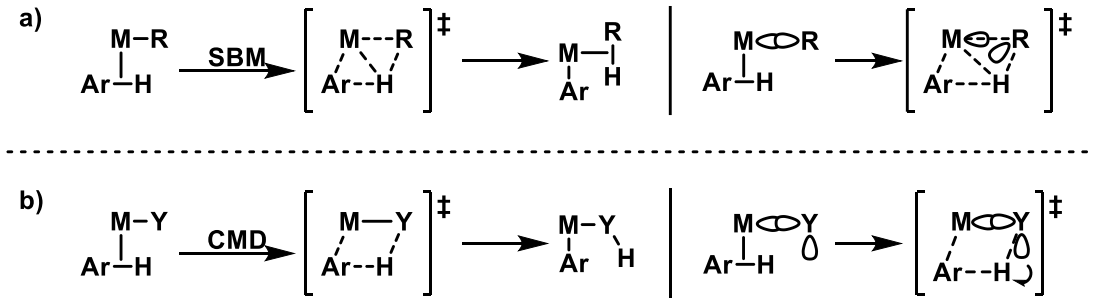

Scheme 2.7 Mechanisms and orbital diagrams of C–H bond activation by a) σ-bond metathesis; b) concerted metalation deprotonation

CMD is has advantages over SBM in reactions involving mid to late transition metals. SBM requires the orbitals of the M–R bond to change direction to interact with the aryl hydrogen.[129] CMD is more favorable because the orbital containing the Y lone pair is already oriented towards the hydrogen so the directionality of the orbitals does not need to change.

Periana et al.[130] observed a C–H activation reaction of benzene by iridium(III) methoxide complex **2.17** (Scheme 2.8). Analysis of the localized DFT molecular orbitals showed that a lone pair on methoxide is involved in the bond activation step, suggesting the mechanism is CMD and not SBM. When toluene was used instead of benzene, only the C–H bonds *meta* and *para* to the methyl group were activated, indicating that this method of bond activation is selective for less sterically hindered C–H bonds.

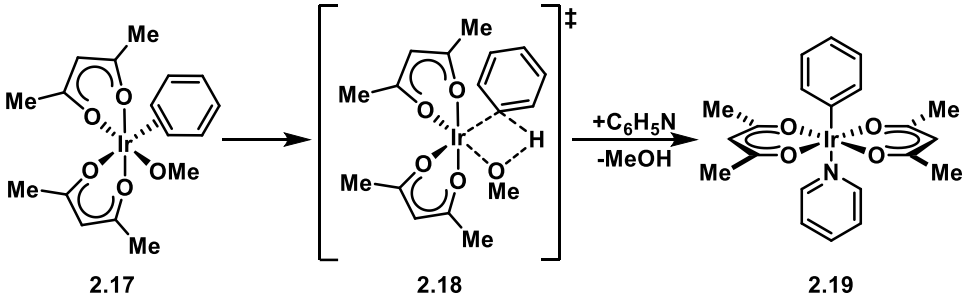

Scheme 2.8 Concerted metalation deprotonation at an iridium(III) center

Late transition metals in low oxidation states typically undergo CMD more easily than metals in higher oxidation states. This is likely due to the decreased amount of back-bonding between the metal center and the Y-group. The reactivity of a complex towards CMD can be enhanced by increasing the basicity of the ligand Y or disrupting ligand-to-metal π-donation.

The thermodynamic and kinetic barriers to CMD are difficult to predict due to the changes in bond energies over the course of the reaction. The Y-ligand is often converted from an X-type donor to an L-type donor during this transformation and any π-back-bonding is diminished or lost entirely. The strength of the M–Ar and Y–H bonds being formed must also be considered as their strengths will affect the transition state energy.

2.2.4 Integrated C–O/C–H Bond Activation Methodologies

While numerous types of reactions involving traditionally inert C–Y bond activations have been developed, most of these methods still involve one metal/halogen pre-functionalized coupling partner. Combining two metal-catalyzed C−Y activations into a single C−C bond-forming reaction is a unique challenge. The earliest examples of C–C bond formation via dual C–Y bond activation are dehydrogenative couplings merging two C–H bond activations of arenes or heteroarenes.[131–135] Examples coupling C–C and C–H bond activations have become more prevalent in recent years.[136,137] Integration of C–N and C–H bond activation processes are rare, but a few examples have been reported by Szostak and coworkers.[138,139] Our work merges C–O and C–H bond activation. This type of dual bond activation has been reported previously relying on the activation of anhydrides. Gooβen et al. developed a carboxylate directed *o*-acylation of benzoic acids **2.20** via Rh-catalyzed C–O bond activation of anhydrides **2.21** (Scheme 2.9a).[140] Other examples of integrated C–O and C–H bond activation methods utilize a Catellani-type[141–144] transient directing group (Scheme 2.9b and c). These processes begin with oxidative addition of the C–I bond of aryl iodides **2.23** or **2.27** and migratory insertion of norbornene or substituted norbornene **2.25**. This places the Pd center in close proximity to the C_{aryl}–H bond to direct bond activation forming metallacycle intermediate **2.31**. subsequent C–O bond activation of anhydrides **2.24** or **2.28** and reductive elimination form the new C–C bond. This process allows for *ortho*-functionalization and *ipso*-dehalogenation[145] or *ortho*- and *ipso*-functionalization[128] of aryl iodides **2.23** and **2.27** to form arenes **2.26** or **2.30** respectively.

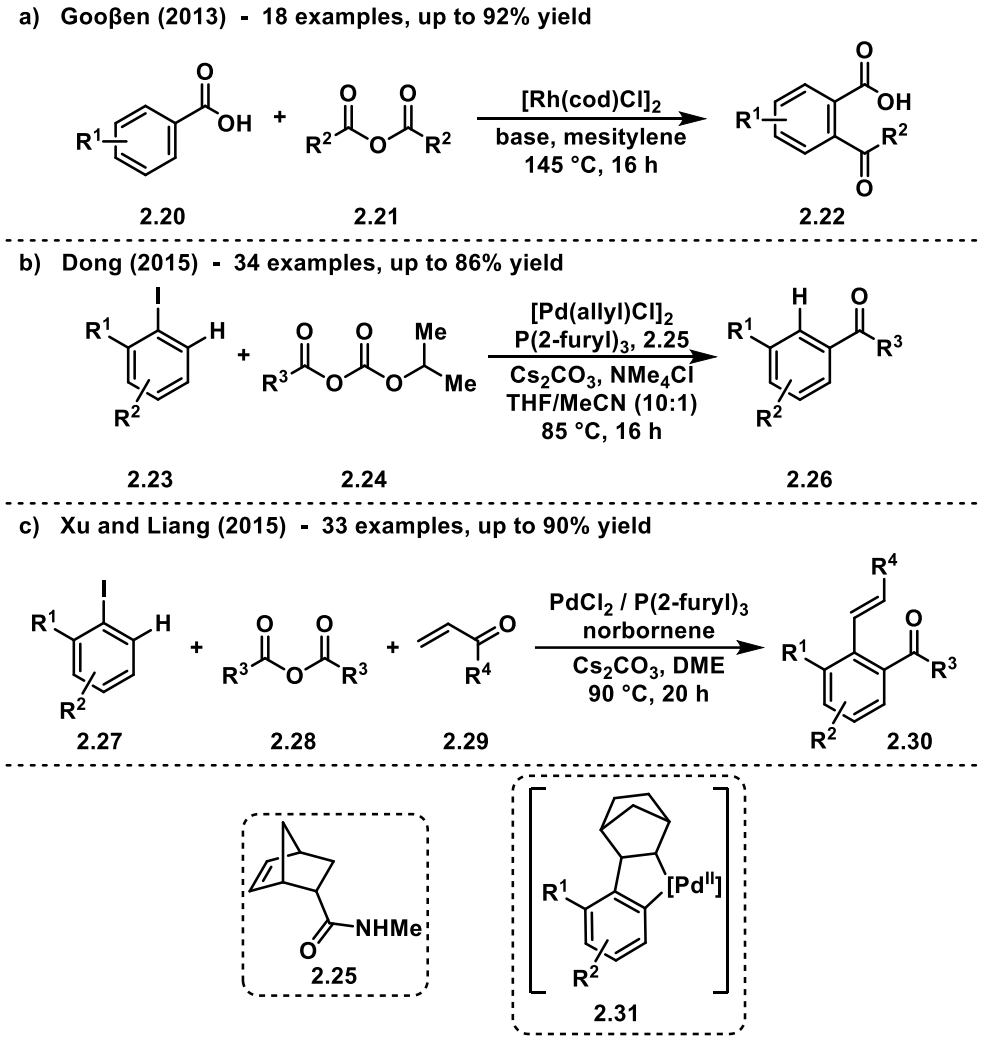

Scheme 2.9 Integrated C–O/C–H bond activation methods

While dual C–Y bond activation is a significant achievement and eliminates the need for exogenous oxidant additives, all previous examples of integrated C–O/C–H bond activation still required a stoichiometric amount of exogenous base. Exogenous oxidant additives are not required because initial addition into the C–Y bond oxidizes the metal center to the higher oxidation state typically required for C–H bond activation. In our

sterically-controlled arene acylation, activation of the ester C–O bond provides an endogenous oxidant and base.

2.3 Reaction Optimization

After the initial serendipitous discovery of the C–O/C–H coupling reaction during the study of oxyacylation, T.G. Hoang and N. A. Serratore worked to optimize the reaction. The starting ester was simplified to **2.4a**, removing the alkenyl side chain to prevent any possibility of a Heck-type insertion reaction.

To begin, the effect of the precatalyst identity was examined. $[Ir(cod)OPh]_2$ was compared to other iridium precatalysts with base additives (Table 2.1). Iridium complexes

Table 2.1 Effect of precatalyst choice

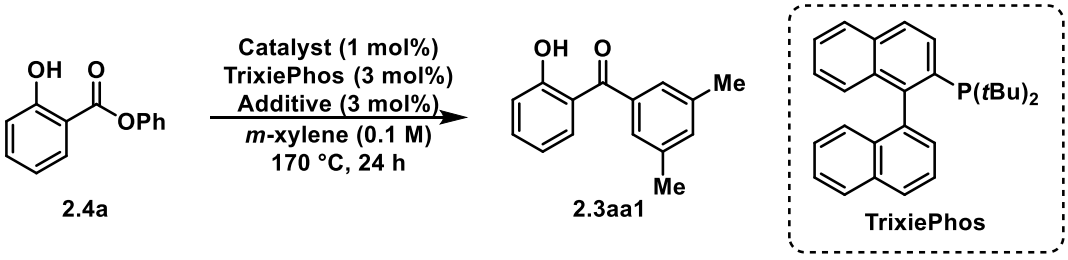

Entry	Catalyst	Additive	Yield 2.3aa1 (%)[a]
1	$[Ir(cod)OPh]_2$	—	81
2	$[Ir(cod)Cl]_2$	KOPh	44
3	$[Ir(cod)Cl]_2$	K_2CO_3	3
4	$[Ir(coe)_2Cl]_2$	KOPh	49
5	$[Ir(coe)_2Cl]_2$	K_2CO_3	1

a) Determined by quantitative ^1H NMR (qNMR)

with 1,5-cyclooctadiene (COD) ligands combined with KOPh additives performed best (Table 2.1 entries 2 and 4). These conditions were presumed to form $[Ir(cod)OPh]_2$ *in situ*, but were still less effective than preformed $[Ir(cod)OPh]_2$ (Table 2.1 entry 1).

A screen of catalyst loadings from 0.5 mol% to 10 mol% indicated that 1 mol% $[Ir(cod)OPh]_2$ was optimal (Table 2.2 entry 2). Interestingly, above 1 mol%, yields of **2.3aa1** went down as catalyst loading increased. This is likely due to an increased amount catalyst decomposition (see Section 2.4.2) or substrate/product sequestration by iridium. Higher catalyst loadings also resulted in lower steric selectivity, forming more significant quantities of **2.3aa2**.

Table 2.2 Effect of catalyst loading on yield and product distribution

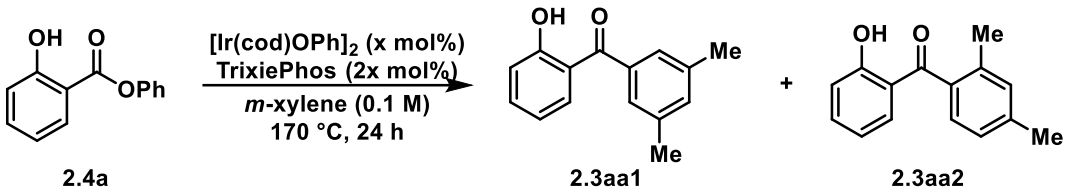

2.4a 2.3aa1 2.3aa2

Entry	[Ir] (mol%)	Yield 2.3aa1 (%)[a]	Ratio 2.3aa1:2.3aa2[a]
1	0.5	49	>20:1
2	1	70	18:1
3	2.5	69	15:1
4	5	60	11:1
5	10	43	7:1

a) Determined by qNMR

Various Buchwald-type ligands and P(*o*-tol)$_3$ were tested (Table 2.3). While all phosphines tested promoted the reaction to some extent, those with the general (bi-aryl)P(*t*-

Table 2.3 Phosphine ligand optimization

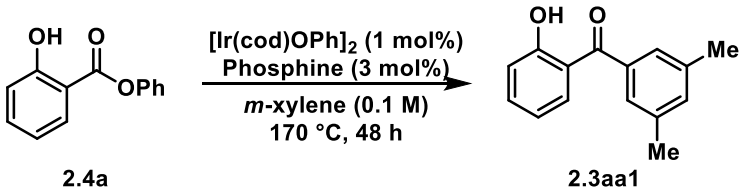

2.4a 2.3aa1

Entry	**Phosphine**	**Yield 2.3aa1 (%)[a]**
1	*t*-Bu XPhos	44
2	XPhos	6
3	*t*-Bu BrettPhos	58
4	BrettPhos	4
5	Cy-JohnPhos	8
6	JohnPhos	61
7	*t*-Bu MePhos	55
8	MePhos	7
9	*t*-Bu DavePhos	47
10	DavePhos	6
11	RuPhos	11
12	S-Phos	10
13	TrixiePhos	60
14	P(*o*-tol)$_3$	2

a) Determined by qNMR

Bu)$_2$ structure were found to give the best yields (Table 2.3 entries 1, 3, 6, 7, 9, and 13). Of these, JohnPhos and TrixiePhos were the best (Table 2.3 entries 6 and 13). JohnPhos gave a 1% higher yield, but as the reactions were run on a 0.1 mmol scale, this difference was deemed negligible. The higher molecular weight of TrixiePhos made quantitative measurement of the ligand more feasible on a small scale so this was used for further reaction optimization.

Next, the effect of TrixiePhos loading was determined (Table 2.4). Graphing yield versus phosphine loading showed a steep increase in yield up to 2 mol% phosphine, and a

Table 2.4 Phosphine loading optimization

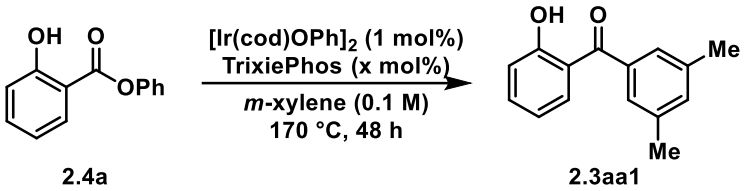

2.4a 2.3aa1

Entry	**TrixiePhos (mol%)**	**Yield 2.3aa1 (%)[a]**
1	0.5	29
2	1	50
3	2	75
4	4	78
5	8	53
6	16	23
7	32	15

a) Determined by qNMR

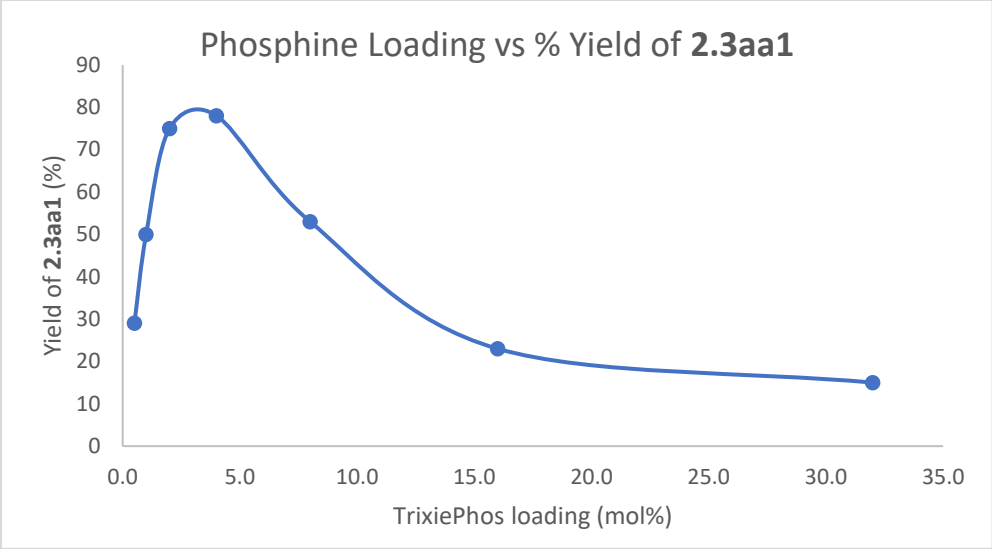

Figure 2.2 Dependence of yield on phosphine loading

sharp decline after 4 mol% (Figure 2.1), indicating that phosphine is needed to promote the reaction, but excess phosphine inhibits product formation. Through extrapolation of this plot, 3 mol% TrixiePhos, or a 2:3 ratio of [Ir]:phosphine, was deemed optimal to maximize yield and limit catalyst decomposition.

Initial reaction optimization was done with solvent quantities of the arene coupling partner *m*-xylene. The effect of arene concentration on product yield was examined using mixtures of *m*-xylene with decalin or mesitylene as a co-solvent, maintaining an overall concentration of 0.1 M **2.4a**. The concentration of the arene coupling partner *m*-xylene had a significant effect on the yield of **2.3aa1** (Table 2.5). Yield of **2.3aa1** dropped significantly with decreasing equivalents of *m*-xylene, decreasing roughly 20% when the amount of *m*-xylene was halved (Table 2.5 entries 1 vs. 2 and 6 vs. 7). Although kinetic studies were not performed at this time, these results indicate that the reaction rate is dependent on the

concentration of arene and conversion to **2.3aa1** decreased while the reaction time remained constant.

Table 2.5 Effect of arene dilution on yield

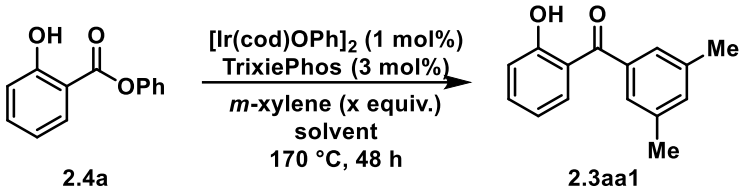

2.4a 2.3aa1

Entry	*m*-xylene (equiv)	Additional Solvent	Yield 2.3aa1 (%)[a]
1	40.5	Decalin	51
2	20.3	Decalin	33
3	8.1	Decalin	13
4	4.0	Decalin	6
5	2.0	Decalin	3
6	40.5	Mesitylene	59
7	20.3	Mesitylene	39
8	8.1	Mesitylene	18
9	4.0	Mesitylene	9
10	2.0	Mesitylene	5

a) Determined by qNMR

Next, we examined effect of salicylate concentration on product yield (Table 2.6). Yield of **2.3aa1** was found to increase slightly with increasing concentration up to 0.14 M **2.4a** in *m*-xylene (Table 2.6 entries 1–4). Above 0.14 M, yield significantly decreases with

increasing concentration, dropping to 51% at 0.40 M (Table 2.6 entries 5–7). This decrease in yield could be due to the decrease in effective concentration of *m*-xylene as the concentration of salicylate **2.4a** increases.

Table 2.6 Optimization of salicylate **2.4a** concentration

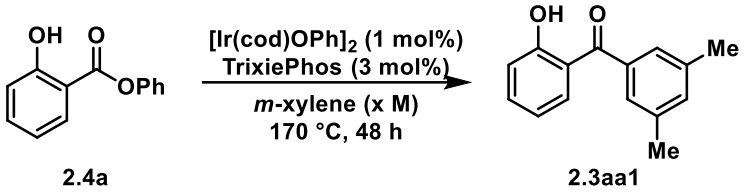

2.4a **2.3aa1**

Entry	**2.4a (mmol)**	**2.4a (M)**	**Yield 2.3aa1 (%)[a]**
1	0.05	0.05	76
2	0.05	0.07	77
3	0.1	0.10	80
4	0.1	0.14	80
5	0.2	0.20	69
6	0.2	0.29	61
7	0.2	0.40	51

a) Determined by qNMR

Monitoring the rate of formation of ketone **2.3ag** by acylation of 1,2-dimethoxybenzene (1,2-DMB) in the presence of either COD or COE showed that COD is a better ancillary ligand for arene acylation, resulting in a greater rate increase than COE (Figure 2.3). Norbornene was also examined as a potential alkene ligand, but no conversion of **2.4a** to **2.3ag** was observed after 45 minutes.

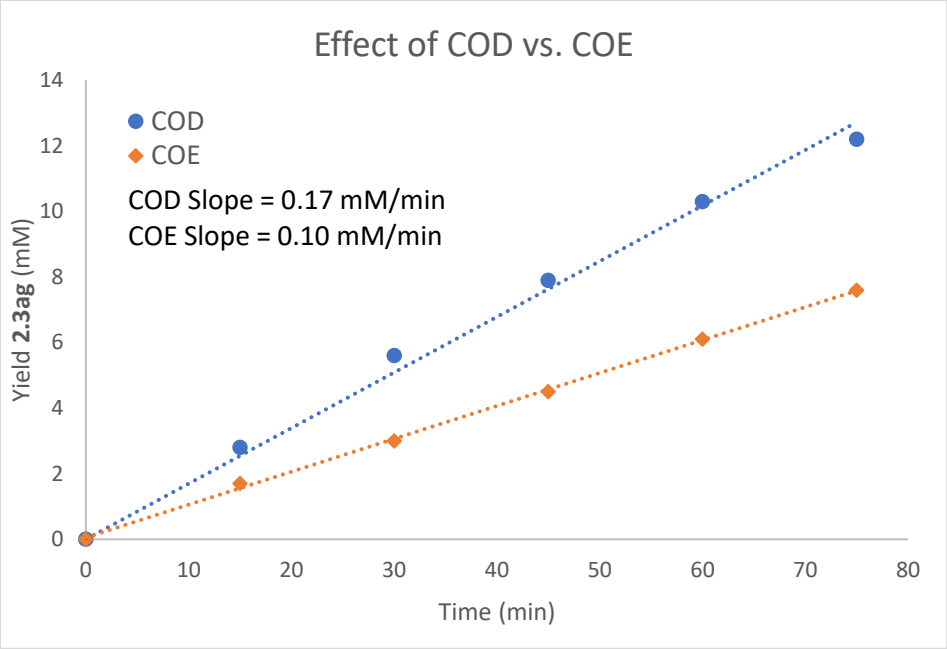

Figure 2.3 Effect of alkene additive on reaction rate

We next examined the effect of the concentration of COD on the reaction. Addition of COD increased conversion to **2.3ag**, resulting in increased yields after 4 hours (Table 2.7). No inhibitory effect was observed up to 5 equivalents of COD. Addition of COD also appeared to stabilize the catalyst, preventing the formation of iridium mirror on the reaction vials, keeping the catalyst in solution.

Although optimization experiments were done with $[Ir(cod)OPh]_2$, $[Ir(cod)OMe]_2$ was selected as the optimum precatalyst as it is commercially available, has better solubility in a variety of arene solvents, and gave comparable results to the phenoxide-substituted precatalyst. The enhanced solubility of the methoxide dimer in aromatic solvents allows us to use premade stock solutions in kinetic experiments, reducing the error in catalyst loadings and ensuring consistency across reactions. Notably, the alkoxide

Table 2.7 Effect of COD additive on the yield of **2.3ag**

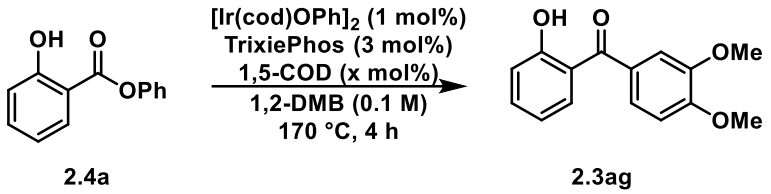

2.4a 2.3ag

Entry	1,5-COD (mol%)	Yield 2.3ag (%)[a]
1	0	39
2	2	47
3	4	50
4	6	53
5	8	49
6	12	53
7	16	59
8	20	59
9[b]	20	20
10[b]	100	27
11[b]	500	52

a) Determined by qNMR; b) Reactions run for 2 hours

released from the precatalyst (phenoxide or methoxide) does undergo transesterification with phenyl salicylate in the reaction conditions. With phenoxide, this transesterification regenerates phenyl salicylate but with methoxide, 2 mol% methyl salicylate is generated. Methyl salicylate was observed by NMR in the resulting reaction mixtures. Methyl

salicylate is unreactive in our reaction conditions, lowering the maximum possible yield of arene acylation by 2%.

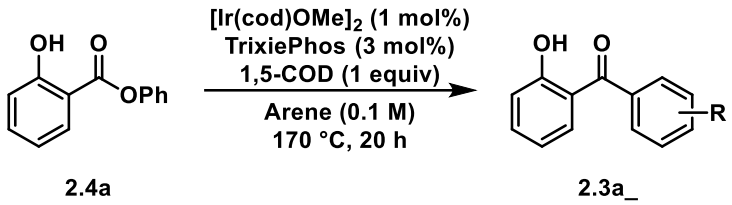

Scheme 2.10 Optimized reaction conditions for hydroxyl-directed arene acylation

Based on the results presented above, we chose the conditions illustrated in Scheme 2.10 as the optimum conditions. Control experiments without the iridium catalyst, without phosphine, and without both iridium and phosphine were done to confirm that the transformation was iridium catalyzed (Table 2.8). When iridium was eliminated from the reaction mixture, there was no conversion to ketone **2.3ag** (Table 2.8 entries 1 and 3). Interestingly, when TrixiePhos was eliminated from the reaction mixture, the reaction still

Table 2.8 Arene acylation control experiments

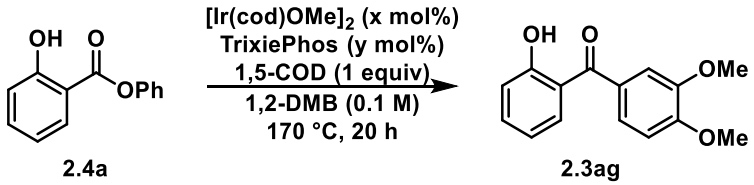

Entry	[Ir(cod)OMe]$_2$ (mol%)	TrixiePhos (mol%)	Yield 2.3ag (%)[a]
1	0	3	0
2	1	0	24
3	0	0	0

a) Determined by qNMR

proceeded, forming **2.3ag** in 24% yield. This result indicates that while iridium is required for the reaction, phosphine is not, but phosphine is required to achieve high catalyst turnover.

2.4 Mechanistic Studies

2.4.1 Mechanistic Questions

Next, we began to investigate the reaction mechanism. We sought to elucidate the pathways of catalyst decomposition, the role of phosphine, and the rate limiting step of the reaction. Mechanistic studies of C–C bond activation processes often found C–C bond activation to be the rate limiting step[78,79] (Section 1.3.2 so we initially thought that C–O bond activation may be rate limiting. As *o*-hydroxyl groups have been known to direct bond activation and prevent decarbonylation, we proposed that the reaction is proceeding through chelated intermediates with the hydroxyl group bound to iridium (Scheme 2.11). Optimization reactions where COD was found to influence the rate of the reaction suggest that COD remains coordinated to iridium as an ancillary ligand throughout the catalytic cycle. To determine the reaction mechanism, we analyzed reaction mixtures with ^{31}P NMR and IR spectroscopy, performed kinetic isotope effect (KIE) experiments, determined the effect of reactant concentration and electronic changes to phenolic leaving groups on reaction rate, and studied reaction reversibility.

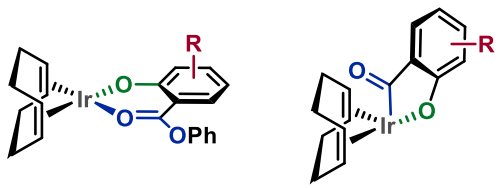

Scheme 2.11 General structure of proposed catalytic intermediates

2.4.2 Role of Phosphine and Iridium Decomposition Pathway

Heating $[Ir(cod)OMe]_2$ with 2 equivalents of TrixiePhos in 1,2- DMB to 170 °C for 1 hour did not result in a change in the ^{31}P NMR spectrum of the reaction mixture. When this same experiment was performed on a reaction mixture containing salicylate **2.4a**, the phosphine signal decreased in intensity over 20 hours. This suggests that phosphine does not bind to the iridium precatalyst. Instead, phosphine may be in a dynamic equilibrium between catalytic intermediates **I** and **II**, potentially slowing the decomposition of the catalyst. Phosphine loading studies during reaction optimization showed that initial addition of phosphine enhances the reaction but excess phosphine acts as an inhibitor (Table 2.4), this is consistent with the proposed role of phosphine shown in Scheme 2.12.

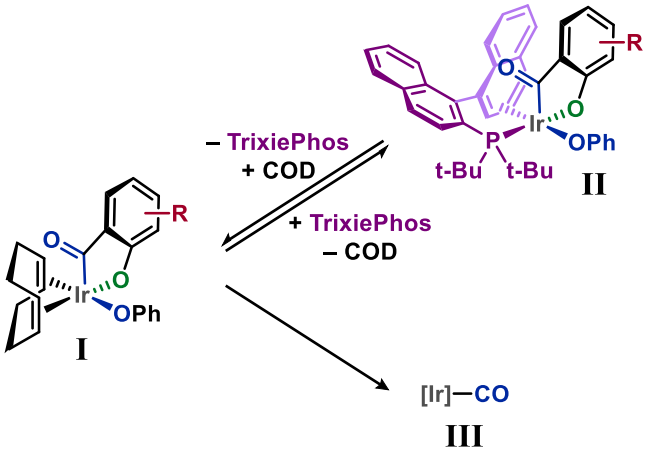

Scheme 2.12 Proposed catalyst decomposition pathway and role of phosphine

As metal-acyl species are known to α-eliminate CO,[87,98–101] we hypothesize that decarbonylation is the main catalyst decomposition pathway. The infrared spectrum of a crude reaction mixture after 20 hours was taken and showed peaks at 1981 and 2027 cm^{-1}, consistent with a catalytically inactive iridium carbonyl complex **III**.[146] If decarbonylation

to form **III** proceeds via a bimetallic mechanism, we expect that lower concentrations of **I**, induced by phosphine, would decrease the rate of decarbonylation relative to the rate of acylation. A bimetallic catalyst decomposition pathway is also consistent with the observation of higher catalyst loadings resulting in lowered yields. Our data are consistent with this hypothesis, suggesting that iridium sequestration by phosphine leads to higher turnover numbers under the optimized conditions. In addition, catalyst poisoning under a CO atmosphere inhibits the reaction. An attempted acylation of 1,2-DMB with phenyl salicylate under 1 atm CO resulted in <10% conversion after 20 hours. We attempted to increase the lifetime of our catalyst by acylating 1,2,3-trimethoxybenzene with phenyl salicylate using a reflux apparatus under a flow of N_2, hoping to sweep away CO formed via decarbonylation. We observed similar results with this setup as in a sealed vessel.

2.4.3 Kinetic Isotope Effects

We investigated the C–H bond activation step of the mechanism using H/D kinetic isotope effect (KIE) experiments[147] with *d*$_4$-1,2-dimethoxybenzene (DMB-D_4) and 4-*d*$_1$-1,2-dimethoxybenzene (DMB-D_1) (Scheme 2.13a). These experiments added insight into the details of arene coordination and C−H cleavage. For the simplification of discussion, our KIE data analysis is presented in the context of the phenoxide-assisted four-membered CMD transition state though our data are also consistent with a carboxylate-assisted six-membered CMD transition state.

The method of initial rates was used to determine independent rates for proteo-1,2-DMB and DMB-D_4, and the value $KIE_{\text{initial rates}} = 1.8 \pm 0.1$ was measured. Product ratios were used to determine the KIEs of intramolecular and intermolecular competition

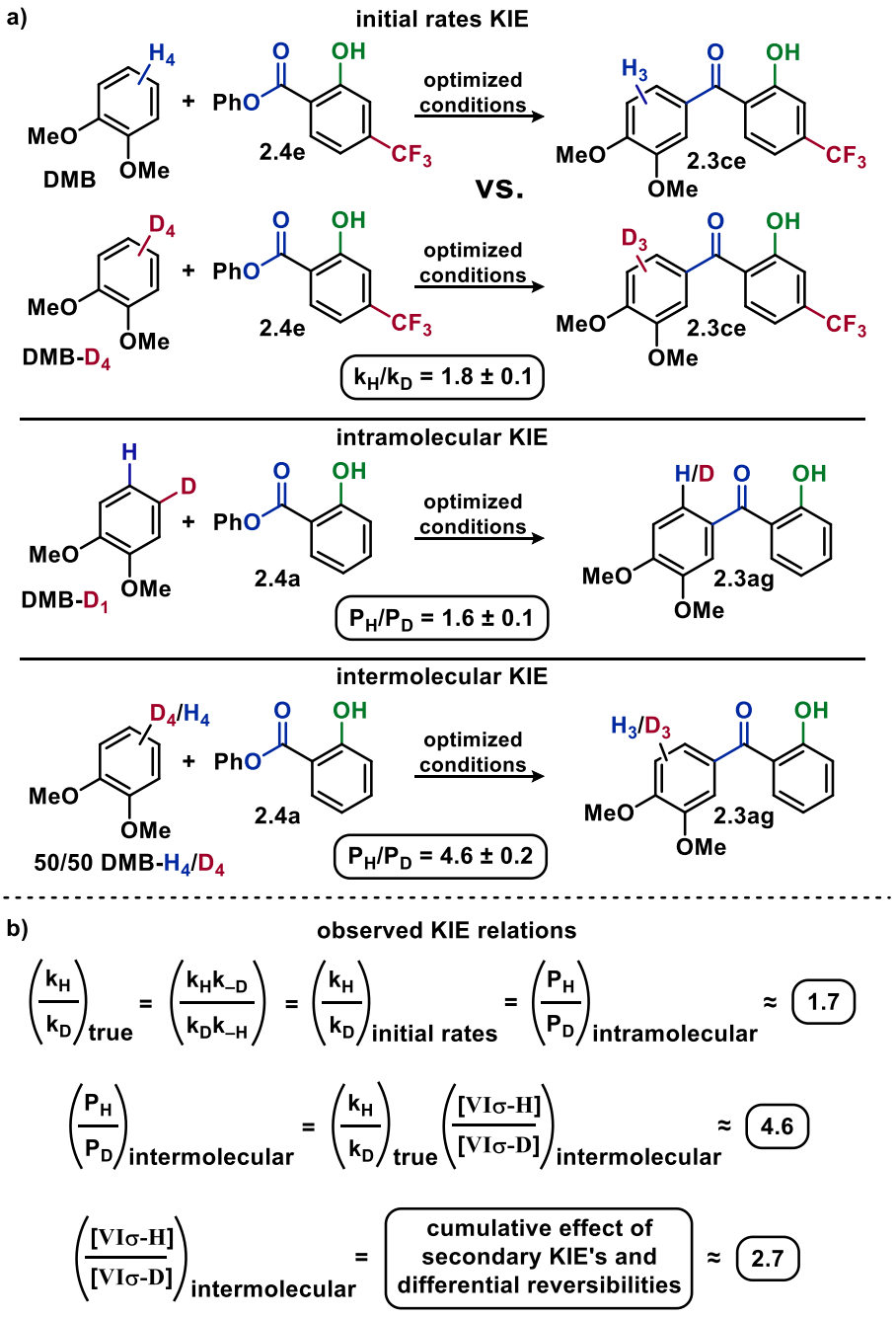

Scheme 2.13 a) KIE experiments; b) Observed KIE relationships and explanations

experiments. The intramolecular competition with DMB-D_1 gave a similar value, $KIE_{intramolecular}$ = 1.6 ± 0.1, but interestingly, the intermolecular competition with a 1:1

mixture of DMB-D_4 and proteo-1,2-DMB gave an amplified value, $KIE_{intermolecular} = 4.6 \pm 0.2$.

The observation of separate KIE values for the set of experiments suggests a multistep mechanism from arene coordination to C−H cleavage.[148,149] A primary $KIE_{initial\ rates}$ is evidence that C−H cleavage is the rate-limiting step of the mechanism and a measure of the true KIE of C−H/D cleavage ($(k_H/k_D)_{true}$) (Scheme 2.13b). Our analysis of the intra- and intermolecular KIEs was primarily influenced by the work of Song and Beak[150] and Adam et al.[151] In the case of the intramolecular KIE, we propose that the selectivity bias for H over D abstraction arises from equilibration of the general arene complex **VI** between σ-adducts (Scheme 2.14a). $\mathbf{VI_{\sigma\text{-}H}}$ and $\mathbf{VI_{\sigma\text{-}D}}$ may interconvert through $\mathbf{VI_{\pi}}$.[149,152] This is further evidenced by the fact that $KIE_{intermolecular} \neq KIE_{intramolecular}$, which implies that arene coordination is a separate step from the intramolecular selectivity-determining step. If **VI** fully equilibrates between σ-adducts and C−H/D cleavage is rate-limiting ($k_{\sigma H}$, $k_{-\sigma H}$, $k_{\sigma D}$, $k_{-\sigma D} \gg k_H$, k_D), then the observed $KIE_{intramolecular}$ should theoretically reflect $(k_H/k_D)_{true}$.[150] Our experimental KIE values, $KIE_{initial\ rates} = 1.8 \pm 0.1$ and $KIE_{intramolecular} = 1.6 \pm 0.1$, are the same within the experimental error and therefore in accordance with this analysis.

In the intermolecular competition reaction, the value $KIE_{intermolecular} = 4.6 \pm 0.2$ may arise from differential reversibility of arene coordination to **I** (Scheme 2.14b). This would result in an increased [$\mathbf{VI_{\pi\text{-}H}}$] relative to [$\mathbf{VI_{\pi\text{-}D}}$], which in turn would lead to an increased [$\mathbf{VI_{\sigma\text{-}H}}$] relative to [$\mathbf{VI_{\sigma\text{-}D}}$]. The relationship of [$\mathbf{VI_{\sigma\text{-}H}}$]/[$\mathbf{VI_{\sigma\text{-}D}}$] can be expressed in terms of forward and reverse rate constants by a derivation using multiple steady-state approximations (see Section 2.4.3).

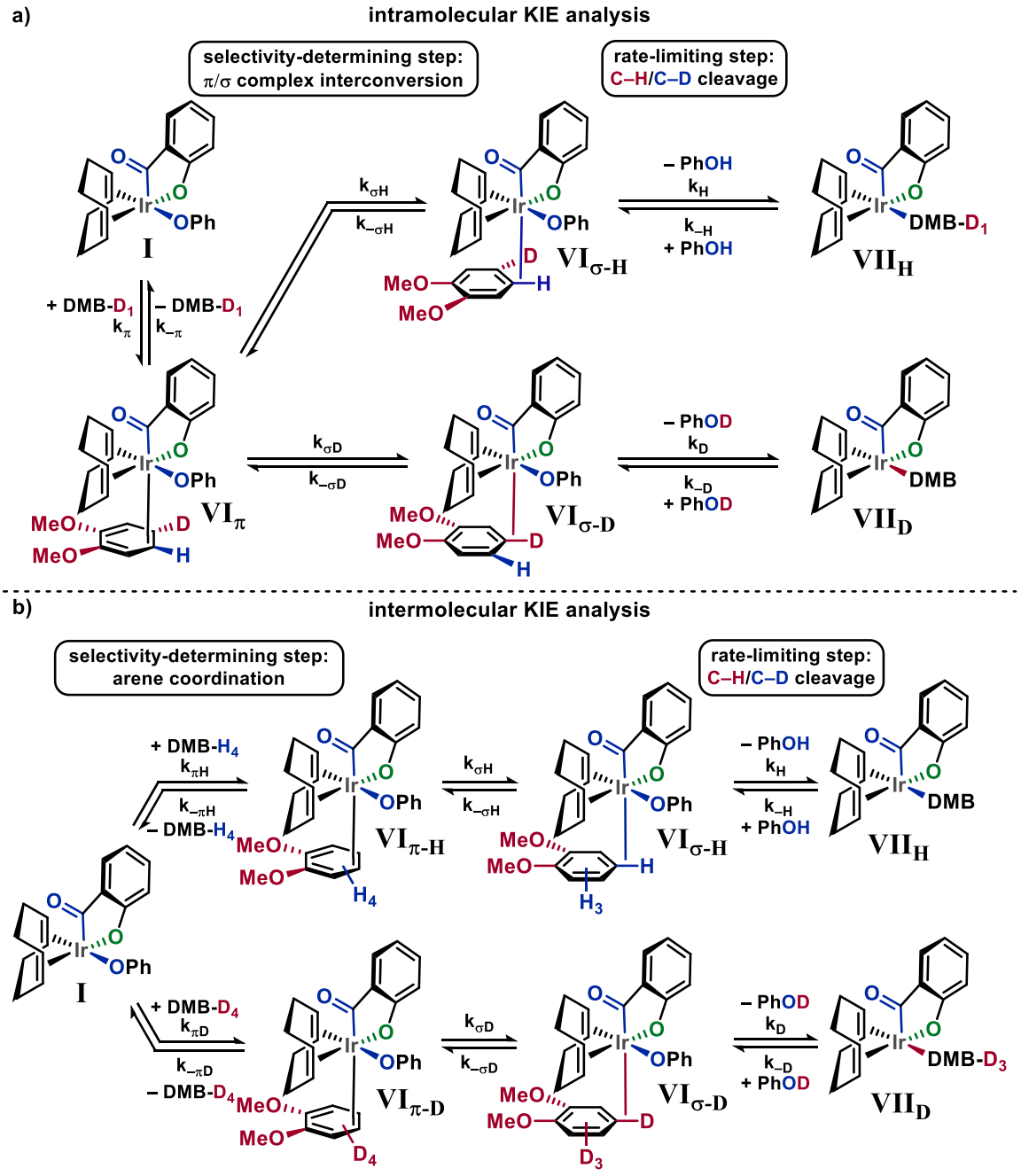

Scheme 2.14 Mechanistic analysis of observed KIEs a) Intramolecular KIEs; b) intermolecular KIEs

The differential reversibility may be explained by secondary isotope effects and/or the preference for H abstraction over D abstraction leading to a higher rate of DMB-D_4

dissociation. This would channel more reacting arene through the proteo-1,2-DMB path.[151] The net effect is measured as an amplification of $(k_H/k_D)_{true}$ by a factor of 2.7. We also note that $KIE_{intermolecular} = 4.6 \pm 0.2$ is comparable to the intermolecular competition KIE found in arene borylation via iridium-catalyzed C−H functionalization (5.0 ± 0.4)[124] and contrasts with the analogous Friedel−Crafts KIE (1.010 ± 0.0007).[124]

2.4.4 Reaction Order Determination with Initial Rates Kinetics

To elucidate the kinetic orders of the components of the reaction, rate data were collected for the reaction of phenyl salicylate and 1,2-DMB using the method of initial rates. This data showed the reaction to be zeroth-order with respect to salicylate and COD. The reaction appeared to be greater than first-order in 1,2-DMB, although solvent polarity effects could have caused an accelerated reaction at relatively high concentrations of 1,2-

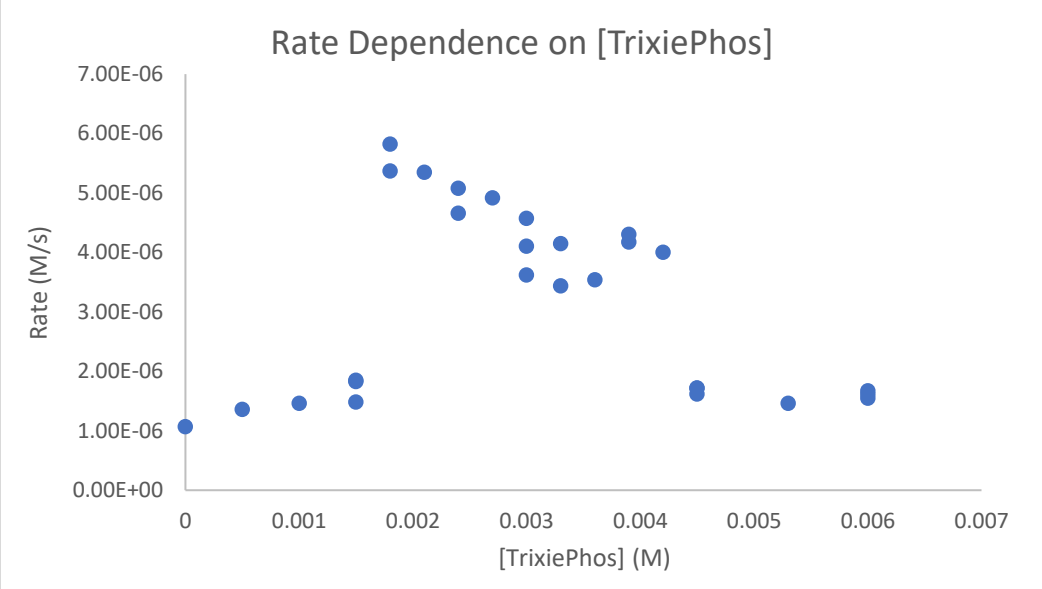

Figure 2.4 Initial rate dependence on TrixiePhos loading

DMB. When TrixiePhos was present at concentrations of ≥1.8 mM, the reaction was inverse order with respect to phosphine (Figure 2.4). Our optimized 3 mol% loading gives 3.0 mM TrixiePhos in solution. This observed region of inverse order is consistent with the proposed off-cycle role of phosphine (Scheme 2.12).

2.4.5 Effect of *p*-Substituted Phenolic Leaving Groups

We used salicylate esters with varied substituents to alter the electron density of the phenolic leaving groups. Initial studies using initial rates kinetics indicated that phenol leaving groups with strong electron withdrawing groups increased the rate of the reaction relative to unsubstituted phenyl salicylate (Figure 2.5). Attempts to perform multiple trials

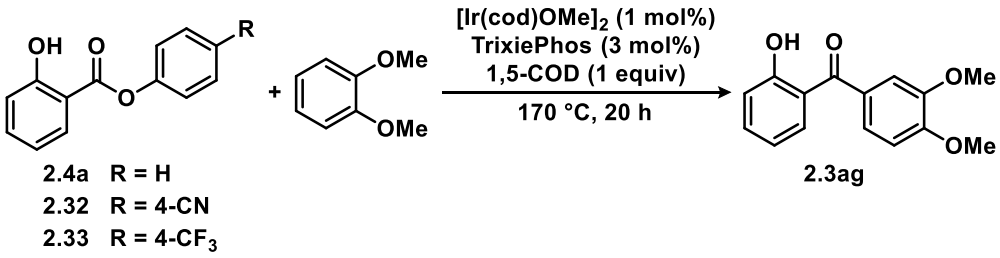

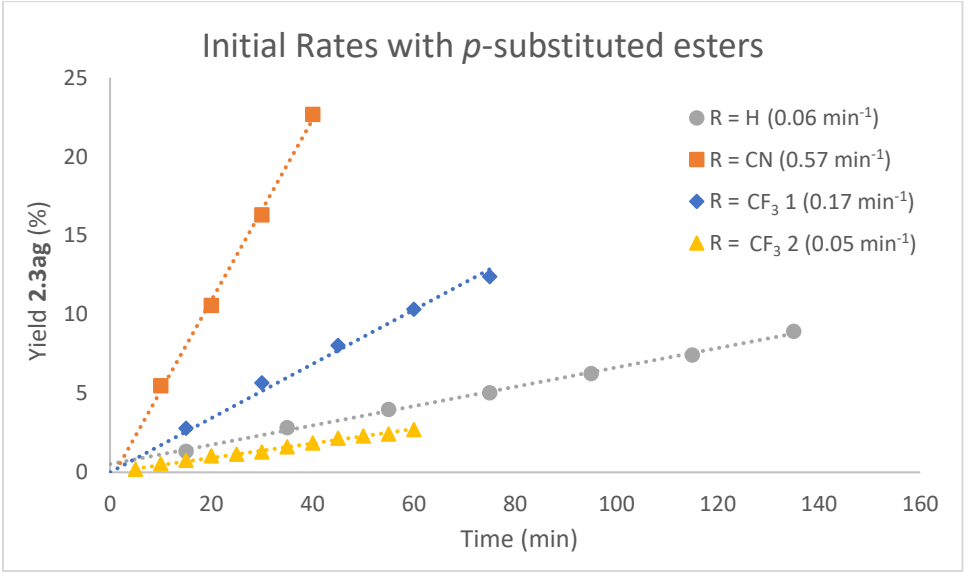

Figure 2.5 Initial rates kinetics with *p*-substituted salicylate esters

to obtain error bars for a Hammett analysis showed significant irreproducibility. This is demonstrated in the difference between the two trials using 4-CF_3 substituted phenyl salicylate **2.33** shown in Figure 2.5. Further attempts at obtaining kinetic data with substituted phenolic leaving groups confirmed that the data was erratic and not suitable for Hammett analysis.

2.4.6 Reversibility

A crucial control experiment to test the reversibility of the reaction was performed. The reaction of **2.3cd** with excess phenol in mesitylene resulted in the formation of salicylate **2.4d** in 24% yield (Scheme 2.15). This confirms that the mechanism of arene acylation is fully reversible and likely in equilibrium. Interestingly, phenyl salicylate **2.4a** was also observed in the reaction mixture suggesting that the C_{acyl}–C_{aryl} bond to the phenolic arene is also being activated in the reaction conditions.

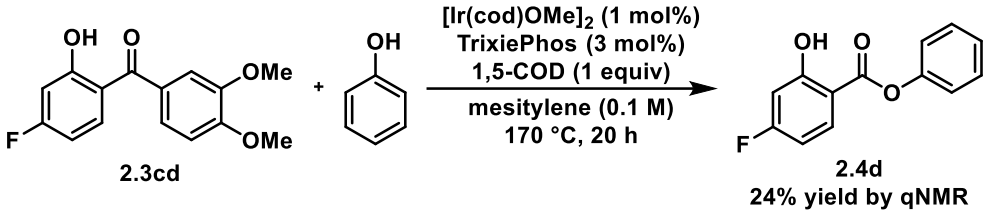

Scheme 2.15 Reversibility of the arene acylation reaction

2.4.7 Proposed Mechanism

Based on the results presented above, we find the two mechanistic paths for our acylation reaction shown in Scheme 2.16 to be most plausible. This proposed mechanism and the stereochemistry of intermediates shown is consistent with computational results.[153,154] Phenyl salicylate **2.4** coordinates to $[Ir(cod)OMe]_2$ (**A**), breaking the dimer,

liberating methanol, and forming square-planar intermediate **IV**, the proposed resting state of the catalyst. Relative to the catalyst loading, approximately 2 equivalents of methyl salicylate **V** are observed, suggesting sacrificial transesterification of **2.4** with methanol (**B**). Oxidative addition into the C_{acyl}–OPh bond of **IV** (**C**) forms square-pyramidal complex **I**. This step and all subsequent steps are proposed to be reversible. From **I**, multiple pathways are plausible. First, the limiting factor in the catalyst lifetime is proposed to be decarbonylation (**D**) to irreversibly form iridium carbonyl complex **III**. TrixiePhos is proposed to inhibit this decomposition by reversibly displacing COD (**E**), stabilizing the C_{acyl}–O oxidative addition intermediate off-cycle as **II**. Intermediate **I** may continue the productive path through coordination of the arene π-bond followed by σ-adduct formation (**F**) with the C_{aryl}–H bond, forming **VI**. This leads to the key steric-controlled C–H bond activation step, a 1,2-addition via concerted metalation–deprotonation (CMD) across the Ir–OPh bond (**G**). In this step, a lone pair on the phenoxide oxygen deprotonates the C_{aryl}–H bond through a four-membered transition state, forming phenol and the new Ir–C_{aryl} complex **VII**.[155] Reductive elimination (**H**) forms the new C_{acyl}–C_{aryl} bond, giving square-planar **VIII** with the new acylation product **2.3** bound to iridium. Finally, ligand exchange of **2.3** for **2.4** (**I**) regenerates intermediate **III**.

While our data are consistent with a 4-membered CMD transition state, they are also consistent with an alternative mechanism involving a more favorable carboxylate-assisted six-membered CMD transition state.[156] We envision that a formal hydrolysis of **2.4** or **V** (**J**) could form salicylic acid **IX** to serve as the carboxylate. Either the presence of

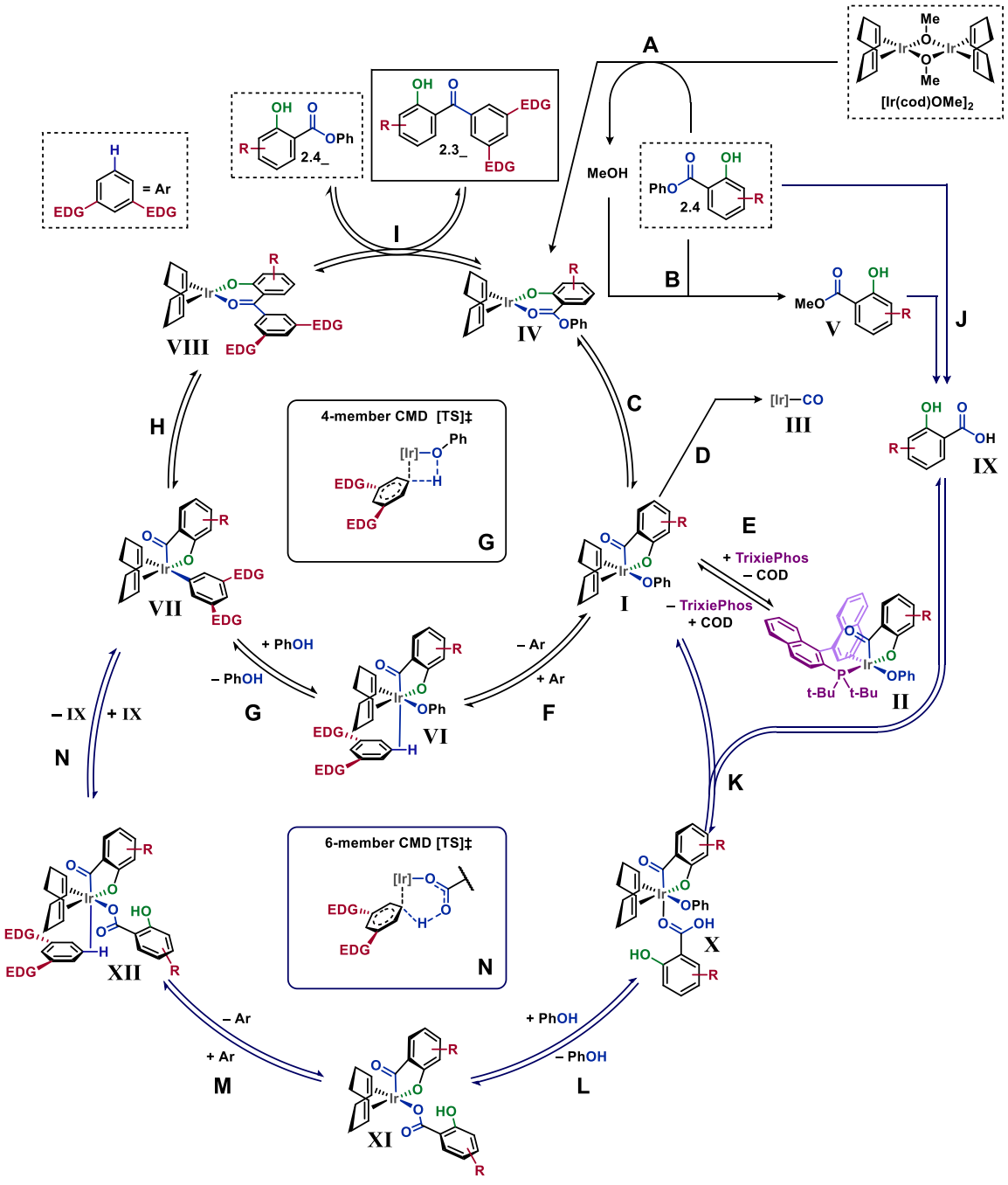

Scheme 2.16 Plausible mechanisms for steric-controlled arene acylation via a four-membered or six-membered CMD transition state

trace H_2O or possibly an alternative oxidative addition of iridium into the Ph–O or Me–O bond and subsequent protonation may account for the formation of **IX**. Intermediate **IX**

may then enter the catalytic cycle by binding to **I** (**K**) to form octahedral complex **X**. Elimination of phenol (**L**) would then form square-pyramidal **XI**. Arene coordination (**M**) would produce **XII**, which may proceed through a less strained six-membered CMD transition state to form **VII**. In either proposed mechanism, the base required to deprotonate the arene is endogenous to the system. In addition, no exogenous oxidant is required for catalyst turnover due to the net reduction of the ester to a ketone over the course of the reaction.

2.5 Substrate Scope

2.5.1 Arene component

With an understanding of the mechanism, we examined the scope of this reaction. The scope with respect to the arene was investigated with mono-, di-, and trisubstituted arenes (Scheme 2.17). Electron-rich arenes react well under these conditions (**2.3aa–ac**, **2.3af–ah**, **2.3an**, **2.3ao**), especially compared with electron-poor arenes (**2.3ad**, **2.3ae**, **2.3ai**, **2.3aj**). Acylation of strongly electron-poor arenes and some functionalized arenes was not observed. Substitution generally occurs preferentially at the most sterically accessible site. When multiple C−H bonds in similar steric environments are available, as in unsymmetrical 1,2-disubstituted arenes **2.3ah**−**aj**, acylation at the more electron-rich position is preferred. In the absence of strong electronic effects, mixtures favoring acylation at the more accessible sites result. For example, acylation of toluene (**2.3am**) provided a 17:17:1 mixture of regioisomers, favoring the *meta*- and *para*-isomers. As arenes with stronger electron donors undergo acylation, as in anisole (**2.3an**) and *N*,*N*-dimethylaniline (**2.3ao**), the *para*-isomer is favored and the *ortho*-isomer is not observed.

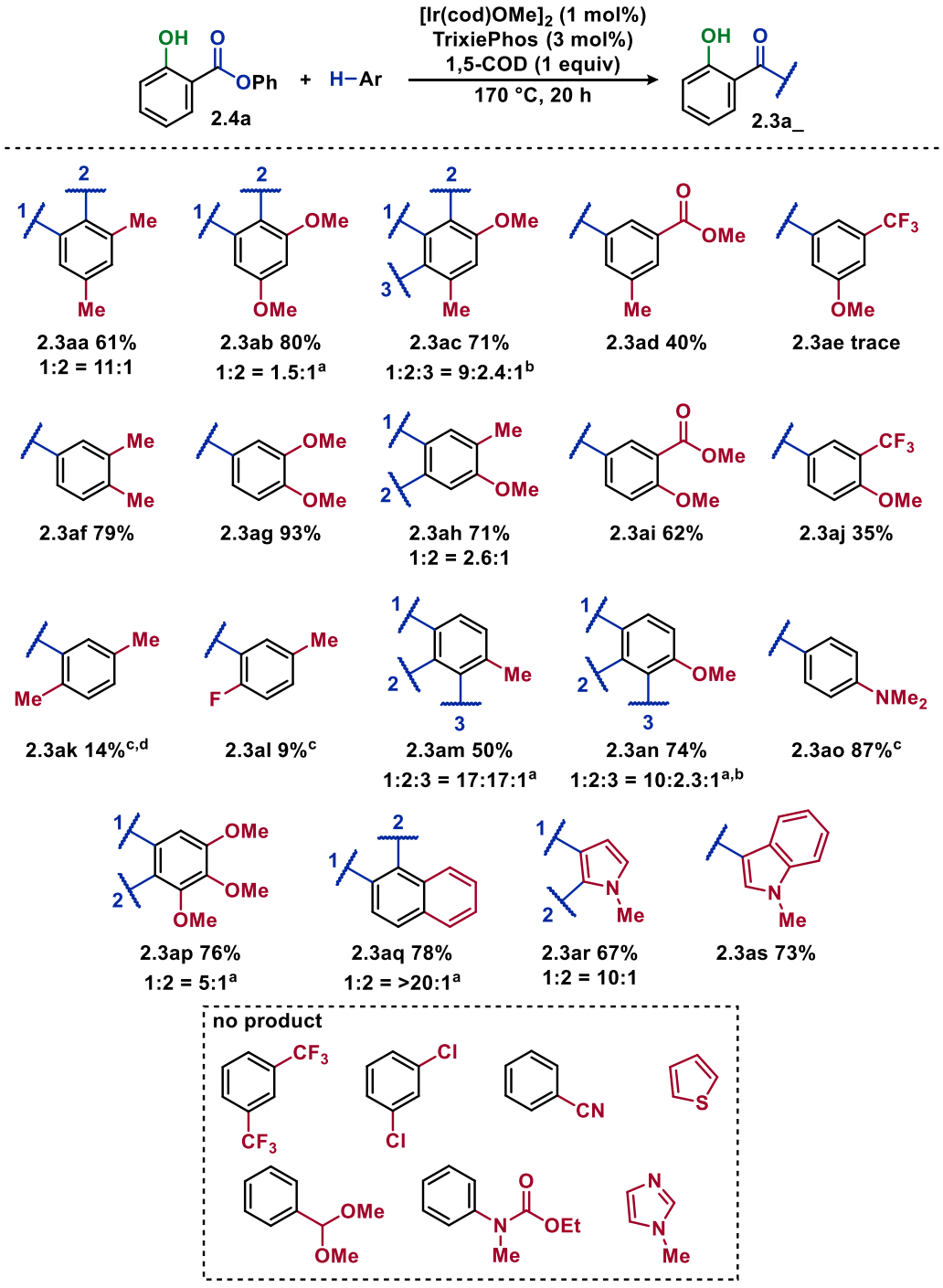

a) isolated as an inseparable mixture, ratio determined by ^{1}H NMR; b) Minor product 2.3a_1 was inseparable from 2.3a_3, ratio determined by ^{1}H NMR; c) After 20 h, a second charge of catalyst (1 mol% [Ir(cod)OMe]2 and 3 mol% TrixiePhos) was added and allowed to react at 170 °C for 20 h; d) Product could not be fully purified, yield given is an uppper bound

Scheme 2.17 Arene Substrate Scope

The acylation reaction tolerates simple arenes with fluoro, trifluoromethyl, methoxy, methyl, methyl ester, and dimethylamino functional groups. *N*-Methylated heteroarenes (**2.3ar**, **2.3as**) were tolerated, with acylation of *N*-methylpyrrole occurring mostly at the sterically favored 3-position (10:1 ratio of regioisomers), contrary to Friedel–Crafts acylation.[157] In the case of *N*-methylindole (**2.3as**), the 3-position relative to the nitrogen is favored both sterically and electronically, and thus, only one product was observed. Interestingly, naphthalene was acylated almost exclusively at the β-position, the opposite selectivity of Friedel–Crafts acylation.[158] The contrasting regioselectivity of this

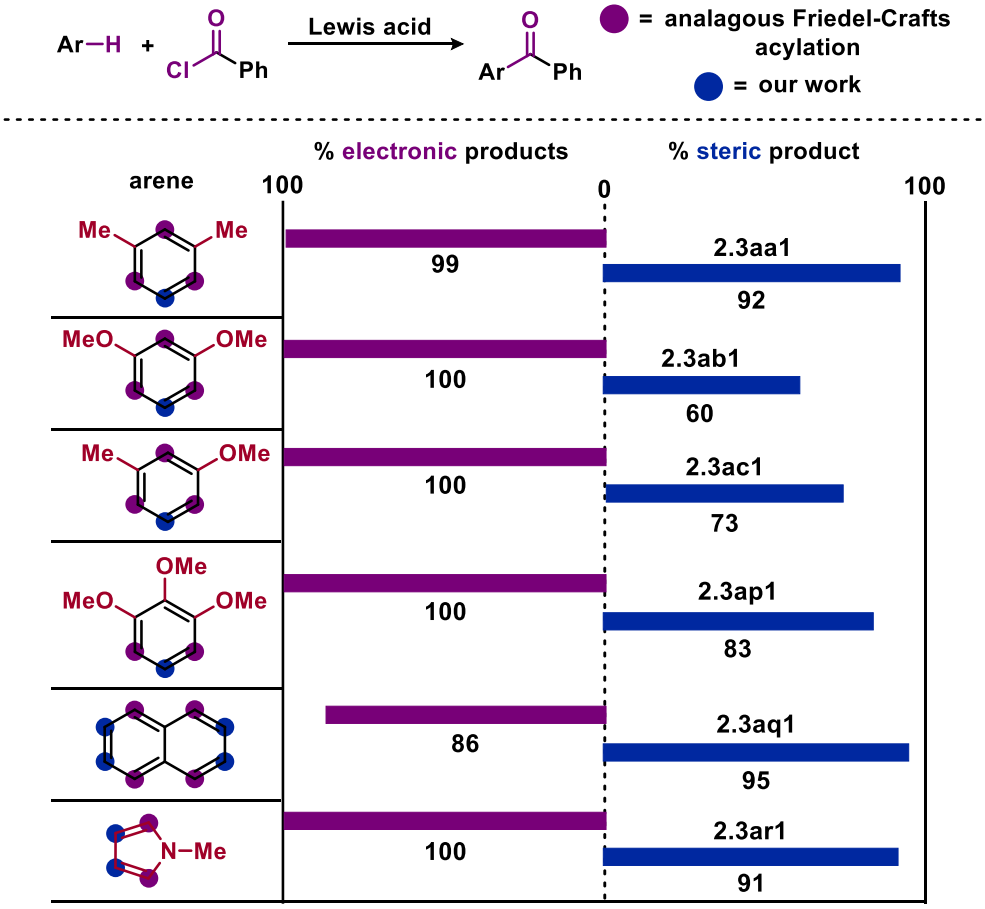

Figure 2.6 Comparison of regioselectivity of Friedel-Crafts acylation with electronic-control to our acylation method with steric-control

reaction is summarized in Figure 2.6. The substrates displayed have distinct electronic- and steric-favored sites. Electron-rich 1,3-disubstituted arenes show universal selectivity at the *ortho*- and *para*-positions with Friedel-Crafts acylation.[157–162] Statistically, the electronically preferred sites for acylation outnumber the sterically accessible sites for many of the arenes in Figure 2.6. Nevertheless, the sterically preferred sites are selectively acylated with our iridium catalyst. Our chemistry shows good selectivity for the steric-controlled product, although with a noticeable decrease in selectivity as the electron density of the ring increases. Very electron-poor arenes were not successful with this methodology. In addition, arenes with Lewis basic functional groups (e.g., nitrile, thiophene, carbamates, and acetals) were not successful.

2.5.2 Salicylate Substrate Scope

Next, the scope of arene acylation with respect to the salicylate ester was examined. We examined the scope of the acylation of *m*-xylene with substituted salicylate esters to determine the reaction efficiency and regioselectivity (Scheme 2.18). Acylation with two charges of iridium-catalyst gave the corresponding ketones **2.3b_** in moderate yields with good regioselectivity (>10:1) favoring the 1,3,5-substituted isomers. There was no clear trend in yield or regioselectivity due to electronic-effects from substitution at the 4-position (**2.3bb–bg**) or the 5-position (**2.3bh** and **bi**). Methyl-substitution at the 3-position was tested to determine if steric hinderance around the hydroxyl-directing group would have a negative effect but yield and regioselectivity were not substantially affected (**2.3bk** vs **2.3bb**). Additional hydroxyl-substituents on the salicylate esters had a negative effect on the reaction, resulting in very poor (**2.3bf**) or trace (**2.3bn**) yields. Amino, bromo, and nitro

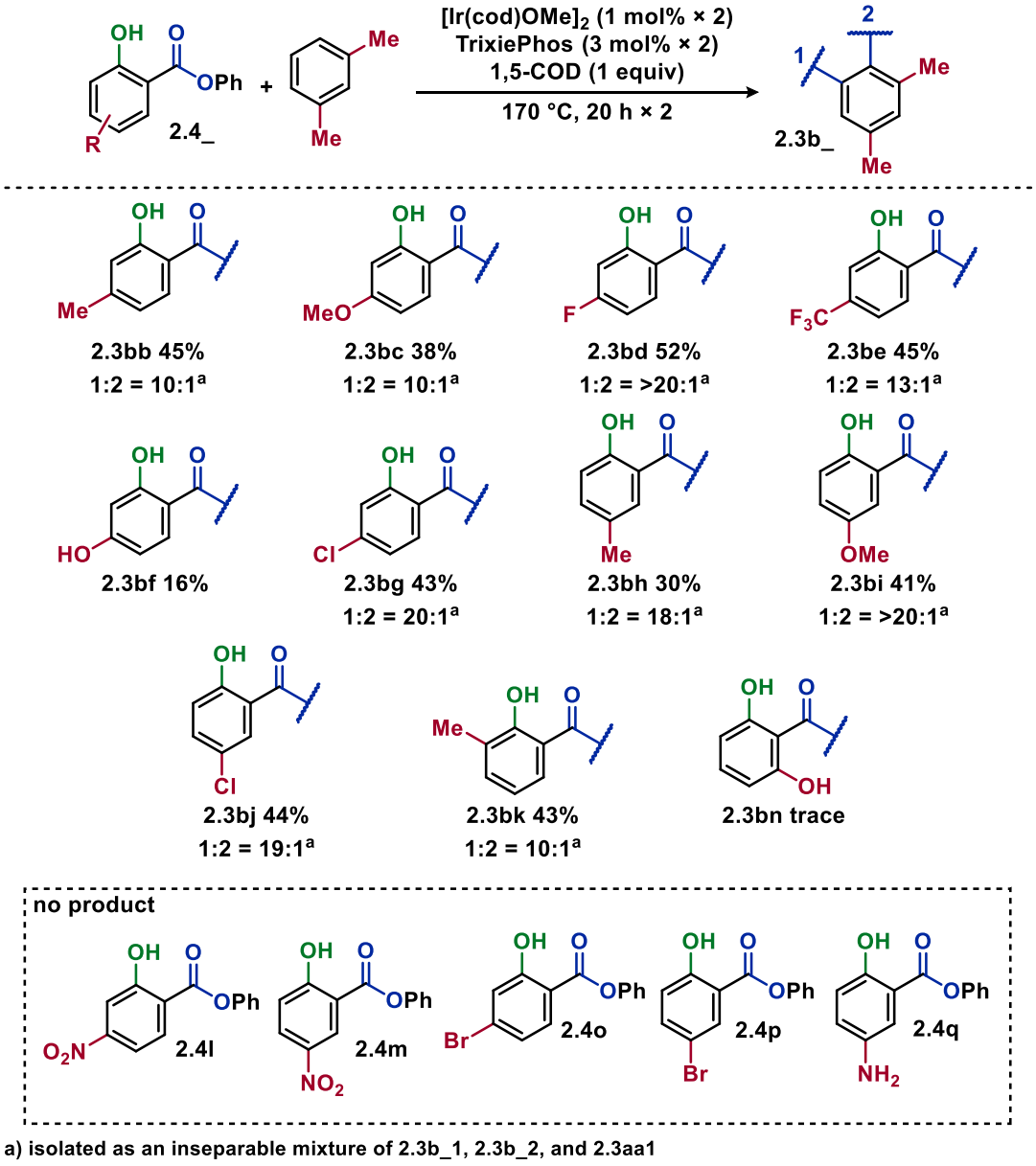

Scheme 2.18 Salicylate ester scope with *m*-xylene

groups (**2.4l, m, o**–**q**) were not tolerated in the reaction, resulting in no biaryl ketone formation. For amino-substituted salicylate ester **2.4q** this was likely due to insolubility in the reaction conditions. Interestingly, ketone **2.3aa1** was also observed as a minor product

in many of the reaction mixtures with apparent loss of the functional group R. This is presumed to be due to C–C bond activation of the biaryl ketone **2.3b_** and C–H bond activation of unsubstituted phenol generated as a byproduct of acylation (Scheme 2.19). This transformation will be studied further in Chapter 3.

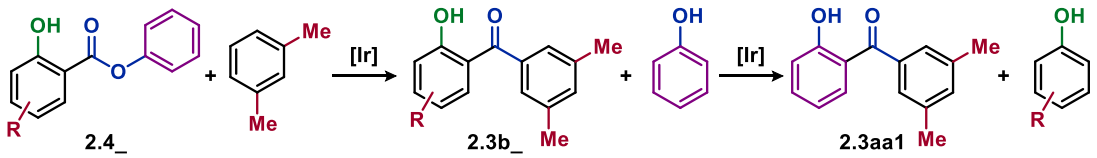

Scheme 2.19 Side products generated in the salicylate substrate scope with *m*-xylene

Each salicylate derivative was used in the acylation of more reactive arene 1,2-DMB to assess the reactivity of the salicylate (Scheme 2.20). Due to the higher reactivity of 1,2-DMB, only one charge of catalyst was required. The steric and electronic effects of the methoxy groups direct to the same site of acylation so only one regioisomer was formed in the reactions. Additionally, no functional group R loss was observed in these reactions. Salicylates with methyl (**2.4b**, **h**, **k**), methoxy (**2.4c**, **i**), fluoro (**2.4d**), and trifluoromethyl (**2.4e**) substitutents gave products in good yields (77–97%). Hydroxyl groups were well tolerated in the 4-position giving product **2.3cf** in good yield. Compound **2.3cf** was unstable to silica and could not be isolated so yield was determined by qNMR. Hydroxyl substitution in the 6-position (**n**) gave significantly lower yield (23%). Chloro-substitution in the 5-position (**j**) only resulted in a small reduction in yield relative to other salicylates with substitutions in the 5-position, giving product **2.3cj** in 80% yield. Chloro-substitution in the 4-position (**g**) and nitro-substitutions at the 4-position (**l**) or 5 position (**m**) gave significantly lower yields (46–49%).

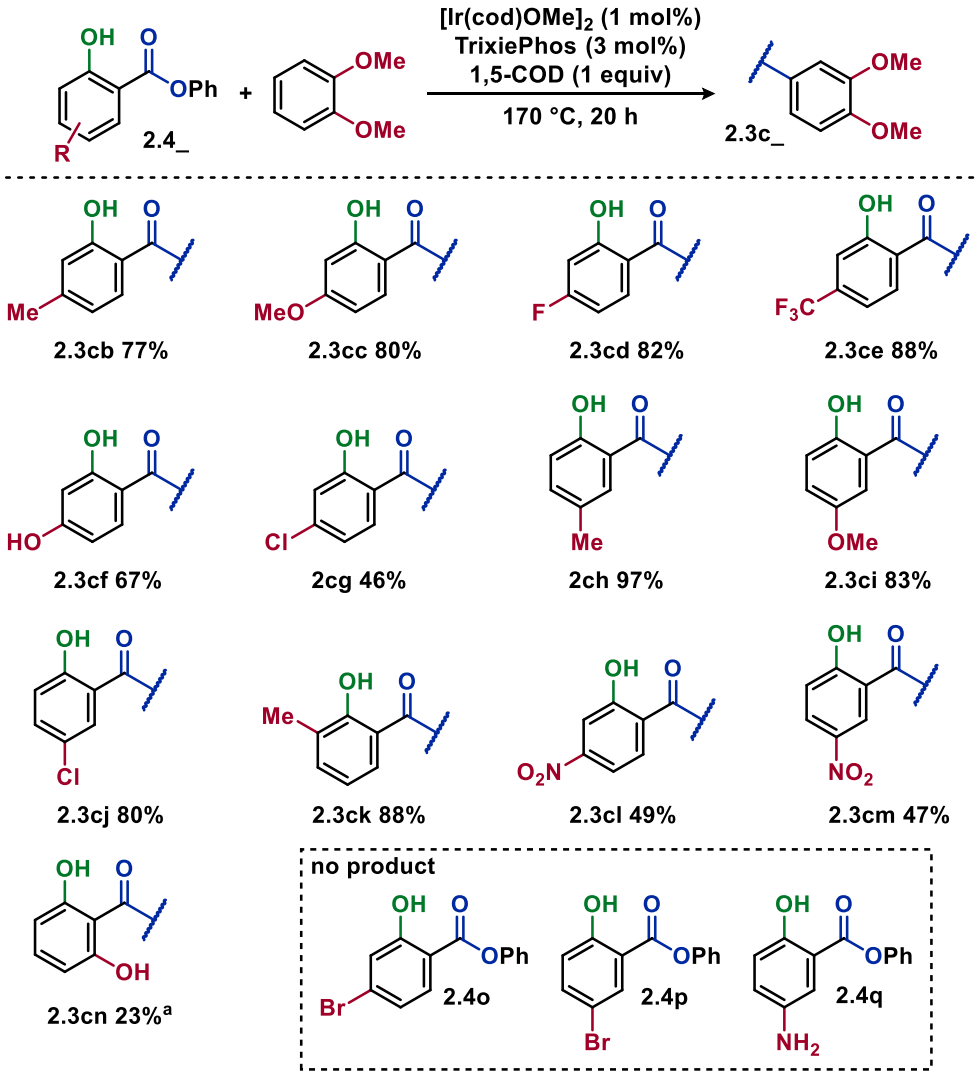

a) Yield was determined by ^{1}H NMR spectroscopy; the product decomposed during attempted purification on silica

Scheme 2.20 Salicylate ester scope with 1,2-dimethoxybenzene

We attempted to use quinoline groups to direct bond activation for arene acylation using 8-acylquinoline ester **2.34** (Scheme 2.21). Reactions were attempted using various rhodium and iridium precatalysts, the best results were obtained with $[Rh(cod)Cl]_2$. A wide variety of phosphines were tested along with reaction temperatures from 150–200 °C. All conditions examined yielded less than 13% of ketone **2.35**.

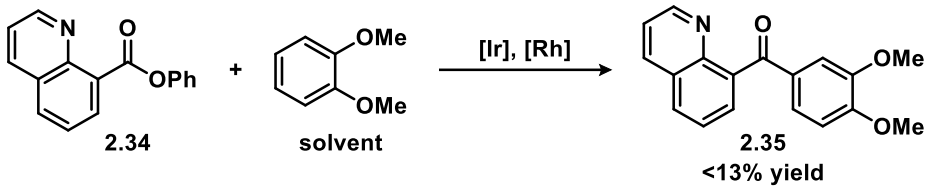

Scheme 2.21 Quinoline directed arene acylation

2.5.3 Dilution studies

A noted drawback of this and related C−H borylation/silylation reactions are that a large excess of arene is used, typically in solvent quantities. We sought to do additional experiments into the effect of lower quantities of arene (Table 2.9). 1,2-DMB was used for these studies as it is highly reactive under standard conditions yielding **2ag** in 93% yield (Table 2.9 entry 1). Dilution with mesitylene to 40 equivalents of 1,2-DMB still formed **2.3ag** in good yield (70%, Table 2.9 entry 2). Further dilution to 20 or 10 equivalents still resulted in fair yields (Table 2.9 entries 2 and 3). Dilution to 5 equivalents of 1,2-DMB resulted in a 30% isolated yield (Table 2.9 entry 5). This is notable as it is a 16-fold reduction in arene equivalency resulting in only a 3-fold reduction in yield. We attempted to improve these yields through modification of the reaction conditions. Additional COD resulted in slightly lowered yields with 40 equivalents of 1,2-DMB (Table 2.9 entries 6 and 7). Adding a second charge of catalyst and phosphine with 5 equivalents of COD also gave slightly lowered yield (Table 2.9 entry 8). Increasing the reaction temperature to 180 °C increased the yield to 37% but led to significant amounts of starting material decomposition (77% conversion) (Table 2.9 entry 9).

Table 2.9 Effect of arene dilution on the acylation of 1,2-DMB

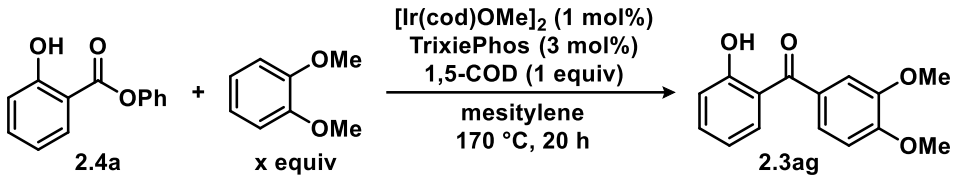

Entry	1,2-DMB (equiv)	Yield 2.3ag (%)[a]
1	78	93[b]
2	40	70
3	20	63
4	10	52
5	5	30[b]
6[c]	40	62
7[d]	40	56
8[e]	5	26
9[f]	5	37

a) Determined by qNMR; b) isolated yield; c) 5 equivalents of COD added; d) 10 equivalents of COD added; e) additional 1 mol% [Ir(cod)OMe]$_2$ and 3 mol% TrixiePhos added after 20 h, 40 h total reaction time; f) 180 °C reaction temperature

2.5.4 Effect of substituted phenolic leaving groups

As discussed in Section 2.4.5 *p*-substituted esters appeared to result in faster reaction rates. We wanted to determine if yield was affected by substituents on the phenolic leaving group. We tested this in the acylation of *o*-xylene and 1,2-DMB (Table 2.10). Acylation of *o*-xylene with salicylates with perfluoro (**2.36**), 3,5-CF_3 (**2.37**), and 4-CN (**2.32**) substituents on the phenolic leaving group did not significantly affect the formation

of **2.3af** (Table 2.10 entries 2–4). Unexpectedly, acylation with 4-CF_3 substituted ester **2.33** decreased the yield of **2.3af** to 69% (Table 2.10 entry 5). Substitution with an electron-rich methoxy group had a similar effect, reducing the yield of **2.3af** to 64% after 20 hours (Table 2.10 entry 6). Substitution with all electron-withdrawing groups resulted in moderately lowered yield (75–76% yield) in the acylation of 1,2-DMB (Table 2.10 entries 2–5). Ester

Table 2.10 Effect of substituted phenolic leaving groups on yield

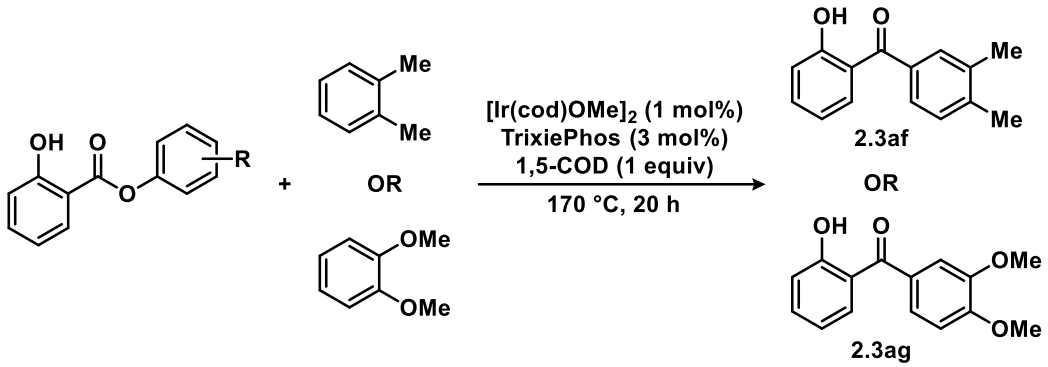

Entry	Ester	R	Yield of 2.3af (%)[a]	Yield of 2.3ag (%)[a]
1[b]	**2.4a**	H	79	93
2	**2.36**	Perfluoro	80	76
3	**2.37**	3,5-CF_3	79	75
4	**2.32**	4-CN	77	76
5	**2.33**	4-CF_3	69	76
6	**2.38**	4-OMe	64	—
7	**2.39**	2,6-Me	—	27

a) Determined by qNMR; b) isolated yields

2.39 with a 2,6-dimethyl substituted phenolic leaving group was tested to determine if additional steric strain around the leaving group oxygen would have any effect on yield. Acylation of 1,2-DMB with **2.39** gave a significantly lower yield (Table 2.10 entry 7).

2.5.5 Hydroxyphenstatin synthesis

With an understanding of the scope of this reaction, we undertook a synthesis of hydroxyphenstatin (**2.40**), a potent anticancer and antimitotic target (Scheme 2.22).[163] The shortest previous route to synthesize **2.40** employs a low-yielding, *ortho*-selective Friedel-Crafts acylation of 1,2,3-trihydroxybenzene (25% yield).[164] Our new acylation reaction opens a new disconnection of this target molecule. Dihydroxycarboxylic acid **2.41** can be synthesized in one step using a literature procedure.[165] Salicylate ester **2.42** was synthesized from **2.41** using phenol and phosphorus oxychloride in 75% yield. Acylation

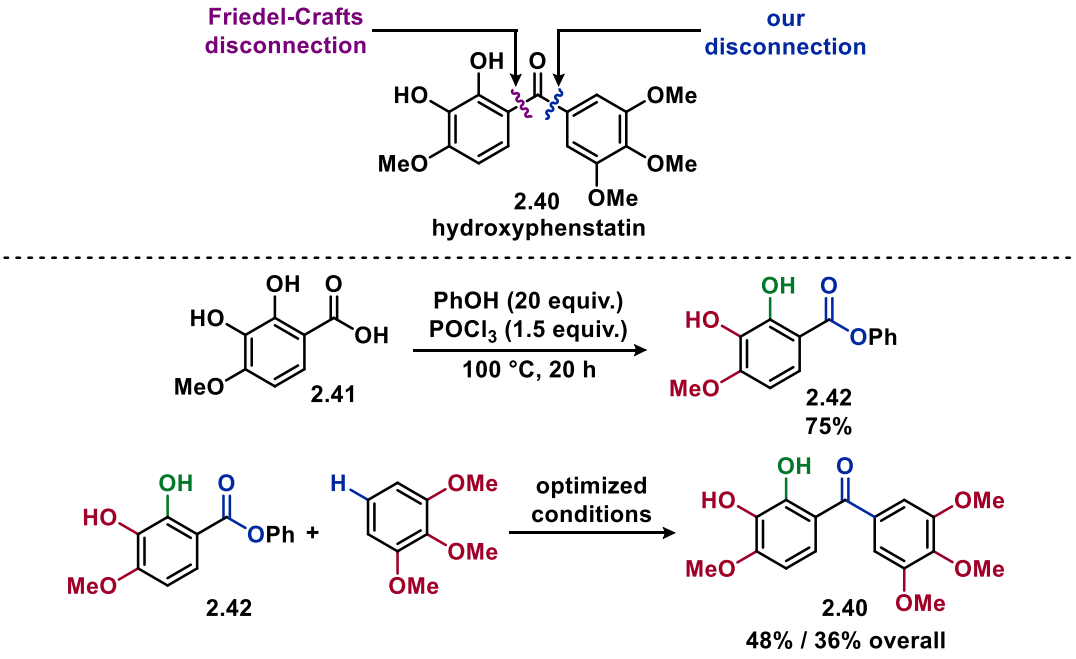

Scheme 2.22 Synthesis of hydroxyphenstatin **2.40**

of 1,2,3-trimethoxybenzene using **2.42** gave **2.40** in 48% yield (36% yield from **2.41**). This synthesis demonstrates a new disconnection available for the synthesis of biologically relevant molecules.

2.6 Conclusion

We have demonstrated the unique mechanistic and synthetic aspects of arene acylation via sequential C−O/C−H activation. The observed KIEs and regioselectivity support that this mechanism is distinct from Friedel−Crafts acylation and offers a pathway to substitution patterns previously inaccessible in a single synthetic step. Steric-controlled acylation is achieved via a proposed concerted metalation-deprotonation C−H activation, as supported by experimental and computational evidence. Simple electron-rich arenes are the most successful, and a broad range of functional groups are tolerated on the salicylate ester. Steric-controlled acylation was utilized to concisely synthesize the anticancer target molecule hydroxyphenstatin. The reaction is a first breakthrough toward forming new C_{acyl}−C_{aryl} bonds under steric control in a single synthetic step using an iridium catalyst.

2.7 Experimental Details

2.7.1 General Information

General Experimental Procedures: All acylation reactions were prepared under inert atmosphere in an oxygen-regulated glovebox. Reaction progress was monitored using thin-layer chromatography (TLC) on 0.25 mm silica plates from SiliCycle. Eluted plates were visualized with UV light. Silica Gel Flash Column Chromatography was performed on 230–400 mesh (particle size 0.04–0.063 mm) silica gel purchased from SiliCycle.

Materials: Unless otherwise indicated, chemicals were obtained from commercial sources and used without further purification. All arenes were degassed by bubbling a stream of argon through the liquid in a Schlenk flask and stored over 3 Å molecular sieves in a nitrogen-filled glovebox.

Instrumentation: NMR characterization data were collected at 300 K on Bruker FT NMR instruments. ^{1}H NMR spectra were internally referenced to TMS (δ = 0 ppm). ^{13}C NMR spectra were internally referenced to the residual solvent signal (δ = 77.2 ppm). Data from ^{1}H NMR are reported as follows: chemical shift (δ ppm), multiplicity (s = singlet, d = doublet, t = triplet, q = quartet, m = multiplet, br = broad), coupling constant (Hz), integration. Quantitative NMR data was collected with an acquisition time of 5 seconds and a d1 relaxation delay of 10 seconds.

Melting point ranges for solid products were determined on a MEL-TEMP instrument and are reported uncorrected.

IR Spectra were obtained as films either neat or from CH_2Cl_2 on sodium chloride plates on a Thermo Scientific FT-IR or with an ATR source using a Nicolet iS5 FT-IR spectrometer. Data are presented as absorption frequency (cm^{-1}).

High-resolution mass spectrometry (HRMS) using GC-MS was performed on an Agilent 7200-QTOF GC-MS, GC column RTX-5MS 30 m length, 0.255 mm ID, 0.25 µm df. Method: inlet temperature 250 °C, source temperature 280 °C. The initial column temperature of 120 ˚C was held for 4 minutes after injection. Column temperature was ramped to 325 °C over 10 minutes and then held for 31 minutes. High-resolution mass spectrometry (HRMS) using ESI experiments were performed on a Bruker BioTOF II instrument using sodium trifluoroacetate internal standard and ammonium bicarbonate additive.

2.7.2 Reaction Optimization Experiments

Control Experiments: Reactions were prepared using phenyl salicylate (0.2 mmol, 1.0 equiv) *Rac*-2-(di-*t*-butyldiphosphino)-1,1'-binapthyl (TrixiePhos, y mol%), $[Ir(cod)OMe]_2$ (x mol%), 1,5-cyclooctadiene (1,5-COD, 1.0 equiv), and 1,2-dimethoxybenzene (1,2-DMB, 0.1 M) in PTFE-lined crimp-top vials. The vials sealed, removed from the glovebox, and heated to 170 °C in an oil bath for twenty hours. Product yields were determined by ^1H NMR using 1,3,5-trimethoxybenzene internal standard (0.8 mL, 0.1 M in $CDCl_3$).

Catalyst Optimization: Reactions were prepared using phenyl salicylate (0.1 mmol, 1.0 equiv), TrixiePhos (0.003 mmol, 3 mol%), catalyst (0.001 mmol, 1 mol%), base (0.018 mmol, 3 mol%), and *m*-xylene (1.0 mL, 0.1 M) in PTFE-lined crimp-top vials. The vials were sealed, removed from the glovebox, and heated to 170 °C in an oil bath for 24 h.

Product yields were determined by ^{1}H NMR using 1,3,5-trimethoxybenzene internal standard (0.7 mL, 0.143 M in $CDCl_3$).

Catalyst Loading Optimization : Reactions were prepared using phenyl salicylate (0.1 mmol, 1.0 equiv), $[Ir(cod)OPh]_2$ (x mol%), TrixiePhos (2x mol%) and *m*-xylene (1.0 mL, 0.1 M) in PTFE-lined crimp-top vials. The vials were sealed, removed from the glovebox, and heated to 170 °C in an oil bath for 24 h. Product yields were determined by ^{1}H NMR using 1,3,5-trimethoxybenzene internal standard (0.7 mL, 0.143 M in $CDCl_3$).

Phosphine/Ligand Screen: Reactions were prepared using phenyl salicylate (0.1 mmol, 1.0 equiv), $[Ir(cod)OPh]_2$ (0.001 mmol, 1 mol%), Phosphine (0.003 mmol, 3 mol%) and *m*-xylene (1.0 mL, 0.1 M) in PTFE-lined crimp-top vials. The vials were sealed, removed from the glovebox, and heated to 170 °C in an oil bath for 48 h. Product yields were determined by ^{1}H NMR using 1,3,5-trimethoxybenzene internal standard (0.7 mL, 0.143 M in $CDCl_3$).

Phosphine Loading Optimization: Reactions were prepared using phenyl salicylate (0.1 mmol, 1.0 equiv), $[Ir(cod)OPh]_2$ (0.001 mmol, 1 mol%), TrixiePhos (x mol%) and *m*-xylene (1.0 mL, 0.1 M) in PTFE-lined crimp-top vials. The vials were sealed, removed from the glovebox, and heated to 170 °C in an oil bath for 48 h. Product yields were determined by ^{1}H NMR using 1,3,5-trimethoxybenzene internal standard (0.7 mL, 0.143 M in $CDCl_3$).

Substrate Concentration Optimization: Reactions were prepared using phenyl salicylate (1.0 equiv), $[Ir(cod)OPh]_2$ (1 mol%), TrixiePhos (3 mol%) and *m*-xylene (volume required to obtain listed concentration of phenyl salicylate) in PTFE-lined crimp-top vials. The vials

were sealed, removed from the glovebox, and heated to 170 °C in an oil bath for 48 h. Product yields were determined by ^{1}H NMR using 1,3,5-trimethoxybenzene internal standard (0.7 mL, 0.143 M in $CDCl_3$).

Effect of Arene Dilution: Reactions were prepared in PTFE-lined crimp-top vials using phenyl salicylate (0.1 mmol, 1.0 equiv), $[Ir(cod)OPh]_2$ (0.001 mmol, 1 mol%), TrixiePhos (0.003 mmol, 3 mol%), *m*-xylene (x equiv), and additional solvent to dilute to a final volume of 1.0 mL. The vials were sealed, removed from the glovebox, and heated to 170 °C in an oil bath for 48 h. Product yields were determined by ^{1}H NMR using 1,3,5-trimethoxybenzene internal standard (0.7 mL, 0.143 M in $CDCl_3$).

COD Equivalents Optimization: Reactions were prepared using phenyl salicylate (1.0 equiv), $[Ir(cod)OPh]_2$ (1 mol%), TrixiePhos (3 mol%), 1,5-COD (volume required to obtain listed concentrations) and 1,2-dimethoxybenzene (0.1 M final concentration relative to phenyl salicylate, 1 mL final volume) in PTFE-lined crimp top vials. The vials were sealed, removed from the glovebox, and heated to 170 °C in an oil bath for 4 hr. Product yield was determined by ^{1}H NMR using dibromomethane internal standard.

Alkene Additive Screen: Reactions were prepared using phenyl salicylate (1 equiv), $[Ir(cod)OMe]_2$ (1 mol%), TrixiePhos (3 mol%), alkene additive (1 equiv) and 1,2-dimethoxybenzene (0.8 mL) in a 5 mm J-young NMR tube. The tube was sealed, removed from the glovebox, and heated to 160 °C. Single-scan ^{1}H NMR spectra were taken at regular intervals. The reaction progress was monitored until approximately 10% completion was observed, relative to trimethyl(phenyl)silane internal standard.

2.7.3 Catalyst Decomposition Experiments

Iridium Carbonyl from Catalyst Decomposition: TrixiePhos (10 mg, 0.024 mmol, 3 mol%), $[Ir(cod)OMe]_2$ (50 mg, 0.08 mmol, 10 mol%, phenyl salicylate (0.171 g, 0.8 mmol, 1 equiv), 1,5-COD (98 μL, 0.8 mmol, 1 equiv), and mesitylene (8 mL, 0.1 M) were added to a 10 mL PTFE-lined crimp-top vial. The vial was sealed, removed from the glovebox, and heated to 170 °C in an oil bath for 20 h. The solvent was removed *in vacuo.* An IR spectrum was obtained of the crude product mixture. Distinguishing peaks at 1981 and 2027 cm^{-1} indicated the probable presence of an Ir–CO complex.

Phosphorus Degradation: TrixiePhos (5.0 mg, 0.013 mmol, 3 mol%), $[Ir(cod)OMe]_2$ (3.0 mg, 0.005 mmol, 1 mol%), phenyl salicylate (90.1 mg, 0.421 mmol, 1 equiv), 1.5-COD (51 μL, 0.416 mmol, 1 equiv) and 1,3-dimethoxybenzene (4.3 mL, 0.1 M) were mixed in a 20 mL scintillation vial. 0.6 mL of the solution was transferred to a J-Young NMR tube, the tube was sealed and removed from the glovebox. A ^{31}P NMR spectrum was taken (t=0), and the reaction mixture was heated to 170 °C in an oil bath. ^{31}P NMR spectra were taken at regular increments.

Reaction in CO Atmosphere: TrixiePhos (9.6 mg, 0.024 mmol, 3 mol%), $[Ir(cod)OMe]_2$ (5.3 mg, 0.008 mmol, 1 mol%), phenyl salicylate (171.4 mg, 0.800 mmol, 1 equiv), 1.5-COD (98 μL, 0.800 mmol, 1 equiv) and 1,3-dimethoxybenzene (8.0 mL, 0.1 M) were mixed in a 20 mL scintillation vial. The solution was transferred to a 50 mL Schlenk tube, the tube was sealed and removed from the glovebox. The Schlenk tube was evacuated and backfilled with CO. The tube was sealed and heated to 170 °C in an oil bath for 20 h. Solvent was removed *in vacuo* and the crude product mixture was analyzed by ^{1}H NMR.

2.7.4 Kinetic Experiments

Initial Rates General: Reactions were prepared using phenyl salicylate, $[Ir(cod)OMe]_2$, TrixiePhos, 1,5-COD, in 1,2-dimethoxybenzene (0.8 mL) in a 5 mm J-young NMR tube. The tube was sealed, removed from the glovebox, and heated to 160 °C. Single-scan ^{1}H N MR spectra were taken at regular intervals. The reaction progress was monitored until approximately 10% completion was observed, relative to 1,3,5-trimethoxybenzene internal standard.

One reagent concentration was varied at a time to determine the reaction order of that component, all other reagent concentrations were held constant at the concentration used in standard reactions (phenyl salicylate (0.100 M), $[Ir(cod)OMe]_2$ (1.0 mM), TrixiePhos (3.0 mM), 1,5-COD (0.100 M)). When varying arene solvent concentration, 1,2-dimethoxybenzene was diluted with mesitylene.

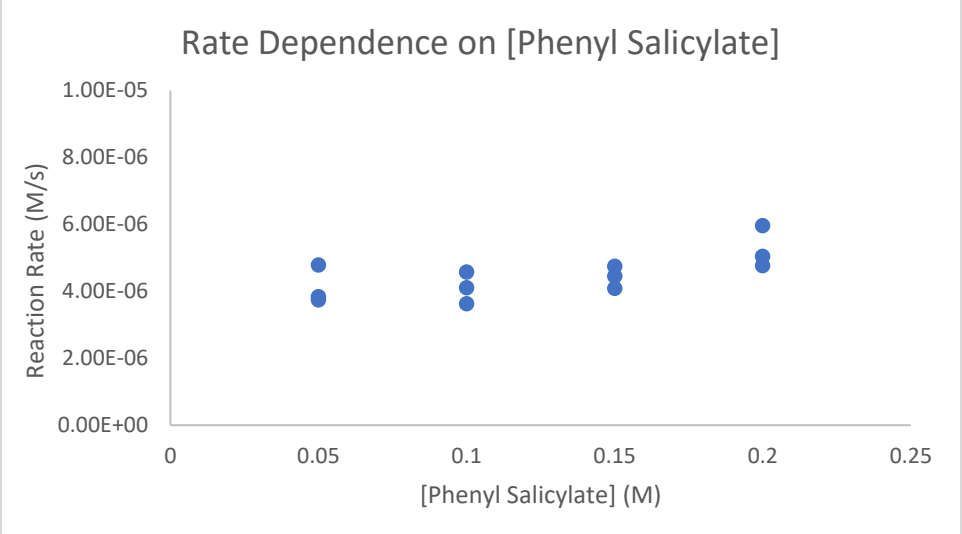

Figure 2.7 Initial rate data showing zeroth order in phenyl salicylate

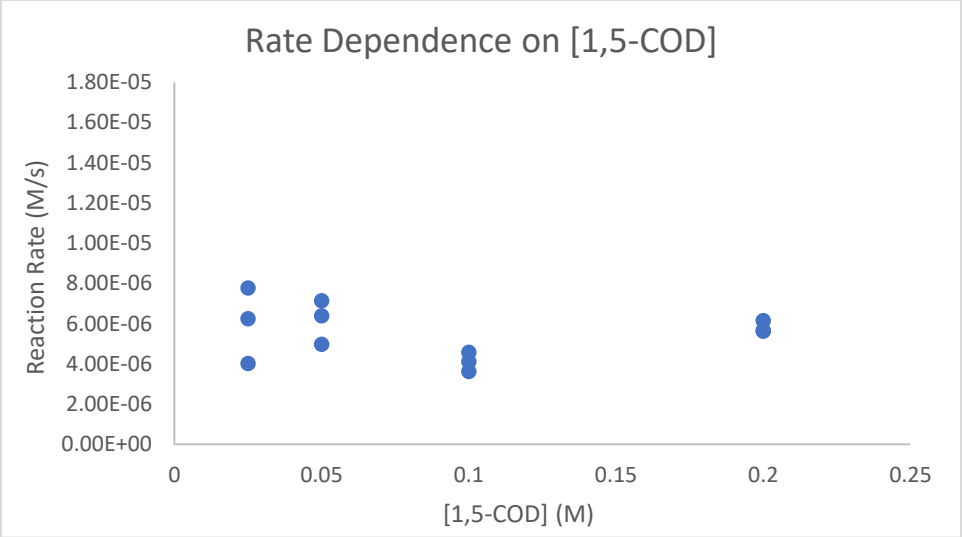

Figure 2.8 Initial rate data showing zeroth order in COD

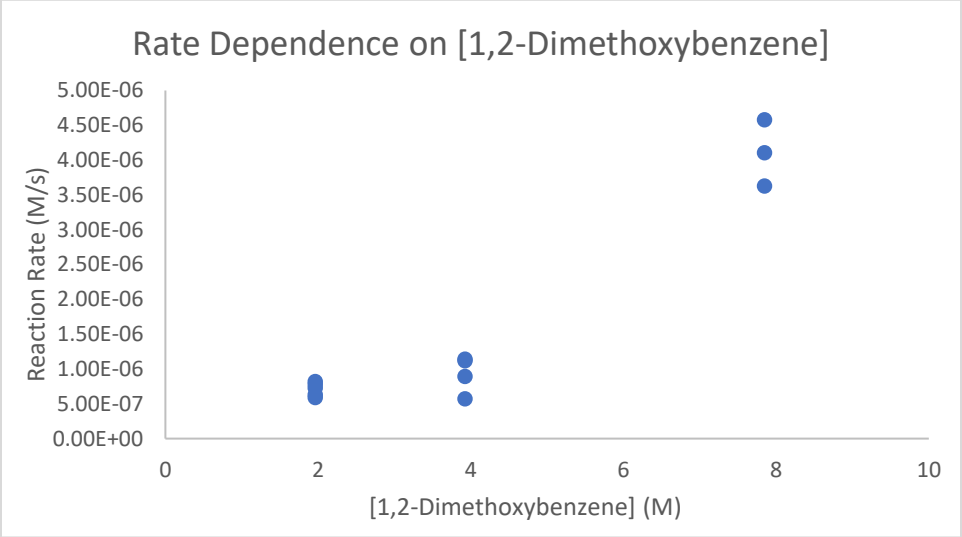

Figure 2.9 Initial rate data showing dependence on 1,2-dimethoxybenzene

Kinetic Isotopes General: The kinetic isotope effects were determined by the following equation:

$$KIE = \frac{Prod_H}{Prod_D} = \frac{k_H}{k_D}$$

Initial Rates

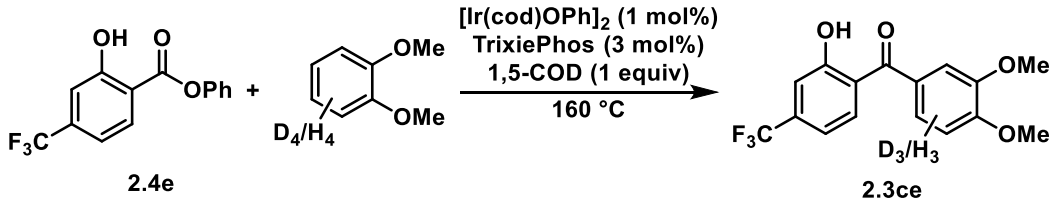

Proteo - Reactions were performed in triplicate using 0.7 mL aliquots from a stock solution containing phenyl 4-(trifluoromethyl)salicylate (0.4 mmol, 1 equiv), $[Ir(cod)OMe]_2$ (0.004 mmol, 1 mol%), TrixiePhos (0.012 mmol, 3 mol%), 1,5-COD (0.4 mmol, 1 equiv), 1-methoxy-3-(trifluoromethyl)benzene (0.463 mmol, 1.16 equiv) and H_4-1,2-dimethoxybenzene (4 mL) in a J-Young NMR tube. Once sealed, the tubes were removed from the glovebox, and single-scan ^1H and ^{19}F NMR spectra were taken for time (t) = 0 min. The reaction mixtures were heated to 160 °C in an oil bath and monitored for 70 minutes. Product formation was monitored by ^{19}F using 1-methoxy-3-(trifluoromethyl)benzene internal standard. Linear fits were obtained, removing the t = 0 data point due to an observed induction period.

Deutero - Reactions were performed in triplicate using 0.7 mL aliquots from a stock solution containing phenyl 4-(trifluoromethyl)salicylate (0.4 mmol, 1 equiv), $[Ir(cod)OMe]_2$ (0.004 mmol, 1 mol%), TrixiePhos (0.012 mmol, 3 mol%), 1,5-COD (0.4 mmol, 1 equiv), 1-methoxy-3-(trifluoromethyl)benzene (0.407 mmol, 1.02 equiv) and D_4-1,2-dimethoxybenzene (4 mL) in a J-Young NMR tube. Once sealed, the tubes were

removed from the glovebox, and single-scan ^{1}H and ^{19}F NMR spectra were taken for time (t) = 0 min. The reaction mixtures were heated to 160 °C in an oil bath and monitored for 90 minutes. Product formation was monitored by ^{19}F using 1-methoxy-3-(trifluoromethyl)benzene internal standard. Linear fits were obtained, removing the t = 0 data point due to an observed induction period.

Table 2.11 Initial rates kinetics results

Entry	**k_H (%/min)**	**k_D (%/min)**	**KIE**
1	0.360	0.198	—
2	0.380	0.220	—
3	0.348	0.201	—
Average	0.363 ± 0.012	0.206 ± 0.016	1.77 ± 0.13

Intermolecular Competition

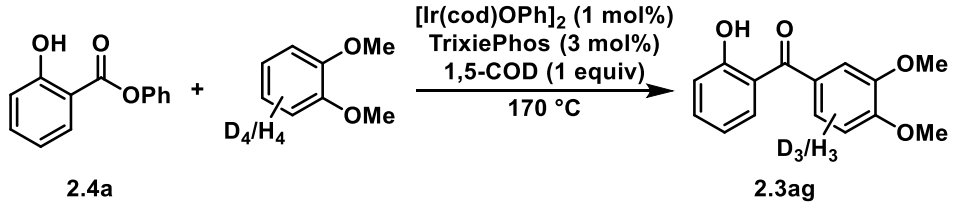

2.4a **2.3ag**

Reactions were prepared in triplicate using phenyl salicylate (1 equiv), $[Ir(cod)OMe]_2$ (1 mol%), TrixiePhos (3 mol%), 1,5-COD (1 equiv), H_4-1,2-dimethoxybenzene (0.5 mL) and D_4-1,2-dimethoxybenzene (92.8% d_4 by ^{1}H NMR, 0.5 mL) in PTFE-lined crimp top vials. The vials were sealed, removed from the glovebox, and heated to 170 °C in an oil bath for 20 hr. Crude mixtures were analyzed by ESI-MS.

$$Prod_H = I_{257}$$

$$Prod_D = I_{260}$$

Intramolecular Competition

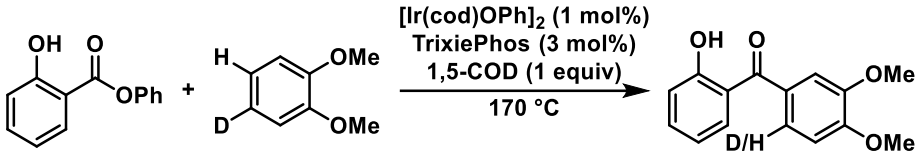

2.4a 2.3ag

Reactions were prepared in triplicate using phenyl salicylate (1 equiv), [Ir(cod)OMe]$_2$ (1 mol%), TrixiePhos (3 mol%), 1,5-COD (1 equiv), 4-*D*$_1$-1,2-dimethoxybenzene (90.4% d_4 by ^{1}H NMR, 1 mL) in PTFE-lined crimp top vials. The vials were sealed, removed from the glovebox, and heated to 170 °C in an oil bath for 20 hr. Crude mixtures were analyzed by ESI-MS. Correction factors are used to account for ^{13}C of products.

$$k_H = I_{259} + (I_{258} - (I_{257} \times 0.16))$$

$$k_D = I_{257} \times 1.16$$

Table 2.12 Product ratios and KIE values from inter- and intramolecular competition experiments

Entry	**$Prod_H/k_H$**	**$Prod_D/k_D$**	**KIE**
Inter1	3332	704	4.73
Inter2	4546	983	4.62
Inter3	5577	1259	4.43
Average			4.59 ± 0.15
Intra1	1057	687	1.54
Intra2	770	457	1.68
Intra3	1437	843	1.70
Average			1.64 ± 0.09

Cumulative effect of secondary isotope effects and differential reversibility on observed intermolecular KIE

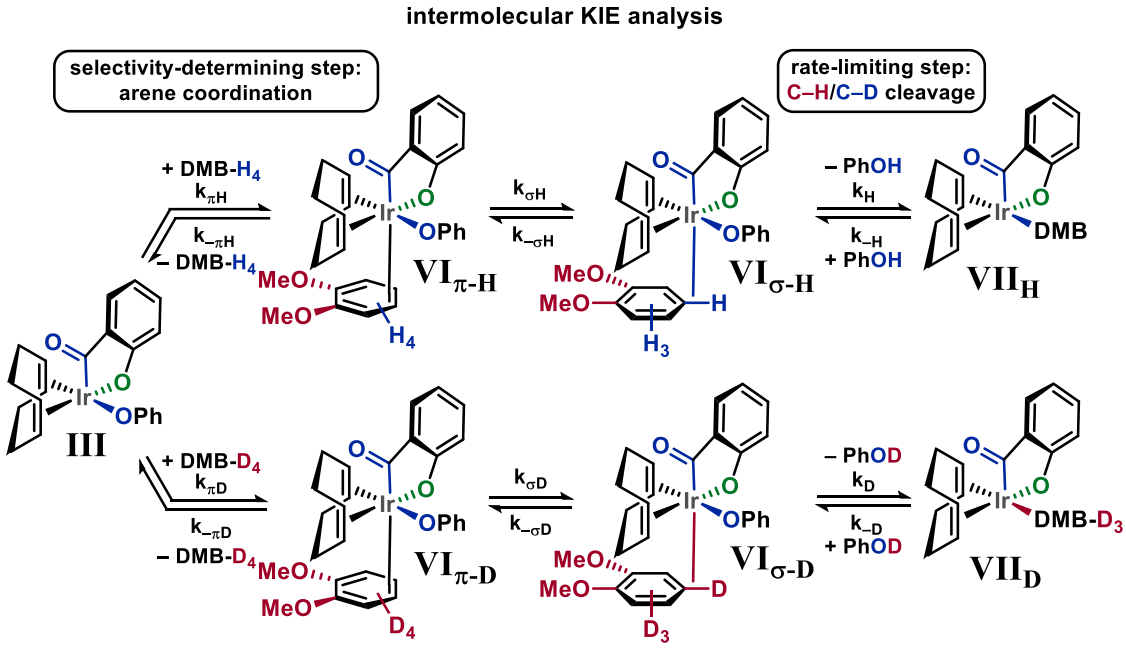

Rate with respect to the formation of $[VII_H]$ is

$$\frac{\Delta[VII_H]}{\Delta t} = k_H[VI_{\sigma H}] - k_{-H}[VII_H] \quad (1)$$

Steady-state approximation on $[VI_{\sigma H}]$

$$0 = \frac{\Delta[VI_{\sigma H}]}{\Delta t} = k_{\sigma H}[VI_{\pi H}] + k_{-H}[VII_H] - k_{-\sigma H}[VI_{\sigma H}] - k_H[VI_{\sigma H}] \quad (2)$$

$$[VI_{\sigma H}] = \frac{k_{\sigma H}[VI_{\pi H}] + k_{-H}[VII_H]}{k_{-\sigma H} + k_H} \quad (3)$$

Substitute Equation 3 into Equation 1

$$\frac{\Delta[VII_H]}{\Delta t} = \frac{k_H k_{\sigma H}[VI_{\pi H}] - k_{-H}k_{-\sigma H}[VII_H]}{k_{-\sigma H}k_H} \quad (4)$$

Steady state approximation on $[VI_{\pi H}]$

$$0 = \frac{\Delta[VI_{\pi H}]}{\Delta t} = k_{\pi H}[III][DMB - H_4] + k_{-\sigma H}[VI_{\sigma H}] - k_{-\pi H}[VI_{\pi H}] - k_{\sigma H}[VI_{\pi H}] \quad (5)$$

Substitute Equation 3 into Equation 5

$$0 = \frac{k_{\sigma H}k_{-\sigma H}[VI_{\pi H}] + k_{-H}k_{-\sigma H}[VII_H]}{k_{-\sigma H} + k_H} + k_{\pi H}[III][DMB - H_4] - k_{-\pi H}[VI_{\pi H}] - k_{\sigma H}[VI_{\pi H}] \quad (6)$$

$$[VI_{\pi H}] = \frac{K_{-\sigma H}k_{\pi H}[III][DMB - H_4] + k_H k_{\pi H}[III][DMB - H_4] + k_{-H}k_{-\sigma H}[VII_H]}{k_{-\sigma H}k_{-\pi H} + k_H k_{-\pi H} + k_H k_{-\sigma H}} \quad (7)$$

Substitute Equation 7 into Equation 4

$$\frac{\Delta[VII_H]}{\Delta t} = \frac{k_H k_{\sigma H} k_{\pi H}[III][DMB - H_4](k_{-\sigma H} + k_H) + k_{-H} k_{-\sigma H} k_{-\pi H}[VII_H](k_{-\sigma H} - k_H)}{k_H^2 k_{\sigma H} + k_H^2 k_{-\pi H} + 2k_H k_{-\sigma H} k_{-\pi H} + k_H k_{\sigma H} k_{-\sigma H} + k_{-\sigma H}^2 k_{-\pi H}} \tag{8}$$

The second term in numerator should be negligible relative to the first term, so Equation 8 simplifies to

$$\frac{\Delta[VII_H]}{\Delta t} = \frac{k_H k_{\sigma H} k_{\pi H}[III][DMB - H_4](k_{-\sigma H} + k_H)}{k_H^2 k_{\sigma H} + k_H^2 k_{-\pi H} + 2k_H k_{-\sigma H} k_{-\pi H} + k_H k_{\sigma H} k_{-\sigma H} + k_{-\sigma H}^2 k_{-\pi H}} \tag{9}$$

Therefore

$$\frac{\Delta[VII_D]}{\Delta t} = \frac{k_D k_{\sigma D} k_{\pi D}[III][DMB - D_4](k_{-\sigma D} + k_D)}{k_D^2 k_{\sigma D} + k_D^2 k_{-\pi D} + 2k_D k_{-\sigma D} k_{-\pi D} + k_D k_{\sigma D} k_{-\sigma D} + k_{-\sigma D}^2 k_{-\pi D}} \tag{10}$$

$KIE_{intermolecular}$ can be described as $\frac{\frac{\Delta[VII_H]}{\Delta t}}{\frac{\Delta[VII_D]}{\Delta t}}$ so

$$\frac{\frac{\Delta[VII_H]}{\Delta t}}{\frac{\Delta[VII_D]}{\Delta t}} = \frac{\frac{k_H k_{\sigma H} k_{\pi H}[III][DMB-H_4](k_{-\sigma H}+k_H)}{k_D k_{\sigma D} k_{\pi D}[III][DMB-D_4](k_{-\sigma D}+k_D)}}{\frac{k_D^2 k_{\sigma D}+k_D^2 k_{-\pi D}+2k_D k_{-\sigma D} k_{-\pi D}+k_D k_{\sigma D} k_{-\sigma D}+k_{-\sigma D}^2 k_{-\pi D}}{k_H^2 k_{\sigma H}+k_H^2 k_{-\pi H}+2k_H k_{-\sigma H} k_{-\pi H}+k_H k_{\sigma H} k_{-\sigma H}+k_{-\sigma H}^2 k_{-\pi H}}} \tag{11}$$

Because $[DMB - H_4]_i = [DMB - D_4]_i$ and $\Delta[DMB] << [DMB]_i$, $[DMB - H_4] = [DMB - D_4]$

$$\frac{\frac{\Delta[VII_H]}{\Delta t}}{\frac{\Delta[VII_D]}{\Delta t}} = \left(\frac{k_H}{k_D}\right) \frac{k_{\sigma H} k_{\pi H}}{k_{\sigma D} k_{\pi D}} \frac{k_{-\sigma H} + k_H}{k_{-\sigma D} + k_D} \frac{k_D^2 k_{\sigma D} + k_D^2 k_{-\pi D} + 2k_D k_{-\sigma D} k_{-\pi D} + k_D k_{\sigma D} k_{-\sigma D} + k_{-\sigma D}^2 k_{-\pi D}}{k_H^2 k_{\sigma H} + k_H^2 k_{-\pi H} + 2k_H k_{-\sigma H} k_{-\pi H} + k_H k_{\sigma H} k_{-\sigma H} + k_{-\sigma H}^2 k_{-\pi H}} \tag{12}$$

2.7.5 Synthetic Experiments

General procedure for salicylate ester synthesis: Salicylic acid (10 mmol, 1 equiv) and phenol (4.70 g, 50 mmol, 5 equiv) were massed in a 5-dram reaction vial, and then 10 mL of dry toluene was added. Phosphorus oxychloride (0.61g, 0.37 mL, 4 mmol, 0.4 equiv) was dripped into the solution via syringe. A stir bar was added and the reaction vial was sealed. The reaction mixture was then heated at 110 °C in an aluminum heating block on a hot plate fitted with a thermocouple for 16-18 h. The mixture was allowed to cool to room temperature, transferred to a separatory funnel, and quenched with saturated aqueous sodium carbonate solution (3 × 10 mL). The aqueous washes were then extracted with diethyl ether (3 × 10 mL). The organic layers were combined, dried with sodium

sulfate, and concentrated *in vacuo*. The crude product was purified by column chromatography.

Arene Acylation General Procedures:

Procedure A: TrixiePhos (10 mg, 0.024 mmol, 3 mol%), $[Ir(cod)OMe]_2$ (5 mg, 0.008 mmol, 1 mol%), phenyl salicylate (0.171 g, 0.8 mmol, 1 equiv), 1,5-COD (98 μL, 0.8 mmol, 1 equiv), and arene (8 mL, 0.1 M) were added to a 10 mL PTFE-lined crimp-top vial. The vial was sealed, removed from the glovebox, and heated to 170 °C in an oil bath for 20 h. The solvent was removed *in vacuo*. Oligomer and residual starting material were hydrolyzed (see general procedure below), and the aqueous layer was extracted with ethyl acetate (EtOAc) (3 × 12 mL). The organic extracts were dried over Na_2SO_4 and concentrated. The crude product was purified by column chromatography.

Procedure B: TrixiePhos (14 mg, 0.036 mmol, 3 mol%), $[Ir(cod)OMe]_2$ (8 mg, 0.012 mmol, 1 mol%), phenyl salicylate (0.257 g, 1.2 mmol, 1 equiv), 1,5-cyclooctadiene (1,5-COD, 147 μL, 1.2 mmol, 1 equiv), and arene (12 mL, 0.1 M) were added to a dry 15 mL pressure tube. The pressure tube was sealed, removed from the glovebox, and heated to 170 °C in an oil bath for 20 h. The solvent was removed *in vacuo*. Oligomer and residual starting material were hydrolyzed (see general procedure below), and the aqueous layer was extracted with EtOAc (3 × 15 mL). The organic extracts were dried over Na_2SO_4 and concentrated. The crude product was purified by column chromatography.

Procedure C: Followed procedure B, then after 20 h, the reaction mixture was cooled to rt, brought into the glovebox, where TrixiePhos (14 mg, 0.036 mmol, 3 mol%) and $[Ir(cod)OMe]_2$ (8 mg, 0.012 mmol, 1 mol%) was added. The pressure tube was sealed,

removed from the glovebox, and heated to 170 °C in an oil bath for 20 h. The solvent was removed *in vacuo*. Oligomer and residual starting material were hydrolyzed (see general procedure below), and the aqueous layer was extracted with EtOAc (3 × 15 mL). The organic extracts were dried over Na_2SO_4 and concentrated. The crude product was purified by column chromatography.

Procedure D: Followed procedure A, then after 20 h, the reaction mixture was cooled to rt, brought into the glovebox, and TrixiePhos (10 mg, 0.024 mmol, 3 mol%) and $[Ir(cod)OMe]_2$ (5 mg, 0.008 mmol, 1 mol%) was added. The vial was sealed, removed from the glovebox, and heated to 170 °C for 20 h. The solvent was removed *in vacuo*. Oligomer and residual starting material were hydrolyzed (see general procedure below), and the aqueous layer was extracted with EtOAc (3 × 12 mL). The organic extracts were dried over Na_2SO_4 and concentrated. The crude product was purified by column chromatography.

General procedure for hydrolysis: Crude material was dissolved in toluene (10 mL), NaOH (30%, 5 mL for procedure A/C, 6.5 mL for procedure B/D) was added, and the mixture was allowed to stir overnight. The mixture was cooled to 0 °C, and HCl (6 M, 7 mL for Procedure A/C, 8 mL for Procedure B or D) was added dropwise.

Hydroxyphenstatin Synthesis:

Synthesis of ester 2.42: In a nitrogen-filled glovebox, 2,3-dihydroxy-4-methoxybenzoic acid[b] (500 mg, 2.72 mmol, 1 equiv), phenol (5.11 g, 54.3 mmol, 20 equiv), and phosphorus oxychloride (631.5 mg, 4.07 mmol, 1.5 equiv) were added to a 25 mL screw top pressure

[b] Prepared using literature reported method.[165]

vessel with a stir bar. The vessel was sealed, removed from the glovebox, and heated to 100 °C for 20 hours. The vessel was cooled to room temperature and the solvent and remaining phenol removed *in vacuo*. The product was purified by flash chromatography (20%→30% EtOAc/Hex).

Synthesis of Hydroxyphenstatin 2.40: TrixiePhos (18 mg, 0.045 mmol, 3 mol%), $[Ir(cod)OMe]_2$ (10 mg, 0.015 mmol, 1 mol%), phenyl salicylate (0.390 g, 1.5 mmol, 1 equiv), 1,5-COD (0.18 mL, 1.5 mmol, 1 equiv), and 1,2,3-trimethoxybenzene (19.8 g, 78.5 equiv) were added to a 75 mL PTFE-sealed screw top pressure vessel. The vessel was sealed, removed from the glovebox, and heated to 170 °C in an oil bath for 20 h. The vessel was then cooled to room temperature and brought into the glovebox and TrixiePhos (18 mg, 0.045 mmol, 3 mol%) and $[Ir(cod)OMe]_2$ (10 mg, 0.015 mmol, 1 mol%) was added. The vessel was sealed, brought out of box, and heated to 170 °C for an additional 20 hours. After 20 hours, the vessel was then cooled and a third charge of iridium and phosphine was added as before. The vessel was heated to 170 °C for an additional 20 hours. The vessel was then cooled to room temperature and contents were transferred to a 50 mL pear-shaped flask. The solvent was removed *in vacuo*. Product was purified by column chromatography (20:80:2 EtOAc:Hex:AcOH for ~10 column volumes, 40:60:2 for ~4 column volumes, 50:50:2 for ~4 column volumes).

2.7.6 Characterization Data

Salicylate Esters:

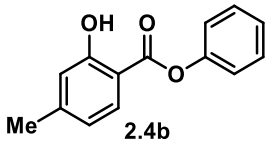

2.4b

Phenyl 2-hydroxy-4-methylbenzoate (**2.4b**). White solid (1.20 g, 5.30 mmol, 53%). mp = 43–44 °C. R_f = 0.33 (5% EtOAc/Hex). ^{1}H NMR (400 MHz, $CDCl_3$) δ 10.45 (s, 1H), 7.94 (d, *J* = 8.1 Hz, 1H), 7.49–7.39 (m, 2H), 7.34–7.25 (m, 1H), 7.21 (d, *J* = 1.3 Hz, 1H), 7.19 (dd, *J* = 2.1, 0.9 Hz, 1H), 2.38 (s, 3H). ^{13}C NMR (101 MHz, $CDCl_3$) δ 169.1, 162.3, 150.3, 148.2, 130.3, 129.7, 126.4, 121.8, 120.9, 118.1, 109.4, 22.1. IR (neat) 1683 cm^{-1}. HRMS (ESI) calcd for $C_{14}H_{12}O_3$ $[M-H]^-$ *m/z* 227.0714, found 227.0724.

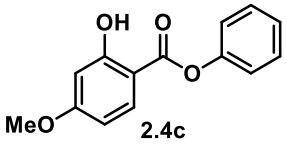

2.4c

Phenyl 2-hydroxy-4-methoxybenzoate (**2.4c**). Phenol (264 mg, 2.8 mmol, 1.4 equiv), 4-methoxysalicylic acid (336.3 mg, 2.0 mmol, 1 equiv), and DMAP (49 mg, 0.4 mmol, 0.2 equiv) were dissolved in methylene chloride (8 mL). DCC (743 mg, 3.6 mmol, 1.8 equiv) was added; the reaction mixture was heated to reflux and allowed to reflux overnight. Removal of the solvent and purification by column chromatography (2% EtOAc/Hex to 3% EtOAc/Hex) ultimately gave a white solid (0.358 g, 1.46 mmol, 73%). mp = 59–61 °C. R_f = 0.28 (5% EtOAc/Hex). ^{1}H NMR (400 MHz, $CDCl_3$) δ 10.72 (s, 1H), 7.97 (d, *J* = 8.8 Hz, 1H), 7.49–7.39 (m, 2H), 7.34–7.25 (m, 1H), 7.24–7.15 (m, 2H), 6.53 (dd, *J* = 8.8, 2.5 Hz, 1H), 6.50 (d, *J* = 2.4 Hz, 1H), 3.86 (s, 3H). ^{13}C NMR (101 MHz, $CDCl_3$) δ 168.9,

166.4, 164.7, 150.4, 131.9, 129.7, 126.3, 121.9, 108.2, 105.0, 101.0, 55.7. IR (neat) 1671 cm^{-1}. HRMS (ESI) calcd for $C_{14}H_{12}O_4$ $[M-H]^-$ *m/z* 243.0663, found 243.0661.

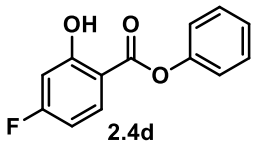

2.4d

Phenyl 4-fluoro-2-hydroxybenzoate (**2.4d**). White solid (1.20 g, 5.20 mmol 52%). mp = 58–60 °C. R_f = 0.32 (5% EtOAc/Hex). ^1H NMR (400 MHz, $CDCl_3$) δ 10.73 (d, *J* = 1.6 Hz, 1H), 8.09 (dd, *J* = 8.9, 6.5 Hz, 1H), 7.51–7.40 (m, 2H), 7.37–7.27 (m, 1H), 7.24–7.16 (m, 2H), 6.77–6.58 (m, 2H). ^{13}C NMR (101 MHz, $CDCl_3$) δ 168.4, 167.9 (d, J_{C-F} = 255.4 Hz), 164.5 (d, J_{C-F} = 14.3 Hz), 150.1, 132.8 (d, J_{C-F} = 11.5 Hz), 129.6, 126.6, 121.7, 108.8 (d, J_{C-F} = 2.4 Hz), 108.0 (d, J_{C-F} = 22.7 Hz), 104.8 (d, J_{C-F} = 24.4 Hz). ^{19}F {^1H} NMR (376 MHz, $CDCl_3$) δ −99.65. IR (neat) 1682 cm^{-1}. HRMS (ESI) calcd for $C_{13}H_9FO_3$ $[M-H]^-$ *m/z* 231.0463, found 231.0473.

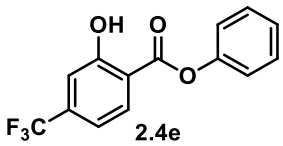

2.4e

Phenyl 2-hydroxy-4-(trifluoromethyl)benzoate (**2.4e**). White solid (1.24 g, 4.40 mmol, 44%). mp = 68–69 °C. R_f = 0.39 (5% EtOAc/Hex). ^1H NMR (400 MHz, $CDCl_3$) δ 10.63 (s, 1H), 8.20 (d, *J* = 8.3 Hz, 1H), 7.52–7.41 (m, 2H), 7.37–7.28 (m, 2H), 7.24–7.18 (m, 3H). ^{13}C NMR (101 MHz, $CDCl_3$) δ 168.2, 162.2, 150.0, 137.7 (q, J_{C-F} = 32.9 Hz), 131.4, 129.9, 127.3, 123.2 (q, J_{C-F} = 273.8 Hz), 121.5, 115.8 (q, J_{C-F} = 3.6 Hz), 115.3 (q, J_{C-F} = 4.0 Hz), 114.6. ^{19}F {^1H} NMR (376 MHz, $CDCl_3$) δ −63.85. IR (neat) 1686 cm^{-1}. HRMS (ESI) calcd for $C_{14}H_9F_3O_3$ $[M-H]^-$ *m/z* 281.0431, found 281.0436.

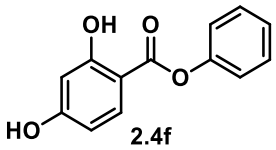

2.4f

Phenyl 2,4-dihydroxybenzoate (**2.4f**). White solid (0.65g, 2.80 mmol, 28%). mp = 144–145 °C. R_f = 0.28 (20% EtOAc/Hex). ^{1}H NMR (400 MHz, $CDCl_3$) δ 10.73 (s, 1H), 7.96 (d, *J* = 8.5 Hz, 1H), 7.44 (t, *J* = 7.9 Hz, 2H), 7.29 (t, *J* = 7.4 Hz, 1H), 7.19 (d, *J* = 7.4 Hz, 1H), 6.47–6.38 (m, 2H), 5.78 (s, 1H). ^{13}C NMR (101 MHz, $CDCl_3$) δ 168.9, 164.3, 162.8, 150.2, 132.6, 129.8, 126.5, 121.8, 108.5, 105.4, 103.5, 77.5, 77.2, 76.8. IR (neat) 1658 cm^{-1}. HRMS (ESI) calcd for $C_{13}H_{10}O_4$ $[M-H]^-$ *m/z* 229.0506, found 229.0510 (avg of 6).

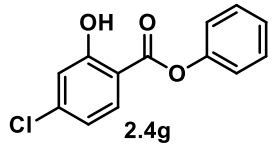

2.4g

Phenyl 4-chloro-2-hydroxybenzoate (**2.4g**). White solid (1.47g, 5.9 mmol, 59%). mp = 52–53 °C. R_f = 0.40 (5% EtOAc/Hex). ^{1}H NMR (400 MHz, $CDCl_3$) δ 10.60 (s, 1H), 8.00 (d, *J* = 8.6 Hz, 1H), 7.50–7.40 (m, 2H), 7.36–7.27 (m, 1H), 7.24–7.16 (m, 2H), 7.06 (d, *J* = 2.0 Hz, 1H), 6.95 (dd, *J* = 8.6, 2.0 Hz, 1H). ^{13}C NMR (101 MHz, $CDCl_3$) δ 168.5, 162.8, 150.1, 142.5, 131.5, 129.8, 126.7, 121.7, 120.4, 118.2, 110.6. IR (neat) 1673 cm^{-1}. HRMS (ESI) calcd for $C_{13}H_9ClO_3$ $[M-H]^-$ *m/z* 247.0167, found 247.0161.

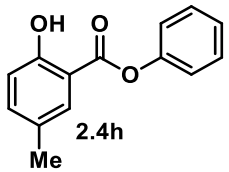

2.4h

Phenyl 2-hydroxy-5-methylbenzoate (**2.4h**). White solid (1.61 g, 7.70 mmol, 77%). mp = 87–89 °C. R_f = 0.36 (5% EtOAc/Hex). ^{1}H NMR (400 MHz, $CDCl_3$) δ 10.31 (s, 1H), 7.86

(d, *J* = 2.2 Hz, 1H), 7.50–7.39 (m, 2H), 7.34 (dd, *J* = 8.5, 2.3 Hz, 1H), 7.35–7.26 (m, 1H), 7.24–7.16 (m, 3H), 6.94 (d, *J* = 8.5 Hz, 1H), 2.34 (s, 3H). ^{13}C NMR (101 MHz, $CDCl_3$) δ 169.1, 160.3, 150.3, 137.6, 130.1, 129.8, 128.8, 126.5, 121.8, 117.7, 111.5, 20.6. IR (neat) 1682 cm^{-1}. HRMS (ESI) calcd for $C_{14}H_{12}O_3$ $[M-H]^-$ *m/z* 227.0714, found 227.0707.

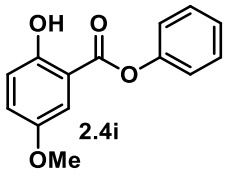

Phenyl 2-hydroxy-5-methoxybenzoate (**2.4i**). White solid (0.75 g, 3.10 mmol, 31%). mp = 40–41 °C. R_f = 0.26 (5% EtOAc/Hex). ^{1}H NMR (400 MHz, $CDCl_3$) δ 10.13 (s, 1H), 7.51 (d, *J* = 3.1 Hz, 1H), 7.51–7.40 (m, 2H), 7.36–7.27 (m, 1H), 7.27–7.15 (m, 2H), 7.16 (dd, *J* = 9.1, 3.2 Hz, 1H), 6.98 (d, *J* = 9.1 Hz, 1H), 3.82 (s, 3H). ^{13}C NMR (101 MHz, $CDCl_3$) δ 168.9, 156.9, 152.3, 150.2, 129.8, 126.6, 125.2, 121.8, 119.0, 112.1, 111.4, 77.5, 77.2, 76.8, 56.1. IR (neat) 1687 cm^{-1}. HRMS (ESI) calcd for $C_{14}H_{12}O_4$ $[M-H]^-$ *m/z* 243.0663, found 243.0653 (avg of 8).

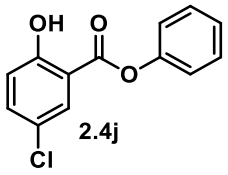

Phenyl 5-chloro-2-hydroxybenzoate (**2.4j**). White solid (1.30 g, 5.20 mmol, 52%). mp = 94–96 °C. R_f = 0.39 (5% EtOAc/Hex). ^{1}H NMR (400 MHz, $CDCl_3$) δ 10.43 (s, 1H), 8.04 (d, *J* = 2.7 Hz, 1H), 7.52–7.41 (m, 3H), 7.37–7.27 (m, 1H), 7.22–7.18 (m, 2H), 6.99 (d, *J* = 8.9 Hz, 1H). ^{13}C NMR (101 MHz, $CDCl_3$) δ 168.1, 160.9, 150.0, 136.5, 129.8, 129.7,

126.7, 124.4, 121.6, 119.6, 112.9, 77.5, 77.2, 76.8. IR (neat) 1685 cm^{-1}. HRMS (ESI) calcd for $C_{13}H_9ClO_3$ $[M-H]^-$ *m/z* 247.0167, found 247.0179 (avg of 6).

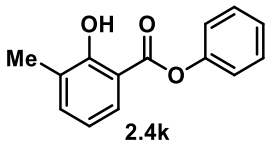

2.4k

Phenyl 2-hydroxy-3-methylbenzoate (**2.4k**). White solid (0.76 g, 3.30 mmol, 33%). mp = 145–145 °C. R_f = 0.45 (5% EtOAc/Hex). ^1H NMR (400 MHz, $CDCl_3$) δ 10.76 (s, 1H), 7.93 (dd, *J* = 8.0, 1.7 Hz, 1H), 7.49–7.40 (m, 2H), 7.39 (ddt, *J* = 7.4, 1.7, 0.8 Hz, 1H), 7.35–7.25 (m, 1H), 7.24–7.17 (m, 2H), 6.87 (t, *J* = 7.7 Hz, 1H), 2.30 (s, 2H). ^{13}C NMR (101 MHz, $CDCl_3$) δ 169.6, 160.8, 150.3, 137.4, 129.8, 128.0, 127.1, 126.5, 121.8, 118.9, 111.2, 15.8. IR (neat) 1685 cm^{-1}. HRMS (ESI) calcd for $C_{14}H_{12}O_3$ $[M-H]^-$ *m/z* 227.0714, found 227.0725 (avg of 6).

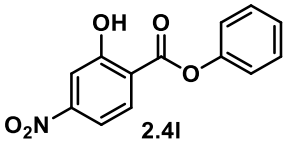

2.4l

Phenyl 2-hydroxy-4-nitrobenzoate (**2.4l**). White solid (3 mmol scale, 0.237 g, 0.90 mmol, 30 %). mp = 148–150 °C. R_f = 0.36 (5% EtOAc/Hex). ^1H NMR (400 MHz, $CDCl_3$) δ 10.73 (s, 1H), 8.27 (d, *J* = 8.7 Hz, 1H), 7.87 (s, 1H), 7.79 (d, *J* = 8.2 Hz, 1H), 7.49 (t, *J* = 7.8 Hz, 2H), 7.36 (t, *J* = 7.5 Hz, 1H), 7.23 (d, *J* = 7.9 Hz, 2H). ^{13}C NMR (101 MHz, $CDCl_3$) δ 167.8, 162.7, 152.7, 149.8, 131.9, 130.0, 127.1, 121.5, 116.8, 113.9, 113.4. IR (neat) 1686 cm^{-1}. HRMS (ESI) calcd for $C_{13}H_9NO_5$ $[M-H]^-$ *m/z* 258.0408, found 258.0420.

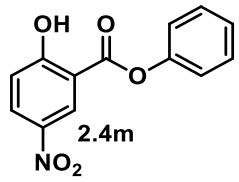

Phenyl 2-hydroxy-5-nitrobenzoate (**2.4m**). White solid (1.558 g, 6.01 mmol 60%). mp = 148–150 °C. R_f = 0.18 (5% EtOAc/Hex). ^{1}H NMR (400 MHz, $CDCl_3$) δ 11.17 (s, 1H), 9.04 (d, *J* = 2.8 Hz, 1H), 8.42 (dd, *J* = 9.2, 2.8 Hz, 1H), 7.54–7.44 (m, 2H), 7.41–7.31 (m, 1H), 7.28–7.20 (m, 2H), 7.16 (d, *J* = 9.2 Hz, 1H). ^{13}C NMR (101 MHz, $CDCl_3$) δ 167.9, 166.8, 149.8, 140.4, 131.3, 130.0, 127.2, 127.1, 121.5, 119.1, 111.9. IR (neat) 1693 cm^{-1}. HRMS (ESI) calcd for $C_{13}H_9NO_5$ $[M-H]^-$ *m/z* 258.0408, found 258.0418.

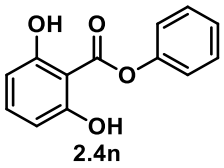

Phenyl 2,6-dihydroxybenzoate (**2.4n**). White solid (0.88 g, 3.80 mmol, 38%). mp = 91–94 °C. R_f = 0.36 (5% EtOAc/Hex). ^{1}H NMR (400 MHz, $CDCl_3$) δ 9.57 (s, 2H), 7.54–7.44 (m, 2H), 7.44–7.33 (m, 2H), 7.27–7.18 (m, 2H), 6.56 (d, *J* = 8.3 Hz, 2H). ^{13}C NMR (101 MHz, $CDCl_3$) δ 168.6, 161.3, 148.6, 137.6, 130.1, 127.5, 122.1, 108.7, 99.8. IR (neat) 1683 cm^{-1}. HRMS (ESI) calcd for $C_{13}H_{10}O_4$ $[M-H]^-$ *m/z* 229.0506, found 229.0508 (avg of 11).

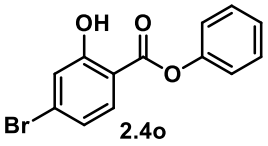

Phenyl 4-bromo-2-hydroxybenzoate (**2.4o**). Off-white solid (5 mmol scale, 1.16g, 3.95 mmol, 79%). mp = 69–72 °C. R_f = 0.38 (5% EtOAc/Hex).^{1}H NMR (400 MHz, $CDCl_3$) δ 10.57 (s, 1H), 7.92 (d, *J* = 8.5 Hz, 1H), 7.50–7.40 (m, 2H), 7.36–7.27 (m, 1H), 7.24 (d, *J* =

1.9 Hz, 1H), 7.24–7.16 (m, 2H), 7.11 (dd, *J* = 8.5, 1.9 Hz, 1H). ^{13}C NMR (101 MHz, $CDCl_3$) δ 168.7, 162.7, 150.0, 131.4, 131.0, 129.8, 126.7, 123.2, 121. 7, 121.3, 111.0. IR (neat) 1673 cm^{-1}. HRMS (ESI) calcd for $C_{13}H_9BrO_3$ $[M-H]^-$ *m/z* 290.9662, found 290.9667.

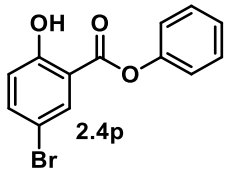

Phenyl 5-bromo-2-hydroxybenzoate (**2.4p**). White solid (1.11 g, 3.80 mmol, 38%). mp = 94–96 °C. R_f = 0.36 (5% EtOAc/Hex). ^{1}H NMR (400 MHz, $CDCl_3$) δ 10.45 (s, 1H), 8.19 (d, *J* = 2.5 Hz, 1H), 7.61 (dd, *J* = 8.9, 2.6 Hz, 1H), 7.51–7.41 (m, 2H), 7.37–7.27 (m, 1H), 7.23–7.18 (m, 2H), 6.94 (d, *J* = 8.9 Hz, 1H). ^{13}C NMR (101 MHz, $CDCl_3$) δ 168.0, 161.3, 150.0, 139.3, 132.7, 129.9, 126.8, 121.6, 120.0, 113.5, 111.3, 77.5, 77.2, 76.8. IR (neat) 1694 cm^{-1}. HRMS (ESI) calcd for $C_{13}H_9BrO_3$ $[M-H]^-$ *m/z* 290.9662, found 290.9653.

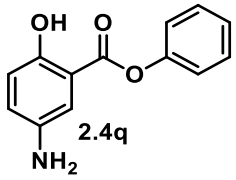

Phenyl 5-amino-2-hydroxybenzoate (**2.4q**). Brown solid (0.383 g, 1.70 mmol, 17%). mp = 72–73 °C. R_f = 0.28 (40% EtOAc/Hex). ^{1}H NMR (400 MHz, $CDCl_3$) δ 9.96 (s, 1H), 7.49–7.39 (m, 2H), 7.37 (d, *J* = 2.9 Hz, 1H), 7.34–7.25 (m, 1H), 7.24–7.15 (m, 2H), 6.94 (dd, *J* = 8.8, 2.8 Hz, 1H), 6.88 (d, *J* = 8.8 Hz, 1H), 3.52 (s, 2H). ^{13}C NMR (101 MHz, $CDCl_3$) δ 168.9, 155.6, 150.3, 138.7, 129.7, 126.4, 125.3, 121.8, 118.6, 114.9, 111.7, 77.5, 77.2, 76.8.

IR (neat) 1678 cm^{-1}. HRMS (ESI) calcd for $C_{13}H_{11}NO_3$ $[M-H]^-$ *m/z* 228.0666, found 228.0679 (avg of 8).

Arene Acylation Products:

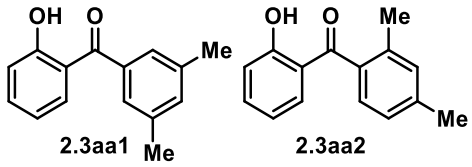

(3,5-dimethylphenyl)(2-hydroxyphenyl)methanone (**2.3aa1**), (2,4-dimethylphenyl)(2-hydroxyphenyl)methanone (**2.3aa2**). Prepared using procedure A. Brown oil (0.110 g, 0.487 mmol, 61%) as an inseparable mixture of regioisomers (11:1 **2.3aa1**:**2.3aa2**). R_f = 0.31 (5% EtOAc/Hex). ^{1}H NMR (400 MHz, $CDCl_3$) **2.3aa1**: δ 12.07 (s, 1H), 7.60 (dd, *J* = 8.0, 1.6 Hz, 1H), 7.50 (ddd, *J* = 8.4, 6.8, 1.6 Hz, 1H), 7.27 (br s, 2H), 7.22 (br s, 1H), 7.06 (dd, *J* = 8.4, 0.8 Hz, 1H), 6.87 (dd, *J* = 8.0, 7.2, 1.2 Hz, 1H), 2.39 (s, 6H); **2.3aa2**: δ 12.28 (s, 1H), 7.33 (dd, *J* = 8.0, 1.6 Hz, 1H), 7.18 (d, *J* = 8.0 Hz, 1H), 7.13– 7.08 (m, 2H), 6.80 (ddd, *J* = 8.4, 7.6, 1.6 Hz, 1H), 2.28 (s, 3H). ^{13}C NMR (101 MHz, $CDCl_3$, only **2.3aa1** observed) δ 202.3, 163.3, 138.2, 138.1, 136.3, 133.8, 133.7, 127.0, 119.4, 118.7, 118.5, 21.4. IR (neat) 1626 cm^{-1}. HRMS (ESI) calcd for $C_{15}H_{13}O_2$ $[M-H]^-$ *m/z* 225.0921; found 225.0927.

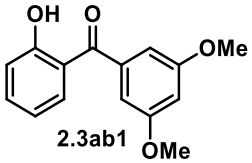

(3,5-dimethoxyphenyl)(2-hydroxyphenyl)methanone (**2.3ab1**). Prepared using procedure C with no hydrolysis in the same reaction as **2.3ab2**; isolated by column chromatography. Brown oil (0.099 g, 0.384 mmol, 48%). R_f = 0.33 (5% EtOAc/Hex with 1% acetic acid

additive). ^{1}H NMR (400 MHz, $CDCl_3$) δ 11.96 (s, 1H), 7.64 (dd, *J* = 8.0, 1.6 Hz, 1H), 7.49 (ddd, *J* = 8.8, 7.2, 2.0 Hz, 1H), 7.05 (dd, *J* = 8.4, 0.8 Hz), 6.86 (ddd, *J* = 8.0, 7.2, 1.2 Hz, 1H), 6.78 (d, *J* = 2.4 Hz, 2H), 6.65 (t, *J* = 2.4 Hz, 1H), 3.82 (s, 6H). ^{13}C NMR (101 MHz, $CDCl_3$) δ 201.5, 163.3, 160.7, 139.8, 136.6, 133.7, 119.2, 118.8, 118.5, 107.1, 104.1, 55.7. IR (neat) 1626 cm^{-1}. HRMS (ESI) calcd for $C_{15}H_{13}O_4$ $[M-H]^-$ *m/z* 257.0819; found 257.0826.

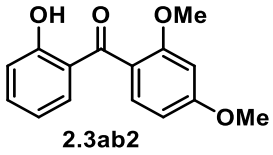

2.3ab2

(2,4-dimethoxyphenyl)(2-hydroxyphenyl)methanone (**2.3ab2**). Prepared using procedure C with no hydrolysis in the same reaction as **2.3ab1**; isolated by column chromatography. Brown oil (0.066 g, 0.256 mmol, 32%). R_f = 0.22 (5% EtOAc/Hex with 1% acetic acid additive). ^{1}H NMR (400 MHz, $CDCl_3$) δ 12.22 (s, 1H), 7.45 (ddd, *J* = 8.7, 7.2, 1.6 Hz, 1H), 7.40 (dd, *J* = 8.0, 1.6 Hz, 1H), 7.28 (d, *J* = 8.4 H, 1H), 7.01 (dd, *J* = 8.4, 1.2 Hz, 1H), 6.80 (ddd, *J* = 8.0, 7.2, 1.2 Hz, 1H), 6.56 (dd, *J* = 8, 2 Hz, 1H), 6.54 (d, *J* = 2.4 Hz, 1H), 3.87 (s, 3H), 3.75 (s, 3H). ^{13}C NMR (101 MHz, $CDCl_3$) δ 201.3, 163.3, 163.0, 158.7, 136.2, 133.9, 131.1, 120.9, 120.6, 118.6, 118.1, 104.7, 99.0, 55.8, 55.7. IR (thin film, CH_2Cl_2) 1606 cm^{-1}. HRMS (ESI) calcd for $C_{15}H_{13}O_4$ $[M-H]^-$ *m/z* 257.0819; found 227.0832.

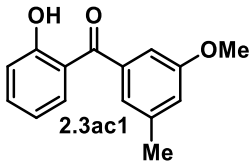

2.3ac1

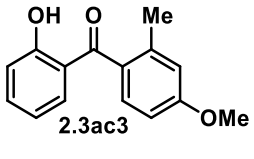

2.3ac3

(3-methoxy-5-methylphenyl)(2-hydroxyphenyl)methanone (**2.3ac1**), (4-methoxy-2-methylphenyl)(2-hydroxyphenyl)methanone (**2ac3**). Prepared using procedure A in the

same reaction as **2.3ac2**; isolated by column chromatography as an inseparable mixture of isomers (9:1 **2.3ac1**: **2.3ac3**). Yellow oil (0.109 mg, 0.450 mmol, 57%) R_f = 0.42 (10% EtOAc/Hex). ^{1}H NMR (400 MHz, $CDCl_3$) **2.3ac1**: δ 12.01 (s, 1H), 7.62 (dd, *J* = 8.0, 1.6 Hz, 1H), 7.51 (ddd, *J* = 8.4, 7.2, 1.6 Hz, 1H), 7.08–7.04 (m, 2H), 7.00–6.98 (m, 1H), 6.95–6.93 (m, 1H), 6.87 (ddd, *J* = 8.0, 7.2, 1.2 Hz, 1H), 3.84 (s, 3H), 2.40 (s, 3H); **2.3ac3**: δ 12.27 (s, 1H), 7.37 (dd, *J* = 8.0, 1.8 Hz, 1H), 6.84–6.76 (m, 3H), 3.86 (s, 3H), 2.34 (s, 3H). ^{13}C NMR (101 MHz, $CDCl_3$, only **2.3ac1** observed) δ 201.8, 163.3, 159.6, 139.9, 139.2, 136.5, 133.8, 122.5, 119.3, 118.81, 118.76, 118.5, 111.3, 55.6, 21.7. IR (thin film, CH_2Cl_2) 1627 cm^{-1}. HRMS (ESI) calcd for $C_{15}H_{14}O_3$ $[M-H]^-$ *m/z* 241.0870; found 241.0870.

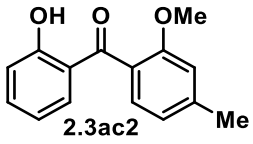

2.3ac2

(2-methoxy-4-methylphenyl)(2-hydroxyphenyl)methanone (**2.3ac2**). Prepared using procedure A in the same reaction as **2.3ac1** and **2.3ac3**; isolated by column chromatography. Yellow solid (0.027 g, 0.11 mmol, 14%). mp = 97–99 °C. R_f = 0.31 (10% EtOAc/Hex). ^{1}H NMR (400 MHz, $CDCl_3$) δ 12.21 (s, 1H), 7.45 (ddd, *J* = 8.8, 7.2, 1.6 Hz, 1H), 7.36 (dd, *J* = 8.0, 1.6 Hz, 1H), 7.19 (d, *J* = 7.6 Hz, 1H), 7.02 (dd, *J* = 8.4, 9.2 Hz, 1H), 6.86 (d, *J* = 7.6 Hz, 1H), 6.82 (s, 1H), 6.79 (t, *J* = 8.0 Hz, 1H), 3.76 (s, 3H), 2.43 (s, 3H). ^{13}C NMR (101 MHz, $CDCl_3$) δ 202.3, 163.0, 156.9, 142.8, 136.4, 134.0, 129.2, 125.2, 121.3, 120.5, 118.7, 118.1, 112.4, 55.7, 22.0. IR (thin film, CH_2Cl_2) 1626 cm^{-1}. HRMS (ESI) calcd for $C_{15}H_{14}O_3$ $[M-H]^-$ *m/z* 241.0870; found 241.0875.

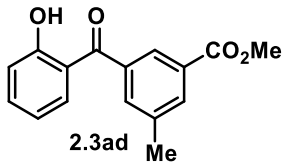

2.3ad

Methyl 5-(2-hydroxybenzoyl)-3-methylbenzoate (**2.3ad**)[c]. Prepared using procedure A with no hydrolysis. Brown oil (0.086 g, 0.321 mmol, 40%). R_f = 0.24 (10% Et_2O/Hex). ^1H NMR (400 MHz, $CDCl_3$) δ 11.94 (s, 1H), 8.12 (br s, 1H), 8.08 (br s, 1H), 7.68 (br s, 1H), 7.53 (ddd, *J* = 8, 6.4, 1.6 Hz, 2H), 7.09 (dd, *J* = 8.8, 1.2 Hz), 6.95–6.85 (m, 2H), 3.94 (s, 3H), 2.50 (s, 3H). ^{13}C NMR (101 MHz, $CDCl_3$) δ 201.0, 166.5, 163.4, 139.1, 138.4, 136.8, 133.8, 133.5, 133.5, 130.4, 127.6, 119.1, 119.0, 118.7, 52.5, 21.4. IR (thin film, CH_2Cl_2) 1725, 1628 cm^{-1}. HRMS (ESI) calcd for $C_{16}H_{13}O_4$ $[M-H]^-$ *m/z* 269.0819; found 269.0830.

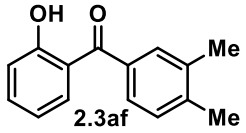

2.3af

(3,4-dimethylphenyl)(2-hydroxyphenyl)methanone (**2.3af**). Prepared using procedure C. Yellow oil (0.143 g, 0.630 mmol, 79%). mp = 74–77 °C. R_f = 0.27 (4% EtOAc/Hex). ^1H NMR (400 MHz, $CDCl_3$) δ 12.06 (s, 1H), 7.63 (dd, *J* = 8.0, 1.6 Hz, 1H), 7.52–7.47 (m, 2H), 7.42 (dd, *J* = 8.0, 2.0 Hz, 1H), 7.06 (dd, *J* = 8.4, 0.8 Hz, 1H), 6.87 (ddd, *J* = 8.4, 7.6, 2.0, 1H), 7.26 (d, *J* = 7.3 Hz, 1H), 2.36 (s, 3H), 2.34 (s, 3H). ^{13}C NMR (101 MHz, $CDCl_3$) δ 201.5, 163.1, 141.4, 136.9, 136.0, 135.6, 133.6, 130.4, 129.5, 127.1, 119.4, 118.5, 118.3, 20.0, 19.8. IR (thin film, CH_2Cl_2) 1626 cm^{-1}. HRMS (ESI) calcd for $C_{15}H_{13}O_2$ $[M-H]^-$ *m/z* 225.0921; found 225.0921.

[c] Arene prepared following literature procedure[213]

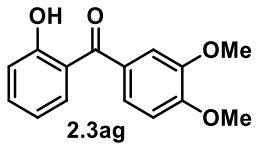

2.3ag

(3,4-dimethoxyphenyl)(2-hydroxyphenyl)methanone (**2.3ag**). Prepared using procedure A with no hydrolysis. Brown solid (0.192 g, 0.74 mmol, 93%). mp = 67–68 °C. R_f = 0.29 (20% EtOAc/Hex). ^{1}H NMR (400 MHz, $CDCl_3$) δ 11.88 (s, 1H), 7.67 (dd, *J* = 8.0, 1.6 Hz, 1H), 7.50 (ddd, *J* = 8.4, 7.2, 1.6 Hz, 1H), 7.33 (dd, *J* = 8.4, 2.0 Hz, 1H), 7.31 (d, *J* = 2.0 Hz, 1H), 7.07 (dd, *J* = 8.4, 0.9 Hz, 1H), 6.95 (d, *J* = 8.2 Hz, 1H), 6.89 (ddd, *J* = 8.2, 7.3, 1.1 Hz, 1H), 3.98 (s, 3H), 3.94 (s, 3H). ^{13}C NMR (101 MHz, $CDCl_3$) δ 200.1, 163.0, 152.8, 149.1, 136.0, 133.4, 130.5, 124.4, 119.5, 118.6, 118.5, 112.2, 110.1, 56.3, 56.2. IR (thin film, CH_2Cl_2) 1624 cm^{-1}. HRMS (ESI) calcd for $C_{15}H_{13}O_4$ $[M-H]^-$ *m/z* 257.0819; found 257.0829.

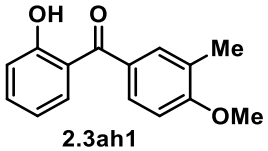

2.3ah1

2-hydroxyphenyl)(4-methoxy-3-methylphenyl)methanone (**2.3ah1**). Prepared using procedure A in the same reaction as **2.3ah2**; isolated by column chromatography. Yellow oil (0.098 g, 0.404 mmol, 50%). R_f = 0.21 (4% EtOAc/Hex). ^{1}H NMR (400 MHz, $CDCl_3$) δ 12.00 (s, 1H), 7.66 (dd, *J* = 8.0, 1.6 Hz, 1H), 7.50 (ddd, *J* = 8.8, 7.6, 1.6 Hz, 1H), 7.24 (dd, *J* = 8.0, 0.8 Hz, 1H), 7.19 – 7.16 (m, 2H), 7.07 (dd, *J* = 8.4, 0.8 Hz, 1H), 6.88 (ddd, *J* = 8.4, 7.2, 1.2 Hz, 1H), 3.89 (s, 3H), 2.31 (s, 3H). ^{13}C NMR (101 MHz, $CDCl_3$) δ 201.4, 163.2, 157.9, 136.7, 136.2, 133.7, 131.9, 130.2, 122.2, 119.4, 118.7, 118.5, 110.3, 55.6,

16.6. IR (neat) 1629 cm^{-1}. HRMS (ESI) calcd for $C_{16}H_{15}O_5$ $[M-H]^-$ *m/z* 241.0870; found 241.0865.

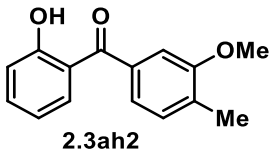

2.3ah2

(2-hydroxyphenyl)(3-methoxy-4-methylphenyl)methanone (**2.3ah2**). Prepared using procedure A in the same reaction as **2.3ah1**; isolated by column chromatography. Yellow solid (0.039 g, 0.16 mmol, 20%). mp = 75-76 °C. R_f = 0.16 (4% EtOAc/Hex). ^{1}H NMR (400 MHz, $CDCl_3$) δ 11.99 (s, 1H), 7.65 (dd, *J* = 8, 1.6 Hz, 1H), 7.61 – 7.55 (m, 2H), 7.49 (ddd, *J* = 8.8, 7.2, 1.6 Hz, 1H), 7.06 (dd, *J* = 8.4, 0.8 Hz, 1H), 6.90 (d, *J* = 8.4 Hz, 1H), 6.88 (ddd, *J* = 8.4, 7.2, 1.2 Hz, 1H), 3.92 (s, 3H), 2.28 (s, 3H). ^{13}C NMR (101 MHz, $CDCl_3$) δ 200.3, 162.9, 161.2, 135.7, 133.4, 132.1, 129.9, 129.7, 127.0, 119.5, 118.4, 118.3, 109.1, 55.6, 16.3. IR (thin film, CH_2Cl_2) 1625 cm^{-1}. HRMS (ESI) calcd for $C_{16}H_{15}O_5$ $[M-H]^-$ *m/z* 241.0870; found 241.0877.

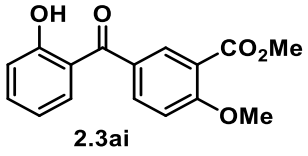

2.3ai

Methyl 5-(2-hydroxybenzoyl)-2-methoxybenzoate (**2.3ai**). Prepared using procedure A with no hydrolysis. Yellow solid (0.113 g, 0.394 mmol, 49%). mp = 117–119 °C. R_f = 0.07 (25% EtOAc/Hex with 2% acetic acid additive). ^{1}H NMR (400 MHz, $CDCl_3$) δ 11.85 (s, 1H), 8.21 (d, *J* = 2.4 Hz), 7.89 (dd, *J* = 8.8, 2.4 Hz, 1H), 7.59 (dd, *J* = 8.0, 1.6 Hz, 1H), 7.52 (ddd, *J* = 8.4, 7.2, 1.6 Hz, 1H), 7.12–7.06 (m, 2H), 6.91 (ddd, *J* = 8.0, 7.2, 1.2 Hz, 1H), 4.01 (s, 3H), 3.91 (s, 3H). ^{13}C NMR (101 MHz, $CDCl_3$) δ 199.3, 165.8, 163.1, 162.1,

136.3, 135.2, 133.7, 133.2, 129.9, 120.1, 119.2, 118.9, 118.6, 111.9, 56.5, 52.5. IR (thin film, CH_2Cl_2) 1731, 1626 cm^{-1}. HRMS (ESI) calcd for $C_{16}H_{13}O_5$ $[M-H]^-$ *m/z* 285.0768; found 285.0762.

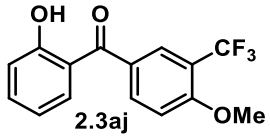

2.3aj

(2-hydroxyphenyl)(4-methoxy-3-(trifluoromethyl)phenyl)methanone (**2.3aj**). Prepared using procedure A light yellow solid (0.083 g, 0.280 mmol, 35%). mp = 68–70 °C. R_f = 0.34 (20% EtOAc/Hex). ^{1}H NMR (400 MHz, $CDCl_3$) δ 11.79 (s, 1H), 7.99 (d, *J* = 1.9 Hz, 1H), 7.91 (dd, *J* = 8.6, 1.9 Hz, 1H), 7.59–7.49 (m, 2H), 7.12 (d, *J* = 8.7 Hz, 1H), 7.09 (d, *J* = 8.4 Hz, 1H), 6.91 (t, *J* = 7.6 Hz, 1H), 4.01 (s, 3H). ^{13}C NMR (101 MHz, $CDCl_3$) δ 199.0, 163.2, 160.6, 136.5, 135.3, 133.0, 129.9, 129.2 (q, *J* = 5.3 Hz), 124.5, 121.8, 119.2 – 118.8 (m), 118.7, 111.7, 56.5. IR (thin film, CH_2Cl_2) 1632 cm^{-1}. HRMS (ESI) calcd for $C_{16}H_{16}O_4$ $[M-H]^-$ *m/z* 295.0588, found 295.0598.

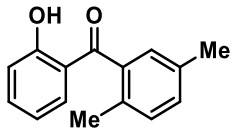

2.3ak

(2,5-dimethylphenyl)(2-hydroxyphenyl)methanone (**2.3ak**). Prepared using procedure C. Due to low yield, the product was unable to be fully purified, and is obtained with minor impurities. Brown oil (0.026 g, 0.114 mmol, 14%). R_f = 0.43 (10% EtOAc/Hex). ^{1}H NMR (400 MHz, $CDCl_3$) δ 12.26 (s, 1H), 7.49 (ddd, *J* = 8.8, 7.6, 1.6 Hz, 2H), 7.31 (dd, *J* = 8.0, 1.6 Hz, 1H), 7.21 (dd, *J* = 8.0, 2.0 Hz, 1H), 7.18 (d, *J* = 7.6 Hz, 1H), 7.07 (br s, 1H), 7.05 (dd, *J* = 8.0, 0.8 Hz, 1H), 2.35 (s, 3H), 2.24 (s, 3H). ^{13}C NMR (101 MHz, $CDCl_3$) δ 204.8,

163.4, 137.9, 136.8, 135.1, 133.9, 132.4, 131.0, 130.9, 128.0, 120.1, 119.0, 118.4, 21.0, 19.2. IR (neat) 1629 cm^{-1}. HRMS (ESI) calcd for $C_{15}H_{13}O_2$ $[M-H]^-$ *m/z* 225.0921; found 225.0932.

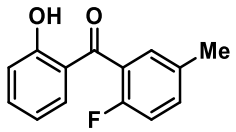

2.3al

(2-fluoro-5-methylphenyl)(2-hydroxyphenyl)methanone (**2.3al**). Prepared using procedure C. Brown oil (0.024 g, 0.104 mmol, 9%). R_f = 0.47 (10% EtOAc/Hex). ^{1}H NMR (400 MHz, $CDCl_3$) δ 11.98 (s, 1H), 7.51 (ddd, *J* = 8.8, 7.2, 1.6 Hz, 1H), 7.43 (ddd, *J* = 8.0, 2.8, 1.6 Hz, 1H), 7.32 (ddddd, *J* = 8.0, 7.2, 4.8, 2.4, 0.4 Hz, 1H), 7.25 (dd, *J* = 6.4, 2.0 Hz, 1H), 7.07 (t, *J* = 9.2 Hz, 1H), 7.05 (dd, *J* = 8.4, 0.8 Hz, 1H), 6.86 (ddd, *J* = 8.4, 7.2, 1.2 Hz, 1H), 2.38 (s, 3H). ^{13}C NMR (101 MHz, $CDCl_3$) δ 199.0, 163.1, 157.2 (d, J_{C-F} = 247.3), 137.1, 134.2 (d, J_{C-F} = 3.7 Hz), 133.6 (d, J_{C-F} = 6.2 Hz), 133.5 (d, J_{C-F} = 12.0 Hz), 130.1 (d, J_{C-F} = 2.7 Hz), 126.1 (d, J_{C-F} = 15.9 Hz), 119.9, 119.2, 118.4, 116.1 (d, *J* = 21.5 Hz), 20.7. ^{19}F {^{1}H} NMR (377 MHz, $CDCl_3$) δ −117.56. IR (neat) 1629 cm^{-1}. HRMS (QTOF) calcd for $C_{14}H_{11}FO_2$ $[M-H]^-$ *m/z* 230.0738; found 230.0742. "Through-space" $^5J_{C-F}$ coupling has been reported in the literature.[166,167]

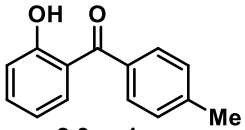

2.3am1

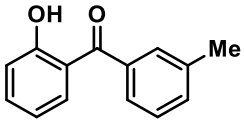

2.3am2

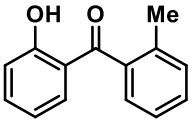

2.3am3

(2-hydroxyphenyl)(*o*-tolyl)methanone (**2.3am1**), (2-hydroxyphenyl)(*m*-tolyl)methanone (**2.3aa2**), (2-hydroxyphenyl)(*p*-tolyl)methanone (**2.3am3**). Prepared using procedure B. Yellow oil (0.128 g, 0.601 mmol, 50%) as an inseparable mixture of regioisomers (1:17:17

2.3am1:**2.3am2**:**2.3am3**). R_f = 0.44 (5% EtOAc/Hex). ^{1}H NMR (500 MHz, $CDCl_3$) **2.3am1**: δ 12.03 (s, 1H), 2.45 (s, 3H); **2.3am2**: δ 12.05 (s, 1H), 7.31 (dd, *J* = 8.0, 0.5 Hz, 2H), 2.44 (s, 3H); **2.3am3**: δ 12.25 (s, 1H), 6.81 (ddd, *J* = 8.5, 8, 1 Hz, 1H), 2.30 (s, 3H); Overlapping signals from **2.3am1** and **2.3am2**: δ 7.63–7.58 (m), 7.53–7.44 (m), 7.41–7.36 (m), 7.07 (m), 6.87 (m). ^{13}C NMR (126 MHz, $CDCl_3$, only **2.3am1** and **2.3am2** observed) δ 202.0, 201.5, 163.3, 163.2, 142.9, 138.4, 138.1, 136.4, 136.2, 135.3, 133.8, 133.7, 132.8, 129.7, 129.6, 129.2, 128.3, 126.5, 119.42, 119.36, 118.74, 118.68, 118.49, 118.48, 21.8, 21.5. IR (neat) 1626 cm^{-1}. HRMS (ESI) calcd for $C_{14}H_{11}O_2$ $[M-H]^-$ *m/z* 211.0765; found 211.0769.

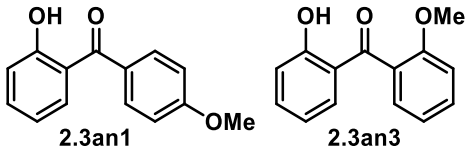

(2-hydroxyphenyl)(4-methoxyphenyl)methanone (**2.3an1**), (2-hydroxyphenyl)(2-methoxyphenyl)methanone (**2.3an3**). Prepared using procedure C in the same reaction as **2.3an2**; isolated by column chromatography as an inseparable mixture (10:1 **2.3an1**:**2.3an3**). Brown oil (0.164 g, 0.719 mmol, 60%) . R_f = 0.24 (8% Et_2O/Hex). ^{1}H NMR (400 MHz, $CDCl_3$) **2.3an1**: δ 11.96 (s, 1H), 7.74–7.70 (m, 2H), 7.63 (dd, *J* = 8.0, 2.0 Hz, 1H), 7.49 (ddd, *J* = 8.8, 7.2, 1.6 Hz, 1H), 7.06 (d, *J* = 8.4 Hz, 1H), 7.02–6.97 (m, 2H), 6.88 (ddd, *J* = 8.4, 7.2, 1.2 Hz), 3.90 (s, 3H); **2.3an3**: δ 12.17 (s, 1H), 7.33 (dd, *J* = 8.0, 1.7 Hz, 1H), 7.29 (dd, *J* = 7.5, 1.8 Hz, 1H), 6.80 (ddd, *J* = 8.1, 7.2, 1.1 Hz, 1H), 3.78 (s, 3H). ^{13}C NMR (101 MHz, $CDCl_3$, only **2.3an1** observed) δ 200.2, 163.1, 136.0, 133.4, 132.0, 130.5, 119.5, 118.6, 118.5, 113.8, 55.7. IR (neat) 1625 cm^{-1}. HRMS (ESI) calcd for $C_{14}H_{11}O_3$ $[M-H]^-$ *m/z* 227.0717; found 227.0711.

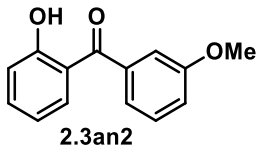

2.3an2

(2-hydroxyphenyl)(3-methoxyphenyl)methanone (**2.3an2**). Prepared using procedure C in the same reaction as **2.3an1**; isolated by column chromatography. Brown oil (0.038 g, 0.166 mmol, 14%). R_f = 0.32 (8% Et_2O/Hex). ^{1}H NMR (400 MHz, $CDCl_3$) δ 11.99 (s, 1H), 7.62 (dd, *J* = 8.0, 1.2 Hz, 1H), 7.51 (app t, *J* = 8.4 Hz, 1H), 7.41 (t, *J* = 8.0 Hz, 1H), 7.23 (d, *J* = 6.8 Hz, 1H), 7.20 (m, 1H) 7.12 (dd, *J* = 8.4, 2.4 Hz, 1H), 7.07 (d, *J* = 8.4 Hz, 1H), 6.87 (t, *J* = 8.0 Hz, 1H) 3.86 (s, 3H). ^{13}C NMR (101 MHz, $CDCl_3$) δ 201.5, 163.4, 159.7, 139.3, 136.5, 133.7, 129.5, 121.8, 119.3, 118.8, 118.5, 118.1, 114.1, 55.6. IR (neat) 1626 cm^{-1}. HRMS (ESI) calcd for $C_{14}H_{11}O_3$ $[M-H]^-$ *m/z* 227.0717; found 227.0714.

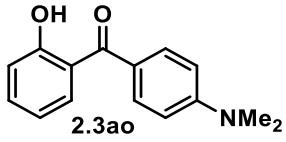

2.3ao

(4-(dimethylamino)phenyl)(2-hydroxyphenyl)methanone (**2.3ao**). Prepared using procedure C with no hydrolysis. Yellow solid (0.167 g, 0.692 mmol, 87%). mp = 58–60 °C. R_f = 0.33 (20% ethyl acetate in hexanes), 0.45 (3% EtOAc/benzene). ^{1}H NMR (400 MHz, $CDCl_3$) δ 12.00 (s, 1H), 7.75–7.70 (m, 2H), 7.68 (dd, *J* = 8.0, 1.6 Hz, 1H), 7.45 (ddd, *J* = 8.4, 7.2, 1.6 Hz, 1H), 7.05 (dd, *J* = 8.4, 0.8 Hz, 1H), 6.87 (ddd, *J* = 8.0, 7.2, 1.2 Hz, 1H), 6.74–6.69 (m, 2H), 3.09 (s, 6H). ^{13}C NMR (101 MHz, $CDCl_3$) δ 199.0, 162.7, 153.3, 135.1, 133.2, 132.5, 125.0, 120.1, 118.4, 118.2, 110.8, 40.2. IR (thin film, CH_2Cl_2) 1621 cm^{-1}. HRMS (ESI) calcd for $C_{15}H_{14}NO_2$ $[M-H]^-$ *m/z* 240.1030; found 240.1033.

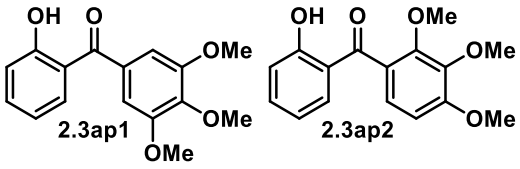

(3,4,5-trimethoxyphenyl)(2-hydroxyphenyl)methanone (**2.3ap1**), (2,3,4-trimethoxy)(2-hydroxyphenyl)methanone (**2.3ap2**). Prepared using procedure A. Yellow oil (0.176 g, 0.610 mmol, 76%) as an inseparable mixture of isomers (5:1 **2.3ap1**:**2.3ap2**). R_f = 0.22 (15% EtOAc/Hex). **2.3ap1**: ^{1}H NMR (500 MHz, $CDCl_3$) δ 11.87 (s, 1H), 7.67 (dd, *J* = 6.4, 1.2 Hz, 1H), 7.52 (ddd, *J* = 7.0, 5.7, 1.4 Hz, 1H), 7.09 (d, *J* = 6.7 Hz, 1H), 6.94 (s, 2H), 6.90 (t, *J* = 6.0 Hz, 1H), 3.95 (s, 3H), 3.90 (s, 6H); **2.3ap2**: δ 12.18 (s, 1H), 7.48 (ddd, *J* = 6.9, 5.7, 1.4 Hz, 1H), 7.41 (dd, *J* = 6.4, 1.2 Hz, 1H), 7.03 (d, *J* = 6.8 Hz, 2H), 6.83 (t, *J* = 5.9 Hz, 1H), 6.74 (d, *J* = 6.8 Hz, 1H), 3.93 (s, 3H), 3.92 (s, 3H), 3.83 (s, 3H). ^{13}C NMR (126 MHz, $CDCl_3$) **2.3ap1**: δ 200.7, 163.3, 153.1, 141.7, 136.4, 133.4, 133.1, 119.3, 118.6, 107.1, 61.2, 56.5; **2.3ap2**: δ 201.0, 163.1, 156.1, 151.9, 142.3, 136.6, 133.9, 125.7, 124.1, 120.4, 118.8, 118.2, 106.9, 62.1, 56.3. IR (neat) 1625 cm^{-1}. HRMS (ESI) calcd for $C_{16}H_{15}O_5$ $[M-H]^-$ *m/z* 287.0925; found 287.0931.

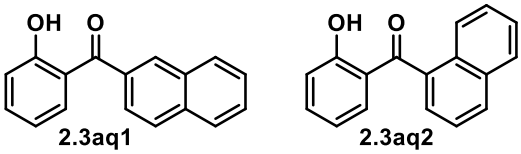

(2-hydroxyphenyl)(napthanlen-2-yl)methanone (**2.3aq1**), (2-hydroxyphenyl)(naphthalen-1-yl)methanone (**2.3aq2**). Prepared using procedure A. Yellow solid (0.150 g, 0.61 mmol, 78%) as an inseparable mixture of isomers (>20:1 ratio). mp = 80–82 °C. R_f = 0.19 (4% EtOAc/Hex). ^{1}H NMR (400 MHz, $CDCl_3$) **2.3aq1**: δ 12.04 (s, 1H), 8.19 (br s, 1H), 7.99–7.91 (m, 3H), 7.78 (dd, *J* = 8.8, 2.0 Hz, 1H), 7.68 (dd, *J* = 8.0, 1.6 Hz, 1H), 7.66–7.56 (m,

2H), 7.54 (ddd, *J* = 8.8, 7.2, 1.6 Hz, 1H), 7.11 (dd, *J* = 8.4, 1.2 Hz, 1H), 6.90 (ddd, *J* = 8.0, 7.2, 1.2 Hz, 1H); **2.3aq2**: δ 12.34 (s, 1 H). ^{13}C NMR (101 MHz, $CDCl_3$, only **2.3aq1** observed) δ 201.6, 163.4, 136.5, 135.3, 135.0, 133.8, 132.3, 130.6, 129.3, 128.5, 128.4, 128.0, 127.2, 125.5, 119.5, 118.9, 118.6. IR (thin film, CH_2Cl_2) 1625 cm^{-1}. HRMS (ESI) calcd for $C_{15}H_{14}O_3$ $[M-H]^-$ *m/z* 247.0765; found 247.0767.

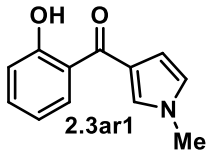

2.3ar1

(2-hydroxyphenyl)(1-methyl-1*H*-pyrrol-3-yl)methanone (**2.3ar1**). Prepared using procedure B in the same reaction as **2.3ar2**; isolated by column chromatography. Brown oil (0.143 g, 0.71 mmol, 59%). R_f = 0.24 (20% EtOAc/Hex). ^{1}H NMR (400 MHz, $CDCl_3$) δ 12.22 (s, 1H), 7.94 (dd, *J* = 8.0, 1.6 Hz, 1H), 7.44 (ddd, *J* = 8.8, 7.2, 1.6 Hz, 1H), 7.28 (t, *J* = 2.0 Hz, 1H), 7.02 (dd, *J* = 8.0, 0.8 Hz, 1H), 6.90 (ddd, *J* = 8.0, 7.2, 1.2 Hz, 1H), 6.70–6.65 (m, 2H), 3.74 (s, 3H). ^{13}C NMR (101 MHz, $CDCl_3$) δ 193.8, 162.5, 135.0, 131.9, 128.5, 123.8, 123.4, 120.7, 118.6, 118.2, 111.6, 36.9. IR (neat) 1621 cm^{-1}. HRMS (ESI) calcd for $C_{12}H_{11}NO_2$ $[M-H]^-$ *m/z* 200.0717; found 200.0720.

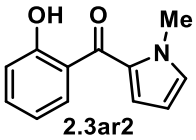

2.3ar2

(2-hydroxyphenyl)(1-methyl-1*H*-pyrrol-2-yl)methanone (**2.3ar2**).Prepared using procedure B in the same reaction as **2.3ar1**; isolated by column chromatography. Brown oil (0.018 g, 0.09 mmol, 7%). R_f = 0.48 (20% EtOAc/Hex). ^{1}H NMR (400 MHz, $CDCl_3$) δ 11.76 (s, 1H), 7.88 (dd, *J* = 8.0, 1.6 Hz, 1H), 7.45 (ddd, *J* = 8.8, 7.6, 1.6 Hz, 1H), 7.01 (dd,

J = 8.0, 0.8 Hz, 1H), 6.94 (t, *J* = 2.0 Hz, 1H), 6.89 (ddd, *J* = 8.0, 7.2, 1.2 Hz, 1H), 6.83 (dd, *J* = 4.0, 1.6 Hz, 1H), 6.20 (dd, *J* = 4.0, 2.4 Hz, 1H), 3.97 (s, 3H). ^{13}C NMR (101 MHz, $CDCl_3$) δ 188.9, 162.2, 134.9, 132.3, 131.7, 129.7, 122.7, 120.7, 118.5, 118.0, 108.5, 37.1. IR (thin film, CH_2Cl_2) 1621 cm^{-1}. HRMS (ESI) calcd for $C_{12}H_{11}NO_2$ $[M-H]^-$ *m/z* 200.0717; found 200.0719.

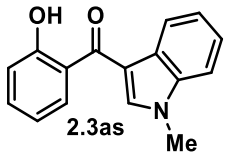

2.3as

(2-hydroxyphenyl)(1-methyl-1*H*-indol-3-yl)methanone (**2.3as**). Prepared using procedure A. Brown solid (0.146 g, 0.581 mmol, 73%). mp = 111–116 °C. R_f = 0.47 (50% EtOAc/Hex). ^{1}H NMR (400 MHz, $CDCl_3$) δ 12.03 (s, 1H), 8.33 – 8.26 (m, 1H), 7.85 (dd, *J* = 8.0, 9.6 Hz, 1H), 7.63 (s, 1H), 7.46 (ddd, *J* = 8.8, 7.6, 2.0 Hz), 7.40 – 7.31 (m, 3H), 7.05 (dd, *J* = 8.4, 1.2 Hz, 1H), 6.91 (ddd, *J* = 8.4, 7.6, 1.2 Hz, 1H), 3.86 (s, 3H). ^{13}C NMR (101 MHz, $CDCl_3$) δ 193.6, 162.0, 137.5, 137.0, 134.7, 131.5, 127.4, 123.9, 122.9, 122.5, 121.5, 118.7, 118.2, 114.8, 109.9, 33.8. IR (thin film, CH_2Cl_2) 1679 cm^{-1}. HRMS (ESI) calcd for $C_{16}H_{13}NO_2$ $[M-H]^-$ *m/z* 250.0874; found 250.0873.

***Meta*-Xylene Acylation Products:**

For all acylations of *m*-xylene, yield determined for the desired products based on relative integration in the ^{1}H NMR.

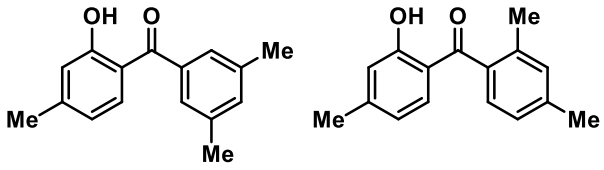

2.3bb1 **2.3bb2**

(3,5-dimethylphenyl)(2-hydroxy-4-methylphenyl)methanone (**2.3bb1**), (2,4-dimethylphenyl)(2-hydroxy-4-methylphenyl)methanone (**2.3bb2**): Prepared using procedure C; isolated by column chromatography. Yellow solid (0.086g, 0.358 mmol, 45%), as an inseparable mixture (2.3:1 **2.3bb1**/**2.3bb2**:**2.3aa1**, 10:1 **2.3bb1**:**2.3bb2**). R_f = 0.36 (5% EtOAc/Hex). ^{1}H NMR (500 MHz, $CDCl_3$) **2.3bb1**: δ 12.15 (s, 1H), 7.48 (d, *J* = 8.1 Hz, 1H), 7.26–7.22 (m, 2H), 7.20 (m, 1H), 6.88–6.85 (m, 1H), 6.68 (dd, *J* = 8.2, 1.6 Hz, 1H), 2.39 (s, 3H), 2.38 (s, 6H); **2.3bb2**: δ 11.95 (s, 1H). ^{13}C NMR (126 MHz, $CDCl_3$, only **2.3bb1** observed) δ 201.7, 163.5, 148.0, 138.3, 138.1, 133.7, 133.4, 126.9, 120.0, 118.5, 117.2, 22.1, 21.4. IR (neat) 1624 cm^{-1}. HRMS (ESI) calcd for $C_{16}H_{16}O_2$ $[M–H]^-$ *m/z* 239.1078, found 239.1086.

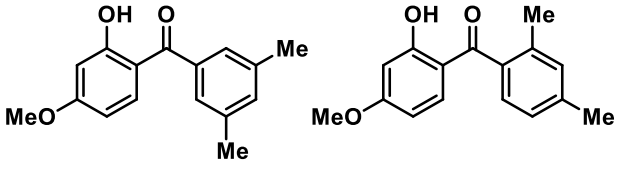

2.3bc1 **2.3bc2**

(3,5-dimethylphenyl)(2-hydroxy-4-methoxyphenyl)methanone (**2.3bc1**) , (2,4-dimethylphenyl)(2-hydroxy-4-methoxyphenyl)methanone (**2.3bc2**). Prepared using procedure C; isolated by column chromatography. Brown oil (0.0769g, 0.300 mmol, 38%),

as an inseparable mixture (4:1 **2.3bc1/2.3bc2**:**2.3aa1**, 10:1 **2.3bc1:2.3bc2**). R_f = 0.28 (5% EtOAc/Hex). ^{1}H NMR (500 MHz, $CDCl_3$) **2.3bc1**: δ 12.72 (s, 1H), 7.52 (d, *J* = 9.0 Hz), 7.22 (br s, 2H), 6.51 (d, *J* = 2.5 Hz, 1H), 6.41 (dd, *J* = 9.0, 2.5 Hz, 1H), 3.86 (s, 3H), 2.38 (s, 6H); **2.3bc2**: δ 12.83 (s, 1H), 3.85 (s, 3H), 2.38 (s, 6H). ^{13}C NMR (126 MHz, $CDCl_3$, only **2.3bc1** observed) δ 200.7, 166.4, 166.3, 138.5, 135.5, 133.9, 133.2, 126.7, 113.4, 107.4, 101.2, 55.8, 21.4. IR (neat) 1621 cm^{-1}. HRMS (ESI) calcd for $C_{16}H_{16}O_3$ $[M–H]^-$ *m/z* 256.1099, found 255.1036.

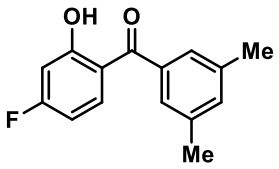

2.3bd1

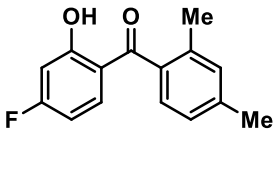

2.3bd2

(3,5-dimethylphenyl)(4-fluoro-2-hydroxyphenyl)methanone (**2.3bd1**), (2,4-dimethylphenyl)(4-fluoro-2-hydroxyphenyl)methanone (**2.3bd2**). Prepared using procedure C; isolated by column chromatography. Yellow oil (0.102g, 0.416 mmol, 52%), as an inseparable mixture (4:1 **2.3bd1**/**2.3bd2**:**2.3aa1**, >20:1 **2.3bd1**:**2.3bd2**). R_f = 0.32 (5% EtOAc/Hex). ^{1}H NMR (500 MHz, $CDCl_3$) **2.3bd1**: δ 12.46 (d, $^5J_{H–F}$ = 1.5 Hz, 1H), 7.62 (dd, *J* = 9.0, 6.6 Hz, 1H), 7.24–7.23 (m, 2H), 7.23–7.21 (m, 1H), 6.74 (dd, *J* = 10.4, 2.5 Hz, 1H), 6.58 (ddd, *J* = 9.0, 8.0, 2.5 Hz, 1H) 2.39 (s, 6H); **2.3bd2**: δ 12.63 (d, $^5J_{H–F}$ = 1.4 Hz, 1H), 2.39 (s, 6H). ^{19}F NMR (471 MHz, $CDCl_3$) -98.79 (q, J = 8.6 Hz). ^{13}C NMR (126 MHz, $CDCl_3$, only **2.3bd1** observed) δ 201.2, 167.5 (d, $^1J_{C–F}$ = 257.1 Hz), 165.9 (d, $^3J_{C–F}$ = 14.2 Hz), 138.3, 138.0, 136.2 (d, $^3J_{C–F}$ = 11.7 Hz), 126.8, 116.5 (d, $^4J_{C–F}$ = 2.2 Hz), 107.0 (d, $^2J_{C–F}$ = 22.5 Hz), 105.1 (d, $^2J_{C-F}$ = 23.8 Hz), 21.4. ^{19}F NMR (471 MHz, $CDCl_3$)

−99.43 (q, J = 8.3 Hz). IR (neat) 1623 cm^{-1}. HRMS (ESI) calcd for $C_{15}H_{13}FO_2$ $[M–H]^-$ *m/z* 243.0827, found 243.0833.

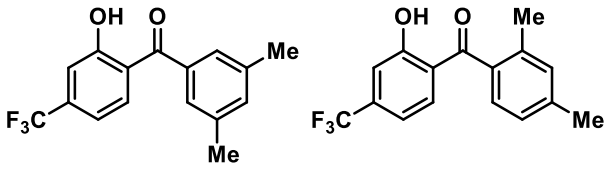

(3,5-dimethylphenyl)(2-hydroxy-4-(trifluoromethyl)phenyl)methanone (**2.3be1**), (2,4-dimethylphenyl)(2-hydroxy-4-(trifluoromethyl)phenyl)methanone (**2.3be2**). Prepared using procedure C; isolated by column chromatography. Brown oil (0.105g, 0.357 mmol, 45%), as an inseparable mixture (7:1 **2.3be1**/**2.3ed2**:**2.3aa1**, 13:1 **2.3be1:2.3be2**). R_f = 0.39 (5% EtOAc/Hex). ^1H (500 MHz, CD_2Cl_2) **2.3be1**: δ 11.99 (s, 1H), 7.77 (d, J = 8.3 Hz, 1H), 7.32 (d, J = 1.3 Hz, 1H), 7.29 (s, 3H), 7.14 (dd, J = 8.3, 1.4 Hz, 1H), 2.40 (s, 3H); **2.3be2**: δ 12.26 (s, 1H), 7.18 (d, J = 7.8 Hz, 1H), 7.17 (s, 1H), 7.07 (dd, J = 8.4, 1.8 Hz, 1H), 2.40 (s, 6H). ^{13}C (126 MHz, CD_2Cl_2, only **2.3be1** observed) δ 201.1, 163.4, 139.0, 137.8, 137.2 (q, $^2J_{C–F}$ = 32.8 Hz), 135.0, 134.8, 127.5, 127.4, 123.8 (q, $^1J_{C–F}$ = 273.4 Hz), 116.0 (q, $^3J_{C–F}$ = 3.9 Hz), 115.5 (q, $^3J_{C–F}$ = 3.6 Hz), 21.5. ^{19}F (471 MHz, CD_2Cl_2) **2.3be1**: δ −64.13; **2.3be2**: δ −64.18. IR (neat) 1639 cm^{-1}. HRMS (ESI) calcd for $C_{16}H_{13}F_3O_2$ $[M–H]^-$ *m/z* 293.0795, found 293.0789.

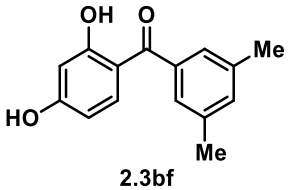

(3,5-dimethylphenyl)(2,4-dihydroxyphenyl)methanone (**2.3bf**). Prepared using procedure C; isolated by column chromatography. Yellow solid (0.0306g, 0.126 mmol, 16%). R_f =

0.16 (10% EtOAc/Hex). ^{1}H NMR (500 MHz, Acetone-d_6) δ 12.70 (s, 1H), 9.64 (br s, 1H), 7.52–7.48 (m, 1H), 7.25 (s, 1H), 7.24 (s, 2H), 6.45–6.41 (m, 2H), 2.38 (s, 6H). ^{13}C NMR (126 MHz, Acetone-d_6) δ 201.2, 167.3, 165.8, 139.5, 138.9, 136.9, 133.7, 127.2, 113.5, 108.7, 103.8, 21.3. IR (neat) 1623 cm^{-1}. HRMS (ESI) calcd for $C_{15}H_{14}O_3$ $[M–H]^-$ *m/z* 241.0870, found 241.0874.

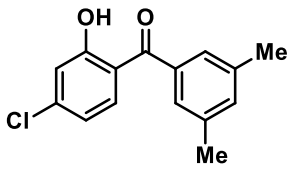

2.3bg1

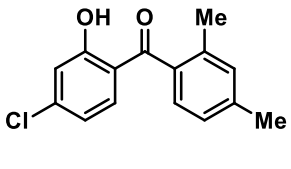

2.3bg2

(3,5-dimethylphenyl)(4-chloro-2-hydroxyphenyl)methanone (**2.3bg1**), (2,4-dimethylphenyl)(4-chloro-2-hydroxyphenyl)methanone (**2.3bg2**). Prepared using procedure C; isolated by column chromatography. Brown solid (0.0897g, 0.344 mmol, 43%), as an inseparable mixture (18:1 **2.3bg1**/**2.3bg2**:**2.3aa1**, 20:1 **2.3bg1**:**2.3bg2**). R_f = 0.40 (5% EtOAc/Hex). ^{1}H NMR (500 MHz, $CDCl_3$) **2.3bg1**: δ 12.22 (s, 1H), 7.54 (d, *J* = 8.6 Hz, 1H), 7.24 (br s, 2H), 7.23 (br s, 1H), 7.08 (d, *J* = 2.0 Hz, 1H), 6.85 (dd, *J* = 8.6, 2.1 Hz, 1H), 2.39 (s, 6H); **2.3bg2**: δ 12.42 (s, 1H), 2.28 (s, 3H). ^{13}C NMR (126 MHz, $CDCl_3$, only **2.3bg1** observed) δ 201.5, 164.0, 142.2, 138.4, 137.8, 134.7, 134.0, 126.9, 119.4, 118.6, 118.0, 21.4. IR (neat) 1618 cm^{-1}. HRMS (ESI) calcd for $C_{15}H_{13}ClO_2$ $[M–H]^-$ *m/z* 259.0531, found 259.0533.

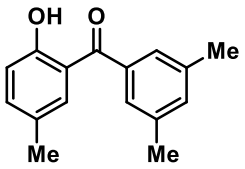

2.3bh1

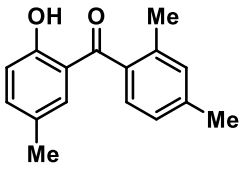

2.3bh2

(3,5-dimethylphenyl)(2-hydroxy-5-methylphenyl)methanone (**2.3bh1**), (2,4-dimethylphenyl)(2-hydroxy-5-methylphenyl)methanone (**2.3bh2**). Prepared using procedure C; isolated by column chromatography. Yellow solid (0.0574g, 0.239 mmol, 30%), as an inseparable mixture (1.8:1 **2.3bh1**/**2.3bh2**:**2.3aa1**, 18:1 **2.3bh1**:**2.3bh2**). R_f = 0.37 (5% EtOAc/Hex). ^{1}H NMR (500 MHz, $CDCl_3$) **2.3bh1**: δ 11.87 (s, 1H), 7.36 (d, *J* = 1.9 Hz, 1H), 7.31 (dd, *J* = 8.5, 2.3 Hz, 1H), 7.26 (m, 1H), 7.22 (br s, 1H), 6.97 (d, *J* = 8.4 Hz, 1H), 2.39 (s, 6H), 2.25 (s, 3H); **2.3bh1**: δ 12.12 (s 1H). ^{13}C NMR (126 MHz, $CDCl_3$, only **2.3bh1** observed) δ 202.3, 161.2, 138.3, 137.4, 133.5, 133.4, 127.8, 126.9, 119.1, 118.4, 118.2, 21.4, 20.6. IR (neat) 1630 cm^{-1}. HRMS (ESI) calcd for $C_{16}H_{16}O_2$ $[M–H]^-$ *m/z* 239.1078, found 239.1089.

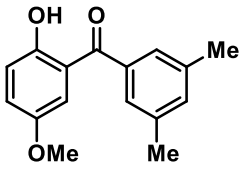

2.3bi1

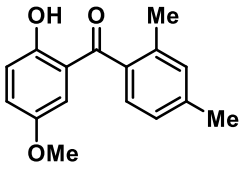

2.3bi2

(3,5-dimethylphenyl)(2-hydroxy-5-methoxyphenyl)methanone (**2.3bi1**), (2,4-dimethylphenyl)(2-hydroxy-5-methoxyphenyl)methanone (**2.3bi2**). Prepared using procedure C; isolated by column chromatography. Orange oil (0.085g, 0.331 mmol, 41%), as an inseparable mixture (2.6:1 **2.3bi1**/**2.3bi2**:**2.3aa1**, >20:1 **2.3bi1**:**2.3bi2**). R_f = 0.26(5% EtOAc/Hex). ^{1}H NMR (500 MHz, $CDCl_3$) δ 11.61 (s, 1H), 7.29 (br s, 2H), 7.22 (br s, 1H), 7.14 (dd, *J* = 9.1, 3.1 Hz, 1H), 7.08 (d, *J* = 3.1 Hz, 1H), 7.01 (d, *J* = 9.1 Hz, 1H), 3.70 (s,

3H), 2.39 (s, 6H) **2.3bi2**: δ 11.89 (s, 1H), 3.64 (s, 3H), 2.30 (s, 3H). ^{13}C NMR (126 MHz, $CDCl_3$, only **2.3bi1** observed) δ 201.8, 157.6, 151.5, 138.2, 138.1, 133.7, 126.9, 124.1, 119.3, 119. 0, 116.6, 56.1, 21.4. IR (neat) 1626 cm^{-1}. HRMS (ESI) calcd for $C_{16}H_{16}O_3$ [M–H]$^-$ *m/z* 255.1027, found 255.1034.

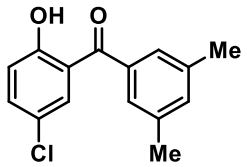

2.3bj1

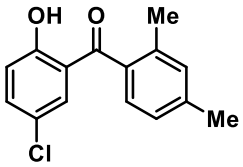

2.3bj2

(3,5-dimethylphenyl)(5-chloro-2-hydroxyphenyl)methanone (**2.3bj1**), (2,4-dimethylphenyl)(5-chloro-2-hydroxyphenyl)methanone (**2.3bj2**). Prepared using procedure C; isolated by column chromatography. Yellow solid (0.092g, 0.351 mmol, 44%), as an inseparable mixture (5.5:1 **2.3bj1/2.3bj2**:**2.3aa1**, 19:1 **2.3bj1**:**2.3bj2**). R_f = 0.39 (5% EtOAc/Hex). ^{1}H NMR (500 MHz, $CDCl_3$) **2.3bj1**: δ 11.94 (s, 1H), 7.56 (d, *J* = 2.6 Hz, 1H), 7.44 (dd, *J* = 8.9, 2.7 Hz, 1H), 7.25 (m, 3H), 7.02 (d, *J* = 8.9 Hz, 1H), 2.40 (s, 6H); **2.3bj2**:z δ 12.18 (s, 1H), 2.29 (s, 3H). ^{13}C NMR (126 MHz, $CDCl_3$, only **2.3bj1** observed) δ 201.3, 161.8, 138.5, 137.5, 136.2, 134.1, 132.6, 126.8, 123.4, 120.10, 120.08, 21.4. IR (neat) 1621 cm^{-1}. HRMS (ESI) calcd for $C_{15}H_{13}ClO_2$ [M–H]$^-$ *m/z* 259.0531, found 259.0535.

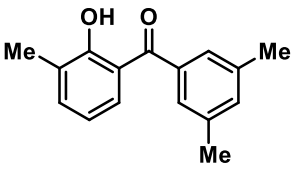

2.3bk1

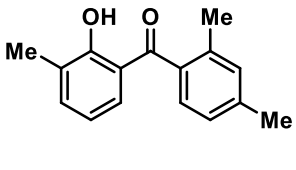

2.3bk2

(3,5-dimethylphenyl)(2-hydroxy-3-methylphenyl)methanone (**2.3bk1**), (2,4-dimethylphenyl)(2-hydroxy-3-methylphenyl)methanone (**2.3bk2**). Prepared using

procedure C; isolated by column chromatography. Brown oil (0.082g, 0.343 mmol, 43%), as an inseparable mixture (3:1 **2.3bk1/2.3bk2**:**2.3aa1**, 10:1 **2.3bk1**:**2.3bk2**). R_f = 0.45 (5% EtOAc/Hex). ^{1}H NMR (500 MHz, $CDCl_3$) δ 12.15 (s, 1H), 7.48 (d, *J* = 8.2 Hz, 1H), 7.25 (br s, 2H), 7.20 (br s, 1H) 6.87 (m, 1H), 6.68 (dd, *J* = 8.0, 0.9 Hz, 1H), 2.38 (s, 6H), 2.37 (s, 3H); **2.3bk2**: δ 11.95 (s, 1H), 7.55 (s, 1H), 6.95 (s, 2H), 2.40 (s, 9H). ^{13}C NMR (126 MHz, $CDCl_3$, only **2.3bk1** observed) δ 201.8, 163.5, 148.0, 138.3, 138.1, 133.7, 133.4, 126.9, 126.8, 120.0, 118.4, 117.2, 22.1. IR (neat) 1618 cm^{-1}. HRMS (ESI) calcd for $C_{16}H_{16}O_2$ $[M–H]^-$ *m/z* 239.1078, found 239.1073.

1,2-Dimethoxybenzene Acylation Products:

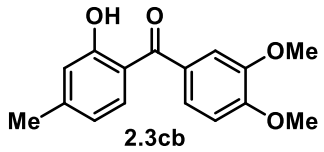

2.3cb

(3,4-dimethoxyphenyl)(2-hydroxy-4-methylphenyl)methanone (**2.3cb**). Prepared using procedure A; isolated by column chromatography. Light yellow solid (0.169g, 0.616 mmol, 77%). mp = 135–138 °C. R_f = 0.39 (30% EtOAc/Hex). ^{1}H NMR (400 MHz, $CDCl_3$) δ 12.00 (s, 1H), 7.55 (d, *J* = 8.1 Hz, 1H), 7.36–7.23 (m, 2H), 6.94 (d, *J* = 8.1 Hz, 1H), 6.88 (s, 1H), 6.70 (d, *J* = 8.2 Hz, 1H), 3.97 (s, 3H), 3.94 (s, 4H), 2.38 (s, 3H). ^{13}C NMR (101 MHz, $CDCl_3$) δ 199.6, 163.2, 152.5, 149.0, 147.6, 133.3, 130.7, 124.1, 119.9, 118.5, 117.2, 112.1, 110.1, 56.2, 56.1, 22.0. IR (thin film, CH_2Cl_2) 1625 cm^{-1}. HRMS (ESI) calcd for $C_{16}H_{16}O_4$ $[M−H]^-$ *m/z* 271.0976, found 271.0977.

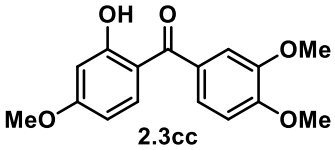

2.3cc

(3,4-dimethoxyphenyl)(2-hydroxy-4-methoxyphenyl)methanone (**2.3cc**). Prepared using procedure A; isolated by column chromatography. Light yellow solid (0.183 g, 0.640 mmol, 80%). mp = 135–137 °C. R_f = 0.29 (30% EtOAc/Hex). ^{1}H NMR (400 MHz, $CDCl_3$) δ 12.62 (s, 1H), 7.59 (d, *J* = 9.0 Hz, 1H), 7.31–7.23 (m, 1H), 6.94 (d, *J* = 8.1 Hz, 1H), 6.52 (d, *J* = 2.5 Hz, 1H), 6.43 (dd, *J* = 8.9, 2.5 Hz, 1H), 3.97 (s, 3H), 3.94 (s, 3H), 3.87 (s, 3H). ^{13}C NMR (101 MHz, $CDCl_3$) δ 198.7, 166.2, 166.0, 152.3, 149.1, 135.1, 130.9, 123.7, 113.4, 112.0, 110.1, 107.3, 101.3, 56.2, 56.2, 55.7. IR (thin film, CH_2Cl_2) 1623 cm^{-1}. HRMS (ESI) calcd for $C_{16}H_{16}O_5$ $[M-H]^-$ *m/z* 287.0925, found 287.0922.

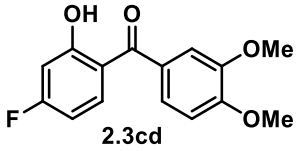

2.3cd

(3,4-dimethoxyphenyl)(4-fluoro-2-hydroxyphenyl)methanone (**2.3cd**). Prepared using procedure A; isolated by column chromatography. Light yellow solid (0.656 mmol, 0.182 g, 82%). mp = 103–105 °C. R_f = 0.37 (30% EtOAc/Hex). ^{1}H NMR (400 MHz, $CDCl_3$) δ 12.31 (s, 1H), 7.69 (dd, *J* = 8.9, 6.6 Hz, 1H), 7.31 – 7.25 (m, 2H), 6.95 (d, *J* = 8.2 Hz, 1H), 6.75 (dd, *J* = 10.4, 2.5 Hz, 1H), 6.60 (td, *J* = 8.6, 2.6 Hz, 1H), 3.98 (s, 3H), 3.94 (s, 3H). ^{13}C NMR (101 MHz, $CDCl_3$) δ 198.9, 168.5, 165.9, 165.5 (d, *J* = 14.3 Hz), 152.8, 149.2, 135.6 (d, *J* = 11.6 Hz), 130.3, 124.1, 116.4 (d, *J* = 2.3 Hz), 111.0 (d, *J* = 189.5 Hz), 106.7 (d, *J* = 22.5 Hz), 105.1 (d, *J* = 23.8 Hz), 56.2, 56.1. ^{19}F {^{1}H} NMR (376 MHz, $CDCl_3$) δ

−100.00. IR (thin film, CH_2Cl_2) 1628 cm^{-1}. HRMS (ESI) calcd for $C_{15}H_{13}FO_4$ $[M-H]^-$ *m/z* 275.0725, found 275.0724.

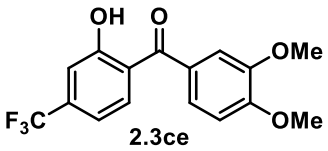

2.3ce

(3,4-dimethoxyphenyl)(2-hydroxy-4-(trifluoromethyl)phenyl)methanone (**2.3ce**). Prepared using procedure A; isolated by column chromatography. Yellow solid (0.230 g, 0.705 mmol, 88%). mp = 74–76 °C. R_f = 0.37 (30% EtOAc/Hex). ^{1}H NMR (400 MHz, $CDCl_3$) δ 11.78 (s, 1H), 7.79 (dd, *J* = 8.3, 1.0 Hz, 1H), 7.36–7.31 (m, 3H), 7.13 (dd, *J* = 8.3, 1.8 Hz, 1H), 6.96 (d, *J* = 8.8 Hz, 1H), 3.99 (s, 3H), 3.95 (s, 3H). ^{13}C NMR (101 MHz, $CDCl_3$) δ 199.0, 162.7, 153.4, 149.4, 136.7 (q, *J* = 33.0 Hz), 133.8, 129.8, 124.8, 123.3 (q, *J* = 273.5 Hz), 121.7, 115.8 (q, *J* = 3.9 Hz), 114.9 (q, *J* = 3.6 Hz), 112.1, 110.2, 56.3, 56.2. ^{19}F {^{1}H} NMR (376 MHz, $CDCl_3$) δ −63.78. IR (thin film, CH_2Cl_2) 1638 cm^{-1}. HRMS (ESI) calcd for $C_{16}H_{13}F_3O_4$ $[M-H]^-$ *m/z* 325.0693, found 325.0689.

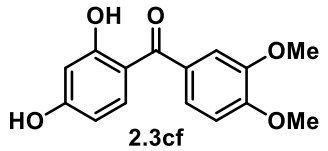

2.3cf

(3,4-dimethoxyphenyl) (2,4-dihydroxyphenyl)methanone (**2.3cf**). Prepared using procedure A; isolated by column chromatography. Light yellow solid (0.146 g, 0.536 mmol, 67%). mp = 174–172 °C. R_f = 0.36 (40% EtOAc/Hex). ^{1}H NMR (400 MHz, Acetone-d_6) δ 12.51 (s, 1H), 7.47 (d, *J* = 9.0 Hz, 1H), 7.18–7.11 (m, 2H), 6.95 (d, *J* = 8.9 Hz, 1H), 6.34–6.27 (m, 2H), 3.78 (s, 3H), 3.75 (s, 3H). ^{13}C NMR (101 MHz, Acetone-d_6) δ 199.4, 167.0, 165.5, 153.5, 150.1, 136.6, 131.6, 124.2, 113.5, 113.2, 111.5, 108.5, 103.9,

56.3, 56.2. IR (thin film, CH_2Cl_2) 1626 cm^{-1}. HRMS (ESI) calcd for $C_{15}H_{14}O_5$ $[M-H]^-$ *m/z* 273.0768, found 273.0766.

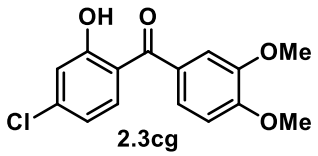

2.3cg

(3,4-dimethoxyphenyl)(4-chloro-2-hydroxyphenyl)methanone (**2.3cg**). Prepared using procedure A; isolated by column chromatography. Light yellow solid (0.108 g, 0.368 mmol, 46%). mp = 114–116 °C. R_f = 0.37 (30% EtOAc/Hex). ^{1}H NMR (400 MHz, $CDCl_3$) δ 12.06 (s, 1H), 7.60 (d, *J* = 8.6 Hz, 1H), 7.32–7.28 (m, 2H), 7.09 (d, *J* = 2.1 Hz, 1H), 6.95 (d, *J* = 8.1 Hz, 1H), 6.87 (dd, *J* = 8.6, 2.1 Hz, 1H), 3.98 (s, 3H), 3.94 (s, 3H). ^{13}C NMR (101 MHz, $CDCl_3$) δ 199.2, 163.7, 153.0, 149.3, 141.8, 134.3, 130.2, 124.3, 119.3, 118.6, 118.1, 112.1, 110.2, 56.3, 56.2. IR (thin film, CH_2Cl_2) 1622 cm^{-1}. HRMS (ESI) calcd for $C_{15}H_{13}ClO_4$ $[M-H]^-$ *m/z* 291.0430, found 291.0432.

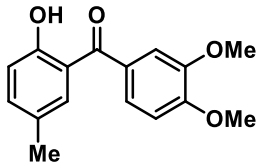

2.3ch

(3,4-dimethoxyphenyl)(2-hydroxy-5-methylphenyl)methanone (**2.3ch**). Prepared using procedure A; isolated by column chromatography. Light yellow solid (0.211 g, 0.776 mmol, 97%). mp = 113–116 °C. R_f = 0.34 (30% EtOAc/Hex). ^{1}H NMR (400 MHz, $CDCl_3$) δ 11.68 (s, 1H), 7.44 (d, *J* = 1.9 Hz, 1H), 7.35–7.29 (m, 3H), 6.98 (d, *J* = 8.4 Hz, 1H), 6.95 (d, *J* = 8.2 Hz, 1H), 3.98 (s, 3H), 3.94 (s, 3H), 2.28 (s, 3H). ^{13}C NMR (101 MHz, $CDCl_3$) δ 200.0, 160.9, 152.7, 149.1, 137.0, 133.1, 130.7, 127.7, 124.3, 119.2, 118.2, 112.2, 110.1,

56.2, 56.2, 20.7. IR (thin film, CH_2Cl_2) 1630 cm^{-1}. HRMS (ESI) calcd for $C_{16}H_{16}O_4$ $[M-H]^-$ *m/z* 271.0976, found 271.0982.

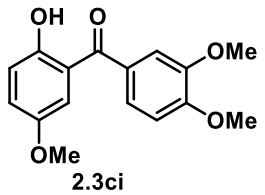

2.3ci

(3,4-dimethoxyphenyl)(2-hydroxy-5-methoxyphenyl)methanone (**2.3ci**). Prepared using procedure A; isolated by column chromatography. Yellow-orange solid (0.192 g, 0.664 mmol, 83%). mp = 86–87 °C. R_f = 0.28 (30% EtOAc/Hex). ^{1}H NMR (400 MHz, $CDCl_3$) δ 11.41 (s, 1H), 7.37 (dd, *J* = 8.3, 2.0 Hz, 1H), 7.33 (d, *J* = 2.0 Hz, 1H), 7.17–7.09 (m, 2H), 7.06–6.98 (m, 1H), 6.95 (d, *J* = 8.3 Hz, 1H), 3.98 (s, 3H), 3.95 (s, 3H), 3.73 (s, 3H). ^{13}C NMR (101 MHz, $CDCl_3$) δ 199.4, 157.1, 152.7, 151.4, 149.0, 130.4, 124.2, 123.5, 119.2, 119.0, 116.2, 112.1, 110.0, 56.1, 56.1, 56.0. IR (thin film, CH_2Cl_2) 1632 cm^{-1}. HRMS (ESI) calcd for $C_{16}H_{16}O_5$ $[M-H]^-$ *m/z* 287.0925, found 287.0931.

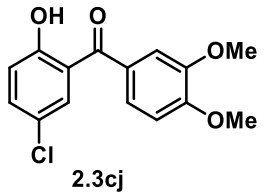

2.3cj

(3,4-dimethoxyphenyl)(5-chloro-2-hydroxyphenyl)methanone (**2.3cj**). Prepared using procedure A; isolated by column chromatography. Light yellow solid (0.187 g, 0.640 mmol, 80%). mp = 127–130 °C. R_f = 0.29 (20% EtOAc/Hex). ^{1}H NMR (400 MHz, $CDCl_3$) δ 11.73 (s, 1H), 7.64 (d, *J* = 2.7 Hz, 1H), 7.44 (dd, *J* = 8.9, 2.7 Hz, 1H), 7.36–7.27 (m, 2H), 7.02 (d, *J* = 8.9 Hz, 1H), 6.96 (d, *J* = 8.3 Hz, 1H), 3.98 (s, 3H), 3.95 (s, 3H). ^{13}C NMR (101

MHz, $CDCl_3$) δ 198.8, 161.4, 153.2, 149.3, 135.7, 132.3, 129.8, 124.5, 123.4, 120.2, 120.1, 112.1, 110.2, 56.3, 56.2. IR (thin film, CH_2Cl_2) 1623 cm^{-1}. HRMS (ESI) calcd for $C_{15}H_{13}ClO_4$ $[M-H]^-$ *m/z* 291.0430, found 291.0424.

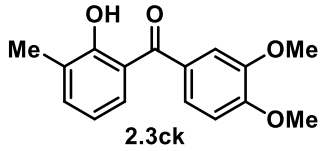

2.3ck

(3,4-dimethoxyphenyl)(2-hydroxy-3-methylphenyl)methanone (**2.3ck**). Prepared using procedure A; isolated by column chromatography. Yellow solid (0.192 g, 0.704 mmol, 88%). mp = 81–84 °C. R_f = 0.26 (20% EtOAc/Hex). ^{1}H NMR (400 MHz, $CDCl_3$) δ 12.17 (s, 1H), 7.50 (d, *J* = 7.9 Hz, 1H), 7.36 (d, *J* = 7.2 Hz, 1H), 7.34–7.28 (m, 2H), 6.93 (d, *J* = 8.0 Hz, 1H), 6.78 (t, *J* = 7.7 Hz, 1H), 3.96 (s, 3H), 3.93 (s, 3H), 2.32 (s, 3H).^{13}C NMR (101 MHz, $CDCl_3$) δ 200.4, 161.4, 152.7, 149.0, 136.8, 131.1, 130.8, 127.5, 124.4, 118.8, 117.9, 112.2, 110.0, 56.2, 56.2, 15.8. IR (neat) 1597 cm^{-1}. HRMS (ESI) calcd for $C_{16}H_{16}O_4$ $[M-H]^-$ *m/z* 279.0976, found 279.0976.

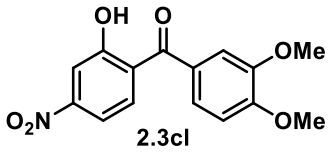

2.3cl

(4-nitro-2-hydroxyphenyl)(3,4-dimethoxyphenyl)methanone (**2.3cl**). Prepared using procedure A; isolated by column chromatography. Orange solid (0.118 g, 0.392mmol, 49%). mp = 128–130 °C. R_f = 0.25 (15% EtOAc/Hex with 5% acetic acid additive). ^{1}H NMR (400 MHz, $CDCl_3$) δ 11.76 (s, 1H), 7.89 (d, *J* = 2.1 Hz, 1H), 7.85 (d, *J* = 8.7 Hz, 1H), 7.73 (d, *J* = 2.2 Hz, 1H), 7.38–7.30 (m, 2H), 6.97 (d, *J* = 8.9 Hz, 1H), 4.00 (s, 3H), 3.96 (s, 3H). ^{13}C NMR (101 MHz, $CDCl_3$) δ 198.6, 163.0, 153.8, 151.7, 149.5, 134.1,

129.5, 125.0, 123.6, 113.8, 113.0, 112.1, 110.2, 56.4, 56.3. IR (thin film, CH_2Cl_2) 1623 cm^{-1}. HRMS (ESI) calcd for $C_{15}H_{13}NO_6$ $[M-H]^-$ *m/z* 302.0670, found 302.0666.

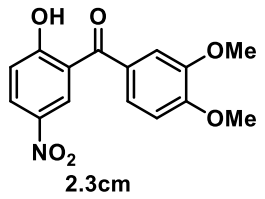

2.3cm

(5-nitro-2-hydroxyphenyl)(3,4-dimethoxyphenyl)methanone (**2.3cm**). Prepared using procedure A; isolated by column chromatography. Light brown solid (0.114 g, 0.376mmol, 47%). mp = 179–182 °C. R_f = 0.25 (15% EtOAc/Hex with 5% acetic acid additive). ^1H NMR (400 MHz, $CDCl_3$) δ 12.59 (s, 1H), 8.69 (d, *J* = 2.7 Hz, 1H), 8.38 (dd, *J* = 9.2, 2.7 Hz, 1H), 7.37 (dd, *J* = 8.3, 1.8 Hz, 1H), 7.34 (d, *J* = 1.7 Hz, 1H), 7.17 (d, *J* = 9.2 Hz, 1H), 7.01 (d, *J* = 8.3 Hz, 1H), 4.01 (s, 3H), 3.97 (s, 3H).^{13}C NMR (101 MHz, $CDCl_3$) δ ^{13}C NMR (101 MHz, $CDCl_3$) δ 198.5, 167.9, 153.9, 149.6, 139.5, 130.5, 129.5, 128.9, 124.8, 119.5, 118.4, 112.0, 110.5, 56.4, 56.3. IR (thin film, CH_2Cl_2) 1622 cm^{-1}. HRMS (ESI) calcd for $C_{15}H_{13}NO_6$ $[M-H]^-$ *m/z* 302.0670, found 302.0670.

<u>Hydroxyphenstatin Synthesis Products:</u>

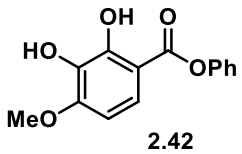

2.42

Phenyl 2,3-dihydroxy-4-methoxybenzoate (**2.42**). Off-white/yellow powder (0.532 g, 2.04 mmol, 75% yield). mpt = 145–147 °C. R_f = 0.16 (20% EtOAc/Hex). ^1H NMR (500 MHz, $CDCl_3$) δ 10.56 (s, 1H), 7.66 (d, *J* = 9.0 Hz, 1H), 7.45 (t, *J* = 7.5 Hz. 2H), 7.30 (t, *J* = 7.3 Hz, 1H), 7.21 (d, *J* = 8.1 Hz, 2H), 6.59 (d, *J* = 9.0 Hz, 1H), 4.97 (br s, 1H), 3.98 (s, 3H).

^{13}C NMR (126 MHz, $CDCl_3$) δ 168.9, 152.3, 150.3, 149.9, 133.6, 129.7, 126.4, 122.1, 121.8, 106.2, 103.4, 56.4. IR (thin film, CH_2Cl_2) 1667 cm^{-1}. HRMS (ESI) calcd for $C_{14}H_{12}O_5$ $[M-H]^-$ *m/z* 259.0612, found 259.0599.

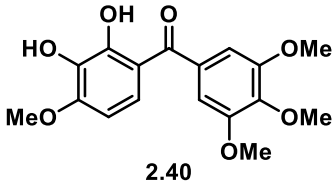

2.40

(2,3-dihydroxy-4-methoxyphenyl)(3,4,5-trimethoxyphenyl)methanone (Hydroxyphenstatin, **2.40**). Yellow/brown solid obtained (0.240 g, 0.718 mmol, 48% yield). R_f = 0.22 (50% EtOAc/Hex). ^{1}H NMR (400 MHz, $CDCl_3$) δ 12.22 (s, 1H), 7.26 (d, *J* = 9.0 Hz, 1H), 6.92 (s, 2H), 6.51 (d, *J* = 9.0 Hz, 1H), 5.56 (bs, 1H), 3.98 (s, 3H), 3.94 (s, 3H), 3.90 (s, 6H). IR (neat) 1635 cm^{-1}. All data are consistent with prior synthesis.[163]

Chapter 3. Phenol Acylation via Hydroxyl-Directed C–C Bond Activation

3.1 Introduction

Based on the reversibility of arene acylation via sequential C–O/C–H bond activation discussed in Chapter 2, we aimed to develop a method converting ketones to esters through C–C bond activation and subsequent coupling with phenol nucleophiles. The proposed mechanism of this transformation begins with coordination of the hydroxyl-directing group to the metal center forming intermediate **I**. Oxidative addition activates the

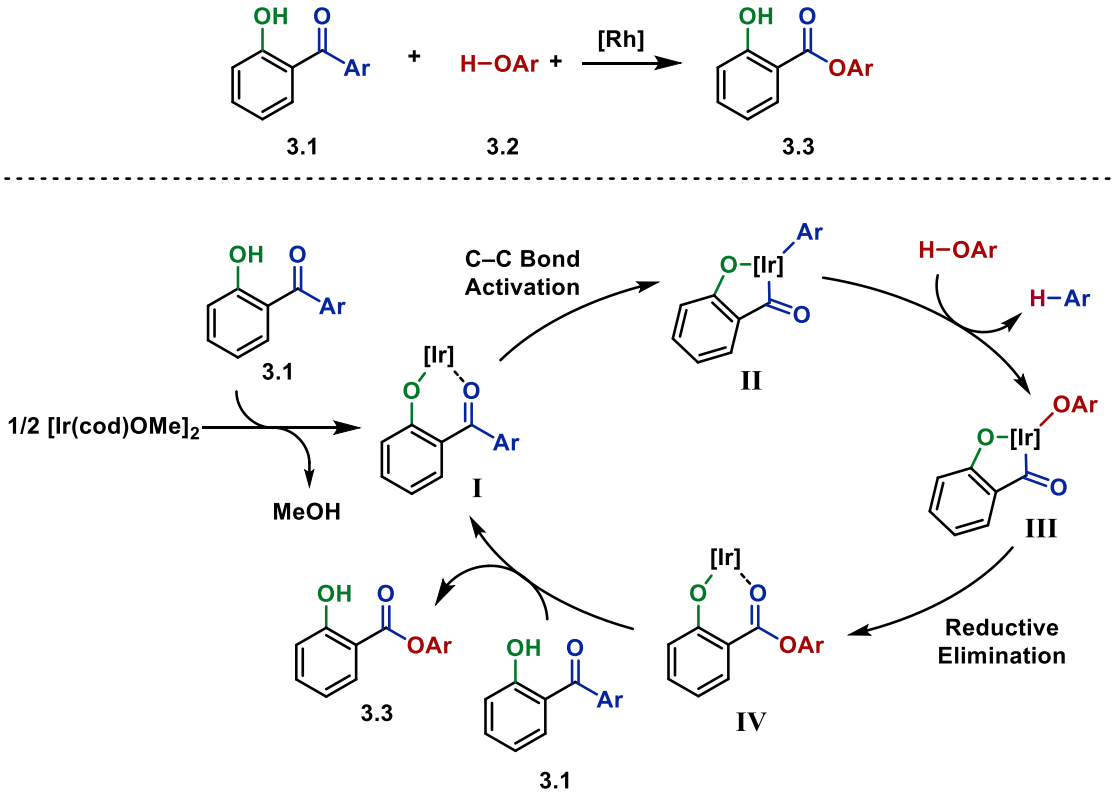

Scheme 3.1 Proposed mechanism of phenol acylation

ketone C–C bond of **3.1** followed by exchange of the arene leaving group for phenol **3.2**, forming metallocycle **III** and a defunctionalized arene. Reductive elimination to **IV** and exchange of the product **3.3** for **3.1** closes the catalytic cycle.

3.1.1 Background of Transition-Metal-Catalyzed C–O Bond Formation

While various methods utilizing C–C bond activation have been developed, there currently are no methods coupling unstrained C–C bond activation products with alcohols. Most research into forming C–O bonds through transition-metal-catalyzed processes focuses on the formation of ethers. These processes rely on an initial oxidative addition into labile C–X bonds (X = Cl, Br, I, NO_2) before coupling to primary, secondary, or aromatic alcohols (Scheme 3.2a).[168–192] Carbonylative coupling of aryl halides can be achieved using a CO atmosphere or reagents that generate metal-carbonyl species.[193–198]

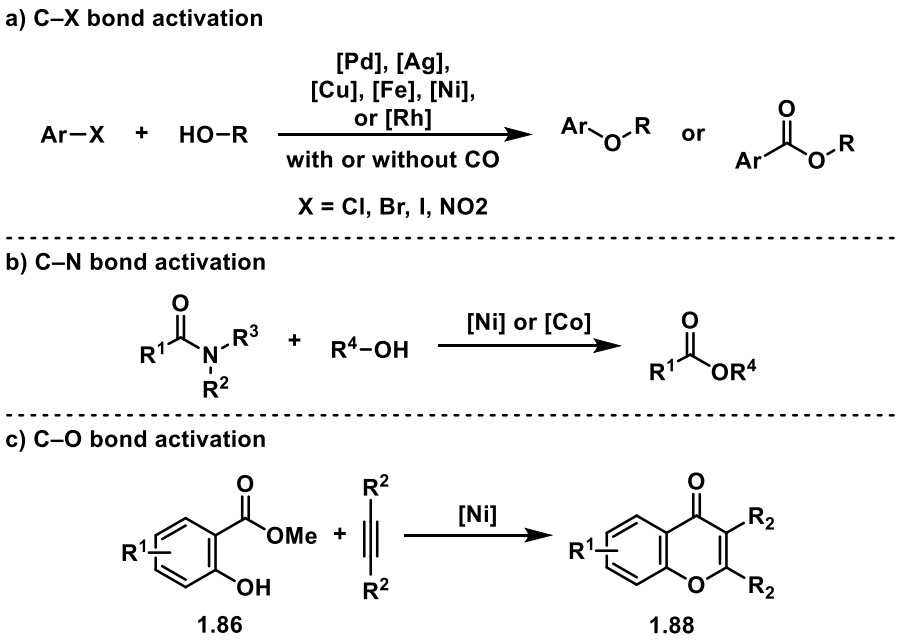

Scheme 3.2 Transition-Metal-Catalyzed C–O bond forming reactions through a) C–X bond activation; b) C–N bond activation; c) C–O bond activation

More recently, Bourne-Branchu et al.[199] and Garg and coworkers[200,201] reported nickel- or cobalt-catalyzed ester syntheses via C–N bond activation of amides (Scheme 3.2b). Iyori and Chatani[116] developed an method of chromone formation via C–O bond activation of ester **1.86** and alkyne insertion using the hydroxyl-directing group as an internal nucleophile to form the new C–O bond of **1.88** (as discussed in Section 1.4.3, Scheme 3.2c).

Previous methods of ester C–O bond formation through C–C bond functionalization use ring strain to drive bond activation. Murakami et al.[202] reported the synthesis of lactones using C–C bond activation. Bond activation was driven by the release of ring strain through the expansion of the cyclobutanone ring of **3.6 (**Scheme 3.3a). The *o*-hydroxyl group acts as a directing group for oxidative addition into the C–C bond and an

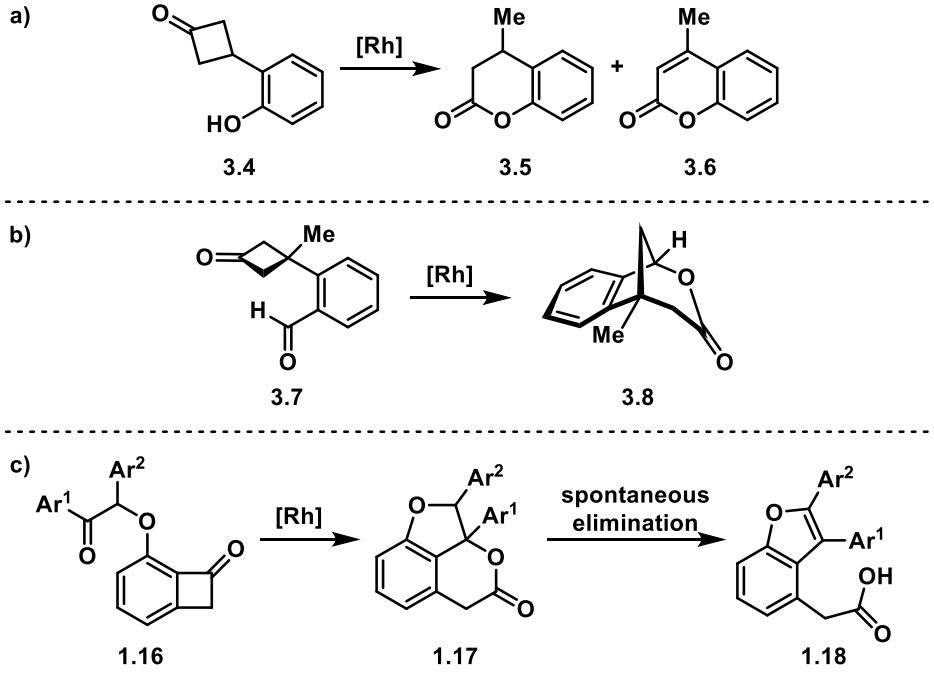

Scheme 3.3 C–O bond formation via strained ring C–C bond functionalization

intramolecular nucleophile for lactone formation. Competition between C–H reductive elimination and β-hydride elimination resulted in a mixture of products **3.5** and **3.6**. Cramer and Souillart[203] reported the C–C bond activation of cyclobutanone **3.9** followed by ketone insertion to form bridged lactone **3.10** (Scheme 3.3b). Xu and coworkers [61,62] used ketone insertion following C–C bond activation of benzocyclobutenones **1.16** to form new C–O bonds in **1.18**, followed by spontaneous carboxylate elimination driven by aromatization (as discussed in Section 1.3.1, Scheme 3.3c). Here we demonstrate an improved method for esterification of ketones through unstrained C–C bond activation using a more diverse set of ketones.

3.2 Reaction Optimization

3.2.1 Initial Reaction Optimization

Symmetric dihydroxylbenzophenone **3.10a** (Scheme 3.4) was chosen as the substrate for optimization of the phenol acylation reaction as we hypothesized that it would simplify the resulting reaction mixtures by regenerating phenol as the sole byproduct. Ketone **3.10a** was readily synthesized in one step through a nucleophilic ring opening of xanthone **3.9**.[204]

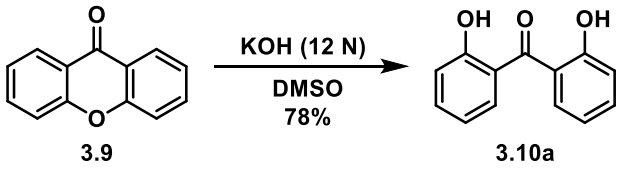

3.9 3.10a

Scheme 3.4 Synthesis of starting material ketone **3.8a**

As phenol acylation was first observed when developing the arene acylation reaction discussed in Chapter 2, these conditions were used as a starting point for

optimization. The reaction was found to be operable at 150 °C with 5 equivalents of phenol, giving **3.11a** in 26% yield on average (Table 3.1 entry 1). Control reactions showed that iridium and phosphine were required for the reaction (Table 3.1 entries 2 and 3). Addition of 1,5-cyclooctadiene (COD) was not required but did improve yields of ester **3.11a**, so it was used in further reaction optimization (Table 3.1 entry 4).

Table 3.1 Phenol acylation control reactions

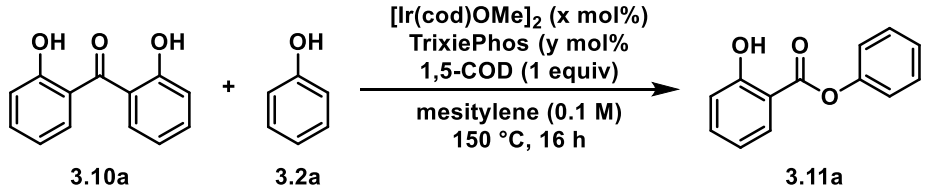

3.10a 3.2a 3.11a

Entry	[Ir(cod)OMe]$_2$ (mol%)	TrixiePhos (mol%)	COD (equiv)	Yield 3.11a (%)[a]
1[b]	1	3	1	26
2	—	3	1	nd
3	1	—	1	tr
4	1	3	—	20

a) Determined by qNMR; b) Average of 3 experiments; nd = not detected; tr = trace

Next, a short solvent screen was performed (Table 3.2). Results indicated that mesitylene was the best solvent of those tested. Attempts at phenol acylation in diglyme gave no detectable product **3.11a** (Table 3.2 entry 2). Reactions in 1,2-dichlorobenzene resulted in lower yields (Table 3.2 entry 3). Phenol acylation in decalin showed yields of **3.11a** comparable to mesitylene, but with higher amounts of decomposition and lower mass balances (Table 3.2 entry 4).

Table 3.2 Phenol acylation in alternate solvents

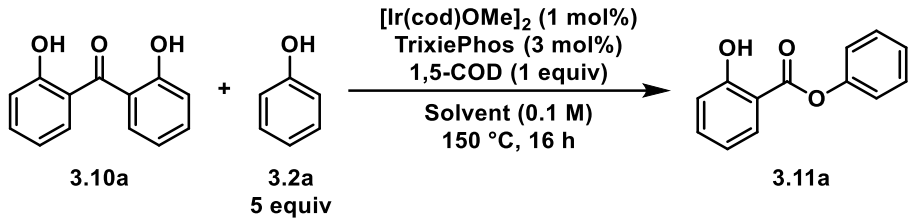

Entry	Solvent	Conversion (%)[a]	Yield 3.11a (%)[a]	Mass balance (%)
1[b]	Mesitylene	57	26	69
2	Diglyme	15	0	85
3	1,2-Dichlorobenzene	23	11	88
4	Decalin	65	25	60

a) Determined by qNMR; b) Average of 3 experiments

A screen of precatalysts and phosphines was performed. Precatalysts $[Rh(cod)OMe]_2$, $[Rh(cod)OH]_2$, $Ni(cod)_2$, $Rh(PPh_3)_3Cl$, $Pd(PPh_3)_4$ showed no or trace product formation. Ir(cod)(acac) and $[Ir(cod)OPh]_2$ promoted minimal reactivity (<10% product formation), with only $[Ir(cod)OMe]_2$ giving reasonable yields (26%). Phosphines varying from bidentate phosphines (BINAP and dppp) to simple phosphines (PPh_3 and P(*t*-Bu)$_3$) and a Buchwald phosphine MePhos all showed no reactivity. Di-*t*-butylbiphenyl phosphines (*t*-BuMePhos and JohnPhos) showed minimal reactivity, with yields of **3.11a** below 5%. Bulky di-*t*-butylbinaphthyl phosphine TrixiePhos was found to be the only phosphine to show appreciable formation of ester **3.11a**. This unique reactivity is consistent with that observed in arene acylation discussed in Chapter 2.

We then examined catalyst loading, finding that yield of **3.11a** increased as catalyst loading increased. As catalyst loading increased, mass balance decreased, likely due to

increased formation of two prominent byproducts. Additionally, the catalyst may be trapping an equivalent of **3.10a** through catalyst decomposition pathways, including decarbonylation, resulting in lower mass balances. A minimal difference was observed between 2 mol% and 2.5 mol% $[Ir(cod)OMe]_2$ (Table 3.3 entries 4 and 5). Optimal loading was determined to be 2 mol% $[Ir(cod)OMe]_2$ based on yield, conversion, and mass balance.

Table 3.3 Catalyst loading optimization

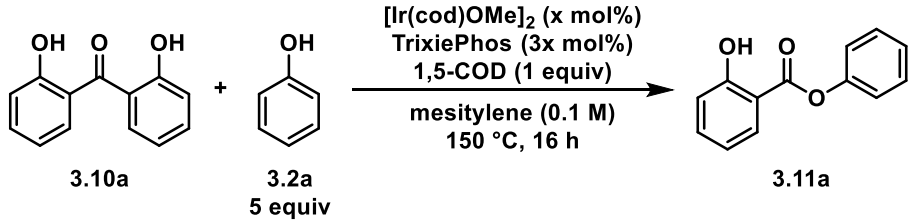

Entry	$[Ir(cod)OMe]_2$ (mol%)	TrixiePhos (mol%)	Conversion (%)[a]	Yield 3.11a (%)[a]	Mass Balance (%)
1	0.5	1.5	41	21	80
2[b]	1	3	57	26	69
3	1.5	4.5	46	25	79
4[b]	2	6	71	34	63
5[b]	2.5	7.5	79	36	57

a) Determined by qNMR; b) Average of 3 experiments

Phosphine loadings were screened to determine the optimal ratio of iridium to phosphine ligand. The amount of phosphine had a marginal effect on the reaction mass balance, with lower yields of **3.11a** observed at phosphine loadings at or below 2 mol% (Ir:phosphine ratios less than or equal to 1) (Table 3.4 entries 1 and 2). With Ir:phosphine ratios above 1, there is little to no effect of increased phosphine (Table 3.4 entries 3–7).

Interestingly, yield of **3.11a** does not decrease until 40 mol% phosphine was used (Table 3.4 entry 8). This contrasts with the reverse arene acylation reaction where excess phosphine inhibits the reaction. Additionally, the consistent mass balances show phosphine loading has no effect on the amount of side reactions or decomposition occurring.

Table 3.4 Phosphine loading optimization

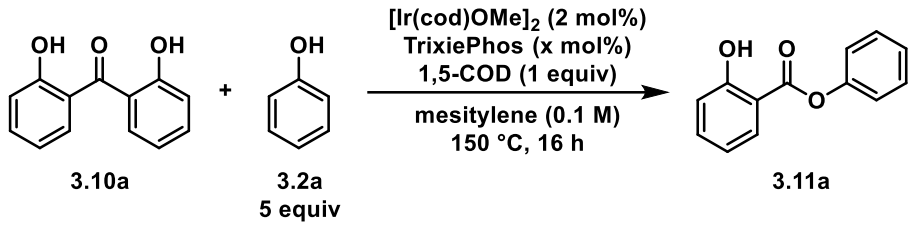

Entry	TrixiePhos (mol%)	Conversion (%)	Yield 3.11a (%)	Mass Balance (%)
1	1	35	11	76
2	2	44	19	75
3	3	67	34	67
4	4	65	34	69
5	6	64	34	70
6	8	65	33	68
7	20	66	32	66
8	40	54	29	75

a) Determined by qNMR

Concentrations from 0.05 to 1 M **3.10a** were examined. The highest yield of **3.11a** was achieved at 0.1 M (Table 3.5 entry 2). As reaction concentration increased, mass balance drastically decreased. NMR analysis of reaction mixtures showed two side

products were being formed in significant quantities and became the major products at concentrations above 0.2 M. The identities of these side products will be discussed in Section 3.2.2 Phenol is a liquid at the reaction temperature so solvent-free "neat" reactions were attempted. At 150 °C, decomposition of **3.10a** was observed with no ester **3.11a** formation after 16 hours (Table 3.5 entry 6). At 170 °C, **3.11a** was formed in 27% yield with 96% conversion of **3.10a** (Table 3.5 entry 7). While there was some decomposition, significant quantities of two side products were also observed in the reaction mixture, making up about 30% of the material.

Table 3.5 Concentration optimization

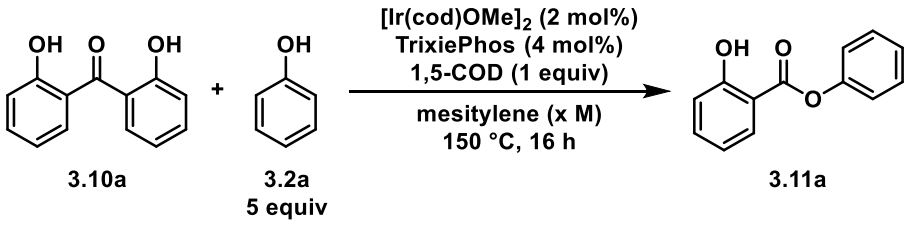

Entry	Concentration (M)	Conversion (%)[a]	Yield 3.11a (%)[a]	Mass Balance (%)
1	0.05	34	8	74
2	0.1	65	34	69
3	0.2	67	18	51
4	0.5	86	19	33
5	1	82	15	33
6	neat	46	0	54
7[b]	neat	96	27	31

a) Determined by qNMR; b) 170 °C

Table 3.6 Temperature and time optimization

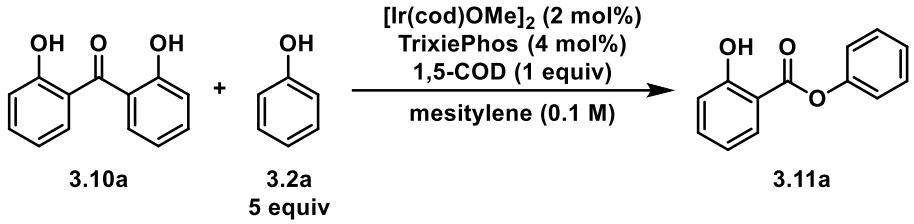

Entry	T (°C)	t (h)	Conversion (%)[a]	Yield 3.11a (%)[a]	Mass Balance (%)
1	150	16	65	34	69
2	150	24	80	39	59
3	150	40	91	45	54
4	150	48	88	44	56
5	160	16	90	48	58
6	160	24	95	51	56
7	160	40	95	50	55
8	160	48	94	47	53
9[b]	170	2	44	16	72
10[b]	170	4	86	44	58
11[b]	170	6	93	48	55
12[b]	170	8	95	49	54
13[b]	170	10	95	51	56
14[b]	170	14	96	49	53
15[c]	170	16	97	49	52
16[b]	170	18	97	47	50
17[b]	170	20	97	45	48
18	170	22	98	43	45
19[c]	170	24	97	44	47
20	170	40	>99	41	41
21	170	48	98	41	43

a) Determined by qNMR; b) Average of 2 experiments; c) Average of 3 experiments

Next, we examined reaction temperature and time (Table 3.6). Since yields of **3.11a** remained relatively low at 150 °C after 16 hours, higher temperatures and longer reaction times were investigated. The maximum yield and mass balance were not strongly dependent on temperature, yields reached approximately 50% at all temperatures then slowly decreased over time (Figure 3.1). The highest yields observed were after 24 hours at 160 °C and 10 hours at 170 °C (51%, Table 3.6 entries 6 and 13). As only these moderate yields were achieved, further optimization was required.

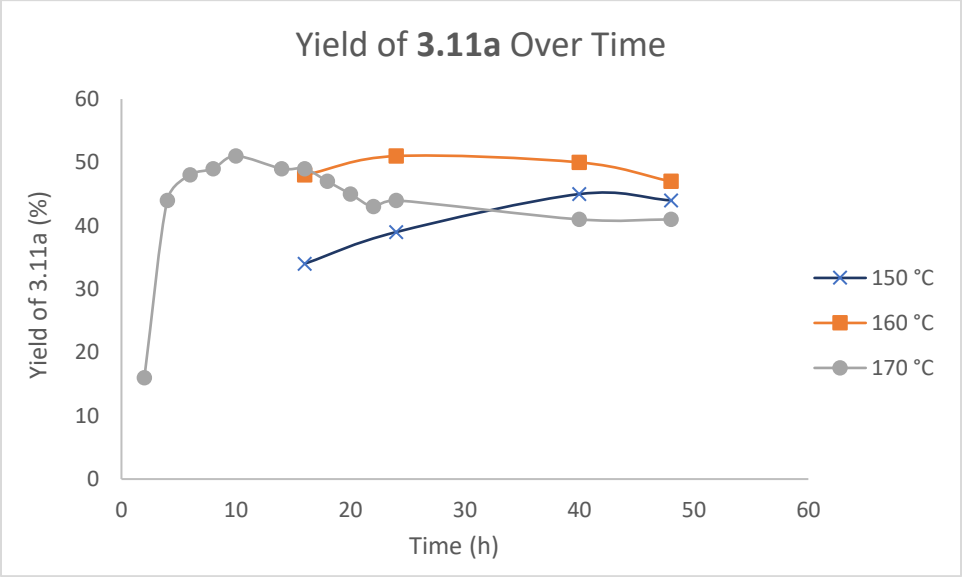

Figure 3.1 Percent yield of **3.11a** over time at 150, 160, and 170 °C

3.2.2 Side product Analysis

Low mass balances were observed due to the formation of two major side products which were isolated and identified as ketone **3.12** and xanthone **3.13** (Scheme 3.5). Ketone **3.12** formed in up to 26% (up to 14% at 0.1 M concentration). Ketone **3.12** is presumed to form through C–C bond activation of **3.10a** followed by *C*-acylation of phenol **3.2a**, via intermediate **V**, following a mechanism as shown in (Scheme 2.16). It was hypothesized

that **3.12** could undergo C–C bond activation and *O*-acylation of phenol to be converted to desired product **3.11a**. Xanthone **3.13** formed in significant quantities, 31% yield in neat conditions or up to 20% at 0.1 M concentration. This product was hypothesized to form through hydroxyl-directed aryl C–H bond activation, forming intermediate **VI**, followed by C–O bond forming reductive elimination. Xanthone **3.13** likely cannot be further converted to product **3.11a**. To increase yields of **3.11a**, formation of **3.13** must be limited.

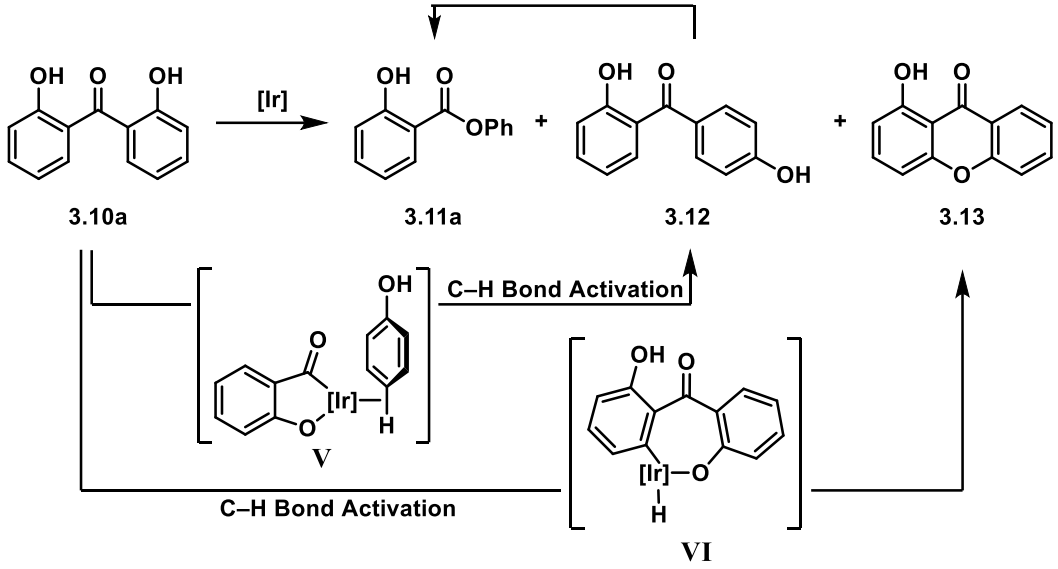

Scheme 3.5 Side products **3.12** and **3.13** formed in phenol acylation reactions

3.2.3 Further Reaction Optimization

Further optimization showed that maximum 60% yield of ester **3.11a** could be obtained through acylation with ketone **3.10a** by increasing the amount of phenol to 10 equivalents (Table 3.7 entry 2). To attempt to increase the yield of **3.11a** and eliminate the formation of side product **3.13**, ketone **3.14a** was tested as a starting material for phenol acylation. With 5 equivalents of phenol, acylation with ketone **3.14a** did not result in higher yields after 8 or 20 hours (Table 3.7 entries 3 and 4). Increasing the amount of phenol to

Table 3.7 Effect of starting material identity and equivalents of phenol

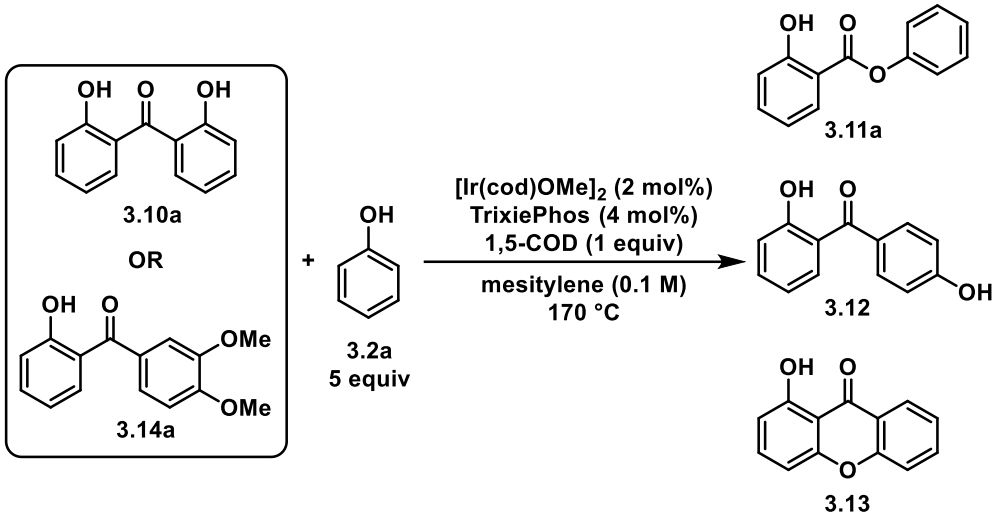

Entry	Starting Material	Time (h)	Phenol (equiv)	Conversion (%)[a]	3.11a (%)[a]	3.12 (%)[a]	3.13 (%)[a]
1	**3.10a**	8	10	90	50	6	6
2	**3.10a**	20	10	89	60	8	8
3	**3.14a**	8	5	80	41	4	0
4	**3.14a**	20	5	90	51	5	0
5	**3.14a**	8	10	90	51	6	tr
6	**3.14a**	18	10	98	54	7	tr
7[b]	**3.14a**	20	10	97	66	8	0
8	**3.14a**	22	10	98	55	7	tr

a) Determined by qNMR; *b) Average of 2 experiments; tr = trace*

10 equivalents gave moderately higher yields, with an optimal 66% yield after 20 hours at 170 °C (Table 3.7 entries 5–8). Switching from **3.10a** to **3.14a** successfully eliminated the formation of side product **3.13**. Interestingly, small amounts of ketone **3.10a** were observed

along with **3.11a** and **3.12** in the resulting reaction mixtures (Scheme 3.6). As both **3.10a** and **3.12** have C–C bonds that can be activated and converted into product **3.11a,** and **3.11a** can undergo C–O bond activation, these three products are likely in equilibrium with each other.

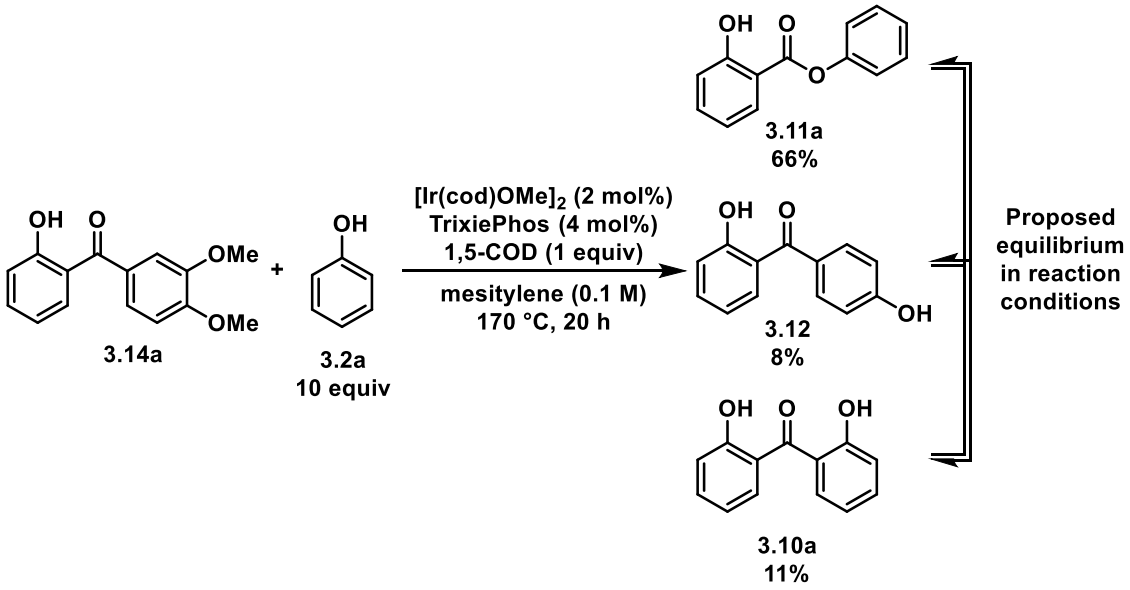

Scheme 3.6 Results of phenol acylation with ketone **3.14a** in optimized conditions

3.3 Reaction Scope

3.3.1 Acylation of Aliphatic Alcohols

Concurrent with reaction condition optimization, reactions with substituted phenols and non-aromatic alcohols were investigated. Two primary aliphatic alcohols, benzyl alcohol and isoamyl alcohol, were chosen as substrates. Initial attempts at acylation of both aliphatic alcohols resulted in only trace formation of esters **3.15** with low conversions of ketone **3.10a** (Scheme 3.7).

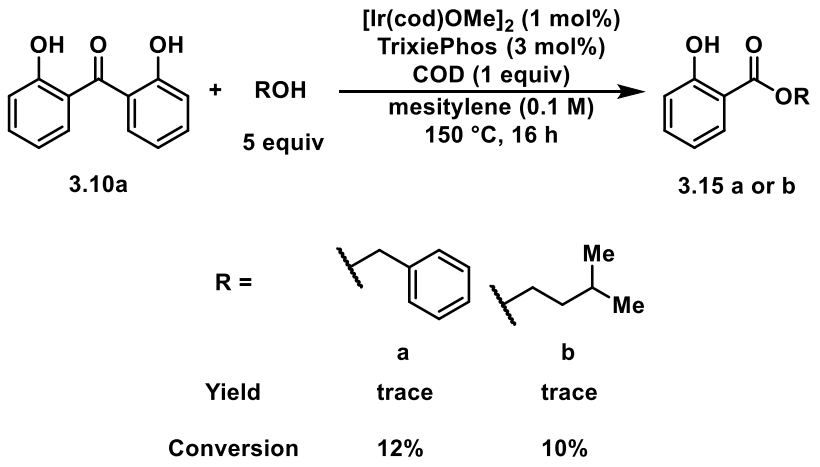

Scheme 3.7 Acylation of non-aromatic alcohols

We hypothesized that the aliphatic alcohols may lack the acidity needed for proton-coupled ligand exchange. Alternatively, once bound the alcohols may promote side reactions forming aldehyde side products by undergoing as β-hydride elimination. Transesterification of phenyl salicylate could potentially be used to circumvent these issues. It was hypothesized that acylation of phenol could occur through C–C bond activation of **3.10a**, forming ester **3.11a**. Ester **3.11a** could then undergo transesterification with the aliphatic alcohol to form ester **3.15a** or **b** *in situ*.

Reacting benzyl and isoamyl alcohols with phenyl salicylate **3.11a** showed that transesterification was possible in the reaction conditions. Esters **3.15a** and **b** were formed in 91% and 55% yield, respectively, with near quantitative conversion of **3.11a** when reacted at 150 °C for 16 hours with iridium catalyst present (Scheme 3.8a). High amounts of transesterification were observed when **3.11a** was heated to 150 °C in the presence of aliphatic alcohols without catalysts present (Scheme 3.8b).

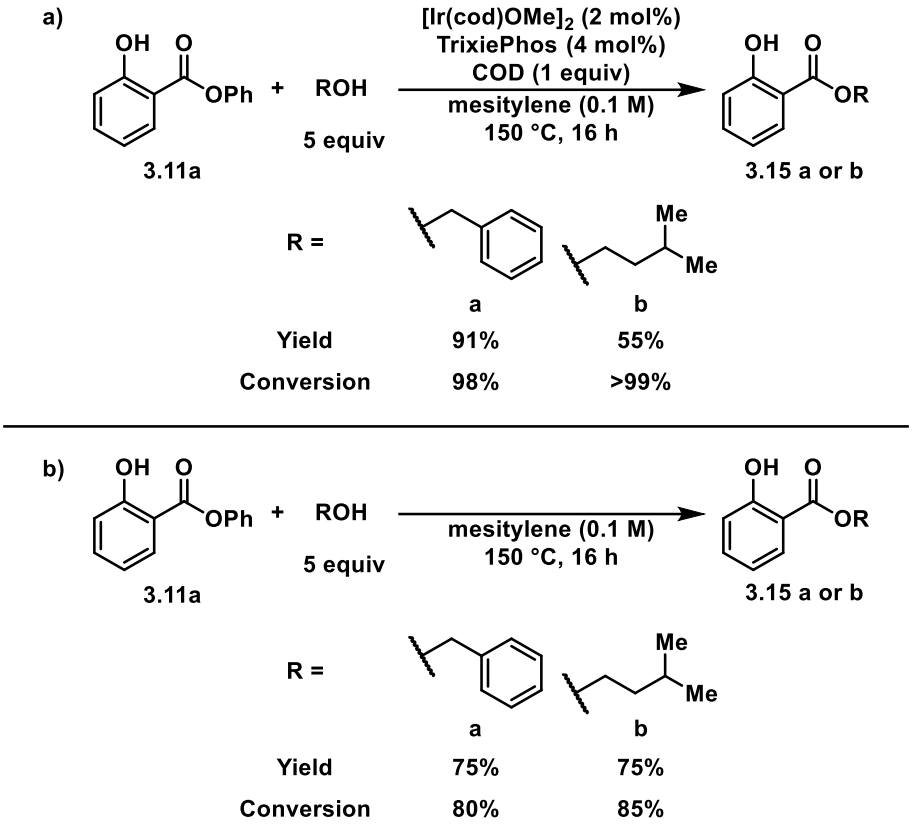

Scheme 3.8 Transesterification of phenyl salicylate **3.11a** with non-aromatic alcohols

Encouraged by these results, we attempted aliphatic alcohol acylation via transesterification. Unfortunately, all attempts at this transformation resulted in only trace formation of products with low conversion of **3.10a** (Scheme 3.9). No formation of **3.11a** was observed in these reaction mixtures.

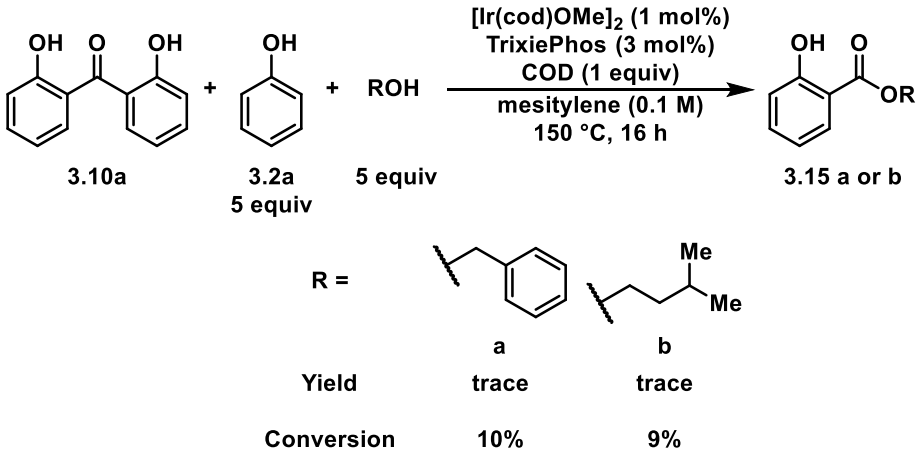

Scheme 3.9 Acylation of non-aromatic alcohols via transesterification

These results reinforce that aliphatic alcohols are not only incompatible nucleophiles for acylation but indicate that they also inhibit phenol acylation. This inhibition could be due to two factors. Benzyl and isoamyl alcohol may be binding tightly to the iridium center, filling all possible coordination sites and inhibiting bond activation. Alternately, the primary alcohols may be binding to the catalyst and undergoing a side reaction, such as β-hydride elimination, forming iridium complexes incapable of entering the phenol acylation catalytic cycle.

3.3.2 Phenol Acylation

Next, acylation of substituted phenols was investigated. Attempts at acylation of 4- or 3,5- substituted phenols with ketone **3.10a** all resulted in complex mixtures (Scheme 3.10). As the C–C, C–O, and C–H bonds of the starting materials and products can be activated by the iridium catalyst, there are many opportunities for side reactions, resulting in a variety of products. While only the substituted phenol species are initially present in

the reaction mixture, unsubstituted phenol **3.2a** forms as a byproduct of bond activation of **3.10a**, increasing the number of potential products.

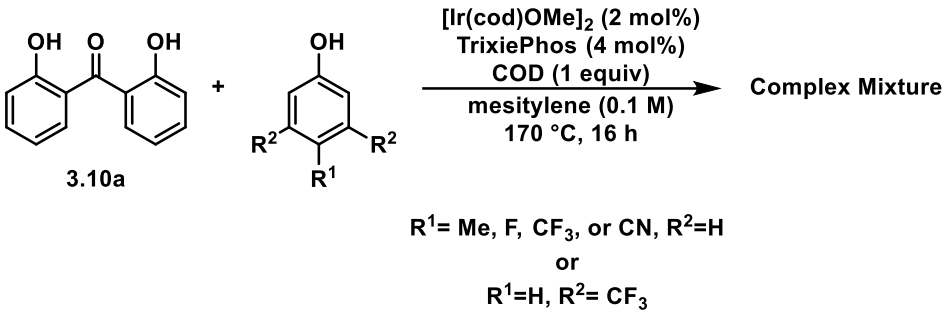

Scheme 3.10 Attempted acylation of substituted phenols

For example, if an acylation reaction was performed between **3.10a** and a *p*-substituted phenol, 6 possible ester and ketone products could form (Scheme 3.11). All combinations of C–C and C–O bond activation followed by *C*- or *O*- acylation of all phenol species present are possible, scrambling the phenol groups in the products. This scrambling is possible starting from both ketones **3.10a** and **3.14a**.

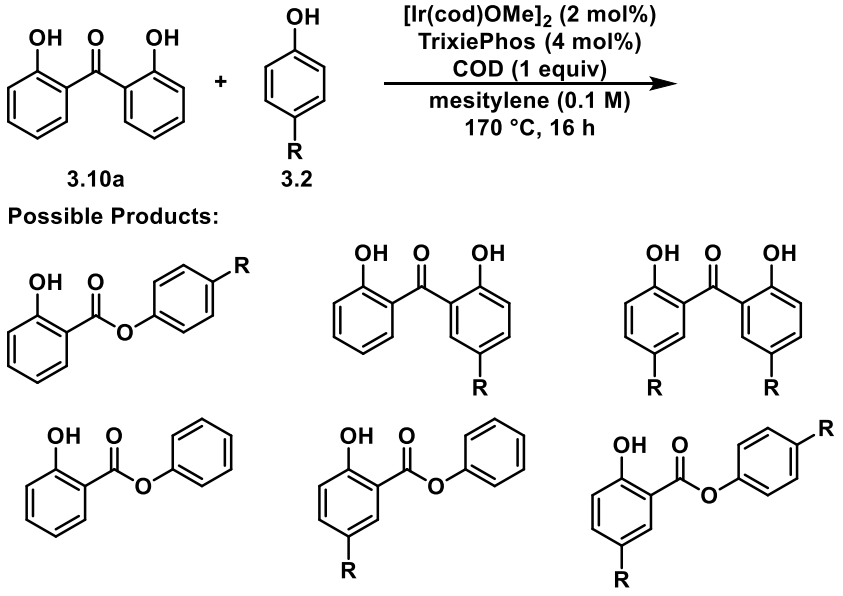

Scheme 3.11 Possible products of acylation of substituted phenols with **3.10a**

To limit the number of possible products, further studies were done using ketone and phenol reactants with matched substituents (Scheme 3.12). It was believed that this would reduce the number of products formed through side reactions as only one phenol species would be present in the reaction mixture. Initial bond activation of **3.14** followed by either *O*- or *C*- acylation would form 1,2-dimethoxybenzene as a byproduct, which is unlikely to be reactivated in the reaction conditions. C–O bond activation of esters **3.11** followed by *C*-acylation of the substituted phenol **3.2** would form symmetric substituted ketone **3.10**. Bond activation of either C_{acyl}–C bond of ketone **3.10** followed by *O*-acylation of **3.2** would regenerate the desired ester product **3.11**. All side reactions shown would regenerate an equivalent of the substituted phenol **3.2**.

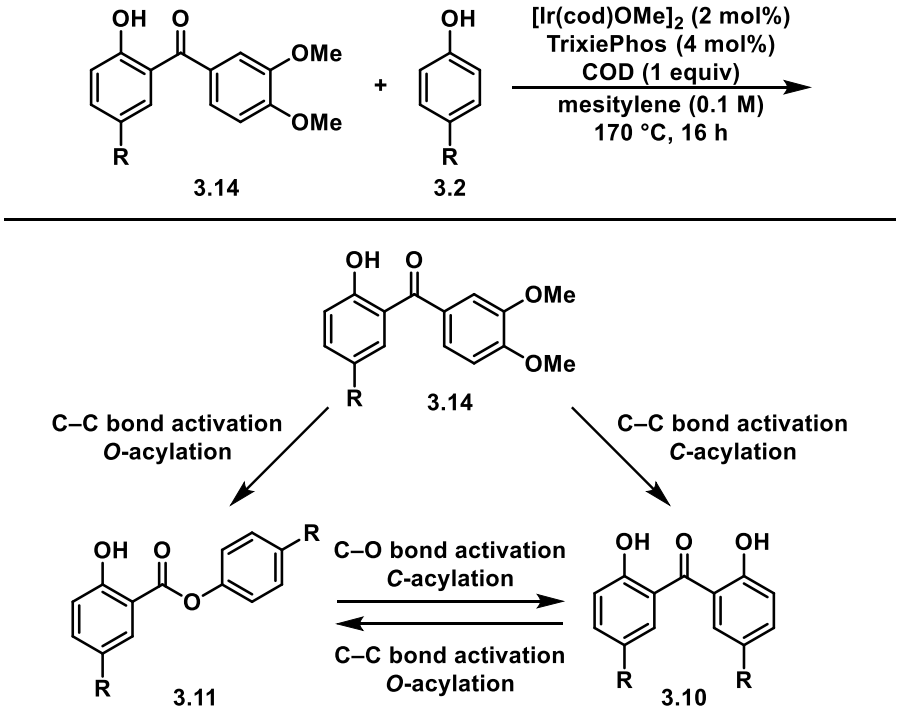

Scheme 3.12 Acylation of substituted phenol with matched ketones

A small substrate screen was performed with matched substituted phenols and ketones was performed (Table 3.8). Multiple catalyst charges were tested for all substrates to achieve the highest yields, the best results are shown. The highest yields and cleanest reaction mixtures were achieved with electron-rich, para-substituted phenols after only one catalyst charge and 20 hours (Table 3.8 entries 1 and 2). This is likely due to two factors. The electron-rich phenols are better nucleophiles for acylation while the steric hinderance resulting from para-substitution inhibits *C*-acylation (as explained in Chapter 2). Lower yields of **3.11d** were obtained from the acylation of electron-poor *p*-chlorophenol **3.2d** even after 3 catalyst charges (Table 3.8 entry 3). No significant side products were observed in the reaction mixture, likely due to the steric inhibition of *C*-acylation. Significant formation of ketones **3.10g** and **3.10h** were observed in reactions with *meta*-substituted phenols with both electron donating (**3.2g**) or electron withdrawing (**3.2h**) groups. Moderate yields were still achieved with electron-rich *meta*-substituted phenols after a single catalyst charge, additional charges and increased reaction time resulted in lowered yields from decomposition (Table 3.8 entries 5 and 6). Poor yields were observed in the acylation of electron deficient phenols (Table 3.8 entries 7–9). Low yields and low mass balances were observed in the acylation of naphthol **3.2k** (Table 3.8 entry 10).

Table 3.8 Substrate scope of phenol acylation

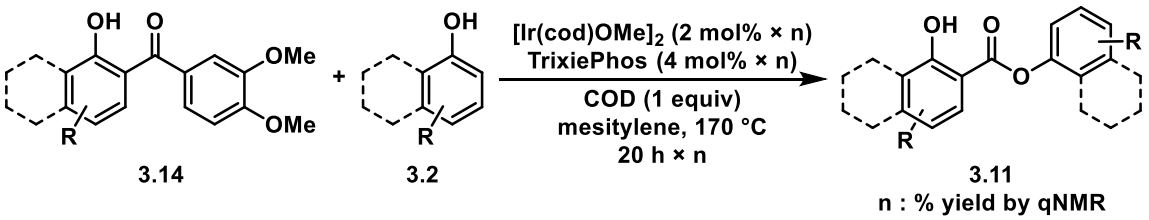

#	Product	#	Product	Other isolated products
1	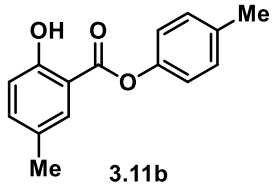 3.11b 1 : 72%	6	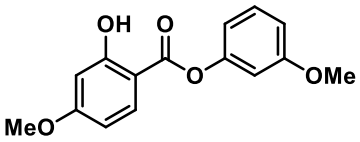 3.11g 1 : 42%	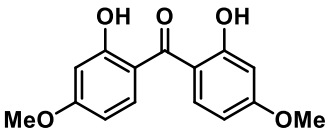 3.10g 21%
2	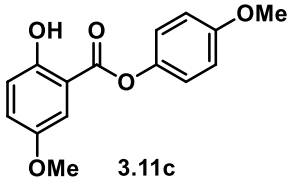 3.11c 1 : 70%	7	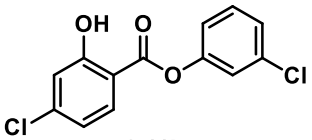 3.11h 2 : 8%	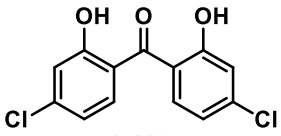 3.10h <1%
3	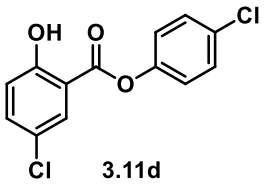 3.11d 3 : 33%	8	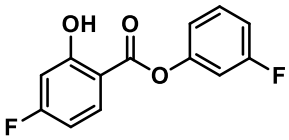 3.11i 1 : 35%	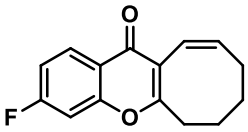 3.16i 4%
4	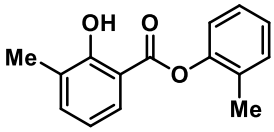 3.11e 1 : 48%	9	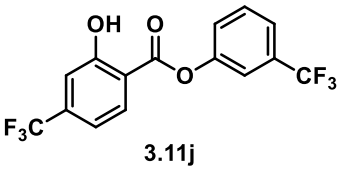 3.11j 1 : 27% 1 : 40%* * no COD	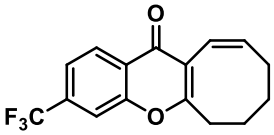 3.16j 8% trace*
5	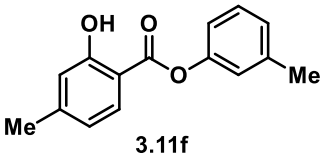 3.11f 1 : 69%	10	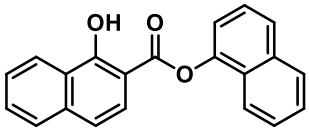 3.11k 2 : 18%	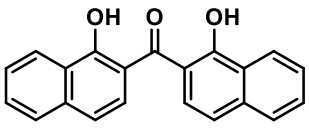 3.10k 9%

3.3.3 Side Product Analysis

Interestingly, an additional side product was isolated from reactions with electron deficient, fluorinated phenols **3.2i** and **3.2j**. These were isolated and identified as tricyclic compounds **3.16i** and **3.16j** respectively (Table 3.8 entries 8 and 9). Following initial isolation and ^{1}H NMR analysis, we found compound **3.16j** contained an unexpected non-aromatic alkene. Due to the stable hydrogen bond between the carbonyl and the hydroxyl proton, the proton of the *o*-hydroxyl ketones and esters produce a distinctive sharp signal in between 10 and 13 ppm in their ^{1}H NMR spectra. This signal was absent in spectra of **3.16j** indicating that it no longer contained a hydroxyl group. Based on these observations and further analysis of ^{1}H and COSY NMR and HRMS data, the structure was determined to be one of the COD containing compounds shown in Figure 3.2a. The location of the second alkene was identified using ^{1}H and ^{19}F decoupled ^{13}C NMR data collected by Dr. Letitia Yao, along with HSQC and HMBC NMR data. Key HMBC signals used for structure assignment are shown in Figure 3.2b. Only a small amount of **3.16i** could be

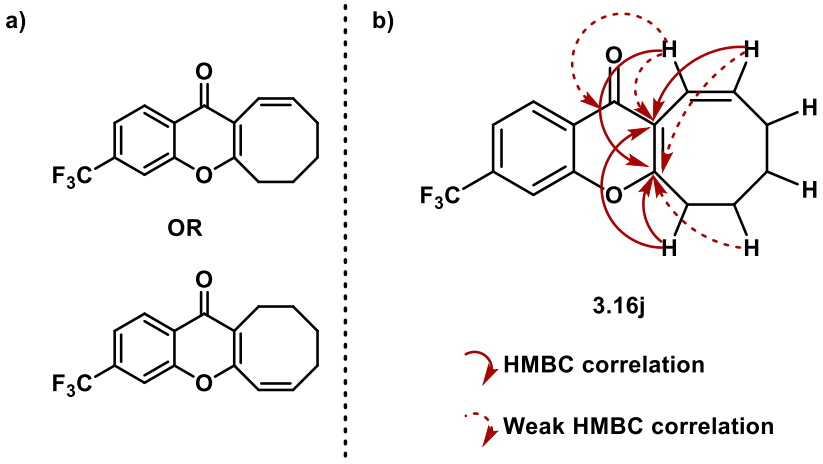

Figure 3.2 Structural assignment of **3.16j**

isolated so this structure was assigned based on HRMS and ^{1}H NMR data and its comparison to data from **3.16j**.

Based on the structure, these products are proposed to form thorough the following mechanism involving insertions of the COD ligand (Scheme 3.13). After C–C or C–O bond activation, intermediate **VII** undergoes migratory insertion of one alkene of COD. While 1,3-COD is shown, this may be occurring with 1,4-COD or 1,5-COD instead as alkene isomerization into conjugation may occur before or after the COD insertion. Following migratory insertion, β-hydride elimination would reform an alkene in **IX**. Reductive elimination of an arene forms **X**. The central ring may then be formed through alkene C–H activation[205] to **XI** followed by reductive elimination forming the new C(sp^2)–O bond of **3.15j** and leaving an iridium hydride species. The increased formation of **3.16** with electron-deficient, trifluoromethyl- and fluoro-substituted ketones **3.14i** and **3.14j** can be

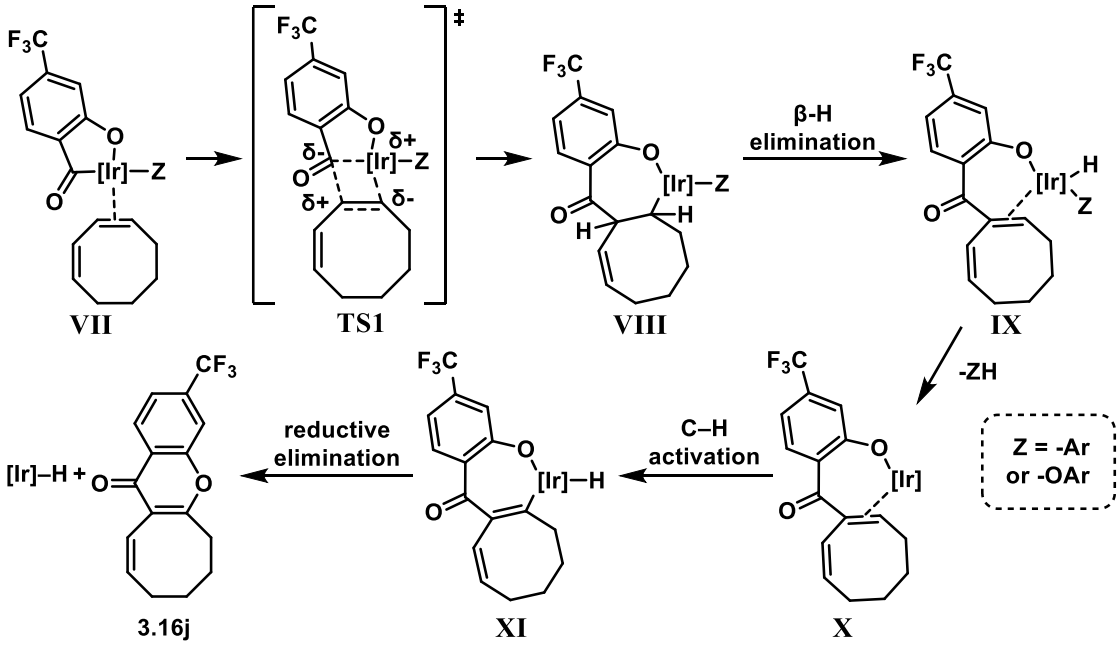

Scheme 3.13 Proposed mechanism for the formation of **3.16j**

explained by the stabilization of the partial charge in transition state **TS1** of the initial migratory insertion of COD. A similar mechanism of C–H bond activation and C–O bond reductive elimination would explain the formation of xanthone **3.13** observed during reaction optimization.

3.4 Conclusion

We have demonstrated the *O*-acylation of phenols as the first known example of C–O bond formation via unstrained C–C bond activation. This is the formal reverse reaction of the arene acylation reaction discussed in Chapter 2 and is proposed to go through the same reaction mechanism. The scope of the reaction with respect to the ketone and phenol substrates was investigated, showing that the reaction proceeds in highest yield and selectivity with 4-substituted phenols

Analysis of isolated side products indicate that C–C, C–O, and C–H bond activation and COD migratory insertion can all occur in the in the standard phenol acylation reaction conditions with $[Ir(cod)OMe]_2$. Further investigation is needed to increase the yields and selectivity of phenol acylation.

3.5 Experimental Details

3.5.1 General Information

General Experimental Procedures: All acylation reactions were prepared under inert atmosphere in an oxygen-regulated glovebox. Reaction progress was monitored using thin-layer chromatography (TLC) on 0.25 mm silica plates from SiliCycle. Eluted plates were visualized with UV light. Silica Gel Flash Column Chromatography was performed on 230–400 mesh (particle size 0.04–0.063 mm) silica gel purchased from SiliCycle.

Materials. Unless otherwise indicated, chemicals were obtained from commercial sources and used without further purification. All solvents for acylation were degassed by bubbling a stream of argon through the liquid in a Schlenk flask and stored over 4 Å molecular sieves in a nitrogen-filled glovebox. Phenols were obtained from a commercial source and were opened and stored in a nitrogen-filled glovebox or, if previously exposed to air, distilled and stored in a nitrogen-filled glovebox.

Instrumentation: NMR characterization data were collected at 300 K on Bruker FT NMR instruments. ^{1}H NMR spectra were internally referenced to TMS (δ = 0 ppm). ^{13}C NMR spectra were internally referenced to the residual solvent signal (δ = 77.16 ppm). Data from ^{1}H NMR are reported as follows: chemical shift (δ ppm), multiplicity (s = singlet, d = doublet, t = triplet, q = quartet, m = multiplet, br = broad), coupling constant (Hz), integration. Quantitative NMR data was collected with an acquisition time of 5 seconds and a d1 relaxation delay of 10 seconds.

Melting point ranges for solid products were determined on a MEL-TEMP instrument and are reported uncorrected.

IR Spectra were obtained as films either neat or from CH_2Cl_2 on sodium chloride plates on a Thermo Scientific FT-IR or with an ATR source using a Nicolet iS5 FT-IR spectrometer. Data are presented as absorption frequency (cm^{-1}).

High-resolution mass spectrometry (HRMS) using ESI experiments were performed on a Bruker BioTOF II instrument using sodium trifluoroacetate internal standard and ammonium bicarbonate additive for negative ion detection or PEG 400 internal standard for positive ion detection.

3.5.2 Reaction Optimization Experiments

Control Experiments: Reactions prepared using benzophenone **3.10a** (0.1 mmol, 1.0 equiv), *Rac*-2-(di-*t*-butyldiphosphino)-1,1'-binapthyl, (TrixiePhos, y mol%), $[Ir(cod)OMe]_2$ (x mol%), 1,5-cyclooctadiene (1,5-COD, 0.1 mmol, 1.0 equiv), phenol (0.5 mmol, 5.0 equiv), and mesitylene (1.00 mL, 0.1 M) in PTFE-lined screw cap vials. The vials were sealed and heated to 150 °C in an aluminum heating block for 16 hours. Product yields were determined by ^1H NMR using 1,3,5-trimethoxybenzene internal standard (0.70 mL, 0.05 M in $CDCl_3$).

Solvent Screen: Reactions prepared using benzophenone **3.10a** (0.1 mmol, 1.0 equiv), TrixiePhos (y mol%), $[Ir(cod)OMe]_2$ (x mol%), 1,5-COD (0.1 mmol, 1.0 equiv), phenol (0.5 mmol, 5.0 equiv), and solvent (1.00 mL, 0.1 M) in PTFE-lined screw cap vials. The vials were sealed and heated to 150 °C in an aluminum heating block for 16 hours. Product yields were determined by ^1H NMR using 1,3,5-trimethoxybenzene internal standard (0.70 mL, 0.05 M in $CDCl_3$).

Catalyst Optimization:

Table 3.9 Catalyst screen

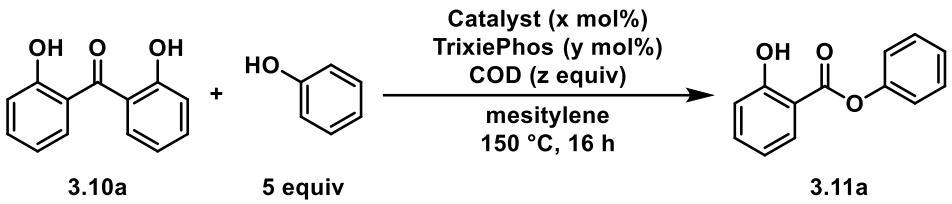

Entry	Catalyst (mol%)	TrixiePhos (mol%)	COD (equiv)	Conversion (%)[a]	3.11a (%)[a]	3.12 (%)[a]	3.13 (%)[a]
1	$[Rh(cod)OMe]_2$ (1)	3	1	44	0	0	11
2	$[Rh(cod)OH]_2$ (1)	3	1	28	0	0	8
3	$Ni(cod)_2$ (1)	3	1	0	0	0	0
4	$[Ir(cod)OPh]_2$ (1)	3	—	37	8	7	tr
5	$Rh(PPh_3)_3Cl$ (2)	—	—	36	0	0	tr
6	$Pd(PPh_3)_4$ (2)	—	—	36	0	0	0
7	Ir(cod)(acac) (1)	3	1	12	6	tr	2

a) Determined by qNMR; tr = trace

Reactions prepared using benzophenone **3.10a** (0.1 mmol, 1.0 equiv), TrixiePhos (y mol%), catalyst (x mol%), 1,5-COD (z equiv), phenol (0.5 mmol, 5.0 equiv), and solvent (1.00 mL, 0.1 M) in PTFE-lined screw cap vials. The vials were sealed and heated to 150 °C in an aluminum heating block for 16 hours. Product yields were determined by ^1H NMR using 1,3,5-trimethoxybenzene internal standard (0.70 mL, 0.05 M in $CDCl_3$).

Phosphine/Ligand Screen:

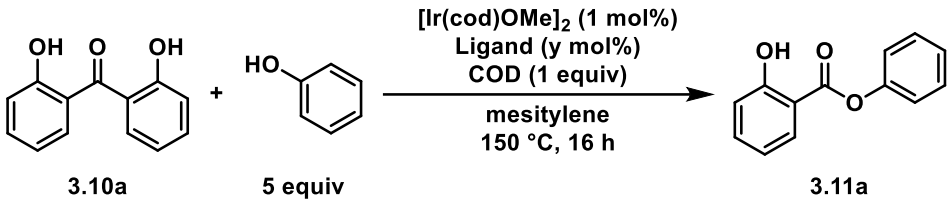

3.10a 5 equiv 3.11a

Entry	Ligand (mol%)	Conversion (%)[a]	3.11a (%)[a]	3.12 (%)[a]	3.13 (%)[a]
1	MePhos (3)	20	0	0	0
2	*t*BuMePhos (3)	13	2	tr	tr
3	BINAP (1.5)	9	tr	0	0
4	dppp (1.5)	12	0	0	0
5	PPh_3 (3)	16	tr	0	0
6	$P(tBu)_3$ (3)	13	tr	0	tr
7[b]	JohnPhos (3)	7	3	0	tr
8	TrixiePhos (3)	62	22	7	8

a) Determined by qNMR; b) No COD added; tr = trace

Reactions prepared using benzophenone **3.10a** (0.1 mmol, 1.0 equiv), ligand (y mol%), $[Ir(cod)OMe]_2$ (0.001 mmol, 1 mol%), 1,5-COD (0.1 mmol, 1 equiv), phenol (0.5 mmol, 5.0 equiv), and mesitylene (1.00 mL, 0.1 M) in PTFE-lined screw cap vials. The vials were sealed and heated to 150 °C in an aluminum heating block for 16 hours. Product yields were determined by ^1H NMR using 1,3,5-trimethoxybenzene internal standard (0.70 mL, 0.05 M in $CDCl_3$).

Catalyst Loading Screen: Reactions prepared using benzophenone **3.10a** (0.1 mmol, 1.0 equiv), TrixiePhos (3x mol%), $[Ir(cod)OMe]_2$ (x mol%), 1,5-COD (0.1 mmol, 1 equiv),

phenol (0.5 mmol, 5.0 equiv), and mesitylene (1.00 mL, 0.1 M) in PTFE-lined screw cap vials. The vials were sealed and heated to 150 °C in an aluminum heating block for 16 hours. Product yields were determined by ^{1}H NMR using 1,3,5-trimethoxybenzene internal standard (0.70 mL, 0.05 M in $CDCl_3$).

Ligand Loading Screen: Reactions prepared using benzophenone **3.10a** (0.1 mmol, 1.0 equiv), TrixiePhos (x mol%), $[Ir(cod)OMe]_2$ (0.002 mmol, 2 mol%), 1,5-COD (0.1 mmol, 1 equiv), phenol (0.5 mmol, 5.0 equiv), and mesitylene (1.00 mL, 0.1 M) in PTFE-lined screw cap vials. The vials were sealed and heated to 150 °C in an aluminum heating block for 16 hours. Product yields were determined by ^{1}H NMR using 1,3,5-trimethoxybenzene internal standard (0.70 mL, 0.05 M in $CDCl_3$).

Concentration Screen: Reactions prepared using benzophenone **3.10a** (0.1 mmol, 1.0 equiv), TrixiePhos (0.004 mmol, 4 mol%), $[Ir(cod)OMe]_2$ (0.002 mmol, 2 mol%), 1,5-COD (0.1 mmol, 1 equiv), phenol (0.5 mmol, 5.0 equiv), and mesitylene (volume required to give listed concentration of **3.10a**, or no solvent added) in PTFE-lined screw cap vials. The vials were sealed and heated to 150 °C or 170 °C in an aluminum heating block for 16 hours. Product yields were determined by ^{1}H NMR using 1,3,5-trimethoxybenzene internal standard (0.70 mL, 0.05 M in $CDCl_3$).

Temperature and Time Screen: Reactions prepared using benzophenone **3.10a** (0.1 mmol, 1.0 equiv), TrixiePhos (0.004 mmol, 4 mol%), $[Ir(cod)OMe]_2$ (0.002 mmol, 2 mol%), 1,5-COD (0.1 mmol, 1 equiv), phenol (0.5 mmol, 5.0 equiv), and mesitylene (1.00 mL, 0.1 M) in PTFE-lined screw cap vials. The vials were sealed and heated to listed temperature an aluminum heating block (for 150 and 160 °C) or a silicon oil bath (170 °C)

for time listed. Product yields were determined by ^{1}H NMR using 1,3,5-trimethoxybenzene internal standard (0.70 mL, 0.05 M in $CDCl_3$).

Acylation of aliphatic alcohols: Reactions prepared using benzophenone **3.10a** (0.1 mmol, 1.0 equiv), TrixiePhos (0.003 mmol, 3 mol%), $[Ir(cod)OMe]_2$ (0.001 mmol, 1 mol%), 1,5-COD (0.1 mmol, 1 equiv), benzyl alcohol or isoamyl alcohol (0.5 mmol, 5 equiv), phenol (if listed, 0.5 mmol, 5.0 equiv), and mesitylene (1.00 mL, 0.1 M) in PTFE-lined screw cap vials. The vials were sealed and heated to 150 °C an aluminum heating block for 16 hours. Product yields were determined by ^{1}H NMR using 1,3,5-trimethoxybenzene internal standard (0.70 mL, 0.05 M in $CDCl_3$) based on literature reported ^{1}H NMR data.[206–208]

Transesterification Experiments:

With catalyst: Reactions prepared using phenyl salicylate **3.11a** (0.1 mmol, 1 equiv), TrixiePhos (0.003 mmol, 3 mol%), $[Ir(cod)OMe]_2$ (0.001 mmol, 1 mol%), benzyl or isoamyl alcohol (0.5 mmol, 5 equiv), 1,5-COD (0.1 mmol, 1 equiv), and mesitylene (1.00 mL, 0.1 M) in PTFE-lined screw cap vials. The vials were sealed and heated to 150 °C for 16 hours. Product yields were determined by ^{1}H NMR using 1,3,5-trimethoxybenzene internal standard (0.70 mL, 0.05 M in $CDCl_3$) based on literature reported ^{1}H NMR data.[206–208]

Without catalyst: Reactions prepared using phenyl salicylate **3.11a** (0.1 mmol, 1 equiv), benzyl or isoamyl alcohol (0.5 mmol, 5 equiv), and mesitylene (1.00 mL, 0.1 M) in PTFE-lined screw cap vials. The vials were sealed and heated to 150 °C for 16 hours. Product

yields were determined by ^{1}H NMR using 1,3,5-trimethoxybenzene internal standard (0.70 mL, 0.05 M in $CDCl_3$) based on literature reported ^{1}H NMR data.[206–208]

3.5.3 Synthetic Experiments

General procedures for phenol acylation: TrixiePhos (1.6 mg, 0.004 mmol, 4 mol%), $[Ir(cod)OMe]_2$ (1.3 mg, 0.002 mmol, 2 mol%), ketone **3.14_** (0.100 mmol, 1 equiv), substituted phenol (1.000 mmol, 10 equiv), 1,5-COD (13 μL, 0.100 mmol, 1 equiv), and mesitylene (1.00 mL, 0.10 M) were added to a 2 mL PTFE-lined crimp top vial. The vial was sealed, removed from the glovebox, and heated to 170 °C in an oil bath for 20 h. If additional catalyst charges were used, the vial was returned to the glovebox and TrixiePhos (1.6 mg, 0.004 mmol, 4 mol%) and $[Ir(cod)OMe]_2$ (1.3 mg, 0.002 mmol, 2 mol%) were added. The vial was sealed and heated to 170 °C for an additional 20 h. Once the reaction was complete, the solvent was removed *in vacuo*. Rection mixtures were analyzed by quantitative ^{1}H NMR using 1,3,5-trimethoxybenzene, dibromomethane, or 4-methoxyacetophenone internal standard. Products were isolated with preparatory TLC.

3.5.4 Characterization Data

Starting materials **3.10a**[204] and **3.14_**[154] synthesized according to literature procedures, all data are consistent with prior synthesis. Characterization data for side products **3.12**[209] and **3.13**[210,211] is consistent with previously reported literature data.

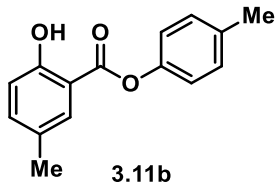

3.11b

p-Tolyl 2-hydroxy-5-methylbenzoate (**3.11b**). Prepared with 1 catalyst charges. Yellow Oil (72% by qNMR). R_f = 0.67 (25% Acetone/Hex). ^{1}H NMR (500 MHz, $CDCl_3$) δ 10.34 (s, 1H), 7.86 (d, *J* = 2.3 Hz, 1H), 7.34 (dd, *J* = 8.4, 2.3 Hz, 1H), 7.24 (d, *J* = 8.6 Hz, 3H), 7.08 (d, *J* = 8.1 Hz, 2H), 6.94 (d, *J* = 8.5 Hz, 1H), 2.39 (s, 3H), 2.34 (s, 3H). ^{13}C NMR (126 MHz, $CDCl_3$) δ 169.3, 160.2, 148.0, 137.6, 136.2, 130.3, 130.1, 128.8, 121.5, 117.7, 111.6, 21.1, 20.6. IR (thin film) 3224, 2924, 2854, 1693 cm^{-1}. HRMS (ESI) calcd for $C_{15}H_{13}O_3$ $[M-H]^-$ *m/z* 241.0870; found 241.0879.

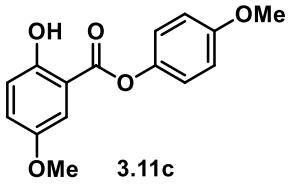

3.11c

4-Methoxyphenyl 2-hydroxy-5-methoxybenzoate (**3.11c**). Prepared with 1 catalyst charge. Yellow Solid (70% by qNMR). R_f = 0.49 (30% Et_2O/Hex). mp = 67.8–68.7 °C. ^{1}H NMR (500 MHz, $CDCl_3$) δ 10.16 (s, 1H), 7.50 (d, *J* = 3.1 Hz, 1H), 7.16 (dd, *J* = 9.1, 3.2 Hz, 1H), 7.16 – 7.10 (m, 2H), 6.99 – 6.94 (m, 3H), 3.84 (s, 3H), 3.83 (s, 3H). ^{13}C NMR (126 MHz, $CDCl_3$) δ 169.2, 157.9, 156.9, 152.3, 143.6, 125.1, 122.6, 119.0, 114.8, 112.1, 111.5, 77.4,

77.2, 76.9, 56.1, 55.8. IR (thin film) 1687, 1616, 1510, 1489 cm^{-1}. HRMS (ESI) calcd for $C_{15}H_{13}O_3$ $[M-H]^-$ *m/z* 273.0768; found 273.0778.

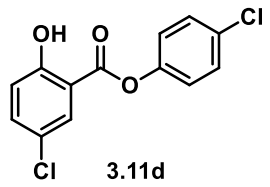

3.11d

4-chlorophenyl 5-chloro-2-hydroxybenzoate (**3.11d**). Prepared with 3 catalyst charges. White Solid (33% by qNMR). R_f = 0.68 (40% Et_2O/Hex). mp = 98.2–98.9 °C. ^1H NMR (400 MHz, $CDCl_3$) δ 10.32 (s, 1H), 8.02 (d, *J* = 2.6 Hz, 1H), 7.49 (dd, *J* = 8.9, 2.6 Hz, 1H), 7.45 – 7.41 (m, 2H), 7.20 – 7.12 (m, 2H), 7.01 (d, *J* = 8.9 Hz, 1H). ^{13}C NMR (126 MHz, $CDCl_3$) δ 167.9, 160.9, 148.4, 136.8, 132.3, 129.9, 129.6, 124.5, 123.1, 119.7, 112.6. IR (thin film) 1692, 1491, 1474 cm^{-1}. HRMS (ESI) calcd for $C_{13}H_7Cl_2O_3$ $[M-H]^-$ *m/z* 280.9778; found 280.9781.

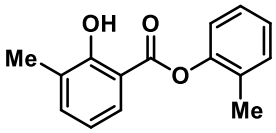

3.11e

o-Tolyl 2-hydroxy-3-methylbenzoate (**3.11e**). Prepared with 1 catalyst charges. Yellow Oil (48% by qNMR). R_f = 0.63 (20% Acetone/Hex). ^1H NMR (400 MHz, $CDCl_3$) δ 10.79 (s, 1H), 7.96 (dd, *J* = 8.0, 1.7 Hz, 1H), 7.41 (d, *J* = 7.2 Hz, 1H), 7.33 – 7.25 (m, 2H), 7.23 (dd, *J* = 7.3, 1.5 Hz, 1H), 7.13 (dd, *J* = 7.9, 1.5 Hz, 1H), 6.88 (t, *J* = 7.7 Hz, 1H), 2.30 (s, 4H), 2.24 (s, 3H). ^{13}C NMR (126 MHz, $CDCl_3$) δ 169.3, 160.8, 149.0, 137.4, 131.5, 130.5, 128.0, 127.2, 127.1, 126.7, 122.0, 119.0, 111.1, 16.3, 15.9. IR (thin film) 2925, 2853, 1683 cm^{-1}. HRMS (ESI) calcd for $C_{15}H_{13}O_3$ $[M-H]^-$ *m/z* 241.0870; found 241.0870.

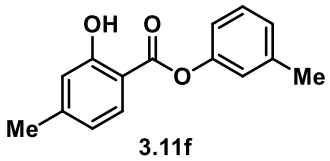

3.11f

m-Tolyl 2-hydroxy-4-methylbenzoate (**3.11f**). Prepared with 1 catalyst charges. Yellow Oil (69% by qNMR). R_f = 0.57 (20% Acetone/Hex). ^{1}H NMR (400 MHz, $CDCl_3$) δ 10.47 (s, 1H), 7.93 (d, *J* = 8.1 Hz, 1H), 7.32 (t, *J* = 7.8 Hz, 1H), 7.11 (d, *J* = 7.6 Hz, 1H), 7.04 – 6.96 (m, 2H), 6.85 (s, 1H), 6.78 (d, *J* = 8.1 Hz, 1H), 2.40 (s, 4H), 2.38 (s, 3H). ^{13}C NMR (126 MHz, $CDCl_3$) δ 169.2, 162.3, 150.3, 148.1, 140.0, 130.3, 129.5, 127.2, 122.4, 120.9, 118.8, 118.1, 109.5, 22.1, 21.5. IR (thin film) 1680 cm^{-1}. HRMS (ESI) calcd for $C_{15}H_{13}O_3$ $[M-H]^-$ *m/z* 241.0870; found 241.0882.

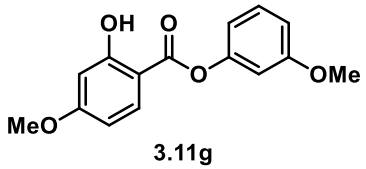

3.11g

3-Methoxyphenyl 2-hydroxy-4-methoxybenzoate (**3.11g**). Prepared with 1 catalyst charge in the same reaction as **3.10g**. Yellow Solid (42% by qNMR). R_f = 0.66 (30% Et_2O/Hex). mp = 70.2–71.5 °C ^{1}H NMR (400 MHz, $CDCl_3$) δ 10.71 (s, 1H), 7.96 (d, J = 8.8 Hz, 1H), 7.33 (t, J = 8.2 Hz, 1H), 6.84 (ddd, J = 8.4, 2.5, 0.9 Hz, 1H), 6.80 (ddd, J = 8.1, 2.2, 0.9 Hz, 1H), 6.75 (t, J = 2.3 Hz, 1H), 6.52 (dd, J = 8.8, 2.5 Hz, 1H), 6.50 (d, J = 2.4 Hz, 1H), 3.86 (s, 3H), 3.82 (s, 3H). ^{13}C NMR (126 MHz, $CDCl_3$) δ 168.8, 166.4, 164.7, 160.8, 151.3, 131.9, 130.1, 114.1, 112.2, 108.2, 107.9, 104.9, 100.9, 55.8, 55.6. IR (thin film) 1668, 1606, 1590 cm^{-1}. HRMS (ESI) calcd for $C_{15}H_{13}O_3$ $[M-H]^-$ *m/z* 273.0768; found 273.0781.

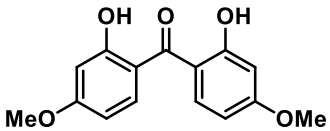

3.10g

bis(2-hydroxy-4-methoxyphenyl)methanone (**3.10g**). Prepared with 1 catalyst charge in the same reaction as **3.11g**. Yellow Solid (21% by qNMR). R_f = 0.53 (30% Et_2O/Hex). mp = 134.5–135.7 °C. ^{1}H NMR (400 MHz, $CDCl_3$) δ 11.33 (s, 1H), 7.55 (d, *J* = 8.9 Hz, 1H), 6.53 (d, *J* = 2.5 Hz, 1H), 6.48 (dd, *J* = 8.9, 2.5 Hz, 1H), 3.87 (s, 3H). ^{13}C NMR (126 MHz, $CDCl_3$) δ 199.3, 165.7, 164.8, 134.6, 113.6, 107.3, 101.7, 55.8. IR (thin film) 1617, 1590, 1575 cm^{-1}. HRMS (ESI) calcd for $C_{15}H_{13}O_3$ $[M-H]^-$ *m/z* 273.0768; found 273.0767.

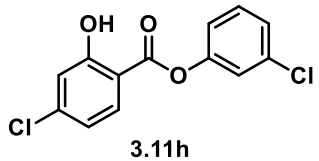

3.11h

3-chlorophenyl 4-chloro-2-hydroxybenzoate (**3.11h**). Prepared with 2 catalyst charges in the same reaction as **3.10h**. White Solid (8% by qNMR). R_f = 0.72 (25% Et_2O/Hex). mp = 106.4–107.5 °C. ^{1}H NMR (400 MHz, CD_2Cl_2) δ 10.44 (s, 1H), 8.00 (d, *J* = 8.6 Hz, 1H), 7.42 (t, *J* = 8.1 Hz, 1H), 7.33 (ddd, *J* = 8.1, 2.0, 1.0 Hz, 1H), 7.28 (t, *J* = 2.1 Hz, 1H), 7.16 (ddd, *J* = 8.1, 2.3, 1.1 Hz, 1H), 7.08 (d, *J* = 2.0 Hz, 1H), 7.00 (dd, *J* = 8.6, 2.1 Hz, 1H). ^{13}C NMR (126 MHz, $CDCl_3$) δ 168.1, 162.9, 150.5, 142.9, 135.2, 131.4, 130.6, 127.0, 122.5, 120.5, 120.1, 118.3, 110.3. IR (thin film) 1678, 1572 cm^{-1}. HRMS (ESI) calcd for $C_{13}H_7Cl_2O_3$ $[M-H]^-$ *m/z* 280.9778; found 280.9784.

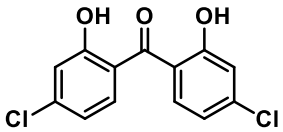

3.10h

bis(4-chloro-2-hydroxyphenyl)methanone (**3.10h**). Prepared with 2 catalyst charges in the same reaction as **3.11h**. Yellow Solid (<1% by qNMR). R_f = 0.43 (25% Et_2O/Hex). ^1H NMR (500 MHz, $CDCl_3$) δ 10.66 (s, 1H), 7.51 (d, *J* = 8.6 Hz, 1H), 7.12 (d, *J* = 2.0 Hz, 1H), 6.94 (dd, *J* = 8.6, 2.0 Hz, 1H). IR (thin film) 3094, 2961, 2921, 1805, 1723, 1615, 1584 cm^{-1}. HRMS (ESI) calcd for $C_{13}H_7Cl_2O_3$ $[M-H]^-$ *m/z* 280.9778; found 280.9769.

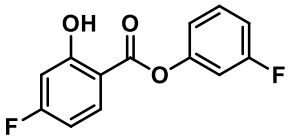

3.11i

3-fluorophenyl 4-fluoro-2-hydroxybenzoate (**3.11i**). Prepared with 1 catalyst charge in the same reaction as **3.16i**. White solid (35% by qNMR). R_f = 0.65 (15% EtOAc/Hex). mp = 57.0–58.5 °C. ^1H NMR (500 MHz, $CDCl_3$) δ 10.61 (d, *J* = 1.6 Hz, 1H), 8.06 (dd, *J* = 8.9, 6.5 Hz, 1H), 7.42 (td, *J* = 8.3, 6.4 Hz, 1H), 7.07 – 7.00 (m, 2H), 6.98 (dt, *J* = 9.2, 2.3 Hz, 1H), 6.74 (dd, *J* = 10.2, 2.5 Hz, 1H), 6.70 (ddd, *J* = 9.0, 8.0, 2.5 Hz, 1H). ^{13}C {^1H, ^{19}F} NMR (126 MHz, $CDCl_3$) δ 168.1, 168.0, 164.6, 163.1, 150.9, 132.8, 130.6, 117.6, 113.7, 110.0, 108.4, 108.1, 104.9. ^{19}F {^1H} NMR (376 MHz, CDCl3) δ -99.1, -110.3.IR (thin film) 1679, 1599, 1506 cm^{-1}. HRMS (ESI) calcd for $C_{13}H_7F_2O_3$ $[M-H]^-$ *m/z* 249.0369; found 249.0381.

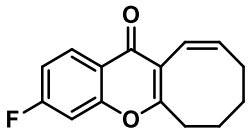

3.16i

(*Z*)-3-fluoro-6,7,8,9-tetrahydro-12H-cycloocta[*b*]chromen-12-one (**3.16i**). Prepared with 1 catalyst charge in the same reaction as **3.11i**. Colorless oil (4% by qNMR). R_f = 0.41 (15% EtOAc/Hex). ^{1}H NMR (500 MHz, $CDCl_3$) δ 8.29 – 8.20 (m, 1H), 7.18 – 7.09 (m, 2H), 6.48 (dt, *J* = 11.4, 1.4 Hz, 1H), 6.03 (dt, *J* = 11.3, 7.0 Hz, 1H), 2.87 – 2.72 (m, 3H), 2.19 (bs, 2H), 1.81 (bs, 2H), 1.60 (bs, 2H). ^{19}F {^{1}H} NMR (376 MHz, $CDCl_3$) δ -103.9. IR (thin film) 2929, 1732, 1657, 1616 cm^{-1}. HRMS (ESI) calcd for $C_{15}H_{13}FO_2$ $[M+Na]^+$ *m/z* 267.0792; found 267.0795.

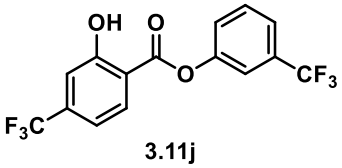

3.11j

3-(trifluoromethyl)phenyl 2-hydroxy-4-(trifluoromethyl)benzoate (**3.11j**). Prepared with 1 catalyst charge in the same reaction as **3.16j**. Yellow Oil (27% by qNMR). R_f = 0.57 (20% Et_2O/Hex). ^{1}H NMR (400 MHz, $CDCl_3$) δ 10.46 (s, 1H), 8.19 (d, *J* = 8.3 Hz, 1H), 7.66 – 7.56 (m, 2H), 7.53 (s, 1H), 7.49 – 7.36 (m, 1H), 7.33 (d, *J* = 1.7 Hz, 1H), 7.23 (dd, *J* = 8.5, 1.7 Hz, 1H). ^{13}C {^{1}H, ^{19}F} (126 MHz, $CDCl_3$) δ 167.8, 162.4, 150.0, 138.1, 132.6, 131.4, 130.5, 125.3, 123.7, 123.5, 123.2, 119.1, 116.1, 115.6, 114.2. ^{19}F {^{1}H} NMR (376 MHz, $CDCl_3$) δ -62.7, -63.9. IR (thin film) 2928, 2856, 1704 cm^{-1}. HRMS (ESI) calcd for $C_{15}H_7F_6O_3$ $[M-H]^-$ *m/z* 349.0305; found 349.0320.

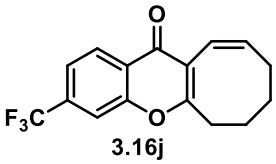

3.16j

(Z)-3-(trifluoromethyl)-6,7,8,9-tetrahydro-12H-cycloocta[b]chromen-12-one (**3.16j**). Prepared with 1 catalyst charge in the same reaction as **3.11j**. Yellow Solid (8% by qNMR). R_f = 0.29 (20% Et_2O/Hex). mp = 98.7–91.0 °C. ^{1}H NMR (500 MHz, $CDCl_3$) δ 8.34 (d, *J* = 8.3 Hz, 1H), 7.74 (s, 1H), 7.60 (dd, *J* = 8.5, 1.5 Hz, 1H), 6.46 (dt, *J* = 11.4, 1.4 Hz, 1H), 6.04 (dt, *J* = 11.4, 7.0 Hz, 1H), 2.85 – 2.78 (m, 2H), 2.20 – 2.14 (m, 2H), 1.81 (t, *J* = 6.0 Hz, 2H), 1.66 – 1.55 (m, 2H). ^{13}C {^{1}H, ^{19}F} NMR (126 MHz, $CDCl_3$) δ 176.6, 165.8, 155.6, 135.0, 134.7, 127.4, 125.3, 123.4, 121.1, 120.9, 119.9, 115.9, 32.4, 29.0, 24.3, 22.7. ^{19}F {^{1}H} NMR (376 MHz, $CDCl_3$) δ -63.0.IR (thin film) 2929, 2857, 1652 cm^{-1}. HRMS (ESI) calcd for $C_{16}H_1F_6O_3$ $[M+Na]^+$ *m/z* 317.0760; found 317.0763. The structure was confirmed by COSY, HSQC, and HMBC NMR.

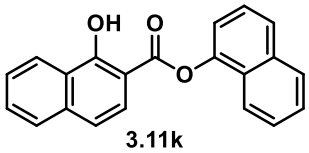

3.11k

naphthalen-1-yl 1-hydroxy-2-naphthoate (**3.11k**). Prepared with 2 catalyst charges in the same reaction as **3.10k**. Yellow Solid (18% by NMR). R_f = 0.15 (1% Et_2O/Hex). mp = 98.5–99.8 °C. ^{1}H NMR (500 MHz, $CDCl_3$) δ 11.72 (s, 1H), 8.47 (d, *J* = 8.3 Hz, 1H), 8.19 (d, *J* = 8.8 Hz, 1H), 7.98 – 7.88 (m, 2H), 7.85 (dd, *J* = 8.0, 5.4 Hz, 2H), 7.68 (ddd, *J* = 8.2, 7.0, 1.3 Hz, 1H), 7.61 – 7.49 (m, 5H), 7.44 (d, *J* = 8.7 Hz, 1H), 7.42 (dd, *J* = 7.4, 1.1 Hz, 1H). ^{13}C NMR (126 MHz, $CDCl_3$) δ 170.1, 162.3, 146.3, 137.8, 134.9, 130.1, 128.3, 127.8, 127.0, 127.0, 126.8, 126.7, 126.2, 125.6, 125.0, 124.5, 124.2, 121.3, 119.4, 118.5, 105.0.

IR (thin film) 2917, 2850, 1627, 1584, 1567 cm^{-1}. HRMS (ESI) calcd for $C_{21}H_{13}O_3$ $[M-H]^-$ *m/z* 313.0870; found 313.0866.

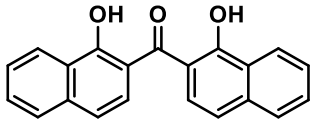

3.10k

bis(1-hydroxynaphthalen-2-yl)methanone (**3.10k**). Prepared with 2 catalyst charges in the same reaction as **3.11k**. Yellow Solid (9% by NMR). R_f = 0.20 (1% Et_2O/Hex). mp = 164.2–167.0 °C. ^1H NMR (500 MHz, $CDCl_3$) δ 12.45 (s, 2H), 8.52 (d, *J* = 8.7 Hz, 2H), 7.81 (d, *J* = 8.1 Hz, 2H), 7.74 – 7.62 (m, 4H), 7.58 (ddd, *J* = 8.2, 6.9, 1.3 Hz, 2H), 7.33 (d, *J* = 8.9 Hz, 2H). ^{13}C NMR (126 MHz, $CDCl_3$) δ 201.7, 162.1, 137.0, 130.3, 127.6, 127.4, 126.2, 125.5, 124.5, 118.2, 113.5. IR (thin film)3061, 2951, 2923, 2851, 1674, 1633, 1599, 1578 cm^{-1}. HRMS (ESI) calcd for $C_{21}H_{13}O_3$ $[M-H]^-$ *m/z* 313.0870; found 313.0875.

Chapter 4. Hydroxyl-Directed Carboacylation of Alkenes

4.1 Introduction

Previously, our group has studied alkene carboacylation, but initial carboacylation reactions were limited to quinolinyl ketones (Scheme 1.9).[77] Quinoline groups are useful for directing bond activation and preventing decarbonylation, but all attempts to remove the quinoline group were unsuccessful.[212] Based on this work, we have developed a more versatile, hydroxyl-directed variant of the carboacylation reaction. Using benzophenone **4.1** we can form dihydrobenzofuran **4.2** through directed ketone C–C bond activation and alkene carboacylation (Scheme 4.1).

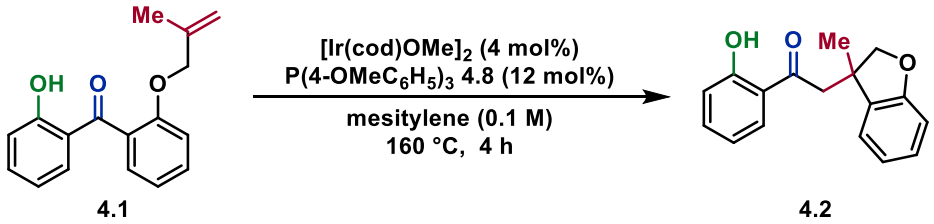

Scheme 4.1 Hydroxyl-directed alkene carboacylation

4.2 Reaction Optimization

We began our optimization of the hydroxyl-directed carboacylation reaction by testing catalyst and ligand systems that were used in our arene acylation[154] (Table 4.1 entry 1), oxyacylation[112,113,115] (Table 4.1 entries 2 and 3), and carboacylation[77] reactions (Table 4.1 entries 4 and 5). Only reactions with $[Ir(cod)OMe]_2$ resulted in any formation of cyclized **4.2**. Using $[Ir(cod)OMe]_2$ with (*R*)-MOP gave **4.2** in 24% yield with 15% of isomerized side product **4.3**. Reactions with Rh-catalysts gave **4.3** as the only product

Table 4.1 Initial carboacylation conditions screened

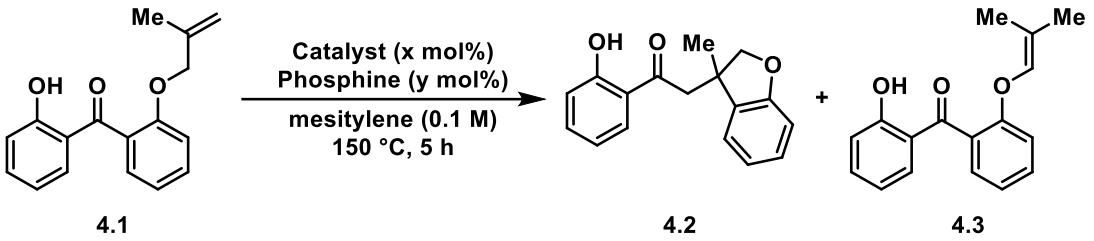

4.1 4.2 4.3

Entry	Catalyst (mol%)	Ligand (mol%)	Conversion (%)[a]	Yield of 4.2 (%)[a]	Yield of 4.3 (%)[a]
1	$[Ir(cod)OMe]_2$ (4)	TrixiePhos (12)	57	2	29
2	$[Ir(cod)OMe]_2$ (4)	*(R)*-MOP (12)	45	24	15
3	$Rh(cod)BF_4$ (10)	dppp (12)	98	0	85
4	$Rh(PPh_3)_3Cl$ (10)	—	64	tr	56
5	$[Rh(C_2H_4)_2Cl]_2$ (5)	—	92	0	63
6	$[Rh(cod)OMe]_2$ (4)	*(R)*-MOP (12)	15	0	0
7	$Pd(PPh_3)_4$ (10)	—	>99	0	0
8	$Ni(cod)_2$ (10)	—	16	0	0
9	$Ni(cod)_2$ (10)	**4.8** (12)	—[b]	0	0
10[c]	$Ni(cod)_2$ (10)	**4.8** (12)	—[b]	0	0

a) Determined by qNMR; b) not determined due to NMR signal broadening; c) 10 mol% K_2CO_3 added; tr = trace

(Table 4.1 entries 3–6). Attempted carboacylation with $Pd(PPh_3)_4$ resulted in full conversion of **4.1** to a mixture of unidentified products (Table 4.1 entry 7). Reactions with $Ni(cod)_2$, with and without ligand **4.8** and K_2CO_3 resulted in no product **4.2** or **4.3**

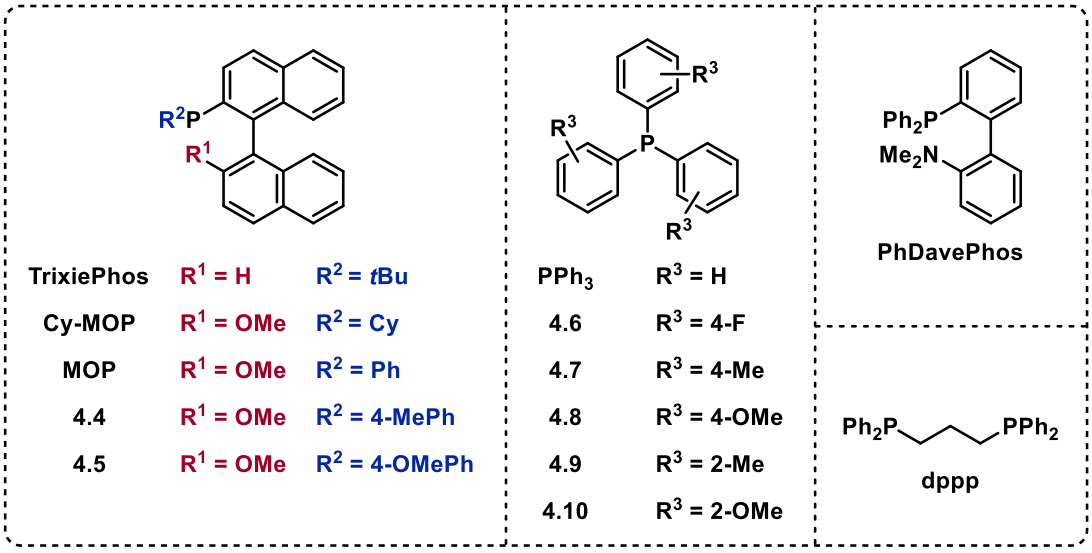

Scheme 4.2 Structure of phosphines used in reaction optimization

formation (Table 4.1 entries 8–10). $[Ir(cod)OMe]_2$ appeared to be the best catalyst and was used moving forwards.

Next, we examined the effect of ligand choice on carboacylation (Table 4.2). The structures of the ligands tested are shown in Scheme 4.2. Methoxy-substituted triarylphosphine **4.8** gave the best result overall, yielding 79% of **4.2** after 5 hours with no alkene isomerization to **4.3** (Table 4.2 entry 13). A control reaction using $[Ir(cod)OMe]_2$ with no phosphine present indicated that phosphine was required for carboacylation, only alkene isomerized product **4.3** was observed without it (Table 4.2 entry 1). Not all phosphines were effective, for example, tri-*tert*-butylphosphine resulted in only alkene isomerization to **4.3** (Table 4.2 entry 2). Reaction with tricyclohexylphosphine gave 8% of desired product **4.2** along with 5% of **4.3** with a low mass balance (Table 4.2 entry 3). Binaphthyl phosphines with *t*-butyl or cyclohexyl groups gave little to no product formation (Table 4.2 entries 4 and 5). Triarylphosphines gave the best results overall.

Table 4.2 Phosphine ligand optimization

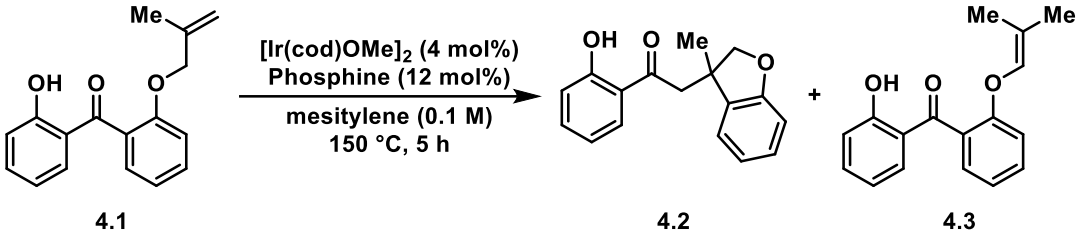

4.1 4.2 4.3

Entry	Ligand	Conversion (%)[a]	Yield of 4.2 (%)[a]	Yield of 4.3 (%)[a]
1	—	91	0	78
2	$P(tBu)_3$	31	0	21
3	PCy_3	42	8	5
4	TrixiePhos	57	2	29
5	Cy-MOP	20	0	6
6	PhDavePhos	66	16	28
7	(*R*)-MOP	45	24	15
8	**4.4**	56	32	7
9	**4.5**	80	50	8
10	**4.6**	*75*	*48*	*4*
11	PPh_3	*95*	*69*	*0*
12	**4.7**	*75*	*68*	*6*
13	**4.8**	*95*	*79*	*0*
14	**4.9**	*67*	*0*	*50*
15	**4.10**	*28*	*0*	*7*

a) Determined by qNMR

Electron-rich Buchwald-type phosphine PhDavePhos gave 16% of **4.2** with significant alkene isomerization (Table 4.2 entry 6). Reactions with a variety of MOP-style ligands showed that yield increased with increasing electron-richness of the non-binaphthyl aryl rings (Table 4.2 entries 7–9). A similar trend was observed with symmetric, 4-substituted triaryl phosphines (Table 4.2 entries 10–13). Yield increased going from -F < -H < -Me < -OMe with methoxy substituted phosphine **4.8** giving 79% of **4.2** after 5 hours. Reactions with electron-rich but sterically-hindered 2-substituted phenyl phosphines **4.9** and **4.10** showed no formation of product **4.2** with varying amounts of alkene isomerization (Table 4.2 entries 14 and 15). Triarylphosphine **4.8** gives the highest yield and was used for further optimization. As reactions with binaphthyl-substituted **4.5** formed **4.2** in moderate yield, this has potential to be used for an asymmetric carboacylation reaction.

A screen of catalyst loadings showed 4 mol% of $[Ir(cod)OMe]_2$ gave the best yield of **4.2** (Table 4.3 entry 4). Yield increased with catalyst loading up to 4 mol%, increasing to 5 mol% resulted in lower yield. No alkene isomerization to **4.3** was observed at any catalyst loading tested.

An iridium to phosphine ratio of 1:1.5, or a 1:3 ratio of $[Ir]_2$ to phosphine, was found to be optimal. Alkene isomerization to **4.3** was observed when the ratio was below 1:1 (Table 4.3 entry 1). At a 1:2 ratio, phosphine inhibited the reaction, lowering conversion and yield of **4.2** (Table 4.4 entry 4).

Table 4.3 Catalyst loading optimization

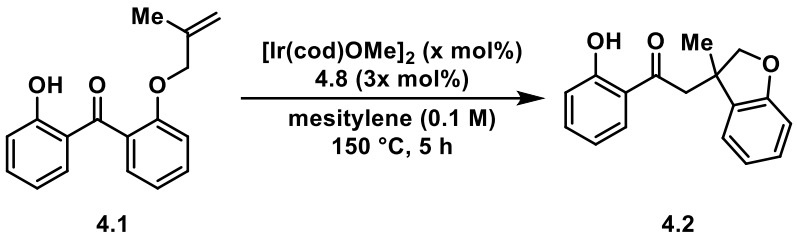

4.1 4.2

Entry	[Ir(cod)OMe]$_2$ (mol%)	4.8 (mol%)	Conversion (%)[a]	Yield of 4.2 (%)[a]
1	1	3	40	24
2	2	6	70	50
3	3	9	88	64
4	4	12	95	79
5	5	15	>99	69

a) Determined by qNMR

Table 4.4 Ligand loading optimization

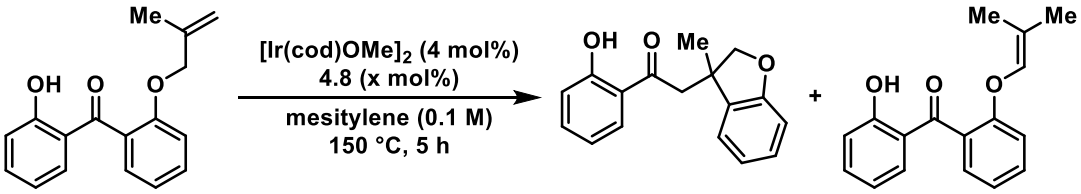

4.1 4.2 4.3

Entry	4.8 (mol%)	[Ir]:P	Conversion (%)[a]	Yield of 4.2 (%)[a]	Yield of 4.3 (%)[a]
1	4	1:0.5	75	38	8
2	8	1:1	97	68	0
3	12	1:1.5	95	79	0
4	16	1:2	64	30	0

a) Determined by qNMR

Various solvents were screened to determine the effect on the yield of carboacylation product **4.2** (Table 4.5). The best yield was achieved in mesitylene at 150 °C (Table 4.5 entry 1). Addition of 10 mol% K_2CO_3 to the reaction in mesitylene did not significantly alter the yield of **4.2**.

Table 4.5 Effect of solvent on yield

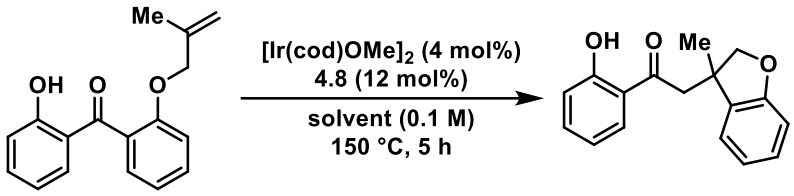

4.1 **4.2**

Entry	**Solvent**	**Temperature (°C)**	**Conversion (%)[a]**	**Yield of 4.2 (%)[a]**
1	Mesitylene	150	95	79
2	Decalin	150	98	65
3	1.2-Dichloroethane	150	77	54
4[b]	1,4-Dioxane	130	41	26
5[b]	Toluene	130	14	9

a) Determined by qNMR; b) 130 °C

Next, we determined the effect of temperature and time on the yield of **4.2** by carboacylation. As we observed nearly full conversion of **4.1** after 5 hours of heating to 150 °C, we examined lower reaction temperatures and longer reaction times. The mass balance of the reaction was around 80%, so shorter reaction times at 150 °C and 160 °C were also tested. The full results of this screen are shown in Figure 4.1. The maximum yield of the reaction was not strongly influenced by temperature, reaching a maximum just

over 70% yield. Some variability in yield of **4.2** was observed so reactions at 150 and 160 °C were repeated multiple times. Average yields over time indicate that 4 hours at 160 °C is optimum (Figure 4.1).

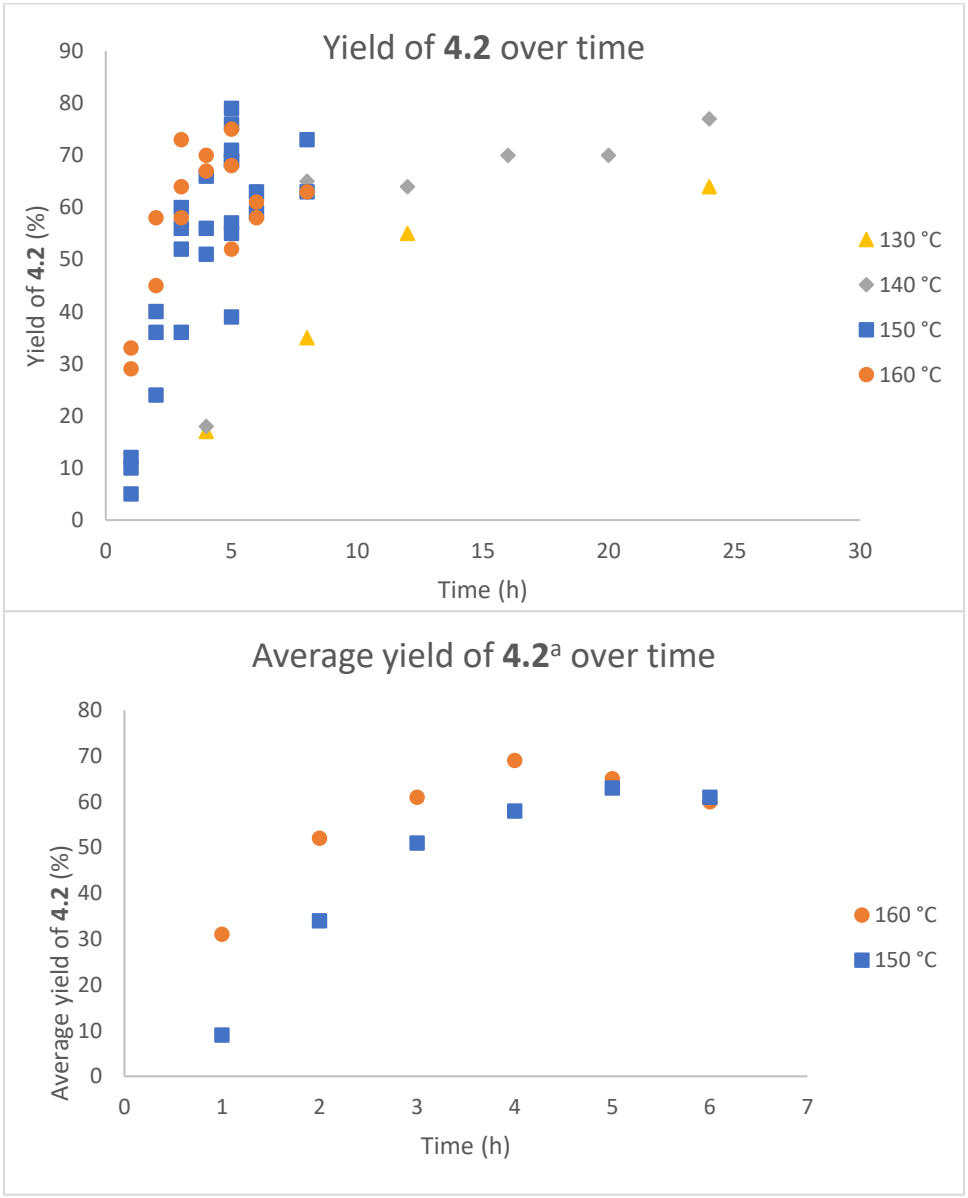

a) average of 2-7 reactions

Figure 4.1 Effect of temperature and time on reaction yield

Attempts to perform alkene carboacylation on a preparatory scale resulted in incomplete conversion of starting material **4.1**. This complicated purification as **4.1** and **4.2** are not easily separable. I examined purification conditions using TLC and was unable to separate the compounds using eluent from mixtures of ethyl acetate, acetone, diethyl ether, and dichloromethane with hexanes, pentane, petroleum ether, toluene, or benzene. Addition of 1-2% acetic acid or pretreatment with triethylamine did not improve separation. Using alumina instead of silica also resulted in no separation of compounds **4.1** and **4.2** by TLC.

4.3 Proposed Mechanism

We have proposed the following reaction mechanism of carboacylation (Scheme 4.3). The transformation would begin with deprotonation and association of the hydroxyl-

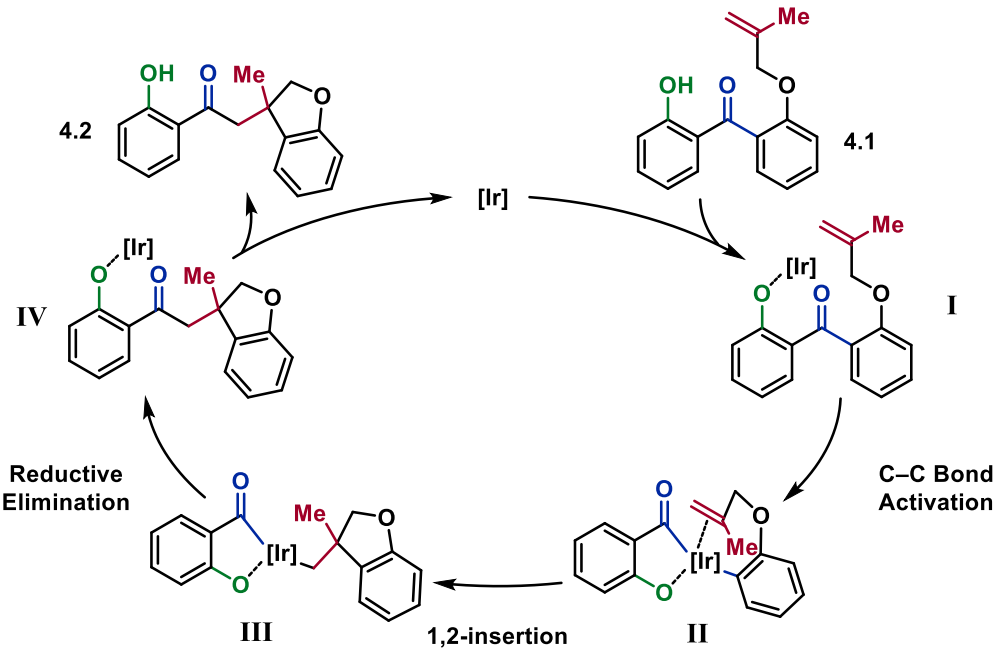

Scheme 4.3 Proposed mechanism of hydroxyl-directed carboacylation of alkenes

directing group to the catalyst forming intermediate **I**. Oxidative addition activates the C–C bond forming 5-membered metallocycle **II**. The coordinated pendent alkene undergoes a 1,2-insertion into the M–C bond forming cyclized **III**. Reductive elimination forming a new C–C bond followed by dissociation of the metal center forms **4.2** and closes the catalytic cycle.

4.4 Future Work

To conclude the work on hydroxyl-directed alkene carboacylation, we must improve purification conditions, attempt asymmetric induction using chiral ligands, and investigate the scope of the reaction. As discussed in Section 4.2, separation of compounds **4.1** and **4.2** is a significant challenge. To use alkene carboacylation on a preparatory scale, we must improve separation conditions or ensure that the reaction occurs with full conversion of the starting material.

Further experiments will be done attempting to induce asymmetry in product **4.2** using chiral ligands. Electron-rich MOP-style ligands are promising candidates, forming **4.2** in up to 50% yield by qNMR (Table 4.2), but we have not determined if this is occurring with any significant enantioinduction. I have developed an HPLC method to separate the enantiomers of **4.2**, but further optimization is needed to separate **4.1** from these products. To develop an asymmetric variant of this carboacylation reaction, we would need to improve the yield with MOP ligands. As yield appears to increase with increasingly electron-rich phosphines, reactions with dimethylamino-substituted MOP ligands should be performed. Other chiral ligand scaffolds should also be tested, such as ferrocene-based phosphines, electron-rich chiral NHCs, and phosphoramidite ligands.

Carboacylation with substituted analogues of **4.1** should be performed to determine the effect that steric and electronic changes have on the reaction (Scheme 4.4). Substituents with varied electronic properties such as methyl, methoxy, acetyl, and trifluoromethyl should be tested on both aryl rings. Methyl substitutions at each open position on the aryl rings can be used to determine the effect of altered steric-hinderance around the directing group and activated C–C bond. Other substrate modifications that should be investigated include alternate alkenes including other 1,1-disubstituted alkenes, and a mono- and a tri-substituted alkene. The length of the alkene tether should be modified to attempt to form 6- and 7-membered rings through carboacylation. Additional modifications could include altering the ether tether to an alkyl or amine group to form indane or indoline rings or replacing one arene with a heteroarene like pyrrole or indole.

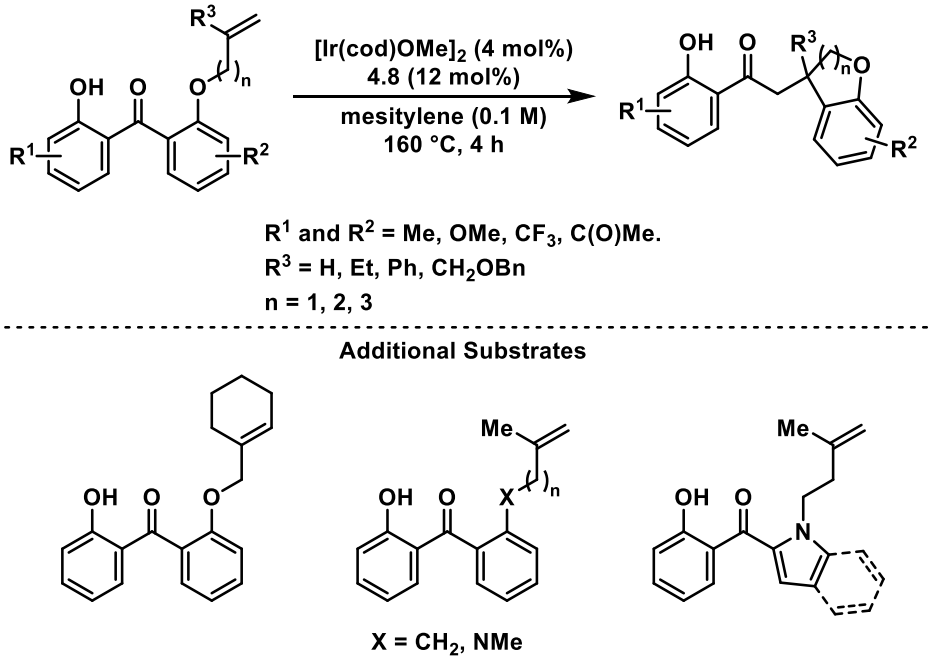

Scheme 4.4 Proposed substrate scope for carboacylation

4.5 Conclusion

We have developed a method for hydroxyl-directed carboacylation of alkenes using iridium-catalyzed C–C bond activation. This transformation forms dihydrobenzofuran rings with a quaternary carbon center in good yield after 3 hours. Preliminary results indicate potential for asymmetric induction with chiral phosphine ligands to develop an enantioselective carboacylation reaction. Further work is needed to optimize product purification, examine reaction scope, and study asymmetric carboacylation.

4.6 Experimental Details

4.6.1 General Information

General Experimental Procedures: All acylation reactions were prepared under inert atmosphere in an oxygen-regulated glovebox. Reaction progress was monitored using thin-layer chromatography (TLC) on 0.25 mm silica plates from SiliCycle. Eluted plates were visualized with UV light. Silica Gel Flash Column Chromatography was performed on 230–400 mesh (particle size 0.04–0.063 mm) silica gel purchased from SiliCycle.

Materials. Unless otherwise indicated, chemicals were obtained from commercial sources and used without further purification. All solvents for carboacylation were degassed by bubbling a stream of argon through the liquid in a Schlenk flask and stored over 4 Å molecular sieves in a nitrogen-filled glovebox.

Instrumentation: NMR characterization data were collected at 300 K on Bruker FT NMR instruments. ^{1}H NMR spectra were internally referenced to TMS (δ = 0 ppm). ^{13}C NMR spectra were internally referenced to the residual solvent signal (δ = 77.16 ppm). Data from ^{1}H NMR are reported as follows: chemical shift (δ ppm), multiplicity (s = singlet, d = doublet, t = triplet, q = quartet, m = multiplet, br = broad), coupling constant (Hz), integration. Quantitative NMR data was collected with an acquisition time of 5 seconds and a d1 relaxation delay of 10 seconds.

IR Spectra were obtained as films either neat or from CH_2Cl_2 on sodium chloride plates on a Thermo Scientific FT-IR or with an ATR source using a Nicolet iS5 FT-IR spectrometer. Data are presented as absorption frequency (cm^{-1}).

High-resolution mass spectrometry (HRMS) using ESI experiments were performed on a Bruker BioTOF II instrument using sodium trifluoroacetate internal standard and ammonium bicarbonate additive for negative ion detection or PEG 400 internal standard for positive ion detection.

4.6.2 Reaction Optimization Experiments

Catalyst screen: Reactions prepared using catalyst (x mol%), phosphine (y mol%), and premade solution of **4.1** (1.00 mL, 0.1 mmol, 0.1 M in mesitylene) in PTFE-lined screw cap vials. The vials were sealed and heated to 150 °C in an aluminum heating block for 5 hours. Product yields were determined by ^{1}H NMR using 1,3,5-trimethoxybenzene internal standard (0.70 mL, 0.05 M in $CDCl_3$).

Phosphine screen: Reactions prepared using $[Ir(cod)OMe]_2$ (4 mol%), phosphine (x mol%), and a premade solution of **4.1** (1 equiv, 0.1 M in mesitylene) in PTFE-lined screw cap vials. The vials were sealed and heated to 150 °C in an aluminum heating block for 5 hours. Product yields were determined by ^{1}H NMR using 1,3,5-trimethoxybenzene internal standard (0.70 mL, 0.05 M in $CDCl_3$).

Catalyst loading: Reactions prepared using $[Ir(cod)OMe]_2$ (x mol%), tris-(4-methoxyphenyl)phosphine (3x mol%), and a premade solution of **4.1** (0.1 mmol, 1 equiv, 0.1 M in mesitylene) in PTFE-lined screw cap vials. The vials were sealed and heated to 150 °C in an aluminum heating block for 5 hours. Product yields were determined by ^{1}H NMR using 1,3,5-trimethoxybenzene internal standard (0.70 mL, 0.04 M in $CDCl_3$).

Phosphine loading: Reactions prepared using $[Ir(cod)OMe]_2$ (0.004 mmol, 4 mol%), tris-(4-methoxyphenyl)phosphine (x mol%), and a premade solution of **4.1** (0.1 mmol, 1 equiv,

0.1 M in mesitylene) in PTFE-lined screw cap vials. The vials were sealed and heated to 150 °C in an aluminum heating block for 5 hours. Product yields were determined by ^{1}H NMR using 1,3,5-trimethoxybenzene internal standard (0.70 mL, 0.04 M in $CDCl_3$).

Solvent screen: Reactions prepared using $[Ir(cod)OMe]_2$ (0.004 mmol, 4 mol%), tris-(4-methoxyphenyl)phosphine (0.012 mmol, 12 mol%), **4.1** (0.1 mmol, 1 equiv), and solvent (1.00 mL, 0.1 M) in PTFE-lined screw cap vials. The vials were sealed and heated to 150 °C in an aluminum heating block for 5 hours. Product yields were determined by ^{1}H NMR using 1,3,5-trimethoxybenzene internal standard (0.70 mL, 0.04 M in $CDCl_3$).

Temperature and Time screening: Reactions prepared using $[Ir(cod)OMe]_2$ (0.004 mmol, 4 mol%), tris-(4-methoxyphenyl)phosphine (0.012 mmol, 12 mol%), **4.1** (0.1 mmol, 1 equiv), and solvent (1.00 mL, 0.1 M) in PTFE-lined screw cap vials. The vials were sealed and heated in an aluminum heating block for the time listed. Product yields were determined by ^{1}H NMR using 1,3,5-trimethoxybenzene internal standard (0.70 mL, 0.05 M in $CDCl_3$).

Table 4.6 Time screen at 130 and 140 °C

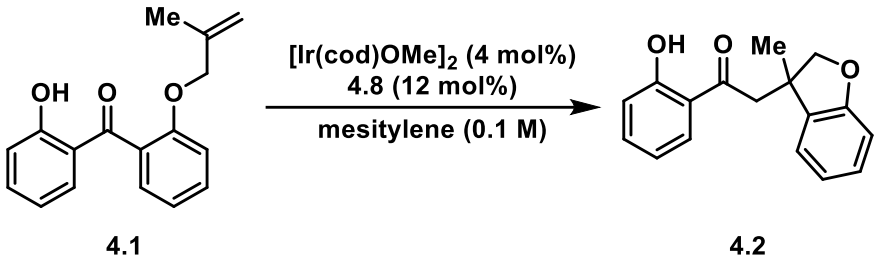

4.1 4.2

Entry	Temperature (°C)	Time (h)	Conversion (%)[a]	Yield 4.2 (%)[a]
1	130	4	39	17
2	130	8	58	35
3	130	12	82	55
4	130	24	89	64
5	140	4	38	18
6	140	8	88	65
7	140	12	94	64
8	140	24	100	77
9	140	16	100	70
10	140	20	100	70

a) Determined by qNMR

Table 4.7 Time screen at 150 °C

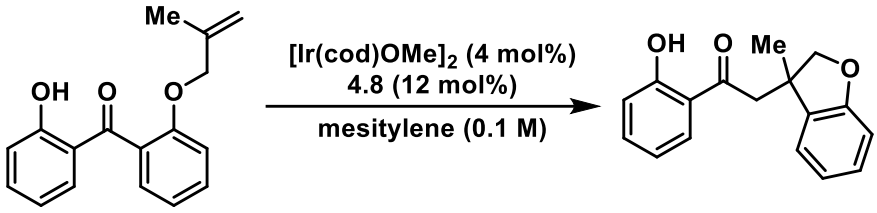

4.1 4.2

Entry	Time (h)	Conversion (%)[a]	Yield 4.2 (%)[a]
1	1	30	10
2	1	31	5
3	1	36	13
Average	1	32	9
4	2	50	24
5	2	65	37
6	2	65	40
Average	2	60	34
7	3	83	60
8	3	66	36
9	3	95	56
10	3	77	52
Average	3	80	51
11	4	81	51
12	4	97	56
13	4	93	66
Average	4	90	58
14	5	70	39
15	5	86	55
16	5	99	57
17	5	96	69
18	5	99	71
19	5	98	69
20	5	95	79
Average	5	92	63
21	6	99	63
22	6	92	59
Average	6	96	61
23	8	98	73
24	8	95	63
Average	8	97	68

a) Determined by qNMR

Table 4.8 Time screen at 160 °C

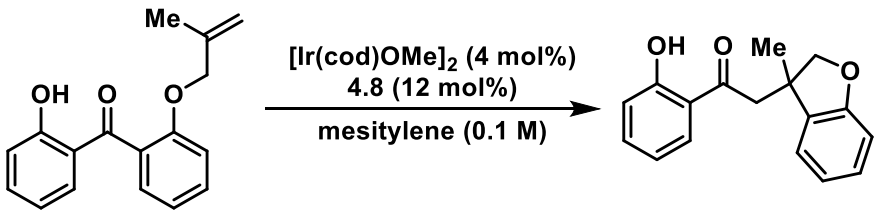

4.1 4.2

Entry	Time (h)	Conversion (%)[a]	Yield 4.2 (%)[a]
1	1	56	33
2	1	58	29
Average	1	57	31
3	2	82	58
4	2	75	45
Average	2	79	52
5	3	99	73
6	3	94	64
7	3	85	58
Average	3	90	61
8	4	97	67
9	4	97	70
Average	4	97	69
10	5	99	75
11	5	97	68
12	5	89	52
Average	5	95	65
13	6	96	61
14	6	99	58
Average	6	98	60
15	8	97	63

a) Determined by qNMR

4.6.3 Synthetic Experiments

Synthesis of 4.1: 2,2'-dihydroxybenzophenone (prepared according to literature procedure[204]) (4 mmol, 1 equiv), 3-chloro-2-methylpropene (4.4 mmol, 1.1 equiv), K_2CO_3 (4.4 mmol, 1.1 equiv), KI (0.4 mmol, 0.1 equiv), and acetone (12 mL, 0.33 M) added to a 6 dram vial and sealed with a PTFE-lined screw cap. The reaction mixture was heated to 50 °C in an aluminum heating block overnight. The resulting reaction mixture was filtered through Celite and rinsed with additional acetone. Solution was concentrated leaving a yellow oil. The oil was dissolved in ethyl acetate (20 mL) and washed with DI water (2 × 20 mL) and brine (10 mL). The organic phase was dried over Na_2SO_4, filtered, and concentrated. The resulting oil was purified with silica column chromatography (3% acetone/hex) to give a yellow oil **4.1** (0.9412 g, 88%).

Carboacylation for isolation of 4.2: $[Ir(cod)OMe]_2$ (0.01 mmol, 4 mol%), tris(4-methoxyphenyl)phosphine (0.03 mmol, 12 mol%), and solution of **4.1** (0.25 mmol, 1 equiv, 0.1 M in mesitylene) added to a vial with a PTFE-lined screw cap. The vial was sealed and heated to 150 °C in an aluminum heating block for 5 hours. Product isolated by preparatory TLC (20% acetone/hex) to give colorless oil **4.2** (51.0 mg, 76%).

4.6.4 Characterization data

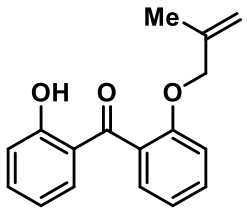

4.1

(2-hydroxyphenyl)(2-((2-methylallyl)oxy)phenyl)methanone (**4.1**). Yellow oil. R_f = 0.26 (5% Acetone/Hex). ^{1}H NMR (400 MHz, $CDCl_3$) δ 12.14 (s, 1H), 7.45 (m, 2H), 7.37 (dd, *J* = 8.0, 1.7 Hz, 1H), 7.32 (dd, *J* = 7.5, 1.8 Hz, 1H), 7.06 (td, *J* = 7.5, 0.9 Hz, 1H), 7.03 (dd, *J* = 8.4, 1.1 Hz, 1H), 6.99 (dd, *J* = 8.4, 0.9 Hz, 1H), 6.79 (ddd, *J* = 8.2, 7.2, 1.2 Hz, 1H), 4.87 – 4.80 (m, 2), 4.40 (bs, 2H), 1.59 (bs, 2H). ^{13}C NMR (101 MHz, $CDCl_3$) δ 202.2, 162.7, 155.7, 140.1, 136.5, 133.9, 131.9, 128.9, 128.2, 120.8, 120.4, 118.8, 118.0, 112.7, 112.6, 72.1, 19.2. IR (neat) 3077, 2976, 2916, 1628, 1600, 1581 cm^{-1}. HRMS (ESI) calcd for $C_{17}H_{16}O_3$ $[M+Na]^+$ *m/z* 291.0992; found 291.1000.

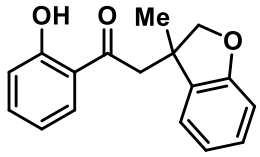

4.2

1-(2-hydroxyphenyl)-2-(3-methyl-2,3-dihydrobenzofuran-3-yl)ethan-1-one (**4.2**). Colorless oil. R_f = 0.6 (20% Acetone/Hex). ^{1}H NMR (400 MHz, $CDCl_3$) δ 12.22 (s, 1H), 7.67 (dd, *J* = 8.1, 1.7 Hz, 1H), 7.46 (ddd, *J* = 8.7, 7.1, 1.7 Hz, 1H), 7.20 – 7.11 (m, 2H), 6.98 (dd, *J* = 8.4, 1.2 Hz, 1H), 6.93 – 6.79 (m, 3H), 4.59 (d, *J* = 9.3 Hz, 1H), 4.50 (d, *J* = 9.4 Hz, 1H), 3.59 (d, *J* = 17.2 Hz, 1H), 3.26 (d, *J* = 17.2 Hz, 1H), 1.51 (s, 3H). ^{13}C NMR (101 MHz, $CDCl_3$) δ 204.4, 162.7, 159.1, 136.7, 134.9, 130.0, 128.7, 122.9, 120.8, 119.9,

119.1, 118.8, 110.1, 82.7, 47.5, 44.1, 25.4. IR(neat) 3047, 2963, 2929, 2890, 1639, 1613, 1598, 1580 cm^{-1}. HRMS (ESI) calcd for $C_{17}H_{16}O_3$ $[M-H]^-$ *m/z* 267.1027; found 267.1043.

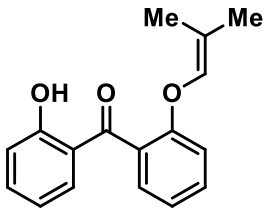

4.3

(2-hydroxyphenyl)(2-((2-methylprop-1-en-1-yl)oxy)phenyl)methanone (**4.3**). Yellow oil. R_f = 0.60 (15% Acetone/Hex). ^1H NMR (400 MHz, $CDCl_3$) δ 12.10 (s, 1H), 7.51 – 7.41 (m, 2H), 7.38 (dd, *J* = 8.0, 1.7 Hz, 1H), 7.35 (dd, *J* = 7.5, 1.7 Hz, 1H), 7.12 (td, *J* = 7.5, 1.0 Hz, 1H), 7.06 (dd, *J* = 8.3, 1.0 Hz, 1H), 7.03 (dd, *J* = 8.4, 1.1 Hz, 1H), 6.81 (ddd, *J* = 8.1, 7.1, 1.2 Hz, 1H), 6.14 (hept, *J* = 1.5 Hz, 1H), 1.60 (d, *J* = 1.4 Hz, 3H), 1.42 (d, *J* = 1.4 Hz, 3H). ^{13}C NMR (101 MHz, $CDCl_3$) δ 201.8, 162.8, 154.8, 136.6, 134.5, 134.0, 132.0, 129.2, 128.3, 122.1, 120.4, 119.6, 118.9, 118.1, 114.9, 19.4, 15.2. IR(neat) 3057, 2966, 2915, 1690, 1629 cm^{-1}. HRMS calcd for $C_{17}H_{16}O_3$ $[M+Na]^+$ *m/z* 291.0992; found 291.0994.

Bibliography

(1) Backvall, J.-E. Scientifc Background on the Nobel Prize in Chemistry 2010 - Palladium-Catalyzed Cross Couplings in Organic Synthesis. *Sci. Backgr. Nobel Prize Chem. 2010* **2010**.

(2) Blanksby, S. J.; Ellison, G. B. Bond Dissociation Energies of Organic Molecules. *Acc. Chem. Res.* **2003**, *36* (4), 255–263. https://doi.org/10.1021/ar020230d.

(3) Miyaura, N.; Yamada, K.; Suzuki, A. A New Stereospecific Cross-Coupling by the Palladium-Catalyzed Reaction of 1-Alkenylboranes with 1-Alkenyl or 1-Alkynyl Halides. *Tetrahedron Lett.* **1979**, *20* (36), 3437–3440. https://doi.org/10.1016/S0040-4039(01)95429-2.

(4) Miyaura, N.; Suzuki, A. Palladium-Catalyzed Cross-Coupling Reactions of Organoboron Compounds. *Chem. Rev.* **1995**, *95* (7), 2457–2483. https://doi.org/10.1021/cr00039a007.

(5) Negishi, E. I.; Hu, Q.; Huang, Z.; Qian, M.; Wang, G. Palladium-Catalyzed Alkenylation by the Negishi Coupling. *Aldrichimica Acta* **2005**, *38* (3), 71–88. https://doi.org/10.1002/chin.200638271.

(6) Negishi, E. I.; King, A. O.; Okukado, N. Selective Carbon-Carbon Bond Formation via Transition Metal Catalysis. 3. A Highly Selective Synthesis of Unsymmetrical Biaryls and Diarylmethanes by the Nickel- or Palladium-Catalyzed Reaction of Aryl- and Benzylzinc Derivatives with Aryl Halides. *J. Org. Chem.* **1977**, *42* (10), 1821–1823. https://doi.org/10.1021/jo00430a041.

(7) Azarian, D.; Dua, S. S.; Eaborn, C.; Walton, D. R. M. Reactions of Organic Halides with R_3 MMR_3 Compounds (M = Si, Ge, Sn) in the Presence of Tetrakis(Triarylphosphine)Palladium. *J. Organomet. Chem.* **1976**, *117* (3), C55–C57. https://doi.org/10.1016/S0022-328X(00)91902-8.

(8) Milstein, D.; Stiile, J. K. A General, Selective, and Facile Method for Ketone Synthesis from Acid Chlorides and Organotin Compounds Catalyzed by Palladium. *J. Am. Chem. Soc.* **1978**, *100* (11), 3636–3638. https://doi.org/10.1021/ja00479a077.

(9) Tamao, K.; Sumitani, K.; Kumada, M. Selective Carbon-Carbon Bond Formation by Cross-Coupling of Grignard Reagents with Organic Halides. Catalysis by Nickel-Phosphine Complexes. *J. Am. Chem. Soc.* **1972**, *94* (12), 4374–4376. https://doi.org/10.1021/ja00767a075.

(10) Biffis, A.; Centomo, P.; Del Zotto, A.; Zecca, M. Pd Metal Catalysts for Cross-Couplings and Related Reactions in the 21st Century: A Critical Review. *Chem. Rev.* **2018**, *118* (4), 2249–2295. https://doi.org/10.1021/acs.chemrev.7b00443.

(11) Nolan, S. P.; Navarro, O. C-C Bond Formation by Cross-Coupling. In *Comprehensive Organometallic Chemistry III*; Elsevier, 2007; Vol. 11, pp 1–37. https://doi.org/10.1016/b0-08-045047-4/00143-6.

(12) Nicolaou, K. C.; Bulger, P. G.; Sarlah, D. Palladium-Catalyzed Cross-Coupling Reactions in Total Synthesis. *Angew. Chemie - Int. Ed.* **2005**, *44* (29), 4442–4489. https://doi.org/10.1002/anie.200500368.

(13) Knappke, C. E. I.; Von Wangelin, A. J. 35 Years of Palladium-Catalyzed Cross-Coupling with Grignard Reagents: How Far Have We Come? *Chem. Soc. Rev.* **2011**, *40* (10), 4948–4962. https://doi.org/10.1039/c1cs15137a.

(14) Paul, D.; Das, S.; Saha, S.; Sharma, H.; Goswami, R. K. Intramolecular Heck Reaction in Total Synthesis of Natural Products: An Update. *European J. Org. Chem.* **2021**, *2021* (14), 2057–2076. https://doi.org/10.1002/ejoc.202100071.

(15) Heravi, M. M.; Mohammadkhani, L. Recent Applications of Stille Reaction in Total Synthesis of Natural Products: An Update. *J. Organomet. Chem.* **2018**, *869*, 106–200. https://doi.org/10.1016/j.jorganchem.2018.05.018.

(16) Heravi, M. M.; Hashemi, E.; Nazari, N. Negishi Coupling: An Easy Progress for C-C Bond Construction in Total Synthesis. *Mol. Divers.* **2014**, *18* (2), 441–472. https://doi.org/10.1007/s11030-014-9510-1.

(17) Xu, S.; Kim, E. H.; Wei, A.; Negishi, E. I. Pd- and Ni-Catalyzed Cross-Coupling Reactions in the Synthesis of Organic Electronic Materials. *Sci. Technol. Adv. Mater.* **2014**, *15* (4). https://doi.org/10.1088/1468-6996/15/4/044201.

(18) Heravi, M. M.; Hashemi, E.; Azimian, F. Recent Developments of the Stille Reaction as a Revolutionized Method in Total Synthesis. *Tetrahedron* **2014**, *70* (1), 7–21. https://doi.org/10.1016/j.tet.2013.07.108.

(19) Heravi, M. M.; Hashemi, E. Recent Applications of the Suzuki Reaction in Total Synthesis. *Tetrahedron* **2012**, *68* (45), 9145–9178. https://doi.org/10.1016/j.tet.2012.08.058.

(20) Heck, K. F.; Nolley, J. P. Palladium-Catalyzed Vinylic Hydrogen Substitution Reactions with Aryl, Benzyl, and Styryl Halides. *J. Org. Chem.* **1972**, *37* (14), 2320–2322. https://doi.org/10.1021/jo00979a024.

(21) Simões, J. A. M.; Beauchamp, J. L. Transition Metal–Hydrogen and Metal–Carbon Bond Strengths: The Keys to Catalysis. *Chem. Rev.* **1990**, *90* (4), 629–688.

https://doi.org/10.1021/cr00102a004.

(22) Halpern, J. Determination and Significance of Transition-Metal-Alkyl Bond Dissociation Energies. *Acc. Chem. Res.* **1982**, *15* (8), 238–244. https://doi.org/10.1021/ar00080a002.

(23) Tipper, C. F. H. Some Reactions of Cyclopropane, and a Comparison with the Lower Olefins. Part II. Some Platinous-Cyclopropane Complexes. *J. Chem. Soc.* **1955**, 2045–2046. https://doi.org/10.1039/JR9550002038.

(24) Adams, D. M.; Chatt, J.; Guy, R. G.; Sheppard, N. 149. The Structure of "Cyclopropane Platinous Chloride." *J. Chem. Soc.* **1961**, 738–742. https://doi.org/10.1039/JR9610000738.

(25) Khoury, P. R.; Goddard, J. D.; Tam, W. Ring Strain Energies: Substituted Rings, Norbornanes, Norbornenes and Norbornadienes. *Tetrahedron* **2004**, *60* (37), 8103–8112. https://doi.org/10.1016/j.tet.2004.06.100.

(26) Wender, P. A.; Takahashi, H.; Witulski, B. Transition Metal Catalyzed [5 + 2] Cycloadditions of Vinylcyclopropanes and Alkynes: A Homolog of the Diels-Alder Reaction for the Synthesis of Seven-Membered Rings. *J. Am. Chem. Soc.* **1995**, *117* (16), 4720–4721. https://doi.org/10.1021/ja00121a036.

(27) Jiao, L.; Lin, M.; Zhuo, L. G.; Yu, Z. X. Rh(I)-Catalyzed [(3 + 2) + 1] Cycloaddition of 1-Yne/Ene-Vinylcyclopropanes and CO: Homologous Pauson-Khand Reaction and Total Synthesis of (±)-α-Agarofuran. *Org. Lett.* **2010**, *12* (11), 2528–2531. https://doi.org/10.1021/ol100625e.

(28) Liu, L.; Montgomery, J. Dimerization of Cyclopropyl Ketones and Crossed Reactions of Cyclopropyl Ketones with Enones as an Entry to Five-Membered Rings. *J. Am. Chem. Soc.* **2006**, *128* (16), 5348–5349. https://doi.org/10.1021/ja0602187.

(29) Ogoshi, S.; Nagata, M.; Kurosawa, H. Formation of Nickeladihydropyran by Oxidative Addition of Cyclopropyl Ketone. Key Intermediate in Nickel-Catalyzed Cycloaddition. *J. Am. Chem. Soc.* **2006**, *128* (16), 5350–5351. https://doi.org/10.1021/ja060220y.

(30) Tamaki, T.; Nagata, M.; Ohashi, M.; Ogoshi, S. Synthesis and Reactivity of Six-Membered Oxa-Nickelacycles: A Ring-Opening Reaction of Cyclopropyl Ketones. *Chem. - A Eur. J.* **2009**, *15* (39), 10083–10091. https://doi.org/10.1002/chem.200900929.

(31) Chen, G. Q.; Zhang, X. N.; Wei, Y.; Tang, X. Y.; Shi, M. Catalyst-Dependent Divergent Synthesis of Pyrroles from 3-Alkynyl Imine Derivatives: A Noncarbonylative and Carbonylative Approach. *Angew. Chemie - Int. Ed.* **2014**, *53*

(32), 8492–8497. https://doi.org/10.1002/anie.201405215.

(32) Kamitani, A.; Chatani, N.; Morimoto, T.; Murai, S. Carbonylative [5 + 1] Cycloaddition of Cyclopropyl Imines Catalyzed by Ruthenium Carbonyl Complex. *J. Org. Chem.* **2000**, *65* (26), 9230–9233. https://doi.org/10.1021/jo000795s.

(33) Wender, P. A.; Pedersen, T. M.; Scanio, M. J. C. Transition Metal-Catalyzed Hetero-[5 + 2] Cycloadditions of Cyclopropyl Imines and Alkynes: Dihydroazepines from Simple, Readily Available Starting Materials. *J. Am. Chem. Soc.* **2002**, *124* (51), 15154–15155. https://doi.org/10.1021/ja0285013.

(34) Zhang, Y.-L.; Guo, R.-T.; He, J.-H.; Wang, X.-C. Catalytic Intermolecular Coupling of Rhodacyclopentanones with Alcohols Enabled by Dual Directing Strategy Scheme 1. Carbonylative C−C Activation Reactions of Poorly Activated Cyclopropanes. *Org. Lett* **2019**, *21*, 4239–4244. https://doi.org/10.1021/acs.orglett.9b01420.

(35) Evans, P. A.; Inglesby, P. A. Intermolecular Rhodium-Catalyzed [3+2+2] Carbocyclization of Alkenylidenecyclopropanes with Activated Alkynes: Regio- and Diastereoselective Construction of Cis-Fused Bicycloheptadienes. *J. Am. Chem. Soc.* **2008**, *130* (39), 12838–12839. https://doi.org/10.1021/ja803691p.

(36) Evans, P. A.; Inglesby, P. A.; Kilbride, K. A Concise Total Synthesis of Pyrovellerolactone Using a Rhodium-Catalyzed [(3 + 2) + 2] Carbocyclization Reaction. *Org. Lett.* **2013**, *15* (8), 1798–1801. https://doi.org/10.1021/ol400165x.

(37) Gulías, M.; Durán, J.; López, F.; Castedo, L.; Mascareñas, J. L. Palladium-Catalyzed [4 + 3] Intramolecular Cycloaddition of Alkylidenecyclopropanes and Dienes. *J. Am. Chem. Soc.* **2007**, *129* (36), 11026–11027. https://doi.org/10.1021/ja0756467.

(38) Liang, Y.; Jiang, X.; Yu, Z. X. Enantioselective Total Synthesis of (+)-Asteriscanolide via Rh(i)-Catalyzed [(5+2)+1] Reaction. *Chem. Commun.* **2011**, *47* (23), 6659–6661. https://doi.org/10.1039/c1cc11005e.

(39) Liang, Y.; Jiang, X.; Fu, X. F.; Ye, S.; Wang, T.; Yuan, J.; Wang, Y.; Yu, Z. X. Total Synthesis of (+)-Asteriscanolide: Further Exploration of the Rhodium(I)-Catalyzed [(5+2)+1] Reaction of Ene-Vinylcyclopropanes and CO. *Chem. - An Asian J.* **2012**, *7* (3), 593–604. https://doi.org/10.1002/asia.201100805.

(40) Yuan, C.; Jiao, L.; Yu, Z. X. Formal Total Synthesis of (±)-Hirsutic Acid C Using the Tandem Rh(I)-Catalyzed [(5+2)+1] Cycloaddition/Aldol Reaction. *Tetrahedron Lett.* **2010**, *51* (43), 5674–5676. https://doi.org/10.1016/j.tetlet.2010.08.028.

(41) Fan, X.; Zhuo, L. G.; Tu, Y. Q.; Yu, Z. X. Formal Syntheses of (±)-Asterisca-

3(15),6-Diene and (±)-Pentalenene Using Rh(I)-Catalyzed [(5+2)+1] Cycloaddition. *Tetrahedron* **2009**, *65* (24), 4709–4713. https://doi.org/10.1016/j.tet.2009.04.020.

(42) Fan, X.; Tang, M. X.; Zhuo, L. G.; Tu, Y. Q.; Yu, Z. X. An Expeditious and High-Yield Formal Synthesis of Hirsutene Using Rh(I)-Catalyzed [(5+2)+1] Cycloaddition. *Tetrahedron Lett.* **2009**, *50* (2), 155–157. https://doi.org/10.1016/j.tetlet.2008.10.023.

(43) Wender, P. A.; Fuji, M.; Husfeld, C. O.; Love, J. A. Rhodium-Catalyzed [5 + 2] Cycloadditions of Allenes and Vinylcyclopropanes: Asymmetric Total Synthesis of (+)-Dictamnol. *Org. Lett.* **1999**, *1* (1), 137–139. https://doi.org/10.1021/ol990599b.

(44) Yu, Z. X.; Wender, P. A.; Houk, K. N. On the Mechanism of [Rh(CO)2Cl]2-Catalyzed Intermolecular (5 + 2) Reactions between Vinylcyclopropanes and Alkynes. *J. Am. Chem. Soc.* **2004**, *126* (30), 9154–9155. https://doi.org/10.1021/ja048739m.

(45) Wender, P. A.; Zhang, L. Asymmetric Total Synthesis of (+)-Aphanamol I Based on the Transition Metal Catalyzed [5 + 2] Cycloaddition of Allenes and Vinylcyclopropanes. *Org. Lett.* **2000**, *2* (15), 2323–2325. https://doi.org/10.1021/ol006085q.

(46) Jiao, L.; Yuan, C.; Yu, Z. X. Tandem Rh(I)-Catalyzed [(5+2)+1] Cycloaddition/Aldol Reaction for the Construction of Linear Triquinane Skeleton: Total Syntheses of (±)-Hirsutene and (±)-1-Desoxyhypnophilin. *J. Am. Chem. Soc.* **2008**, *130* (13), 4421–4430. https://doi.org/10.1021/ja7100449.

(47) Wender, P. A.; Gamber, G. G.; Scanio, M. J. C. Polycyclic Compounds from Simple , Readily Available Starting Materials. *Angew. Chemie Int. Ed.* **2001**, 3895–3897. https://doi.org/10.1002/1521-3773(20011015)40:20<3895::AID-ANIE3895>3.0.CO;2-%23.

(48) Trost, B. M.; Hu, Y.; Horne, D. B. Total Synthesis of (+)-Frondosin A. Application of the RU-Catalyzed [5+2] Cycloaddition. *J. Am. Chem. Soc.* **2007**, *129* (38), 11781–11790. https://doi.org/10.1021/ja073272b.

(49) Trost, B. M.; Waser, J.; Meyer, A. Total Synthesis of (-)-Pseudolaric Acid B. *J. Am. Chem. Soc.* **2007**, *129* (47), 14556–14557. https://doi.org/10.1021/ja076165q.

(50) Ashfeld, B. L.; Martin, S. F. Enantioselective Syntheses of Tremulenediol A and Tremulenolide A. *Tetrahedron* **2006**, *62* (45), 10497–10506. https://doi.org/10.1016/j.tet.2006.05.087.

(51) Goldberg, A. F. G.; Stoltz, B. M. A Palladium-Catalyzed Vinylcyclopropane (3 +

2) Cycloaddition Approach to the Melodinus Alkaloids. *Org. Lett.* **2011**, *13* (16), 4474–4476. https://doi.org/10.1021/ol2017615.

(52) Trost, B. M.; Bai, W. J.; Hohn, C.; Bai, Y.; Cregg, J. J. Palladium-Catalyzed Asymmetric Allylic Alkylation of 3-Substituted 1 H-Indoles and Tryptophan Derivatives with Vinylcyclopropanes. *J. Am. Chem. Soc.* **2018**, *140* (21), 6710–6717. https://doi.org/10.1021/jacs.8b03656.

(53) Wender, P. A.; Christopher Bi, F.; Brodney, M. A.; Gosselin, F. Asymmetric Synthesis of the Tricyclic Core of NGF-Inducing Cyathane Diterpenes via a Transition-Metal-Catalyzed [5 + 2] Cycloaddition. *Org. Lett.* **2001**, *3* (13), 2105–2108. https://doi.org/10.1021/ol0160699.

(54) Houston, S. D.; Xing, H.; Bernhardt, P. V.; Vanden Berg, T. J.; Tsanaktsidis, J.; Savage, G. P.; Williams, C. M. Cyclooctatetraenes through Valence Isomerization of Cubanes: Scope and Limitations. *Chem. - A Eur. J.* **2019**, *25* (11), 2735–2739. https://doi.org/10.1002/chem.201805124.

(55) Cassar, L.; Eaton, P. E.; Halpern, J.; Cassar, L. Catalysis of Symmetry-Restricted Reactions by Transition Metal Compounds. The Valence Isomerization of Cubane. *J. Am. Chem. Soc.* **1970**, *92* (11), 3515–3518. https://doi.org/10.1021/ja00714a075.

(56) Chapman, N. B.; Key, J. M.; Toyne, K. J. The Valence Isomerisation of Homocubane Derivatives. *Tetrahedron Lett.* **1970**, *11* (60), 5211–5214. https://doi.org/10.1016/S0040-4039(00)99975-1.

(57) Griffin, G. W.; Marchand, A. P. Synthesis and Chemistry of Cubanes. *Chem. Rev.* **1989**, *89* (5), 997–1010. https://doi.org/10.1021/cr00095a003.

(58) Xu, T.; Dong, G. Rhodium-Catalyzed Regioselective Carboacylation of Olefins: A C-C Bond Activation Approach for Accessing Fused-Ring Systems. *Angew. Chemie - Int. Ed.* **2012**, *51* (30), 7567–7571. https://doi.org/10.1002/anie.201202771.

(59) Xu, T.; Ko, H. M.; Savage, N. A.; Dong, G. Highly Enantioselective Rh-Catalyzed Carboacylation of Olefins: Efficient Syntheses of Chiral Poly-Fused Rings. *J. Am. Chem. Soc.* **2012**, *134* (49), 20005–20008. https://doi.org/10.1021/ja309978c.

(60) Deng, L.; Xu, T.; Li, H.; Dong, G. Enantioselective Rh-Catalyzed Carboacylation of C=N Bonds via C-C Activation of Benzocyclobutenones. *J. Am. Chem. Soc.* **2016**, *138* (1), 369–374. https://doi.org/10.1021/jacs.5b11120.

(61) Qin, Y.; Zhan, J. L.; Shan, T. tian; Xu, T. Total Synthesis of Penta-Me Amurensin H and Diptoindonesin G Featuring a Rh-Catalyzed Carboacylation/Aromatization Cascade Enabled by C–C Activation. *Tetrahedron Lett.* **2019**, *60* (13), 925–927. https://doi.org/10.1016/j.tetlet.2019.02.040.

(62) Sun, T.; Zhang, Y.; Qiu, B.; Wang, Y.; Qin, Y.; Dong, G.; Xu, T. Rhodium(I)-Catalyzed Carboacylation/Aromatization Cascade Initiated by Regioselective C−C Activation of Benzocyclobutenones. *Angew. Chemie - Int. Ed.* **2018**, *57* (11), 2859–2863. https://doi.org/10.1002/anie.201713179.

(63) Qiu, B.; Li, X. T.; Zhang, J. Y.; Zhan, J. L.; Huang, S. P.; Xu, T. Catalytic Enantioselective Synthesis of 3,4-Polyfused Oxindoles with Quaternary All-Carbon Stereocenters: A Rh-Catalyzed C-C Activation Approach. *Org. Lett.* **2018**, *20* (23), 7689–7693. https://doi.org/10.1021/acs.orglett.8b03412.

(64) Zhang, Y.; Shen, S.; Fang, H.; Xu, T. Total Synthesis of Galanthamine and Lycoramine Featuring an Early-Stage C-C and a Late-Stage Dehydrogenation via C-H Activation. *Org. Lett.* **2020**, *22* (4), 1244–1248. https://doi.org/10.1021/acs.orglett.9b04337.

(65) Deng, L.; Chen, M.; Dong, G. Concise Synthesis of (-)-Cycloclavine and (-)-5-Epi-Cycloclavine via Asymmetric C-C Activation. *J. Am. Chem. Soc.* **2018**, *140* (30), 9652–9658. https://doi.org/10.1021/jacs.8b05549.

(66) Murakami, M.; Amii, H.; Shigeto, K.; Ito, Y. Breaking of the C-C Bond of Cyclobutanones by Rhodium(I) and Its Extension to Catalytic Synthetic Reactions. *J. Am. Chem. Soc.* **1996**, *118* (35), 8285–8290. https://doi.org/10.1021/ja9604525.

(67) Murakami, M.; Amii, H.; Ito, Y. Selective Activation of Carbon-Carbon Bonds next to a Carbonyl Group. *Nature* **1994**, *370* (6490), 540–541. https://doi.org/10.1038/370540a0.

(68) Korotvička, A.; Císařová, I.; Roithová, J.; Kotora, M. Synthesis of Aromatic Compounds by Catalytic C-C Bond Activation of Biphenylene or Angular [3]Phenylene. *Chem. - A Eur. J.* **2012**, *18* (14), 4200–4207. https://doi.org/10.1002/chem.201103888.

(69) Perthuisot, C.; Edelbach, B. L.; Zubris, D. L.; Simhai, N.; Iverson, C. N.; Müller, C.; Satoh, T.; Jones, W. D. Cleavage of the Carbon-Carbon Bond in Biphenylene Using Transition Metals. *J. Mol. Catal. A Chem.* **2002**, *189*, 157–168.

(70) Zhang, X.; Carpenter, G. B.; Sweigart, D. A. Carbon-Carbon Bond Activation in Biphenylene. Effect of η6-Coordination to Manganese Tricarbonyl. *Organometallics* **1999**, *18* (23), 4887–4888. https://doi.org/10.1021/om990634i.

(71) Satoh, T.; Jones, W. D. Palladium-Catalyzed Coupling Reactions of Biphenylene with Olefins, Arylboronic Acids, and Ketones Involving C-C Bond Cleavage. *Organometallics* **2001**, *20* (13), 2916–2919. https://doi.org/10.1021/om010196r.

(72) Edelbach, B. L.; Lachicotte, R. J.; Jones, W. D. Mechanistic Investigation of Catalytic Carbon-Carbon Bond Activation and Formation by Platinum and

Palladium Phosphine Complexes. *J. Am. Chem. Soc.* **1998**, *120* (12), 2843–2853. https://doi.org/10.1021/ja973368d.

(73) William Suggs, J. Activation of Aldehyde C-H Bonds to Oxidative Addition via Formation of 3-Methyl-2-Aminopyridyl Aldimines and Related Compounds: Rhodium Based Catalytic Hydroacylation. *J. Am. Chem. Soc.* **1979**, *101* (2), 489. https://doi.org/10.1021/ja00496a040.

(74) Koh, J. J.; Lee, W. H.; Williard, P. G.; Risen, W. M. The PtP(C6H11)3(C2H4)2 Mediated Activation of Aldehyde C–H Bonds via Chelate-Assisted Oxidative Addition Reactions. *J. Organomet. Chem.* **1985**, *284* (3), 409–419. https://doi.org/10.1016/0022-328X(85)80038-3.

(75) Suggs, J. W.; Jun, C. H. Directed Cleavage of Carbon-Carbon Bonds by Transition Metals: The α-Bonds of Ketones. *J. Am. Chem. Soc.* **1984**, *106* (10), 3054–3056. https://doi.org/10.1021/ja00322a063.

(76) William Suggs, J.; Cox, S. D. Directed Cleavage of sp^2-sp Carbon-Carbon Bonds. *J. Organomet. Chem.* **1981**, *221* (2), 199–201. https://doi.org/10.1016/S0022-328X(00)89055-5.

(77) Dreis, A. M.; Douglas, C. J. Catalytic Carbon-Carbon σ Bond Activation: An Intramolecular Carbo-Acylation Reaction with Acylquinolines. *J. Am. Chem. Soc.* **2009**, *131* (2), 412–413. https://doi.org/10.1021/ja8066308.

(78) Rathbun, C. M.; Johnson, J. B. Rhodium-Catalyzed Acylation with Quinolinyl Ketones: Carbon-Carbon Single Bond Activation as the Turnover-Limiting Step of Catalysis. *J. Am. Chem. Soc.* **2011**, *133* (7), 2031–2033. https://doi.org/10.1021/ja109686v.

(79) Lutz, J. P.; Rathbun, C. M.; Stevenson, S. M.; Powell, B. M.; Boman, T. S.; Baxter, C. E.; Zona, J. M.; Johnson, J. B. Rate-Limiting Step of the Rh-Catalyzed Carboacylation of Alkenes: C-C Bond Activation or Migratory Insertion? *J. Am. Chem. Soc.* **2012**, *134* (1), 715–722. https://doi.org/10.1021/ja210307s.

(80) Ling, T.; Rivas, F. All-Carbon Quaternary Centers in Natural Products and Medicinal Chemistry: Recent Advances. *Tetrahedron* **2016**, *72* (43), 6729–6777. https://doi.org/10.1016/j.tet.2016.09.002.

(81) Prusov, E. V. Construction of Quaternary Stereogenic Centers in the Total Synthesis of Natural Products. *Angew. Chemie - Int. Ed.* **2017**, *56* (46), 14356–14358. https://doi.org/10.1002/anie.201706629.

(82) Marek, I.; Minko, Y.; Pasco, M.; Mejuch, T.; Gilboa, N.; Chechik, H.; Das, J. P. All-Carbon Quaternary Stereogenic Centers in Acyclic Systems through the Creation of Several C-C Bonds per Chemical Step. *J. Am. Chem. Soc.* **2014**, *136*

(7), 2682–2694. https://doi.org/10.1021/ja410424g.

(83) Wang, J. J.; Chen, W.; Zuo, S.; Liu, L.; Zhang, X.; Wang, J. J. Direct Exchange of a Ketone Methyl or Aryl Group to Another Aryl Group through C-C Bond Activation Assisted by Rhodium Chelation. *Angew. Chemie - Int. Ed.* **2012**, *51* (49), 12334–12338. https://doi.org/10.1002/anie.201206693.

(84) Dennis, J. M.; Compagner, C. T.; Dorn, S. K.; Johnson, J. B. Rhodium-Catalyzed Interconversion of Quinolinyl Ketones with Boronic Acids via C-C Bond Activation. *Org. Lett.* **2016**, *18* (14), 3334–3337. https://doi.org/10.1021/acs.orglett.6b01434.

(85) Zhu, J.; Chen, P. hao; Lu, G.; Liu, P.; Dong, G. Ruthenium-Catalyzed Reductive Cleavage of Unstrained Aryl-Aryl Bonds: Reaction Development and Mechanistic Study. *J. Am. Chem. Soc.* **2019**, *141* (46), 18630–18640. https://doi.org/10.1021/jacs.9b11605.

(86) Wagner, C. J.; Salisbury, E. A.; Schoonover, E. J.; VanderRoest, J. P.; Johnson, J. B. Pyridine-Directed Carbon–Carbon Single Bond Activation: Rhodium-Catalyzed Decarbonylation of Aryl and Heteroaromatic Ketones. *Tetrahedron Lett.* **2021**, 153132. https://doi.org/10.1016/j.tetlet.2021.153132.

(87) Gribkov, D. V.; Pastine, S. J.; Schnürch, M.; Sames, D. Ruthenium Catalyzed Decarbonylative Arylation at Sp^3 Carbon Centers in Pyrrolidine and Piperidine Heterocycles. *J. Am. Chem. Soc.* **2007**, *129* (38), 11750–11755. https://doi.org/10.1021/ja072577n.

(88) Jiang, C.; Zheng, Z. J.; Yu, T. Y.; Wei, H. Suzuki-Miyaura Coupling of Unstrained Ketones via Chelation-Assisted C-C Bond Cleavage. *Org. Biomol. Chem.* **2018**, *16* (39), 7174–7177. https://doi.org/10.1039/c8ob02075b.

(89) Zhong, J.; Long, Y.; Yan, X.; He, S.; Ye, R.; Xiang, H.; Zhou, X. Rhodium-Catalyzed Pyridine N-Oxide Assisted Suzuki-Miyaura Coupling Reaction via C(O)-C Bond Activation. *Org. Lett.* **2019**, *21* (23), 9790–9794. https://doi.org/10.1021/acs.orglett.9b04068.

(90) Jun, C. H.; Lee, H. Catalytic Carbon-Carbon Bond Activation of Unstrained Ketone by Soluble Transition-Metal Complex [13]. *J. Am. Chem. Soc.* **1999**, *121* (4), 880–881. https://doi.org/10.1021/ja983197s.

(91) Xia, Y.; Wang, J.; Dong, G. Suzuki-Miyaura Coupling of Simple Ketones via Activation of Unstrained Carbon-Carbon Bonds. *J. Am. Chem. Soc.* **2018**, *140* (16), 5347–5351. https://doi.org/10.1021/jacs.8b02462.

(92) Ko, H. M.; Dong, G. Cooperative Activation of Cyclobutanones and Olefins Leads to Bridged Ring Systems by a Catalytic [4 + 2] Coupling. *Nat. Chem.* **2014**, *6* (8),

739–744. https://doi.org/10.1038/nchem.1989.

(93) Ahn, J. A.; Chang, D. H.; Young, J. P.; Ye, R. Y.; Loupy, A.; Jun, C. H. Solvent-Free Chelation-Assisted Catalytic C-C Bond Cleavage of Unstrained Ketone by Rhodium(I) Complexes under Microwave Irradiation. *Adv. Synth. Catal.* **2006**, *348* (1–2), 55–58. https://doi.org/10.1002/adsc.200505233.

(94) Kim, D. S.; Park, W. J.; Jun, C. H. Metal-Organic Cooperative Catalysis in C-H and C-C Bond Activation. *Chem. Rev.* **2017**, *117* (13), 8977–9015. https://doi.org/10.1021/acs.chemrev.6b00554.

(95) Hou, S. H.; Prichina, A. Y.; Zhang, M.; Dong, G. Asymmetric Total Syntheses of Di- and Sesquiterpenoids by Catalytic C−C Activation of Cyclopentanones. *Angew. Chemie - Int. Ed.* **2020**, *59* (20), 7848–7856. https://doi.org/10.1002/anie.201915821.

(96) Li, Z.; Zhang, S. L.; Fu, Y.; Guo, Q. X.; Liu, L. Mechanism of Ni-Catalyzed Selective C-O Bond Activation in Cross-Coupling of Aryl Esters. *J. Am. Chem. Soc.* **2009**, *131* (25), 8815–8823. https://doi.org/10.1021/ja810157e.

(97) Ishuzu T.; Yamamoto, A.; Yamamoto, A. Selective Cleavage of C-O Bonds in Esters through Oxidative Addition to Nickel(0) Complexes. *Chem. Lett.* **1976**, *5* (10), 1091–1094. https://doi.org/10.1246/cl.1976.1091.

(98) Chatani, N.; Tatamidani, H.; Ie, Y.; Kakiuchi, F.; Murai, S. The Ruthenium-Catalyzed Reductive Decarboxylation of Esters: Catalytic Reactions Involving the Cleavage of Acyl-Oxygen Bonds of Esters [2]. *J. Am. Chem. Soc.* **2001**, *123* (20), 4849–4850. https://doi.org/10.1021/ja0103501.

(99) Dr., L. J. G.; Paetzold, J. Pd-Catalyzed Decarbonylative Olefination Of. *Angew. Chem. Int. Ed.* **2002**, *41* (7), 1237–1241.

(100) Hiraki, K.; Kira, S. I.; Kawano, H. Formation of Di- And Tricarbonylruthenium(0) Species from $[RuH_2(CO)(PPh_3)_3]$ via Decarbonylation of Methyl Benzoates: X-Ray Crystal Structures of $[Ru(CO)_2(PPh_3)_3]$ and $[Ru(O_2)(CO)_2(PPh_3)_2]$. *Bull. Chem. Soc. Jpn.* **1997**, *70* (7), 1583–1592. https://doi.org/10.1246/bcsj.70.1583.

(101) Tatamidani, H.; Yokota, K.; Kakiuchi, F.; Chatani, N. Catalytic Cross-Coupling Reaction of Esters with Organoboron Compounds and Decarbonylative Reduction of Esters with $HCOONH_4$: A New Route to Acyl Transition Metal Complexes through the Cleavage of Acyl−Oxygen Bonds in Esters. *J. Org. Chem.* **2004**, *69* (17), 5615–5621. https://doi.org/10.1021/jo0492719.

(102) Guo, L.; Rueping, M. Transition-Metal-Catalyzed Decarbonylative Coupling Reactions: Concepts, Classifications, and Applications. *Chem. - A Eur. J.* **2018**, *24* (31), 7794–7809. https://doi.org/10.1002/chem.201704670.

(103) Nagayama, K.; Shimizu, I.; Yamamoto, A. Oxidative Addition of Aryl and Benzyl Trifluoroacetates to Zerovalent Palladium Complexes with Two Modes of C–O Bond Cleavage Process. *Bull. Chem. Soc. Jpn* **1999**, *72* (4), 799–803.

(104) Kakino, R.; Shimizu, I.; Yamamoto, A. Synthesis of Trifluoromethyl Ketones by Palladium-Catalyzed Cross-Coupling Reaction of Phenyl Trifluoroacetate with Organoboron Compounds. *Bull. Chem. Soc. Jpn.* **2001**, *74* (2), 371–376. https://doi.org/10.1246/bcsj.74.371.

(105) Wang, J. J.; Zuo, S.; Chen, W.; Zhang, X.; Tan, K.; Tian, Y.; Wang, J. J. Catalytic Formation of Ketones from Unactivated Esters through Rhodium Chelation-Assisted C-O Bond Activation. *J. Org. Chem.* **2013**, *78* (17), 8217–8231. https://doi.org/10.1021/jo400949p.

(106) Tatamidani, H.; Kakiuchi, F.; Chatani, N. A New Ketone Synthesis by Palladium-Catalyzed Cross-Coupling Reactions of Esters with Organoboron Compounds. *Org. Lett.* **2004**, *6* (20), 3597–3599. https://doi.org/10.1021/ol048513o.

(107) Shi, S.; Lei, P.; Szostak, M. Pd-PEPPSI: A General Pd-NHC Precatalyst for Suzuki-Miyaura Cross-Coupling of Esters by C-O Cleavage. *Organometallics* **2017**, *36* (19), 3784–3789. https://doi.org/10.1021/acs.organomet.7b00565.

(108) Ben Halima, T.; Zhang, W.; Yalaoui, I.; Hong, X.; Yang, Y.-F.; Houk, K. N.; Newman, S. G. Palladium-Catalyzed Suzuki–Miyaura Coupling of Aryl Esters. *J. Am. Chem. Soc.* **2017**, *139* (3), 1311–1318. https://doi.org/10.1021/jacs.6b12329.

(109) Hie, L.; Fine Nathel, N. F.; Hong, X.; Yang, Y. F.; Houk, K. N.; Garg, N. K. Nickel-Catalyzed Activation of Acyl C-O Bonds of Methyl Esters. *Angew. Chemie - Int. Ed.* **2016**, *55* (8), 2810–2814. https://doi.org/10.1002/anie.201511486.

(110) Buchspies, J.; Rahman, M. M.; Szostak, M. Transamidation of Amides and Amidation of Esters by Selective N-C(O)/O-C(O) Cleavage Mediated by Air- and Moisture-Stable Half-Sandwich Nickel(II)-NHC Complexes. *Molecules* **2021**, *26* (1), 188. https://doi.org/10.3390/molecules26010188.

(111) Murai, M.; Miki, K.; Ohe, K. A New Route to 3-Acyl-2-Aminobenzofurans: Palladium-Catalysed Cycloisomerisation of 2-(Cyanomethyl)Phenyl Esters. *Chem. Commun.* **2009**, No. 23, 3466–3468. https://doi.org/10.1039/b904127c.

(112) Hoang, G. T.; Reddy, V. J.; Nguyen, H. H. K.; Douglas, C. J. Insertion of an Alkene into an Ester: Intramolecular Oxyacylation Reaction of Alkenes through Acyl C-O Bond Activation. *Angew. Chemie - Int. Ed.* **2011**, *50* (8), 1882–1884. https://doi.org/10.1002/anie.201005767.

(113) Hoang, G. T.; Walsh, D. J.; McGarry, K. A.; Anderson, C. B.; Douglas, C. J. Development and Mechanistic Study of Quinoline-Directed Acyl C-O Bond

Activation and Alkene Oxyacylation Reactions. *J. Org. Chem.* **2017**, *82* (6), 2972–2983. https://doi.org/10.1021/acs.joc.6b03011.

(114) Uson, R.; Oro, L. A.; Cabeza, J. A.; Bryndza, H. E.; Stepro, M. P. Dinuclear Methoxy, Cyclooctadiene, and Barrelene Complexes of Rhodium(I) and Iridium(I). In *Inorganic Syntheses*; John Wiley & Sons, Inc., 1985; Vol. 23, pp 126–130. https://doi.org/10.1002/9780470132548.ch25.

(115) Hoang, G. T.; Pan, Z.; Brethorst, J. T.; Douglas, C. J. Intramolecular Oxyacylation of Alkenes Using a Hydroxyl Directing Group. *J. Org. Chem.* **2014**, *79* (23), 11383–11394. https://doi.org/10.1021/jo501814n.

(116) Iyori, Y.; Chatani, N. Nickel-Catalyzed C–O/O–H Annulation of Salicylate Esters with Alkynes: Activation of C–O Bond in Esters. *Chem. Lett.* **2021**, *50* (3), 510–512. https://doi.org/10.1246/cl.200885.

(117) Banovetz, H. K.; Vickerman, K. L.; David, C. M.; Alkan, M.; Stanley, L. M. Palladium-Catalyzed Intermolecular Alkene Carboacylation via Ester C–O Bond Activation. *Org. Lett.* **2021**, *23*, 37. https://doi.org/10.1021/acs.orglett.1c00940.

(118) Jr., Wade, L. G. *Organic Chemistry*, 6th ed.; Prentice Hall PTR, 2006.

(119) Firouzabadi, H.; Iranpoor, N.; Nowrouzi, F. Aluminum Dodecatungstophosphate (AlPW12O40) as a Non-Hygroscopic Lewis Acid Catalyst for the Efficient Friedel-Crafts Acylation of Aromatic Compounds under Solvent-Less Conditions. *Tetrahedron* **2004**, *60* (48), 10843–10850. https://doi.org/10.1016/j.tet.2004.09.049.

(120) Cho, J.-Y.; Tse, M. K.; Holmes, D.; Maleczka, R. E.; Smith, M. R. Remarkably Selective Iridium Catalysts for the Elaboration of Aromatic C-H Bonds. *Science (80-.).* **2002**, *295* (5553), 305–308. https://doi.org/10.1126/science.1067074.

(121) Ishiyama, T.; Takagi, J.; Ishida, K.; Miyaura, N.; Anastasi, N. R.; Hartwig, J. F. Mild Iridium-Catalyzed Borylation of Arenes. High Turnover Numbers, Room Temperature Reactions, and Isolation of a Potential Intermediate. *J. Am. Chem. Soc.* **2002**, *124* (3), 390–391. https://doi.org/10.1021/ja0173019.

(122) Ishiyama, T.; Takagi, J.; Hartwig, J. F.; Miyaura, N. A Stoichiometric Aromatic C-H Borylation Catalyzed by Iridium (I)/2, 2′-Bipyridine Complexes at Room Temperature. *Angew. Chemie Int. Ed.* **2002**, *41*, 3056–3058. https://doi.org/10.1002/1521-3773(20020816)41:16<3056::AID-ANIE3056>3.0.CO;2-#.

(123) Tamura, H.; Yamazaki, H.; Sato, H.; Sakaki, S. Iridium-Catalyzed Borylation of Benzene with Diboron. Theoretical Elucidation of Catalytic Cycle Including Unusual Iridium(V) Intermediate. *J. Am. Chem. Soc.* **2003**, *125* (51), 16114–

16126. https://doi.org/10.1021/ja0302937.

(124) Boller, T. M.; Murphy, J. M.; Hapke, M.; Ishiyama, T.; Miyaura, N.; Hartwig, J. F. Mechanism of the Mild Functionalization of Arenes by Diboron Reagents Catalyzed by Iridium Complexes. Intermediacy and Chemistry of Bipyridine-Ligated Iridium Trisboryl Complexes. *J. Am. Chem. Soc.* **2005**, *127* (41), 14263–14278. https://doi.org/10.1021/ja053433g.

(125) Chen, C.; Hartwig, J. F. Rhodium-Catalyzed Intermolecular C-H Silylation of Arenes with High Steric Regiocontrol. *Science.* **2014**, *343* (6173), 853–857. https://doi.org/10.1126/science.1248042.

(126) Cheng, C.; Hartwig, J. F. Iridium-Catalyzed Silylation of Aryl C-H Bonds. *J. Am. Chem. Soc.* **2015**, *137* (2), 592–595. https://doi.org/10.1021/ja511352u.

(127) Karmel, C.; Chen, Z.; Hartwig, J. F. Iridium-Catalyzed Silylation of C-H Bonds in Unactivated Arenes: A Sterically Encumbered Phenanthroline Ligand Accelerates Catalysis. *J. Am. Chem. Soc.* **2019**, *141* (17), 7063–7072. https://doi.org/10.1021/jacs.9b01972.

(128) Zhou, P. X.; Ye, Y. Y.; Liu, C.; Zhao, L. B.; Hou, J. Y.; Chen, D. Q.; Tang, Q.; Wang, A. Q.; Zhang, J. Y.; Huang, Q. X.; Xu, P. F.; Liang, Y. M. Palladium-Catalyzed Acylation/Alkenylation of Aryl Iodide: A Domino Approach Based on the Catellani-Lautens Reaction. *ACS Catal.* **2015**, *5* (8), 4927–4931. https://doi.org/10.1021/acscatal.5b00516.

(129) Webb, J. R.; Burgess, S. A.; Cundari, T. R.; Gunnoe, T. B. Activation of Carbon-Hydrogen Bonds and Dihydrogen by 1,2-CH-Addition across Metal-Heteroatom Bonds. *Dalt. Trans.* **2013**, *42* (48), 16646–16665. https://doi.org/10.1039/c3dt52164h.

(130) Oxgaard, J.; Tenn, W. J.; Nielsen, R. J.; Periana, R. A.; Goddard, W. A.; Jonas Oxgaard, *,†; William J. Tenn, I.; Robert J. Nielsen, †; Roy A. Periana, ‡ and; William A. Goddard, I. Mechanistic Analysis of Iridium Heteroatom C-H Activation: Evidence for an Internal Electrophilic Substitution Mechanism. *Organometallics* **2007**, *26* (7), 1565–1567. https://doi.org/10.1021/om061189b.

(131) Yeung, C. S.; Zhao, X.; Borduas, N.; Dong, V. M. Pd-Catalyzed Ortho-Arylation of Phenylacetamides, Benzamides, and Anilides with Simple Arenes Using Sodium Persulfate. *Chem. Sci.* **2010**, *1* (3), 331–336. https://doi.org/10.1039/c0sc00231c.

(132) Zhao, X.; Yeung, C. S.; Dong, V. M. Palladium-Catalyzed Ortho-Arylation of O-Phenylcarbamates with Simple Arenes and Sodium Persulfate. *J. Am. Chem. Soc.* **2010**, *132* (16), 5837–5844. https://doi.org/10.1021/ja100783c.

(133) Xi, P.; Yang, F.; Qin, S.; Zhao, D.; Lan, J.; Gao, G.; Hu, C.; You, J. Palladium(II)-Catalyzed Oxidative C-H/C-H Cross-Coupling of Heteroarenes. *J. Am. Chem. Soc.* **2010**, *132* (6), 1822–1824. https://doi.org/10.1021/ja909807f.

(134) Lyons, T. W.; Sanford, M. S. Palladium-Catalyzed Ligand-Directed C-H Functionalization Reactions. *Chem. Rev.* **2010**, *110* (2), 1147–1169. https://doi.org/10.1021/cr900184e.

(135) Yang, Y.; Lan, J.; You, J. Oxidative C-H/C-H Coupling Reactions between Two (Hetero)Arenes. *Chem. Rev.* **2017**, *117* (13), 8787–8863. https://doi.org/10.1021/acs.chemrev.6b00567.

(136) Nairoukh, Z.; Cormier, M.; Marek, I. Merging C-H and C-C Bond Cleavage in Organic Synthesis. *Nat. Rev. Chem.* **2017**, *1* (5), 1–17. https://doi.org/10.1038/s41570-017-0035.

(137) Wei, Y.; Hu, P.; Zhang, M.; Su, W. Metal-Catalyzed Decarboxylative C-H Functionalization. *Chem. Rev.* **2017**, *117* (13), 8864–8907. https://doi.org/10.1021/acs.chemrev.6b00516.

(138) Meng, G.; Szostak, M. Site-Selective C-H/C-N Activation by Cooperative Catalysis: Primary Amides as Arylating Reagents in Directed C-H Arylation. *ACS Catal.* **2017**, *7* (10), 7251–7256. https://doi.org/10.1021/acscatal.7b02540.

(139) Meng, G.; Szostak, M. Rhodium-Catalyzed C-H Bond Functionalization with Amides by Double C-H/C-N Bond Activation. *Org. Lett.* **2016**, *18* (4), 796–799. https://doi.org/10.1021/acs.orglett.6b00058.

(140) Mamone, P.; Danoun, G.; Gooßen, L. J. Rhodium-Catalyzed Ortho Acylation of Aromatic Carboxylic Acids. *Angew. Chemie - Int. Ed.* **2013**, *52* (26), 6704–6708. https://doi.org/10.1002/anie.201301328.

(141) Catellani, M.; Frignani, F.; Rangoni, A. A Complex Catalytic Cycle Leading to a Regioselective Synthesis of *o,o'*-Disubstituted Vinylarenes. *Angew. Chemie – Int. Ed.* **1997**, *36* (1–2), 119–122. https://doi.org/10.1002/anie.199701191.

(142) Catellani, M.; Motti, E.; Baratta, S. A Novel Palladium-Catalyzed Synthesis of Phenanthrenes from Ortho-Substituted Aryl Iodides and Diphenyl-or Alkylphenylacetylenes. *Org. Lett.* **2001**, *3* (23), 3611–3614. https://doi.org/10.1021/ol016360o.

(143) Catellani, M. Catalytic Multistep Reactions via Palladacycles. *Synlett* **2003**, *2003* (3), 298–313. https://doi.org/10.1055/s-2003-37102.

(144) Catellani, M.; Motti, E.; Della Ca', N. Catalytic Sequential Reactions Involving Palladacycle-Directed Aryl Coupling Steps. *Acc. Chem. Res.* **2008**, *41* (11), 1512–

1522. https://doi.org/10.1021/ar800040u.

(145) Dong, Z.; Wang, J.; Ren, Z.; Dong, G. Ortho C-H Acylation of Aryl Iodides by Palladium/Norbornene Catalysis. *Angew. Chemie - Int. Ed.* **2015**, *54* (43), 12664–12668. https://doi.org/10.1002/anie.201506397.

(146) Vaska, L.; DiLuzio, J. W. Carbonyl and Hydrido-Carbonyl Complexes of Iridium by Reaction with Alcohols. Hydrido Complexes by Reaction with Acid. *J. Am. Chem. Soc.* **1961**, *83* (12), 2784–2785. https://doi.org/10.1021/ja01473a054.

(147) Simmons, E. M.; Hartwig, J. F. On the Interpretation of Deuterium Kinetic Isotope Effects in C-H Bond Functionalizations by Transition-Metal Complexes. *Angew. Chemie - Int. Ed.* **2012**, *51* (13), 3066–3072. https://doi.org/10.1002/anie.201107334.

(148) Sibbald, P. A.; Rosewall, C. F.; Swartz, R. D.; Michael, F. E. Mechanism of N-Fluorobenzenesulfonimide Promoted Diamination and Carboamination Reactions: Divergent Reactivity of a Pd(IV) Species. *J. Am. Chem. Soc.* **2009**, *131* (43), 15945–15951. https://doi.org/10.1021/ja906915w.

(149) Churchill, D. G.; Janak, K. E.; Wittenberg, J. S.; Parkin, G. Normal and Inverse Primary Kinetic Deuterium Isotope Effects for C-H Bond Reductive Elimination and Oxidative Addition Reactions of Molybdenocene and Tungstenocene Complexes: Evidence for Benzene σ-Complex Intermediates. *J. Am. Chem. Soc.* **2003**, *125* (5), 1403–1420. https://doi.org/10.1021/ja027670k.

(150) Song, Z.; Beak, P. Investigation of the Mechanisms of Ene Reactions of Carbonyl Enophiles by Intermolecular and Intramolecular Hydrogen-Deuterium Isotope Effects: Partitioning of Reaction Intermediates. *J. Am. Chem. Soc.* **1990**, *112* (22), 8126–8134. https://doi.org/10.1021/ja00178a042.

(151) Adam, W.; Krebs, O.; Orfanopoulos, M.; Stratakis, M.; Vougioukalakis, G. C. Intramolecular and Intermolecular Kinetic Isotope Effects (KIE) in the Nitrosoarene Ene Reaction: Experimental Evidence for Reversible Intermediate Formation. *J. Org. Chem.* **2003**, *68* (6), 2420–2425. https://doi.org/10.1021/jo0266240.

(152) Jones, W. D. Isotope Effects in C-H Bond Activation Reactions by Transition Metals. *Acc. Chem. Res.* **2003**, *36* (2), 140–146. https://doi.org/10.1021/ar020148i.

(153) Serratore, N. A. Method Development and Mechanistic Insights into Palladium-Catalyzed C–CN Bond Activation and Iridium-Catalyzed Sequential C–O/C–H Bond Activation Reactions, University of Minnesota, 2017.

(154) Serratore, N. A.; Anderson, C. B.; Frost, G. B.; Hoang, T. G.; Underwood, S. J.; Gemmel, P. M.; Hardy, M. A.; Douglas, C. J. Integrating Metal-Catalyzed C-H

and C-O Functionalization to Achieve Sterically Controlled Regioselectivity in Arene Acylation. *J. Am. Chem. Soc.* **2018**, *140* (31), 10025–10033. https://doi.org/10.1021/jacs.8b06476.

(155) Lapointe, D.; Fagnou, K. Overview of the Mechanistic Work on the Concerted Metallation-Deprotonation Pathway. *Chem. Lett.* **2010**, *39* (11), 1118–1126. https://doi.org/10.1246/cl.2010.1118.

(156) Davies, D. L.; Macgregor, S. A.; McMullin, C. L. Computational Studies of Carboxylate-Assisted C-H Activation and Functionalization at Group 8-10 Transition Metal Centers. *Chem. Rev.* **2017**, *117* (13), 8649–8709. https://doi.org/10.1021/acs.chemrev.6b00839.

(157) He, F.; Wu, H.; Chen, J.; Su, W. Unexpectedly High Activity of $Zn(OTf)_2 \cdot 6H_2O$ in Catalytic Friedel-Crafts Acylation Reaction. *Synth. Commun.* **2008**, *38* (2), 255–264. https://doi.org/10.1080/00397910701750292.

(158) Earle, M. J.; Hakala, U.; Hardacre, C.; Karkkainen, J.; McAuley, B. J.; Rooney, D. W.; Seddon, K. R.; Thompson, J. M.; Wähälä, K. Chloroindate(III) Ionic Liquids: Recyclable Media for Friedel-Crafts Acylation Reactions. *Chem. Commun.* **2005**, No. 7, 903–905. https://doi.org/10.1039/b413132k.

(159) Kusama, H.; Narasaka, K. Friedel–Crafts Acylation of Arenes Catalyzed by Bromopentacarbonylrhenium(I). *Bull. Chem. Soc. Jpn.* **1995**, *68* (8), 2379–2383. https://doi.org/10.1246/bcsj.68.2379.

(160) Vekariya, R. H.; Aubé, J. Hexafluoro-2-Propanol-Promoted Intermolecular Friedel-Crafts Acylation Reaction. *Org. Lett.* **2016**, *18* (15), 3534–3537. https://doi.org/10.1021/acs.orglett.6b01460.

(161) Miquel, J. F.; Buu-Hoï, N. P.; Royer, R. Friedel-Crafts Reactions with Methyl m-Tolyl Ether. *J. Chem. Soc.* **1955**, No. 0, 3417–3420. https://doi.org/10.1039/JR9550003417.

(162) Sato, H.; Dan, T.; Onuma, E.; Tanaka, H.; Aoki, B.; Koga, H. Studies on Uricosuric Diuretics. III. Substituted 1,3-Dioxolo[4,5-f]-1,2-Benzisoxazole-6-Carboxylic Acids and 1,3-Dioxolo[4,5-g]-1,2-Benzisoxazole-7-Carboxylic Acids. *Chem. Pharm. Bull.* **1992**, *40* (6), 109–116.

(163) Pettit, G. R.; Grealish, M. P.; Herald, D. L.; Boyd, M. R.; Hamel, E.; Pettit, R. K. Antineoplastic Agents. 443. Synthesis of the Cancer Cell Growth Inhibitor Hydroxyphenstatin and Its Sodium Diphosphate Prodrug. *J. Med. Chem.* **2000**, *43* (14), 2731–2737. https://doi.org/10.1021/jm000045a.

(164) Radha, P. A Simple and Convenient Multigram Scale Synthesis of Hydroxyphenstatin: Potential Cancer Cell Growth Inhibitor. *Synth. Commun.*

2003, *33* (22), 3869–3873. https://doi.org/10.1081/SCC-120026308.

(165) Yanagisawa, A.; Taga, M.; Atsumi, T.; Nishimura, K.; Ando, K.; Taguchi, T.; Tsumuki, H.; Chujo, I.; Mohri, S. I. Process Development of the PDE4 Inhibitor K-34. *Org. Process Res. Dev.* **2011**, *15* (2), 376–381. https://doi.org/10.1021/op100291g.

(166) Jaime-Figueroa, S.; Kurz, L. J.; Liu, Y.; Cruz, R. Synthesis and Experimental Study of Through-Space Hydrogen-Fluorine and Carbon-Fluorine Spin-Spin Coupling in 4,5-Substituted 1-Acetyl-8-Fluoronaphthalenes. *Spectrochim. Acta - Part A Mol. Biomol. Spectrosc.* **2000**, *56* (6), 1167–1178. https://doi.org/10.1016/S1386-1425(99)00215-2.

(167) Chen, J.; Reibenspies, J.; Derecskei-Kovacs, A.; Burgess, K. Through-Space 13C-19F Coupling Can Reveal Conformations of Modified BODIPY Dyes. *Chem. Commun.* **1999**, No. 24, 2501–2502. https://doi.org/10.1039/a907559c.

(168) Palucki, M.; Wolfe, J. P.; Buchwald, S. L. Palladium-Catalyzed Intermolecular Carbon-Oxygen Bond Formation: A New Synthesis of Aryl Ethers. *J. Am. Chem. Soc.* **1997**, *119* (14), 3395–3396. https://doi.org/10.1021/ja9640152.

(169) Mann, G.; Hartwig, J. F. Nickel- vs Palladium-Catalyzed Synthesis of Protected Phenols from Aryl Halides. *J. Org. Chem.* **1997**, *62* (16), 5413–5418. https://doi.org/10.1021/jo970453v.

(170) Bistri, O.; Correa, A.; Bolm, C. Iron-Catalyzed C-O Cross-Couplings of Phenols with Aryl Iodides. *Angew. Chemie - Int. Ed.* **2008**, *47* (3), 586–588. https://doi.org/10.1002/anie.200704018.

(171) Milton, E. J.; Fuentes, J. A.; Clarke, M. L. Palladium-Catalysed Synthesis of Aryl-Alkyl Ethers Using Alkoxysilanes as Nucleophiles. *Org. Biomol. Chem.* **2009**, *7* (12), 2645–2648. https://doi.org/10.1039/b907784g.

(172) Gowrisankar, S.; Sergeev, A. G.; Anbarasan, P.; Spannenberg, A.; Neumann, H.; Beller, M. A General and Efficient Catalyst for Palladium-Catalyzed C-O Coupling Reactions of Aryl Halides with Primary Alcohols. *J. Am. Chem. Soc.* **2010**, *132* (33), 11592–11598. https://doi.org/10.1021/ja103248d.

(173) Wu, X.; Fors, B. P.; Buchwald, S. L. A Single Phosphine Ligand Allows Palladium-Catalyzed Intermolecular C-O Bond Formation with Secondary and Primary Alcohols. *Angew. Chemie - Int. Ed.* **2011**, *50* (42), 9943–9947. https://doi.org/10.1002/anie.201104361.

(174) Kim, H. J.; Kim, M.; Chang, S. Rhodium(NHC)-Catalyzed O -Arylation of Aryl Bromides. *Org. Lett.* **2011**, *13* (9), 2368–2371. https://doi.org/10.1021/ol200603c.

(175) Zheng, X.; Ding, J.; Chen, J.; Gao, W.; Liu, M.; Wu, H. The Coupling of Arylboronic Acids with Nitroarenes Catalyzed by Rhodium. *Org. Lett.* **2011**, *13* (7), 1726–1729. https://doi.org/10.1021/ol200251x.

(176) Gowrisankar, S.; Neumann, H.; Beller, M. A Convenient and Practical Synthesis of Anisoles and Deuterated Anisoles by Palladium-Catalyzed Coupling Reactions of Aryl Bromides and Chlorides. *Chem. - A Eur. J.* **2012**, *18* (9), 2498–2502. https://doi.org/10.1002/chem.201103347.

(177) Maligres, P. E.; Li, J.; Krska, S. W.; Schreier, J. D.; Raheem, I. T. C-O Cross-Coupling of Activated Aryl and Heteroaryl Halides with Aliphatic Alcohols. *Angew. Chemie - Int. Ed.* **2012**, *51* (36), 9071–9074. https://doi.org/10.1002/anie.201203460.

(178) Cheung, C. W.; Buchwald, S. L. Mild and General Palladium-Catalyzed Synthesis of Methyl Aryl Ethers Enabled by the Use of a Palladacycle Precatalyst. *Org. Lett.* **2013**, *15* (15), 3998–4001. https://doi.org/10.1021/ol401796v.

(179) Rangarajan, T. M.; Singh, R.; Brahma, R.; Devi, K.; Singh, R. P.; Singh, R. P.; Prasad, A. K. BrettPhos Ligand Supported Palladium-Catalyzed C-O Bond Formation through an Electronic Pathway of Reductive Elimination: Fluoroalkoxylation of Activated Aryl Halides. *Chem. - A Eur. J.* **2014**, *20* (44), 14218–14225. https://doi.org/10.1002/chem.201404121.

(180) Aranyos, A.; Old, D. W.; Kiyomori, A.; Wolfe, J. P.; Sadighi, J. P.; Buchwald, S. L. Novel Electron-Rich Bulky Phosphine Ligands Facilitate the Palladium-Catalyzed Preparation of Diaryl Ethers. *J. Am. Chem. Soc.* **1999**, *121* (18), 4369–4378. https://doi.org/10.1021/ja990324r.

(181) Rangarajan, T. M.; Brahma, R.; Ayushee; Prasad, A. K.; Verma, A. K.; Singh, R. P. Mild and Efficient Palladium/BrettPhos-Catalyzed Methoxylation and Deuteriomethoxylation of Activated Aryl Bromides. *Tetrahedron Lett.* **2015**, *56* (17), 2234–2237. https://doi.org/10.1016/j.tetlet.2015.03.045.

(182) Begum, T.; Mondal, M.; Borpuzari, M. P.; Kar, R.; Gogoi, P. K.; Bora, U. Palladium-on-Carbon-Catalyzed Coupling of Nitroarenes with Phenol: Biaryl Ether Synthesis and Evidence of an Oxidative-Addition-Promoted Mechanism. *European J. Org. Chem.* **2017**, *2017* (22), 3244–3248. https://doi.org/10.1002/ejoc.201700639.

(183) Takise, R.; Isshiki, R.; Muto, K.; Itami, K.; Yamaguchi, J. Decarbonylative Diaryl Ether Synthesis by Pd and Ni Catalysis. *J. Am. Chem. Soc.* **2017**, *139* (9), 3340–3343. https://doi.org/10.1021/jacs.7b00049.

(184) Zhang, H.; Ruiz-Castillo, P.; Buchwald, S. L. Palladium-Catalyzed C-O Cross-Coupling of Primary Alcohols. *Org. Lett.* **2018**, *20* (6), 1580–1583.

https://doi.org/10.1021/acs.orglett.8b00325.

(185) Capdevila, L.; Andris, E.; Briš, A.; Tarrés, M.; Roldán-Gómez, S.; Roithová, J.; Ribas, X. Silver(I)-Catalyzed C-X, C-C, C-N, and C-O Cross-Couplings Using Aminoquinoline Directing Group via Elusive Aryl-Ag(III) Species. *ACS Catal.* **2018**, *8* (11), 10430–10436. https://doi.org/10.1021/acscatal.8b03257.

(186) Mann, G.; Incarvito, C.; Rheingold, A. L.; Hartwig, J. F. Palladium-Catalyzed C-O Coupling Involving Unactivated Aryl Halides. Sterically Induced Reductive Elimination to Form the C-O Bond in Diaryl Ethers [4]. *J. Am. Chem. Soc.* **1999**, *121* (13), 3224–3225. https://doi.org/10.1021/ja984321a.

(187) Torraca, K. E.; Huang, X.; Parrish, C. A.; Buchwald, S. L. An Efficient Intermolecular Palladium-Catalyzed Synthesis of Aryl Ethers [17]. *J. Am. Chem. Soc.* **2001**, *123* (43), 10770–10771. https://doi.org/10.1021/ja016863p.

(188) Harkal, S.; Kumar, K.; Michalik, D.; Zapf, A.; Jackstell, R.; Rataboul, F.; Riermeier, T.; Monsees, A.; Beller, M. An Efficient Catalyst System for Diaryl Ether Synthesis from Aryl Chlorides. *Tetrahedron Lett.* **2005**, *46* (18), 3237–3240. https://doi.org/10.1016/j.tetlet.2005.03.033.

(189) Vorogushin, A. V.; Huang, X.; Buchwald, S. L. Use of Tunable Ligands Allows for Intermolecular Pd-Catalyzed C-O Bond Formation. *J. Am. Chem. Soc.* **2005**, *127* (22), 8146–8149. https://doi.org/10.1021/ja050471r.

(190) Burgos, C. H.; Barder, T. E.; Huang, X.; Buchwald, S. L. Significantly Improved Method for the Pd-Catalyzed Coupling of Phenols with Aryl Halides: Understanding Ligand Effects. *Angew. Chemie - Int. Ed.* **2006**, *45* (26), 4321–4326. https://doi.org/10.1002/anie.200601253.

(191) Ouali, A.; Spindler, J. F.; Jutand, A.; Taillefer, M. Nitrogen Ligands in Copper-Catalyzed Arylation of Phenols: Structure/Activity Relationships and Applications. *Adv. Synth. Catal.* **2007**, *349* (11–12), 1906–1916. https://doi.org/10.1002/adsc.200600628.

(192) Xia, N.; Taillefer, M. Copper- or Iron-Catalyzed Arylation of Phenols from Respectively Aryl Chlorides and Aryl Iodides. *Chem. - A Eur. J.* **2008**, *14* (20), 6037–6039. https://doi.org/10.1002/chem.200800436.

(193) Takatori, K.; Nishihara, M.; Nishiyama, Y.; Kajiwara, M. An Asymmetric Synthesis of L-[3-13C]Phenylalanine and L-[3-13C]Tyrosine from [13C]Carbon Monoxidet. *Tetrahedron* **1998**, *54*, 5861–15869.

(194) Martinelli, J. R.; Watson, D. A.; Freckmann, D. M. M.; Barder, T. E.; Buchwald, S. L. Palladium-Catalyzed Carbonylation Reactions of Aryl Bromides at Atmospheric Pressure: A General System Based on Xantphos. *J. Org. Chem.* **2008**,

73 (18), 7102–7107. https://doi.org/10.1021/jo801279r.

(195) Park, H. S.; Kim, D. S.; Jun, C. H. Palladium-Catalyzed Carbonylative Esterification of Primary Alcohols with Aryl Chlorides through Dehydroxymethylative C-C Bond Cleavage. *ACS Catal.* **2015**, *5* (1), 397–401. https://doi.org/10.1021/cs501778q.

(196) Min, B. H.; Kim, D. S.; Park, H. S.; Jun, C. H. Pd/C-Catalyzed Carbonylative Esterification of Aryl Halides with Alcohols by Using Oxiranes as CO Sources. *Chem. - A Eur. J.* **2016**, *22* (18), 6234–6238. https://doi.org/10.1002/chem.201600570.

(197) Georgsson, J.; Hallberg, A.; Larhed, M. Rapid Palladium-Catalyzed Synthesis of Esters from Aryl Halides Utilizing Mo(CO)6 as a Solid Carbon Monoxide Source. *J. Comb. Chem.* **2003**, *5* (4), 350–352. https://doi.org/10.1021/cc0201086.

(198) Hajipour, A. R.; Tavangar-Rizi, Z.; Iranpoor, N. Palladium-Catalyzed Carbonylation of Aryl Halides: An Efficient, Heterogeneous and Phosphine-Free Catalytic System for Aminocarbonylation and Alkoxycarbonylation Employing Mo(CO)6 as a Solid Carbon Monoxide Source. *RSC Adv.* **2016**, *6* (82), 78468–78476. https://doi.org/10.1039/c6ra18679c.

(199) Bourne-Branchu, Y.; Gosmini, C.; Danoun, G. Cobalt-Catalyzed Esterification of Amides. *Chem. - A Eur. J.* **2017**, *23* (42), 10043–10047. https://doi.org/10.1002/chem.201702608.

(200) Hie, L.; Baker, E. L.; Anthony, S. M.; Desrosiers, J.-N. N.; Senanayake, C.; Garg, N. K. Nickel-Catalyzed Esterification of Aliphatic Amides. *Angew. Chemie - Int. Ed.* **2016**, *55* (48), 15129–15132. https://doi.org/10.1002/anie.201607856.

(201) Hie, L.; Fine Nathel, N. F.; Shah, T. K.; Baker, E. L.; Hong, X.; Yang, Y.-F. F.; Liu, P.; Houk, K. N.; Garg, N. K. Conversion of Amides to Esters by the Nickel-Catalysed Activation of Amide C-N Bonds. *Nature* **2015**, *524* (7563), 79–83. https://doi.org/10.1038/nature14615.

(202) Murakami, M.; Tsuruta, T.; Ito, Y. Lactone Formation by Rhodium-Catalyzed C-C Bond Cleavage of Cyclobutanone. *Angew. Chemie - Int. Ed.* **2000**, *39* (14), 2484–2486. https://doi.org/10.1002/1521-3773(20000717)39:14<2484::AID-ANIE2484>3.0.CO;2-1.

(203) Souillart, L.; Cramer, N. Highly Enantioselective Rhodium(I)-Catalyzed Carbonyl Carboacylations Initiated by C-C Bond Activation. *Angew. Chemie - Int. Ed.* **2014**, *53* (36), 9640–9644. https://doi.org/10.1002/anie.201405834.

(204) Gardikis, Y.; Tsoungas, P. G.; Potamitis, C.; Zervou, M.; Cordopatis, P. Xanthones in Heterocyclic Synthesis. An Efficient Route for the Synthesis of C-3 o-

Hydroxyaryl Substituted 1, 2-Benzisoxazoles and Their N-Oxides, Potential Scaffolds for Angiotensin(II) Antagonist Hybrid Peptides. *Heterocycles* **2011**, *83* (5), 1077–1091. https://doi.org/10.3987/COM-11-12162.

(205) Alías, F. M.; Daff, P. J.; Paneque, M.; Poveda, M. L.; Carmona, E.; Pérez, P. J.; Salazar, V.; Alvarado, Y.; Atencio, R.; Sánchez-Delgado, R. C-C Bond-Forming Reactions of Ir(III)-Alkenyls and Nitriles or Aldehydes: Generation of Reactive Hydride- and Alkyl-Alkylidene Compounds and Observation of a Reversible 1,2-H Shift in Stable Hydride-Ir(III) Alkylidene Complexes. *Chem. - A Eur. J.* **2002**, *8* (22), 5132–5146. https://doi.org/10.1002/1521-3765(20021115)8:22<5132::AID-CHEM5132>3.0.CO;2-O.

(206) Tao, D. J.; Wu, J.; Wang, Z. Z.; Lu, Z. H.; Yang, Z.; Chen, X. S. SO3H-Functionalized Brønsted Acidic Ionic Liquids as Efficient Catalysts for the Synthesis of Isoamyl Salicylate. *RSC Adv.* **2014**, *4* (1), 1–7. https://doi.org/10.1039/c3ra45921g.

(207) Yamada, K.; Yoshida, S.; Fujita, H.; Kitamura, M.; Kunishima, M. O-Benzylation of Carboxylic Acids Using 2,4,6-Tris(Benzyloxy)-1,3,5-Triazine (TriBOT) under Acidic or Thermal Conditions. *European J. Org. Chem.* **2015**, *2015* (36), 7997–8002. https://doi.org/10.1002/ejoc.201501172.

(208) Lu, B.; Zhu, F.; Sun, H. M.; Shen, Q. Esterification of the Primary Benzylic C-H Bonds with Carboxylic Acids Catalyzed by Ionic Iron(III) Complexes Containing an Imidazolinium Cation. *Org. Lett.* **2017**, *19* (5), 1132–1135. https://doi.org/10.1021/acs.orglett.7b00148.

(209) Wang, D.; Cui, S. Rh(III)-Catalyzed Aldehyde C-H Bond Functionalization of Salicylaldehydes with Arylboronic Acids. *Tetrahedron* **2015**, *71* (45), 8511–8516. https://doi.org/10.1016/j.tet.2015.09.053.

(210) Fujimoto, Y.; Furukawa, C.; Takahashi, K.; Mochizuki, M.; Yanai, H.; Matsumoto, T. An Efficient Two-Step Protocol for the Isoprenylation of Xanthone at the C2 Position Starting from 1-Fluoroxanthone Derivative. *Synlett* **2020**, *31* (14), 1423–1429. https://doi.org/10.1055/s-0039-1690891.

(211) Mo, F.; Trzepkowski, L. J.; Dong, G. Synthesis of Ortho-Acylphenols through the Palladium-Catalyzed Ketone-Directed Hydroxylation of Arenes. *Angew. Chemie - Int. Ed.* **2012**, *51* (52), 13075–13079. https://doi.org/10.1002/anie.201207479.

(212) Dreis, A. M. Carbon–Carbon Sigma Bond Activation: Functionalizing C–C and C–CN Bonds via Carboacylation and Cyanoamidation, University of Minnesota, 2015, Vol. 151. https://doi.org/10.1145/3132847.3132886.

(213) Huang, S. T.; Hsei, I. J.; Chen, C. Synthesis and Anticancer Evaluation of Bis(Benzimidazoles), Bis(Benzoxazoles), and Benzothiazoles. *Bioorganic Med.*

Chem. **2006**, *14* (17), 6106–6119. https://doi.org/10.1016/j.bmc.2006.05.007.

Appendix: NMR Spectra

Only spectra for compounds from previously unpublished work are included.

3.11b 1H NMR Spectrum

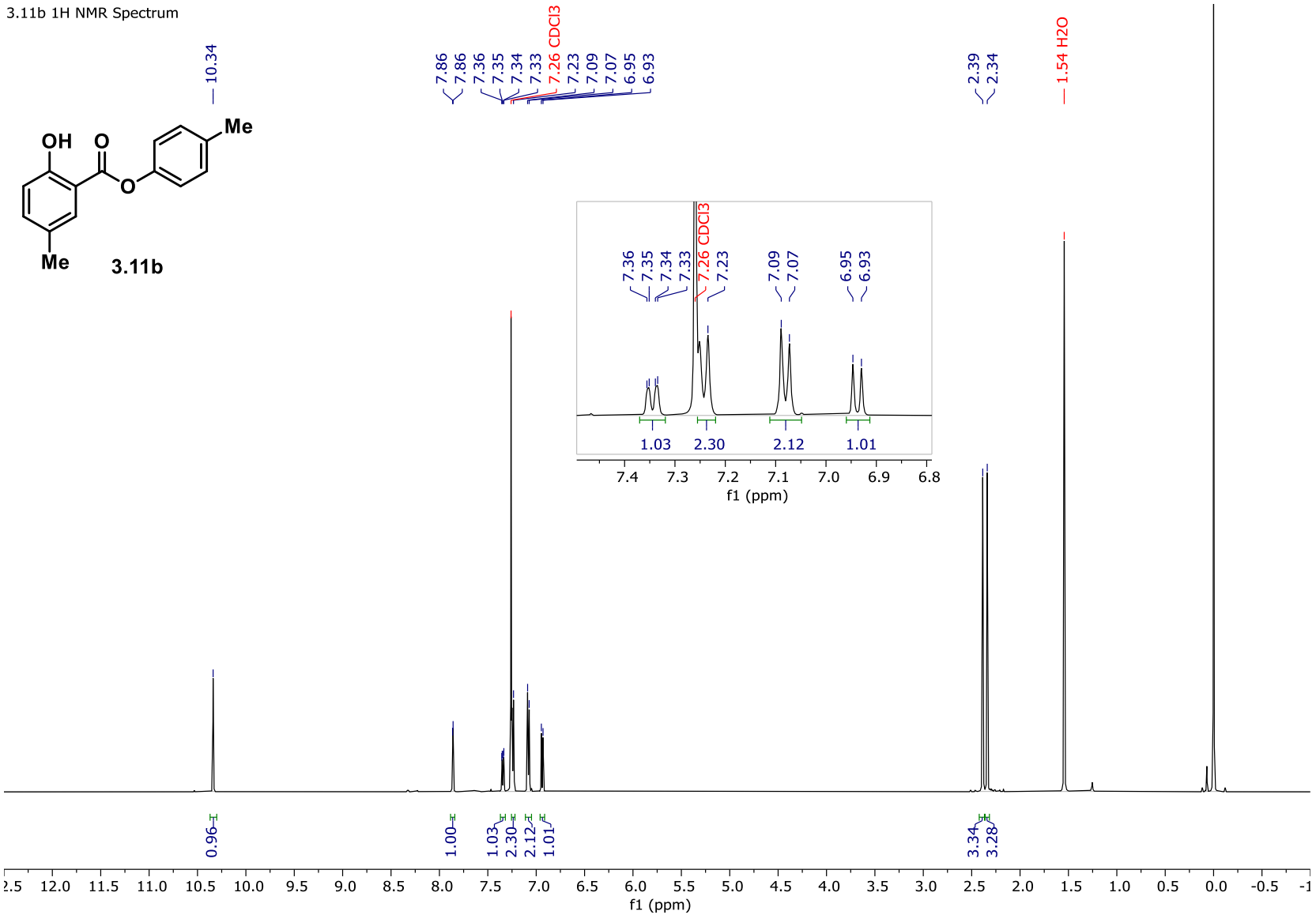

3.11b 13C NMR Spectrum in CDCl3

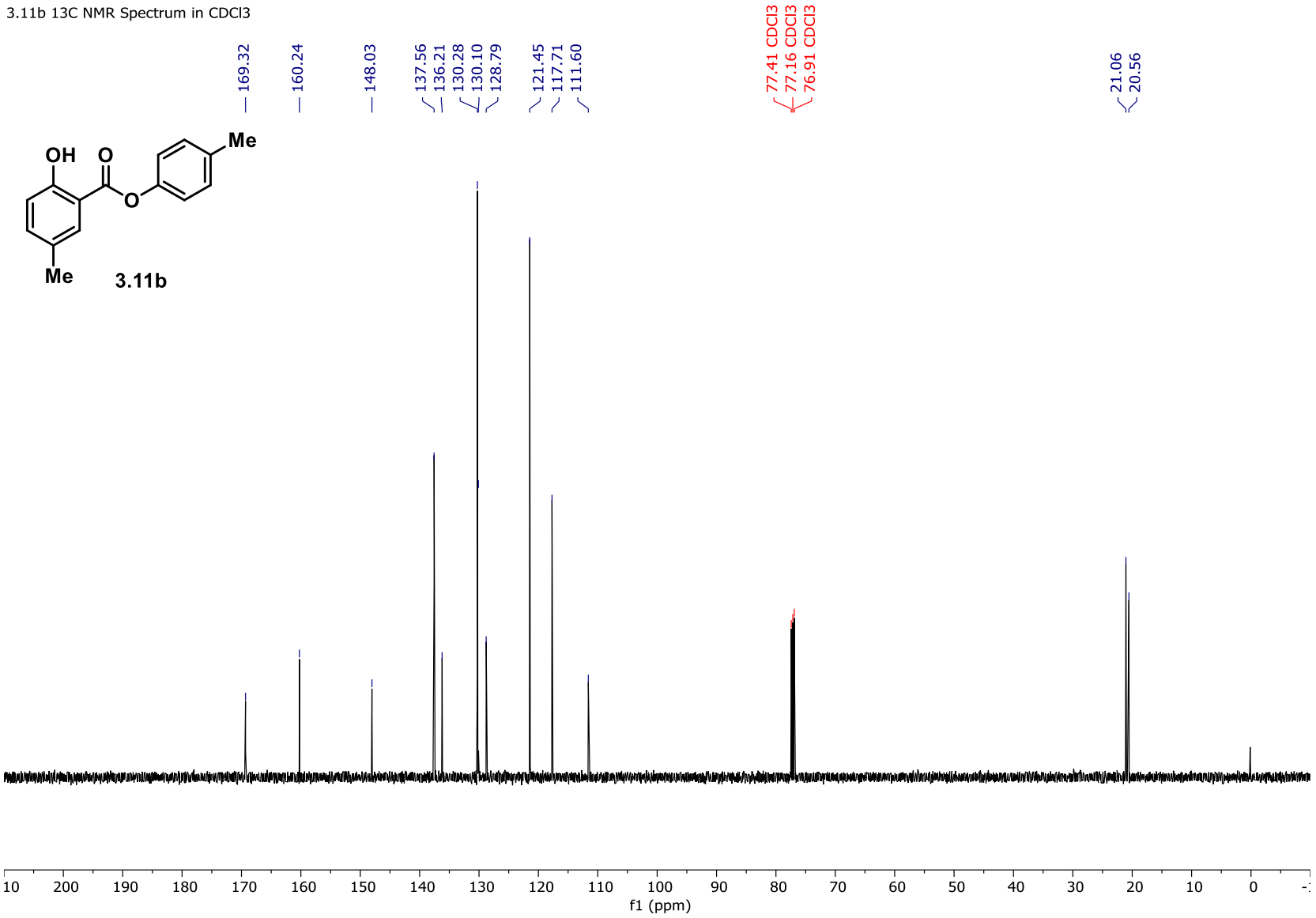

3.11c 1H NMR Spectrum in CDCl3

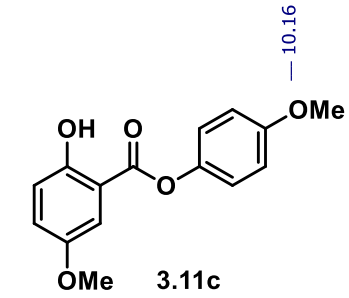

3.11c

3.11c 13C NMR Spectrum in CDCl3

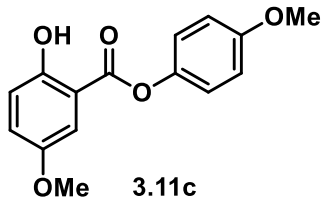

3.11d 1H NMR Spectrum in CDCl3

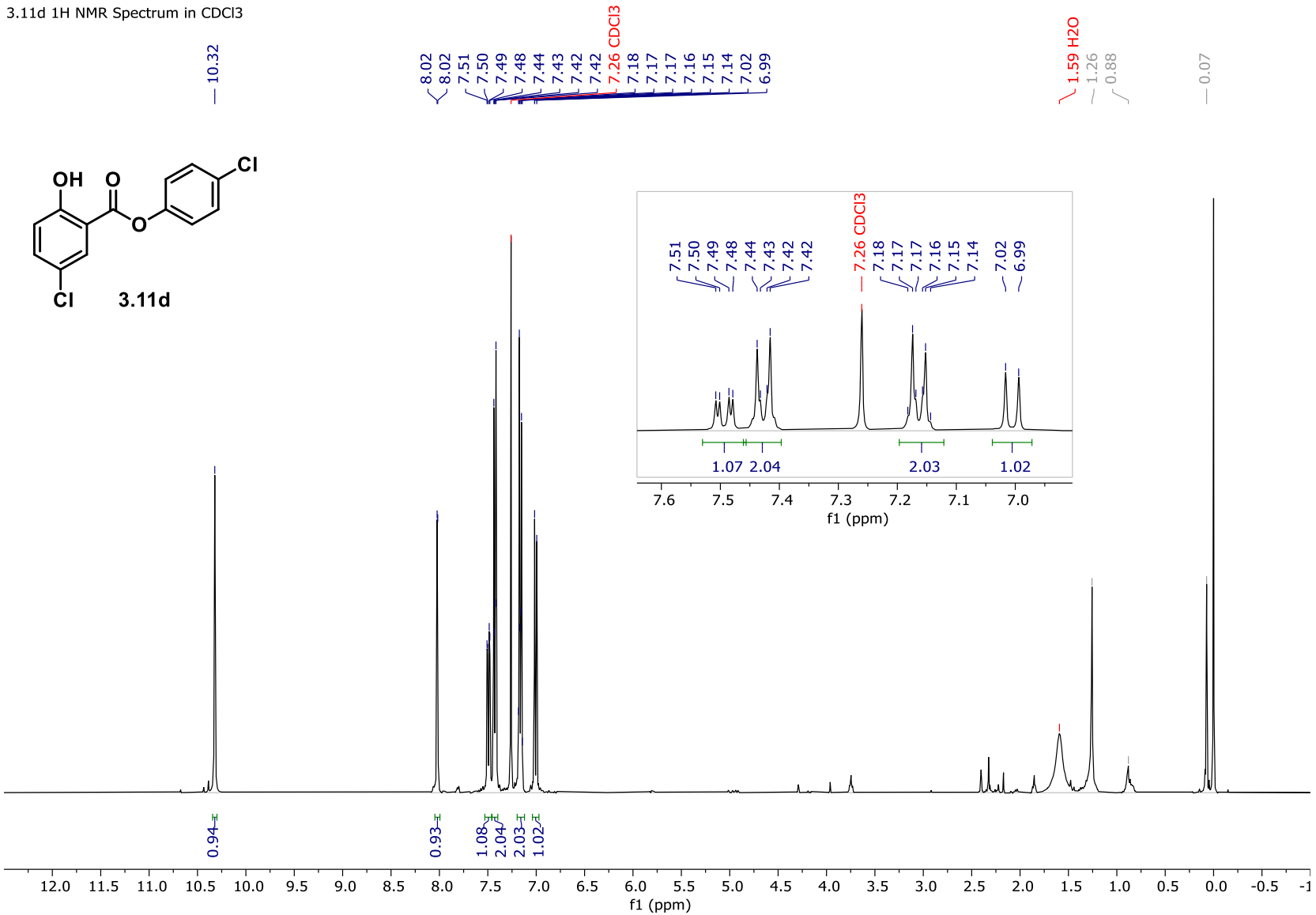

3.11d 13C NMR Spectrum in CDCl3

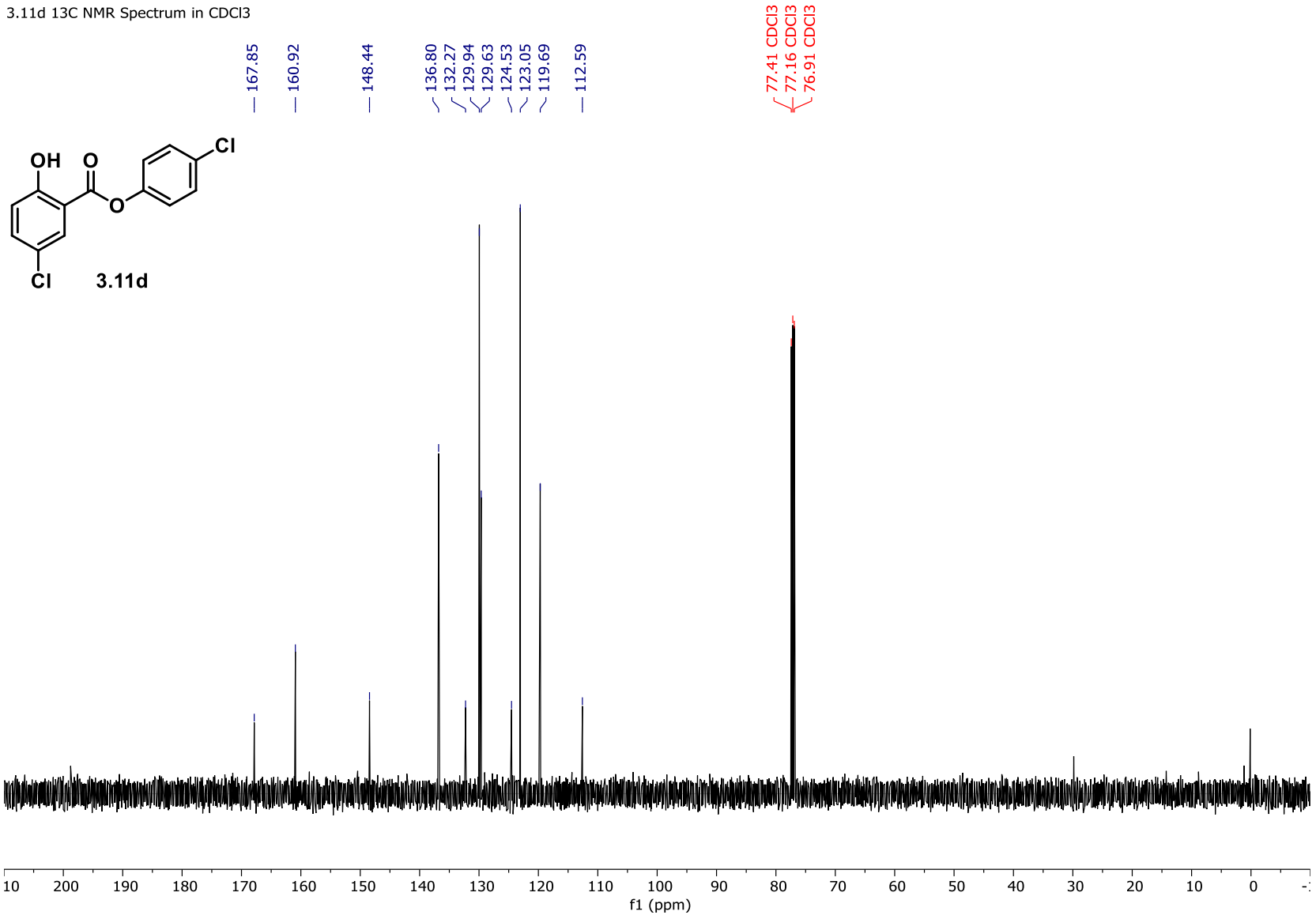

3.11e 1H NMR Spectrum in CDCl3

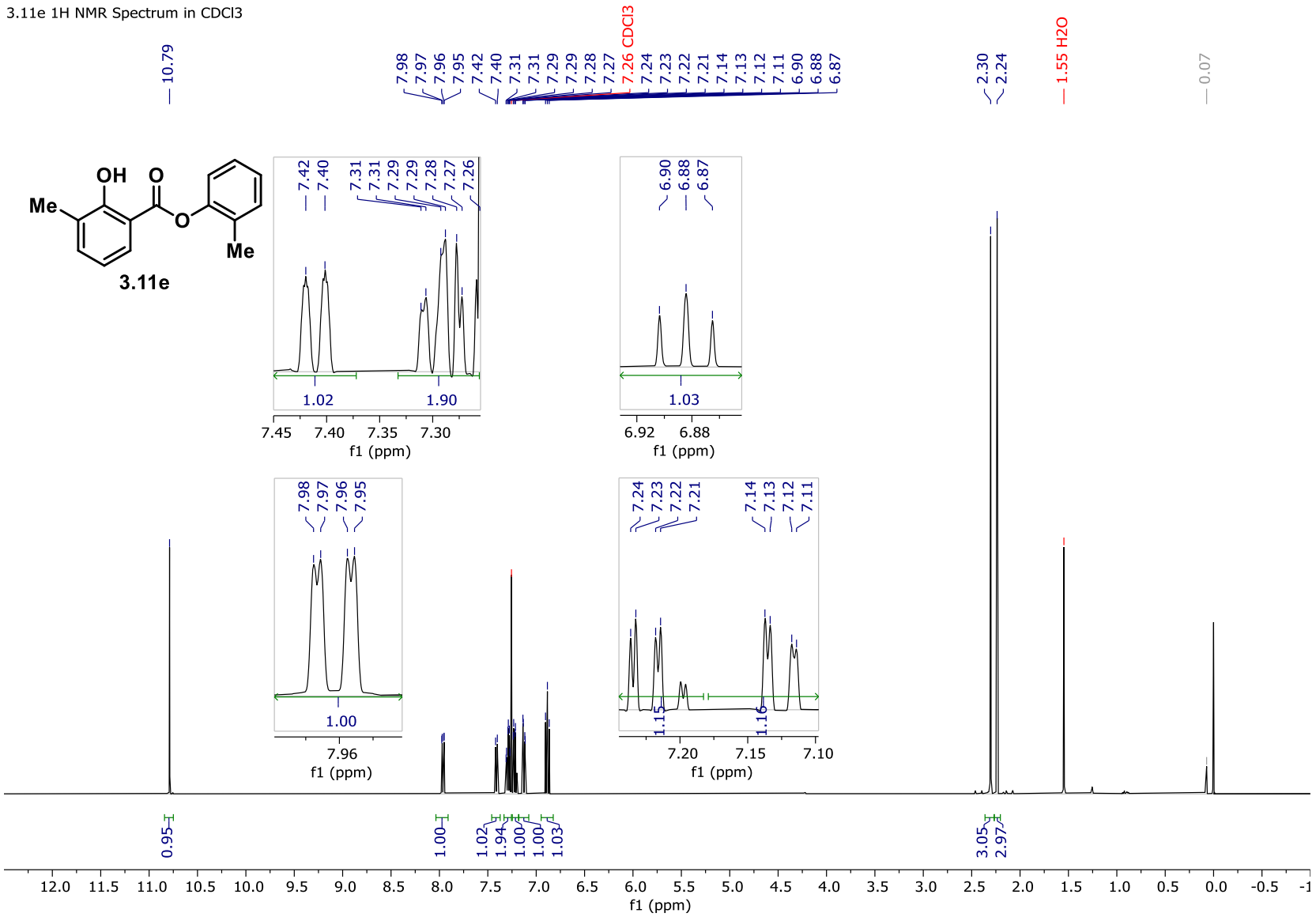

3.11e 13C NMR Spectrum in CDCl3

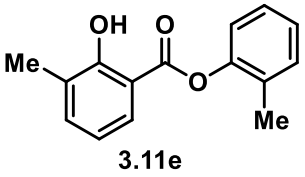

3.11e

3.11f 1H NMR Spectrum in CDCl3

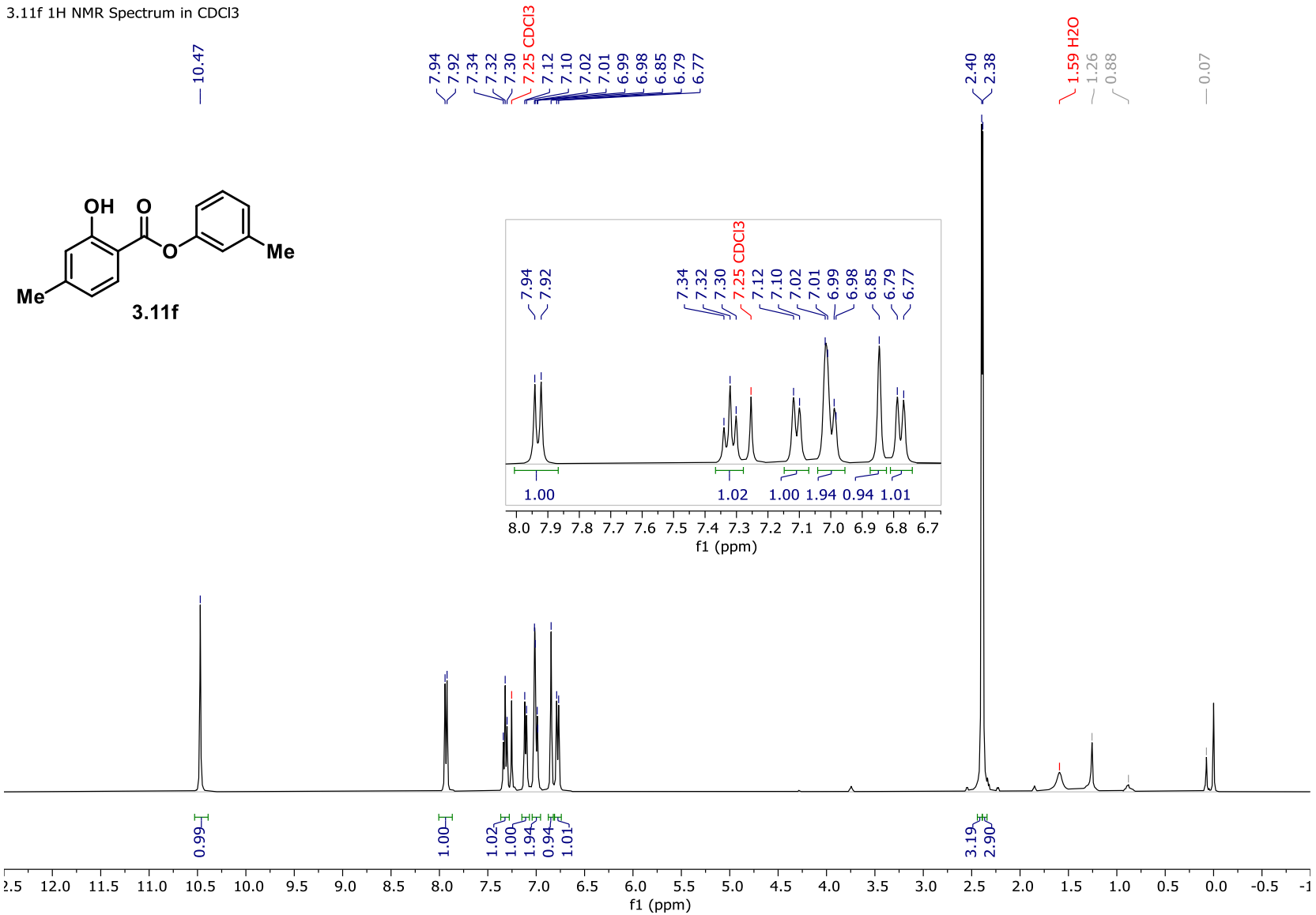

3.11f 13C NMR Spectrum in CDCl3

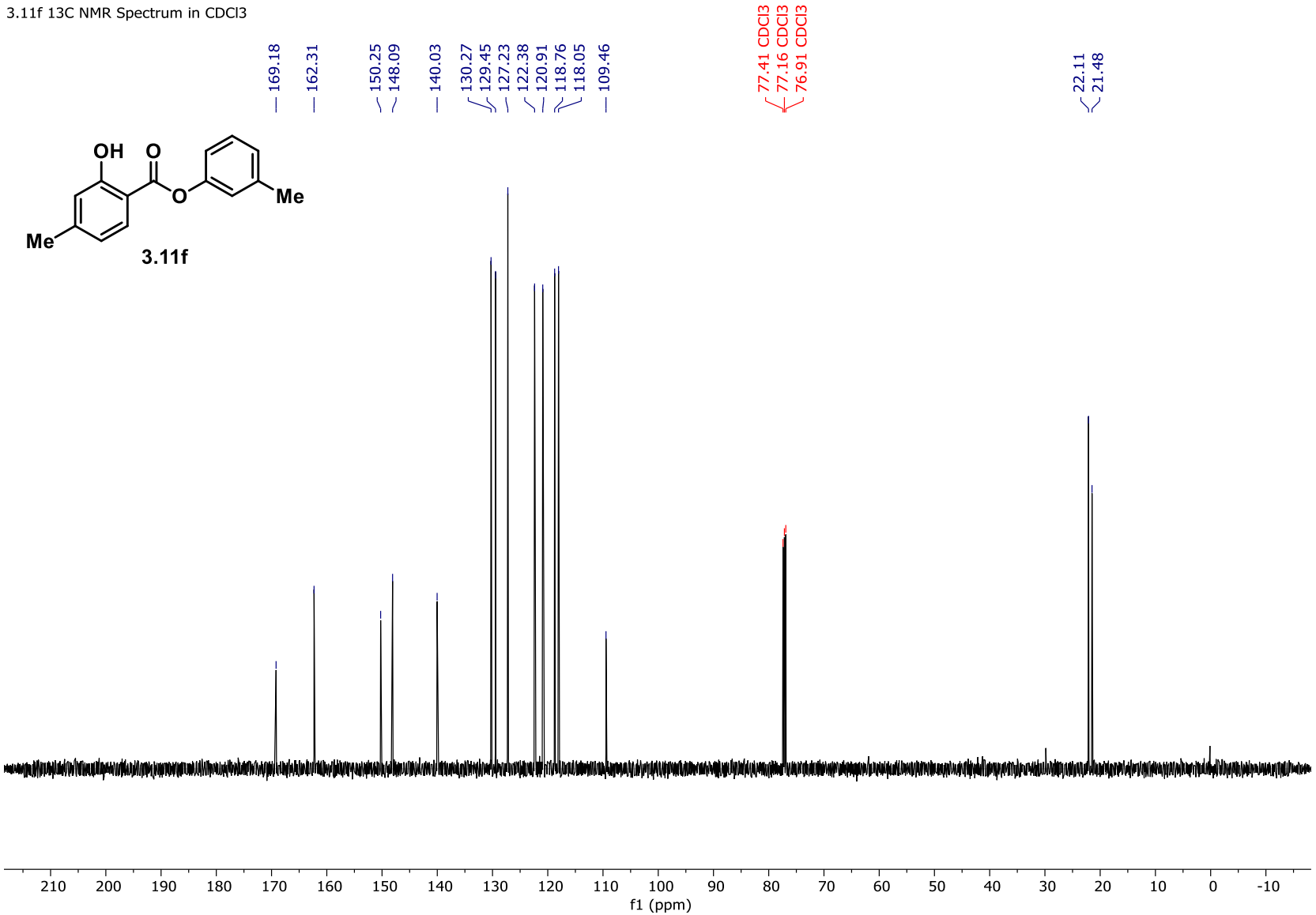

3.11g 1H NMR Spectrum in CDCl3

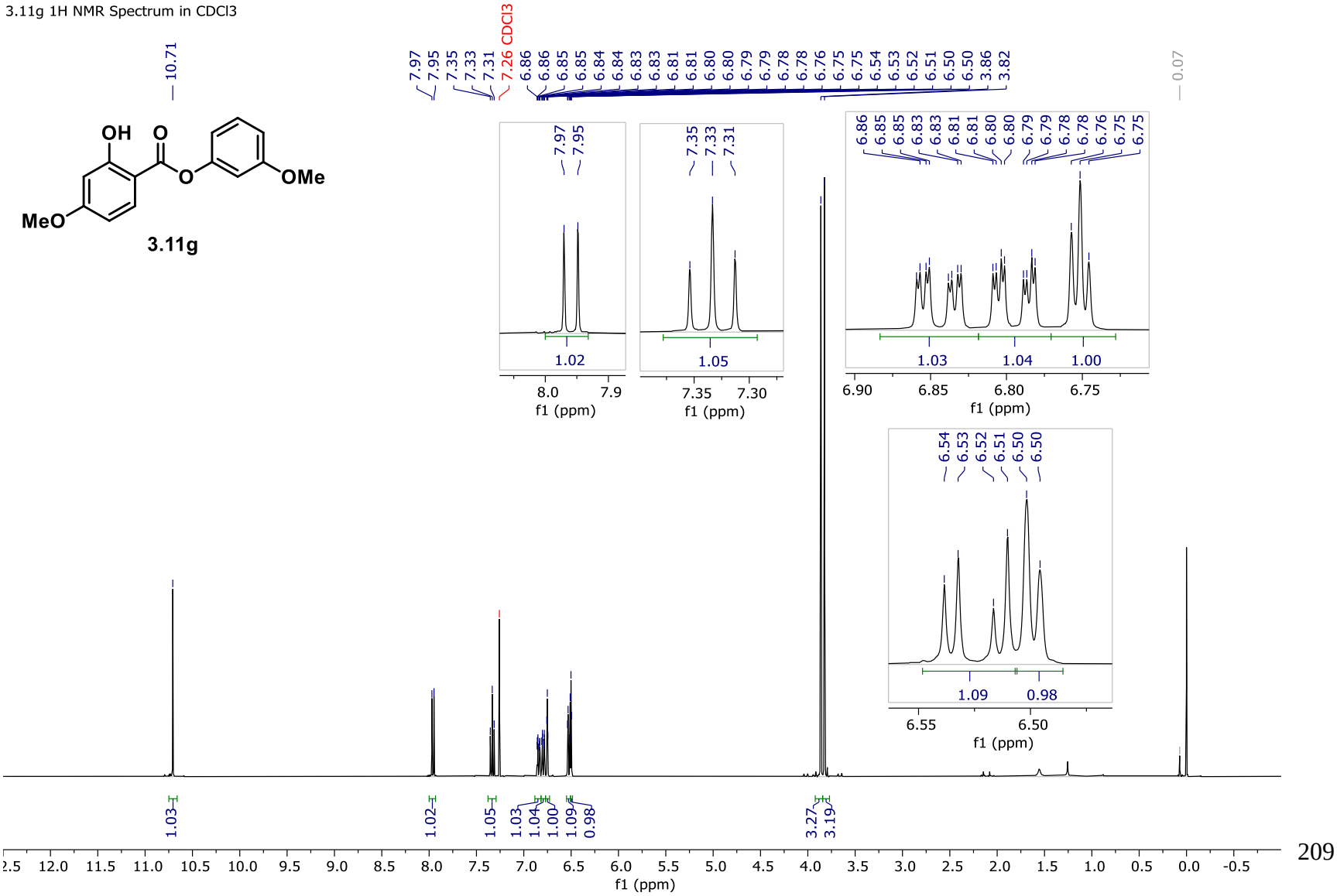

3.11g 13C NMR Spectrum in CDCl3

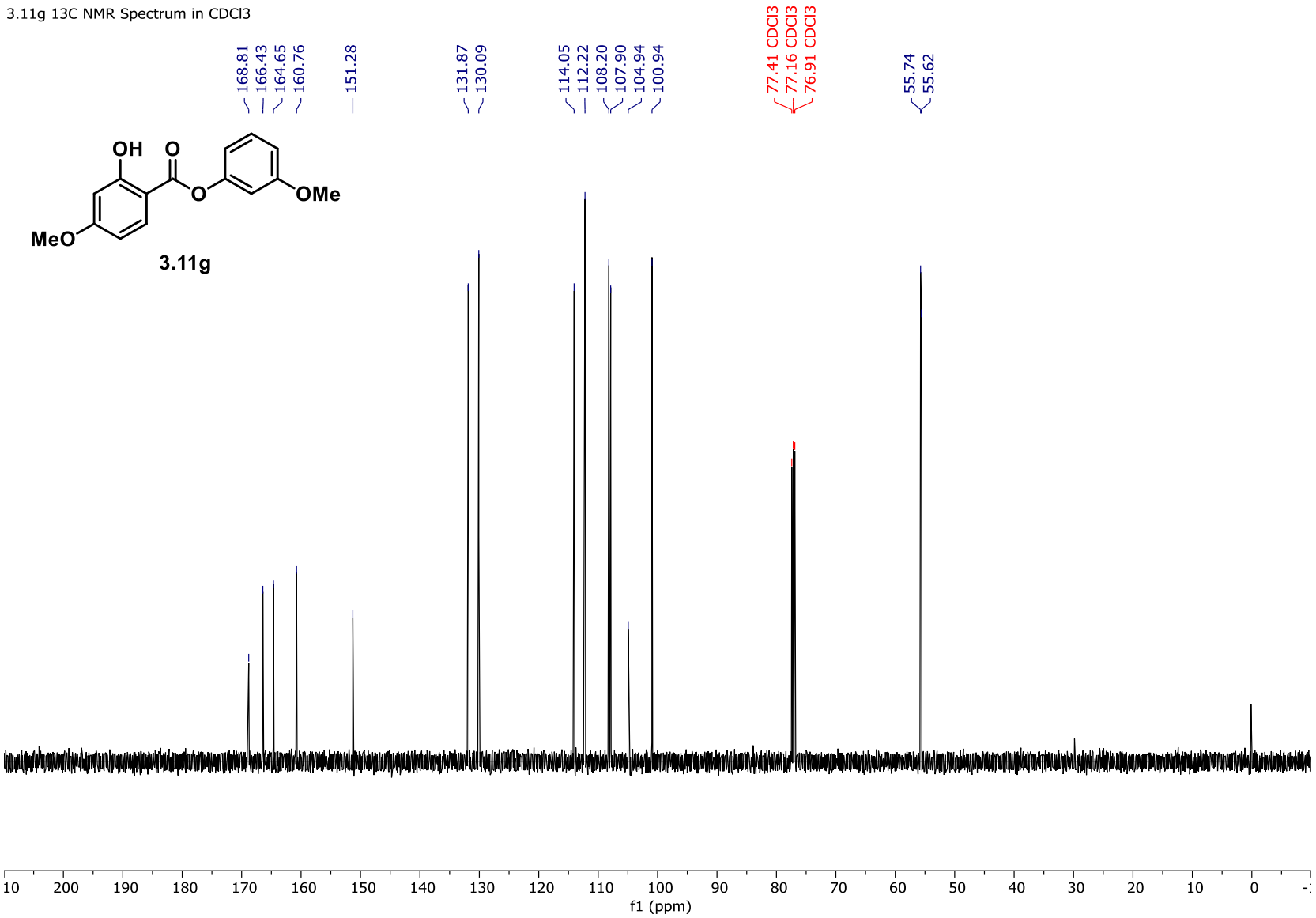

3.10g 1H NMR Spectrum in CDCl3

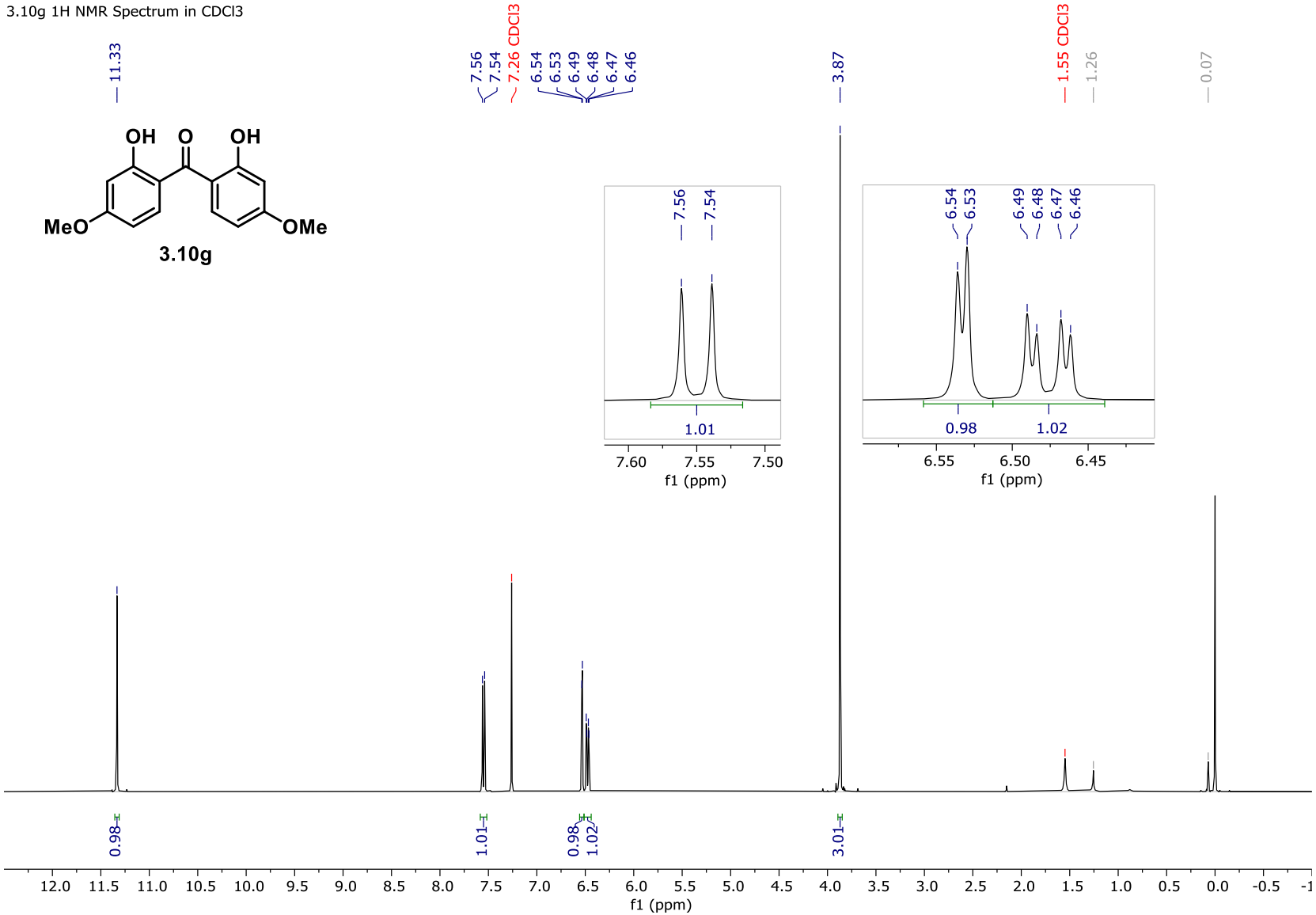

3.10g 13C NMR Spectrum in CDCl3

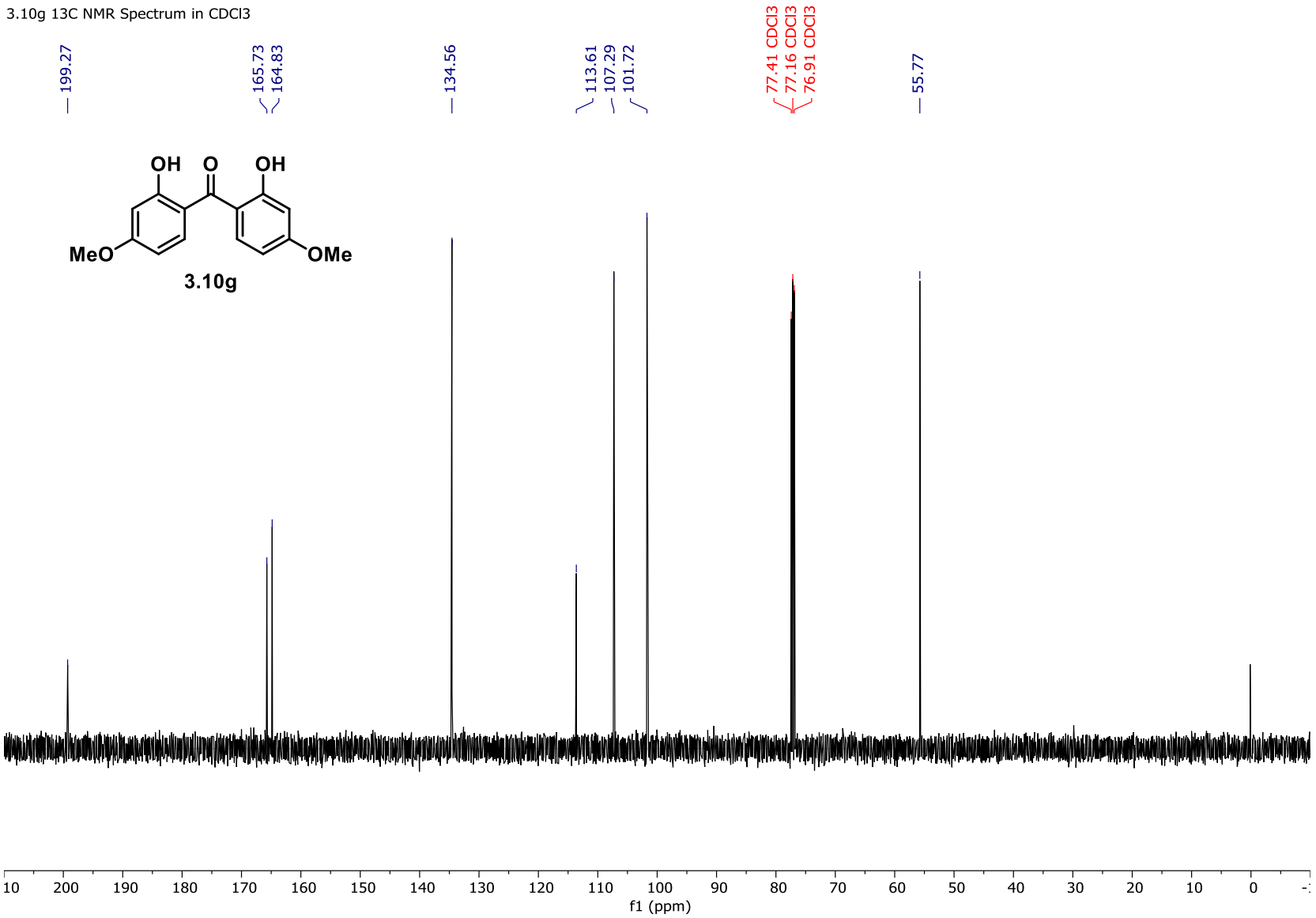

3.11h 1H NMR Spectrum in CD2Cl2

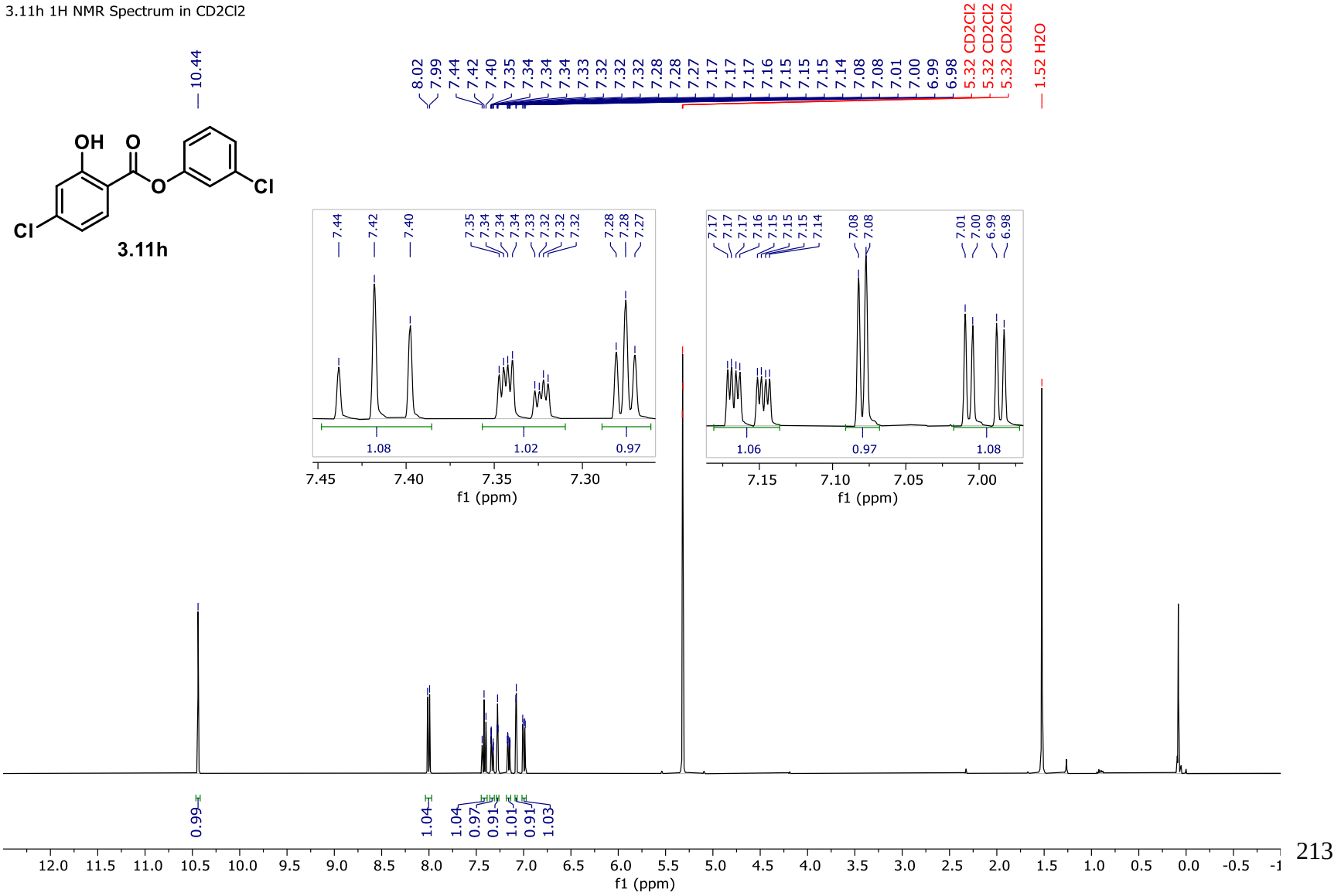

3.11h 13C NMR Spectrum in CDCl3

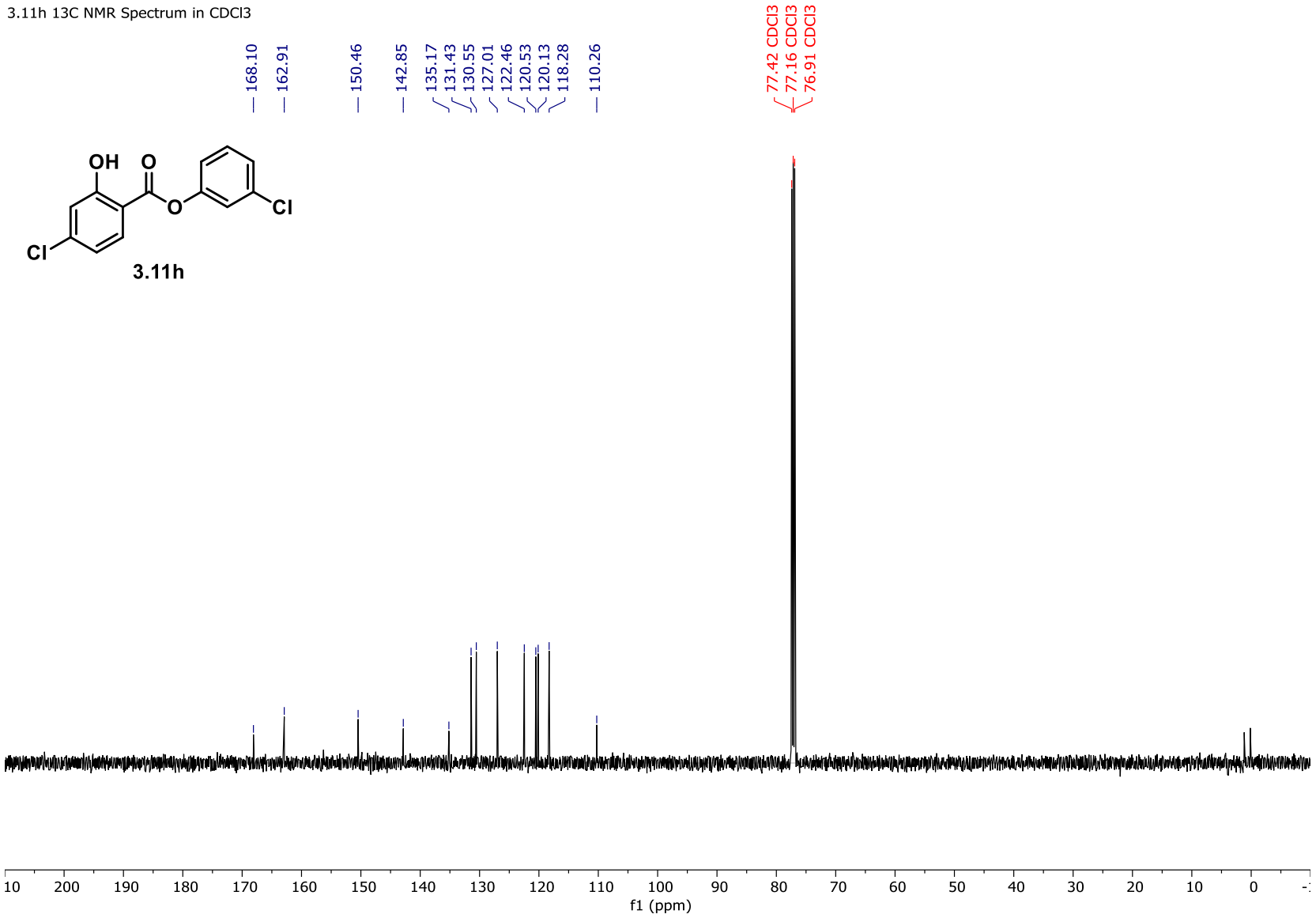

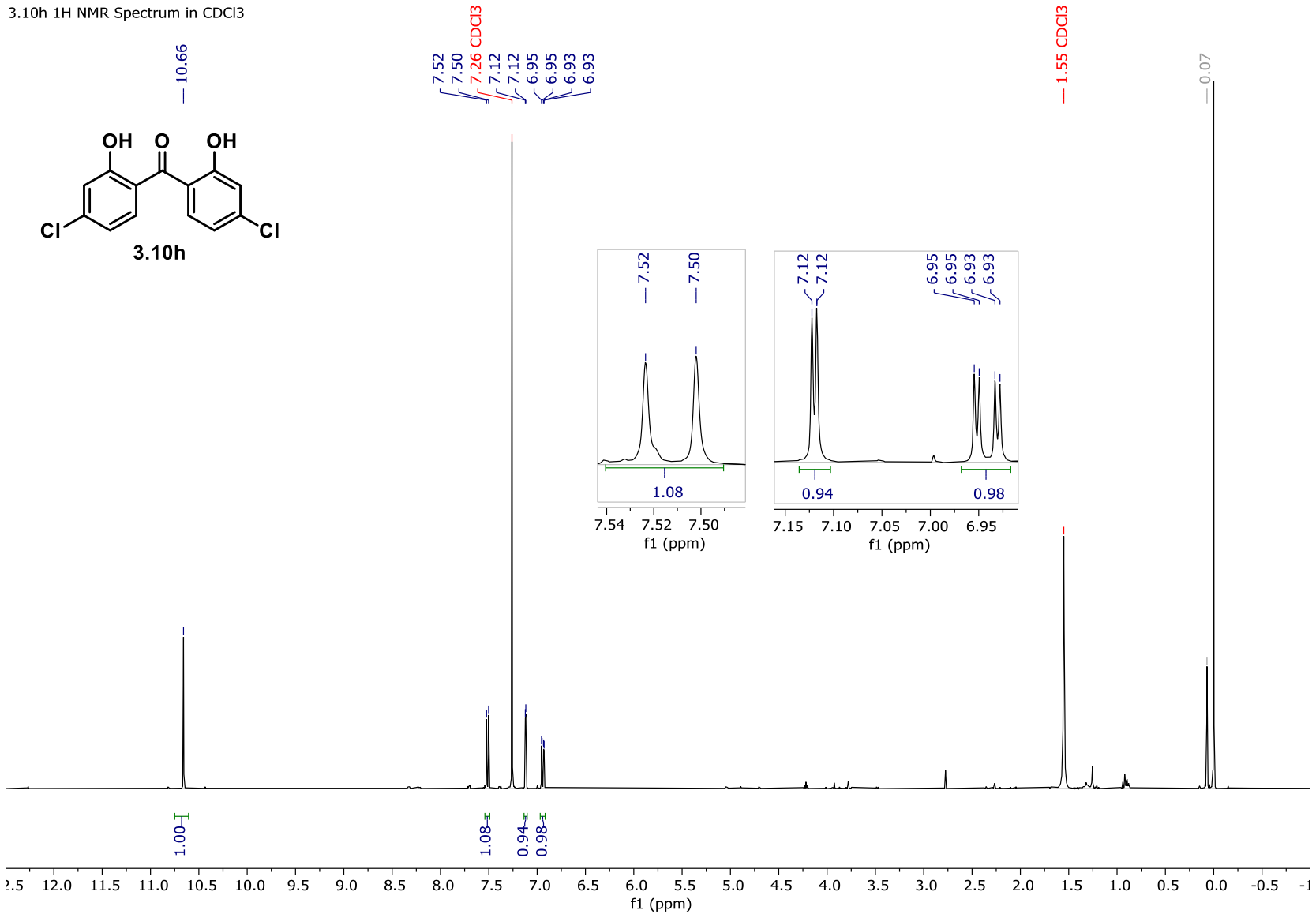
3.10h 1H NMR Spectrum in CDCl3
10.66
7.52
7.50
7.26 CDCl3
7.12
7.12
6.95
6.95
6.93
6.93
1.55 CDCl3
0.07
OH
O
OH
Cl
Cl
3.10h
1.08
0.94
0.98
f1 (ppm)
1.00
1.08
0.94
0.98
f1 (ppm)

3.11i 1H NMR Spectrum in CDCl3

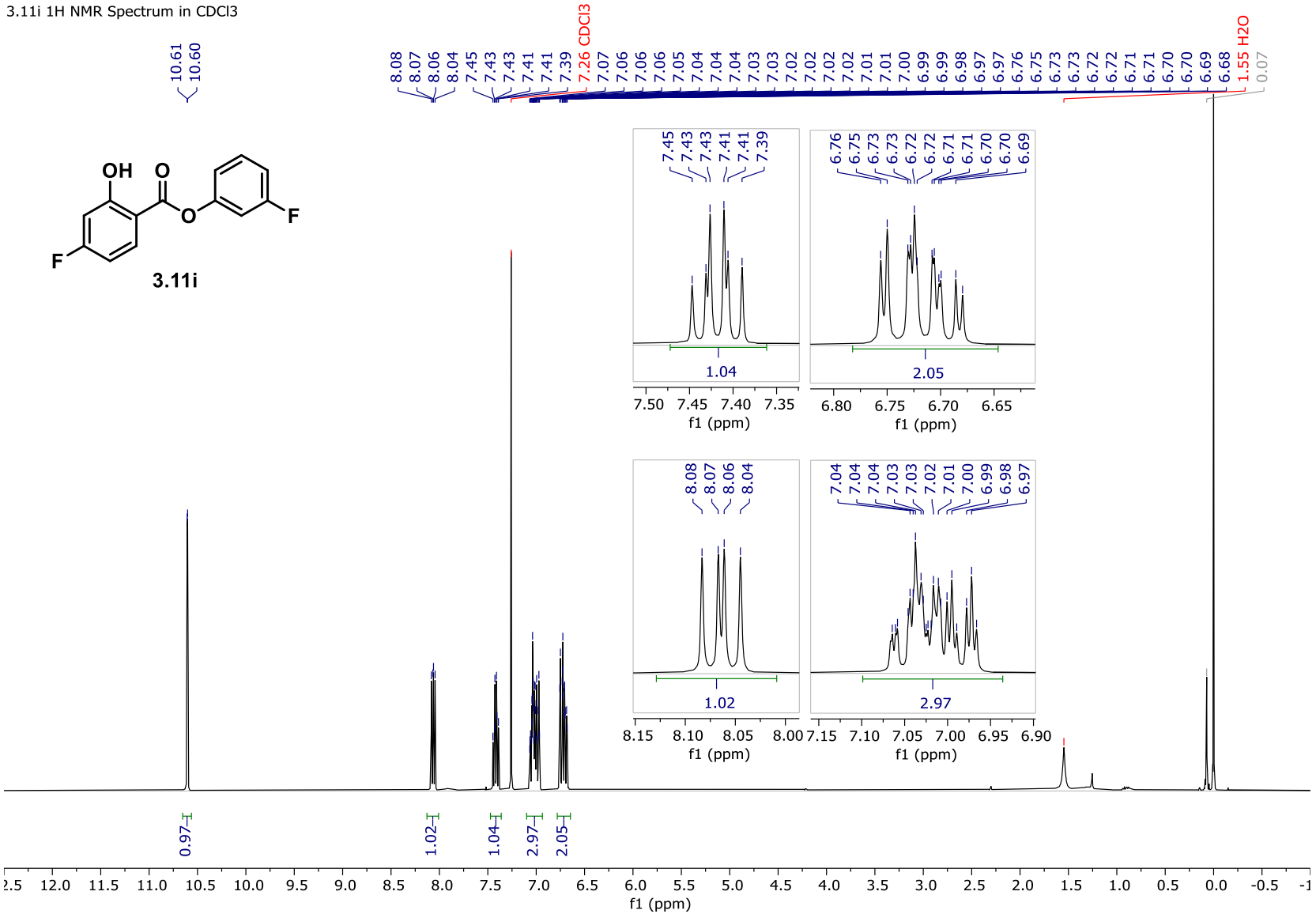

3.11i 13C {1H, 19F} NMR Spectrum in CDCl3

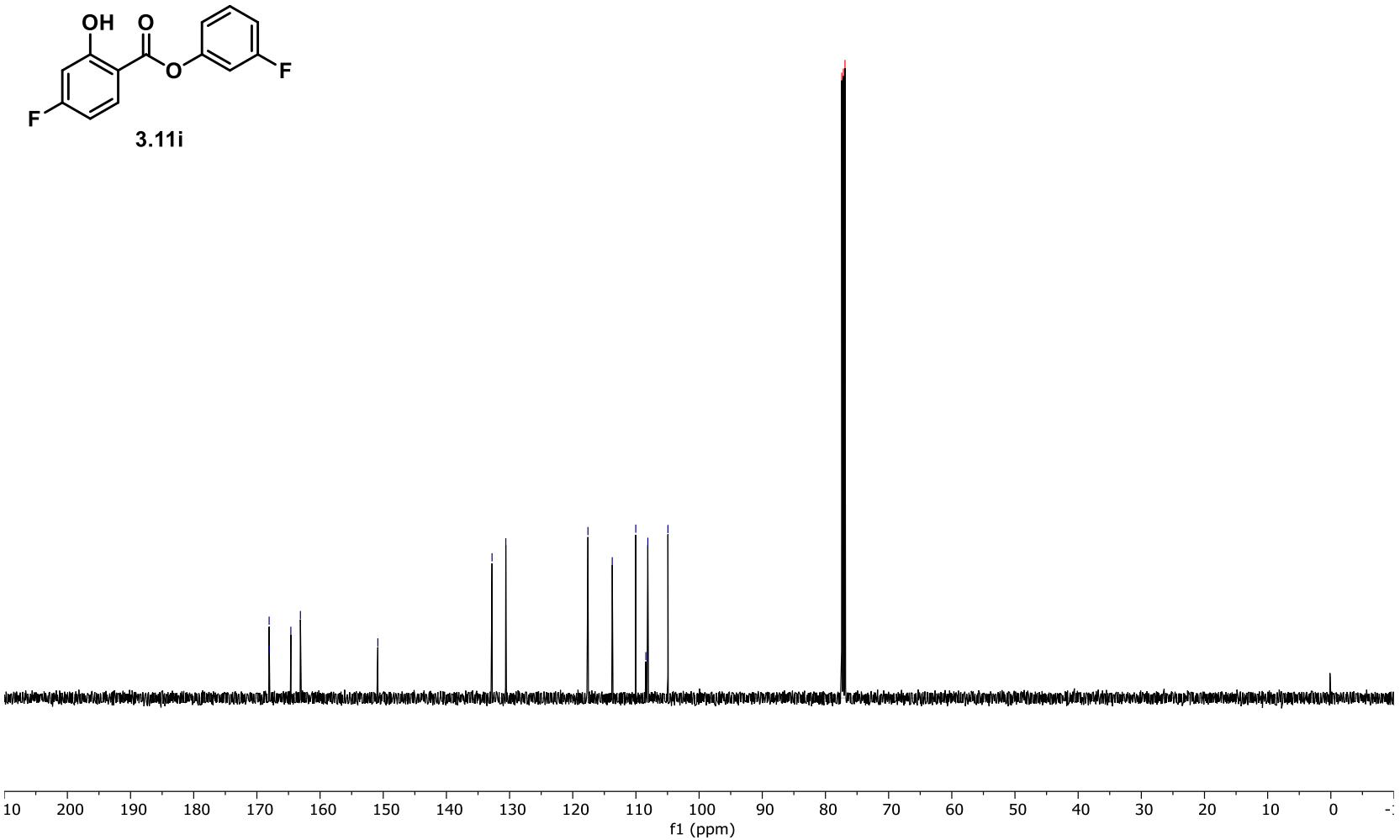

3.11i 19F {1H} NMR Spectrum in CDCl3

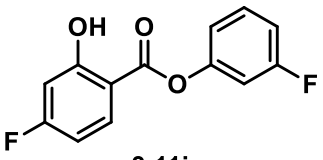

3.11i

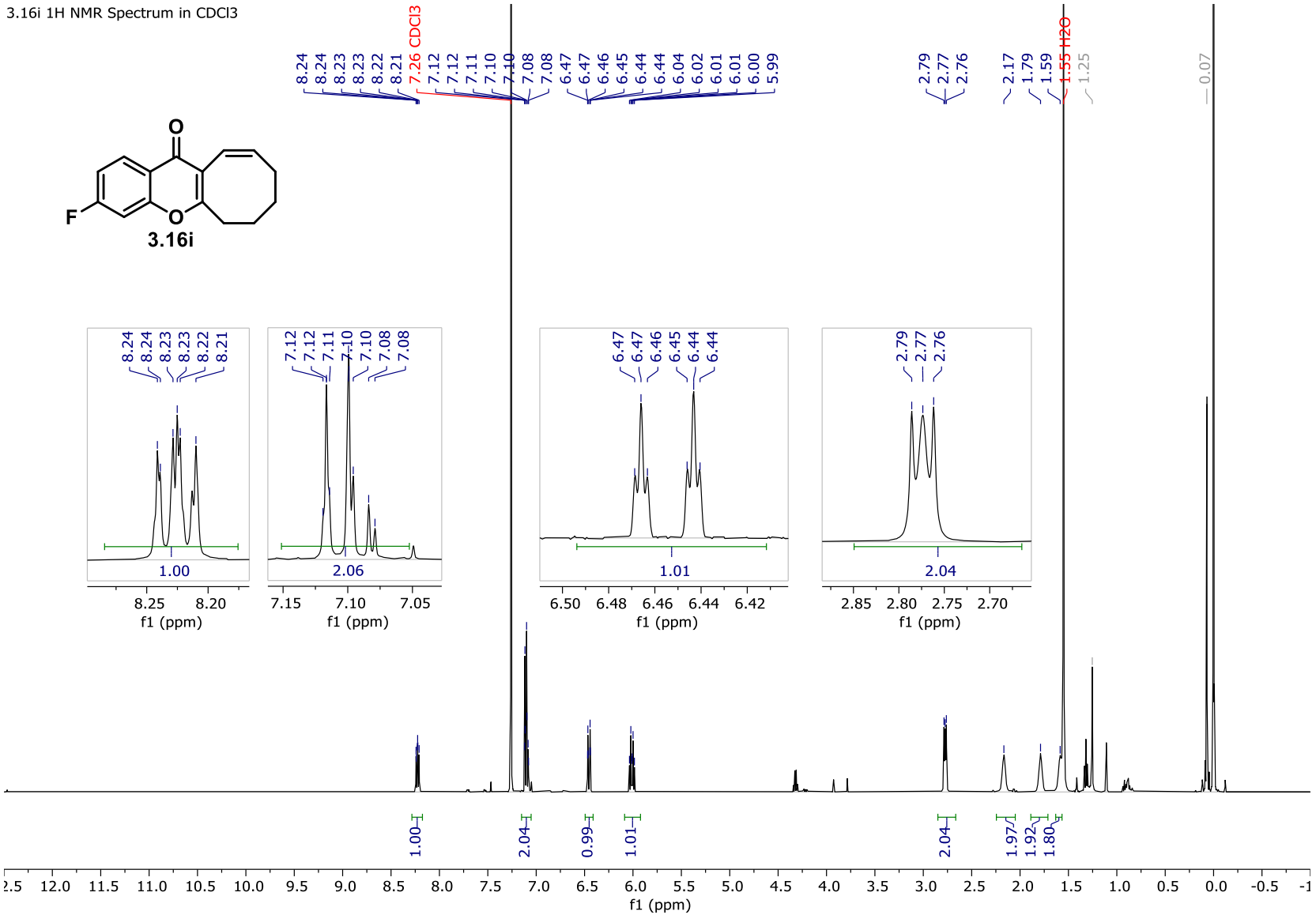
3.16i 1H NMR Spectrum in CDCl3
8.24 8.24 8.23 8.23 8.22 8.21 7.26 CDCl3 7.12 7.12 7.11 7.10 7.10 7.08 7.08 6.47 6.46 6.45 6.44 6.44 6.04 6.02 6.01 6.01 6.00 5.99
2.79 2.77 2.76 2.17 1.79 1.59 1.55 H2O 1.25 0.07
O
F
O
3.16i
1.00
2.06
1.01
2.04
f1 (ppm)
1.00 2.04 0.99 1.01 2.04 1.97 1.92 1.80

3.16i 19F {1H} NMR Spectrum in CDCl3

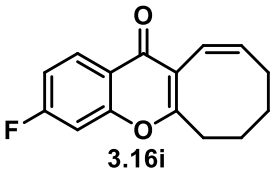

3.16i

3.11j 1H NMR Spectrum in CDCl3

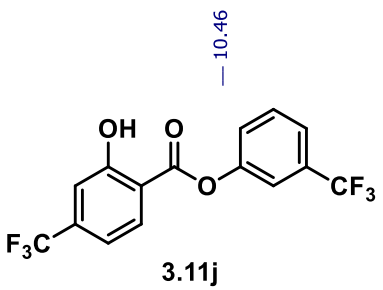

3.11j

3.11j 13C {1H, 19F} NMR Spectrum in CDCl3

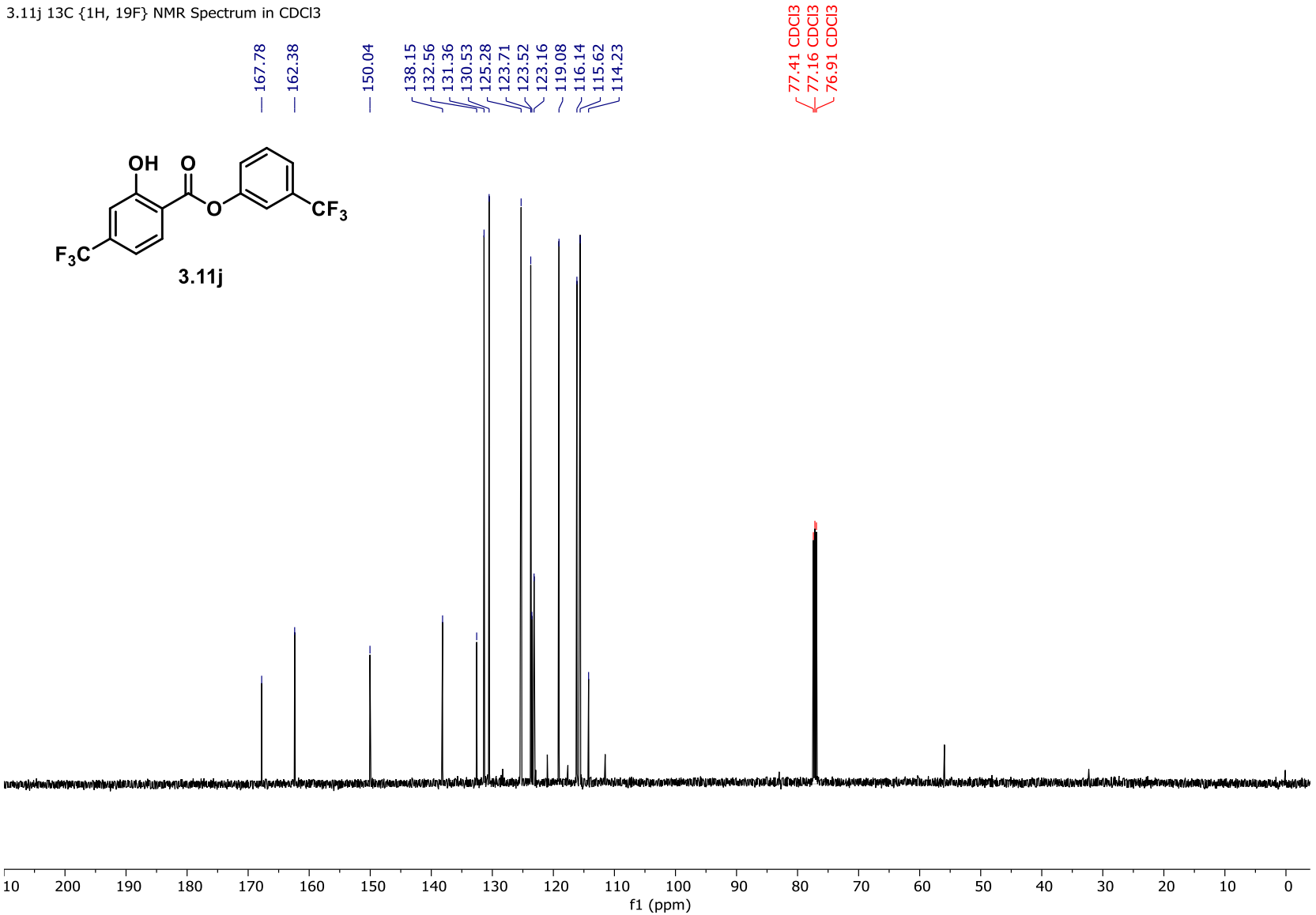

3.11j 19F {1H} NMR Spectrum in CDCl3

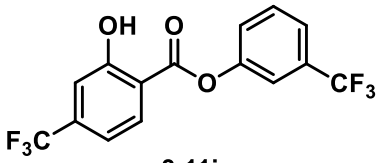

3.11j

3.11j 1H NMR Spectrum in CDCl3

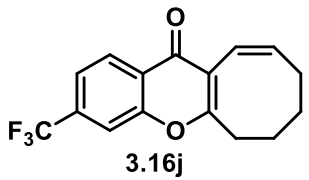

3.16j

3.16j 13C {1H, 19F} NMR Spectrum in CDCl3

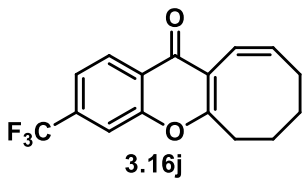

3.16j

3.11j 19F {1H} NMR Spectrum in CDCl3

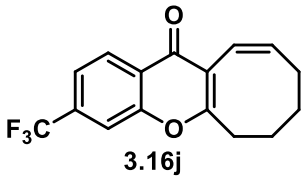

3.16j

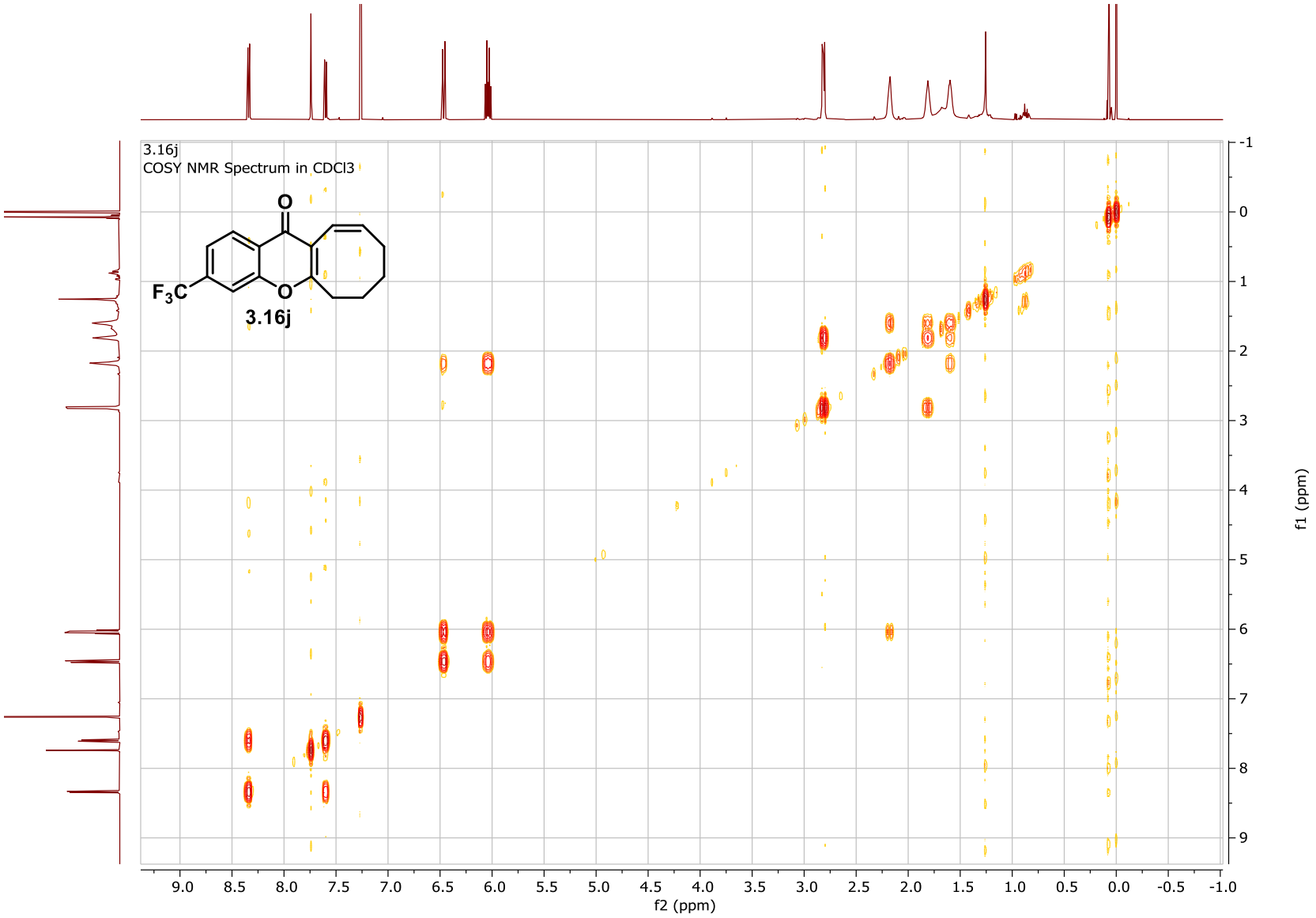
3.16j
COSY NMR Spectrum in CDCl3
O
F3C
O
3.16j
f2 (ppm)
f1 (ppm)

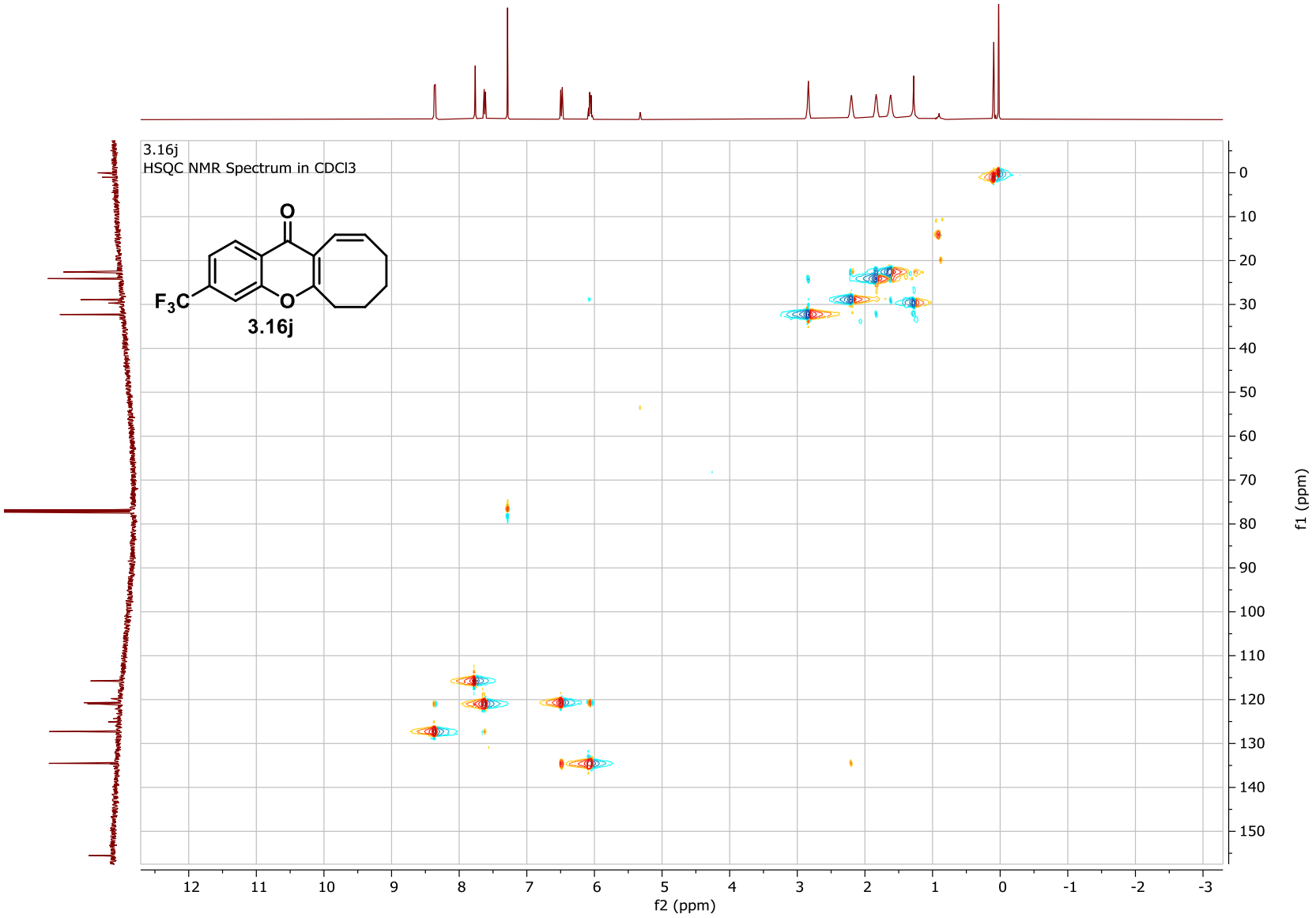
3.16j
HSQC NMR Spectrum in CDCl3
O
F3C
O
3.16j
f2 (ppm)
f1 (ppm)

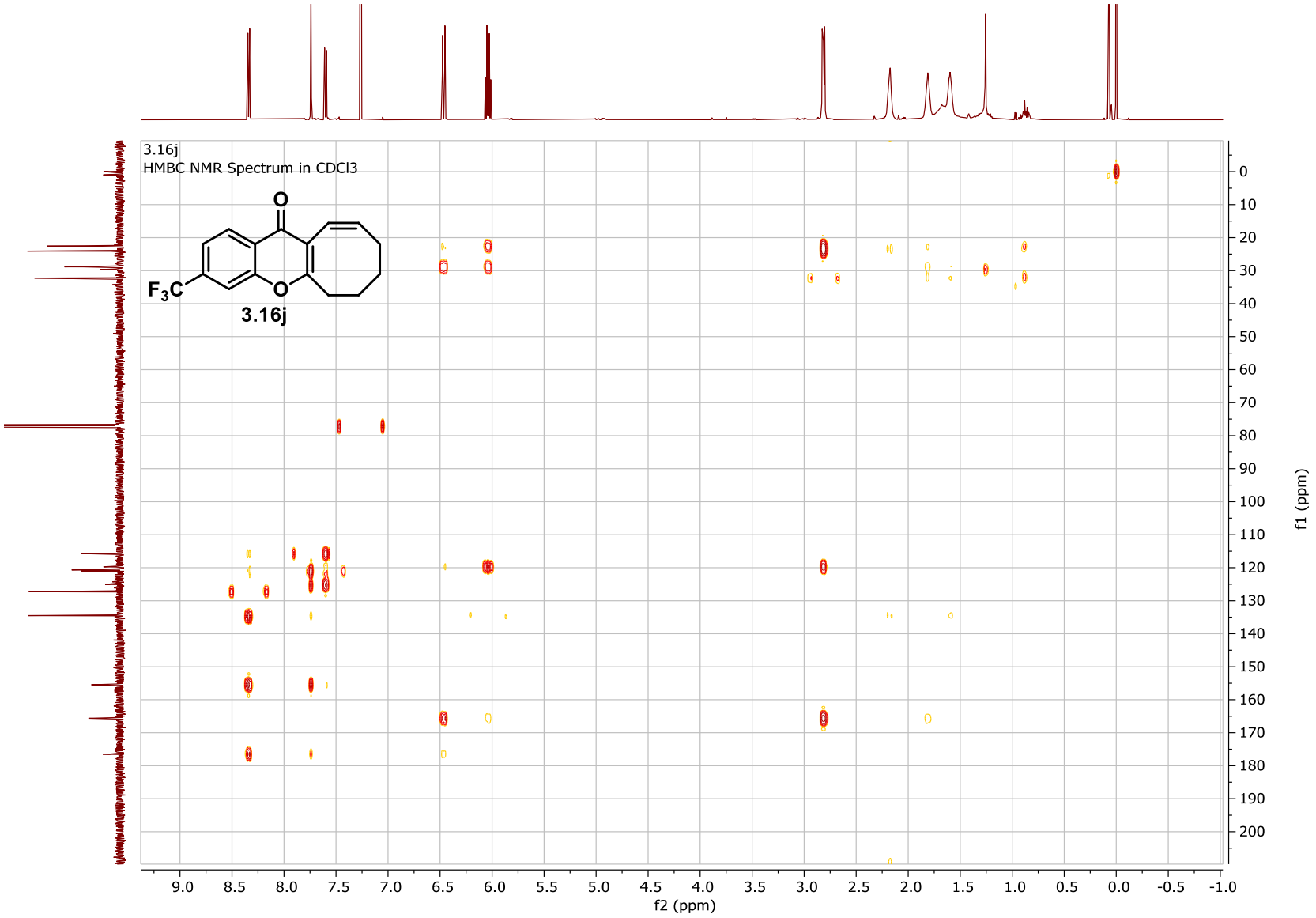
3.16j
HMBC NMR Spectrum in CDCl3
O
F3C
O
3.16j
f2 (ppm)
f1 (ppm)

3.11k 1H NMR Spectrum in CDCl3

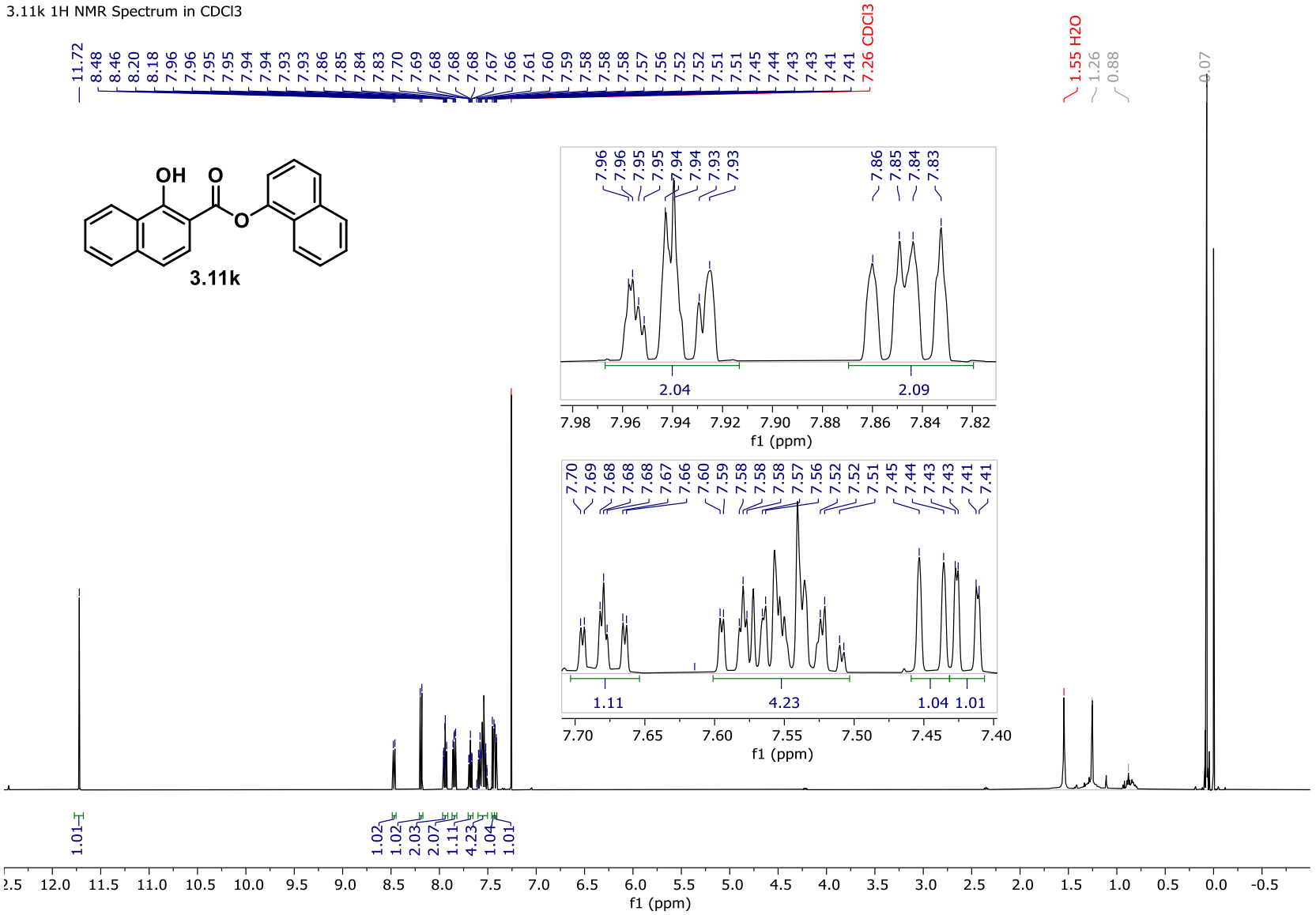

3.11h 13C NMR Spectrum in CDCl3

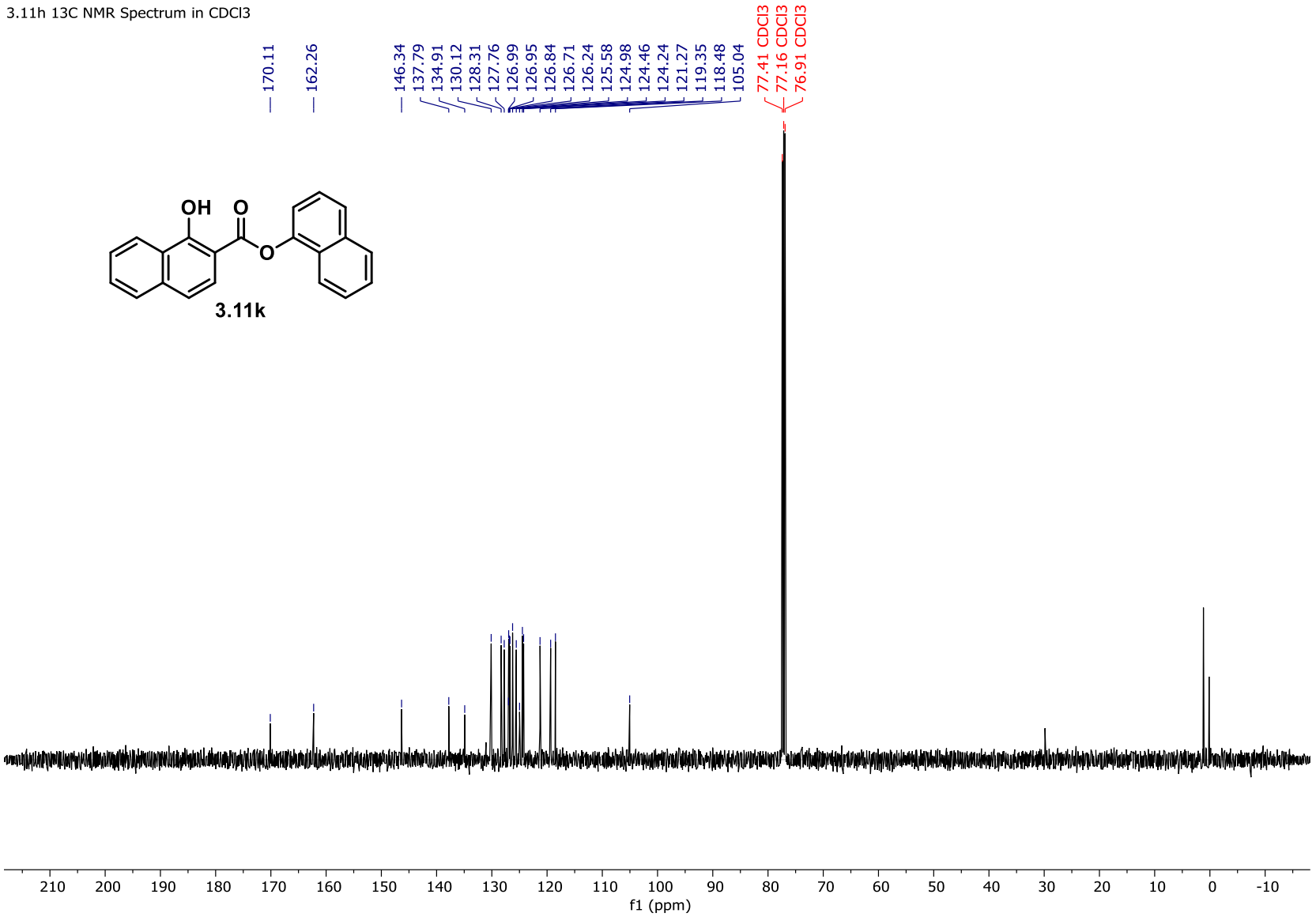

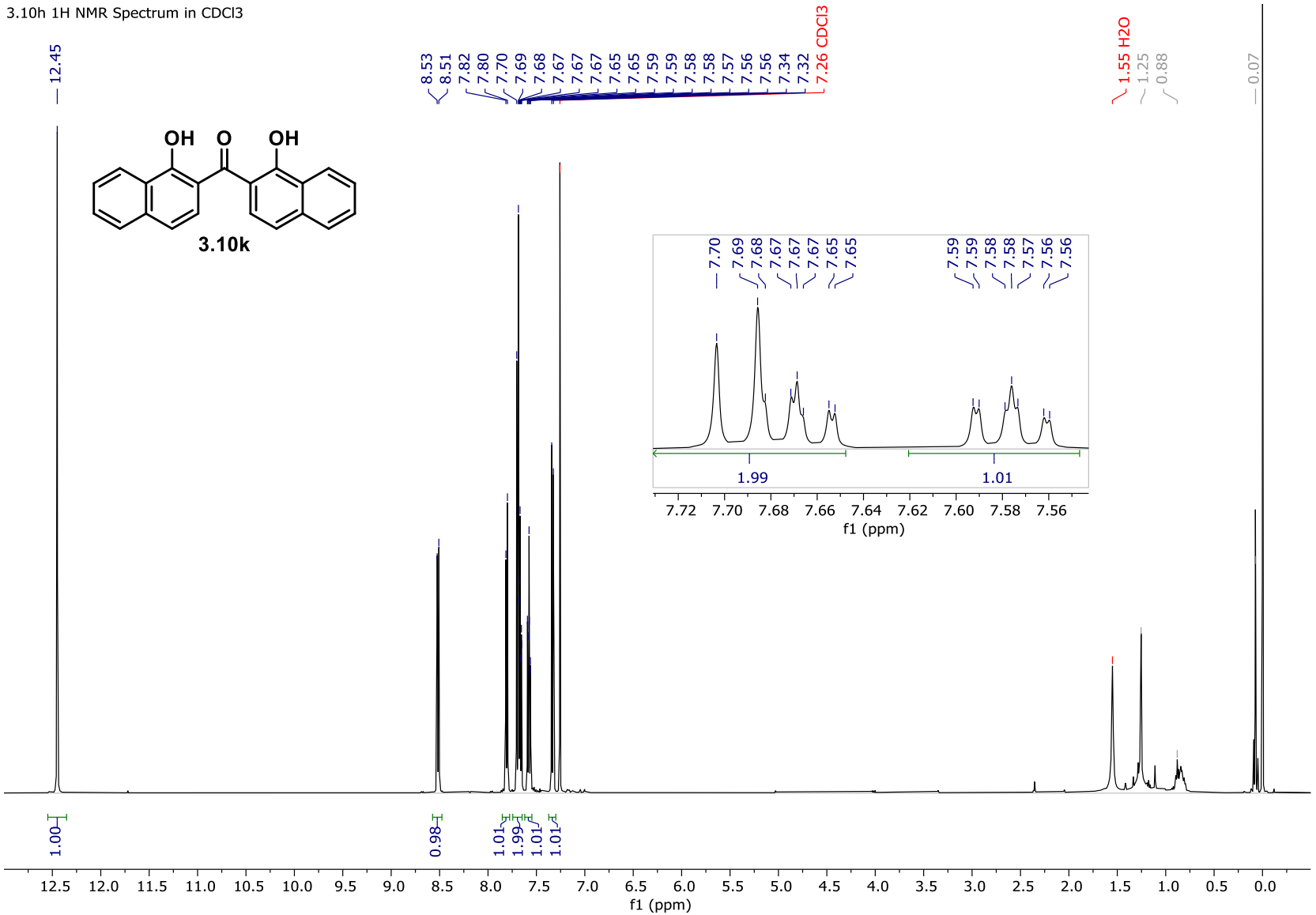
3.10h 1H NMR Spectrum in CDCl3
12.45
8.53
8.51
7.82
7.80
7.70
7.69
7.68
7.67
7.67
7.67
7.65
7.65
7.59
7.59
7.58
7.58
7.57
7.56
7.34
7.32
7.26 CDCl3
1.55 H2O
1.25
0.88
0.07
OH
O
OH
3.10k
7.70
7.69
7.68
7.67
7.67
7.67
7.65
7.65
7.59
7.59
7.58
7.58
7.57
7.56
7.56
1.99
1.01
7.72 7.70 7.68 7.66 7.64 7.62 7.60 7.58 7.56
f1 (ppm)
1.00
0.98
1.01
1.99
1.01
1.01
12.5 12.0 11.5 11.0 10.5 10.0 9.5 9.0 8.5 8.0 7.5 7.0 6.5 6.0 5.5 5.0 4.5 4.0 3.5 3.0 2.5 2.0 1.5 1.0 0.5 0.0
f1 (ppm)

3.10h 13C NMR Spectrum in CDCl3

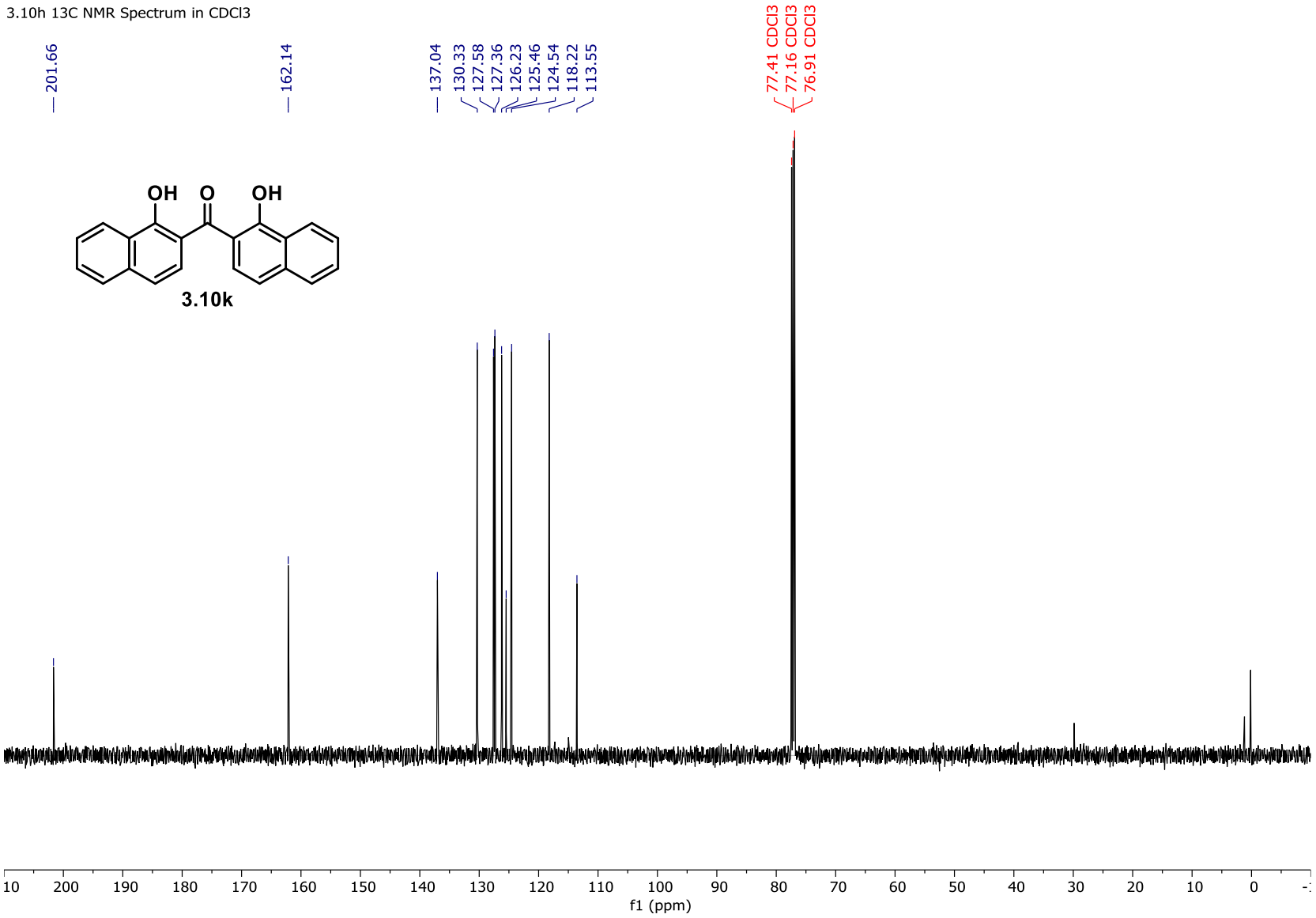

4.1 1H NMR Spectrum in CDCl3

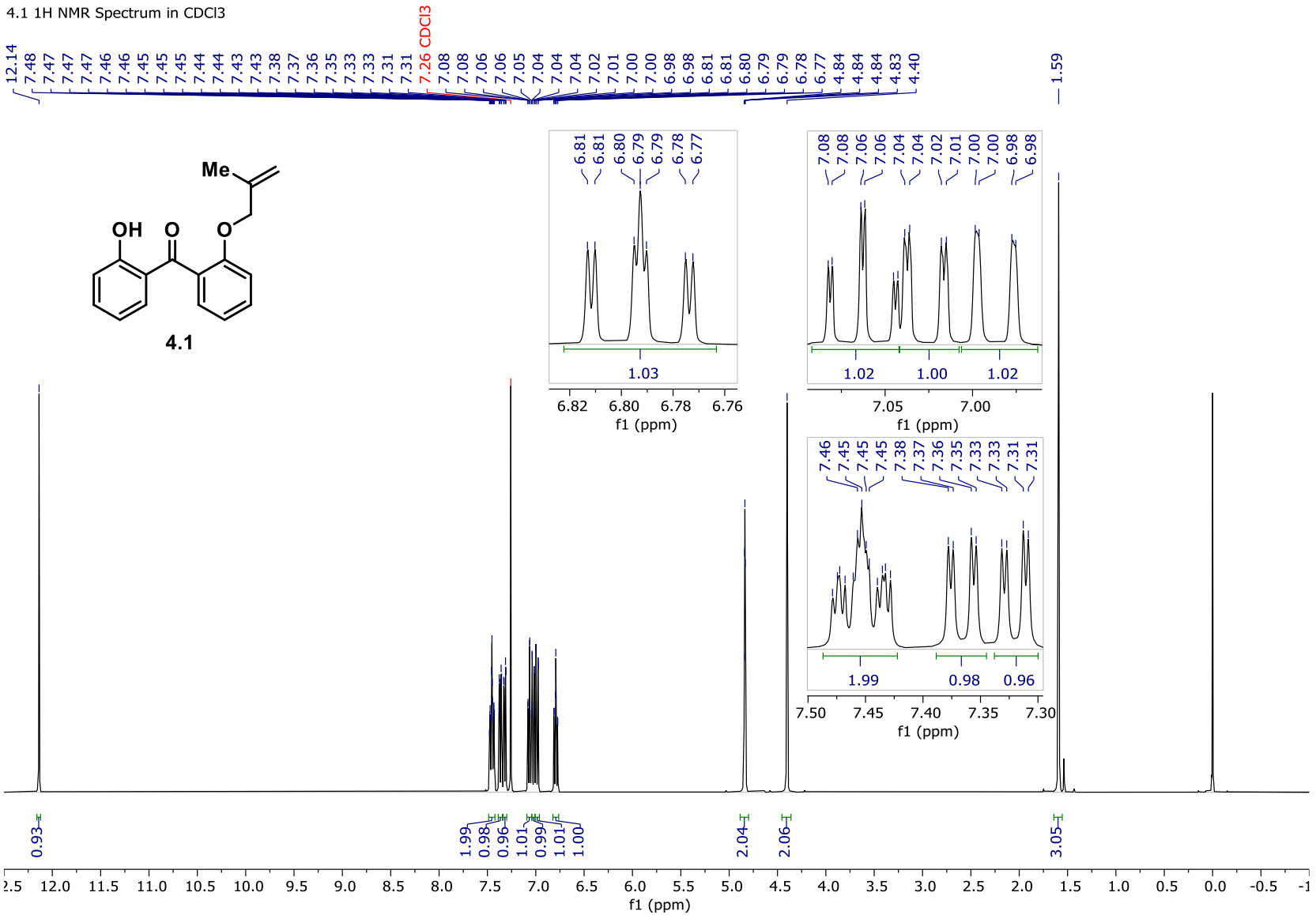

4.1 13C NMR Spectrum in CDCl3

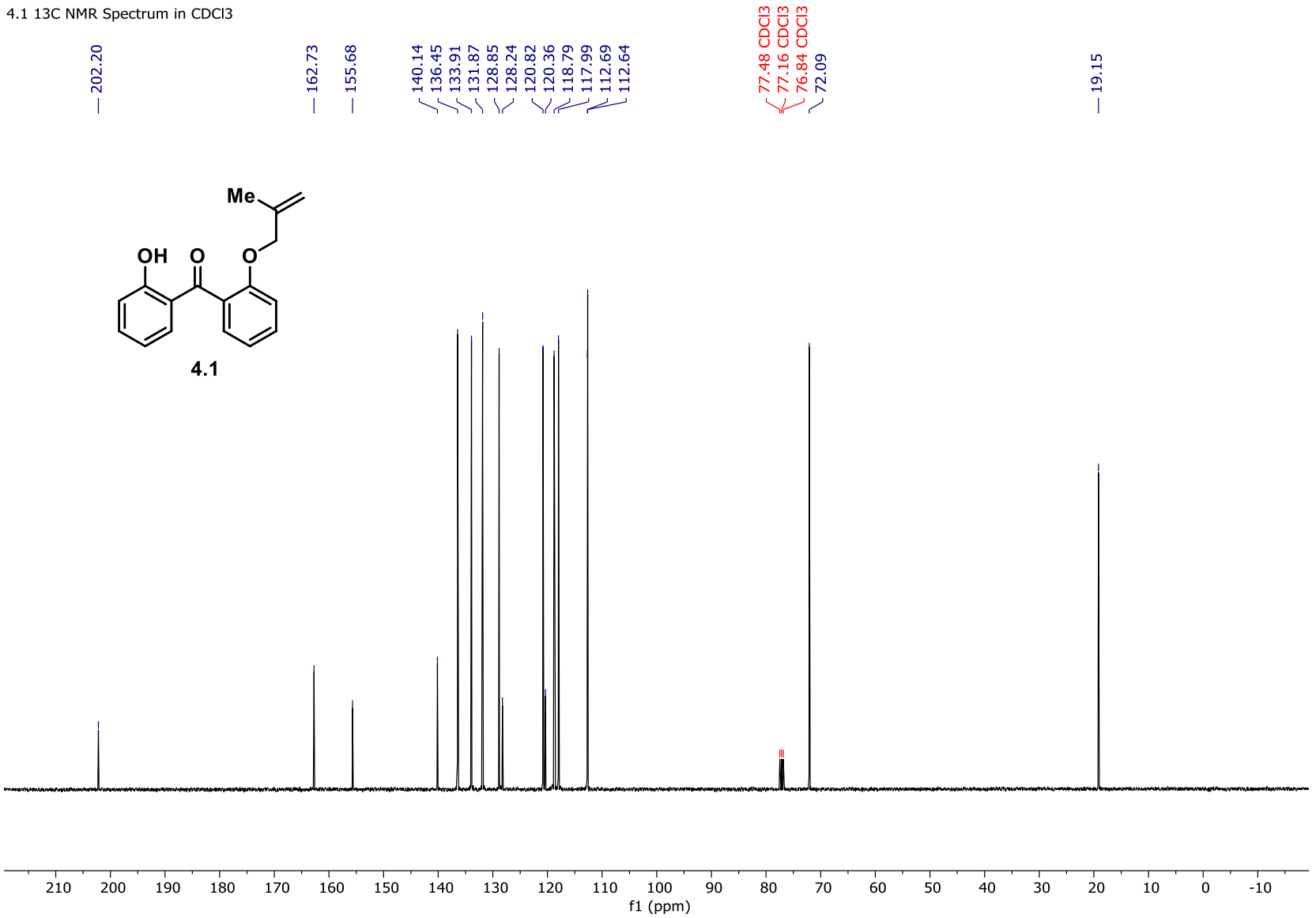

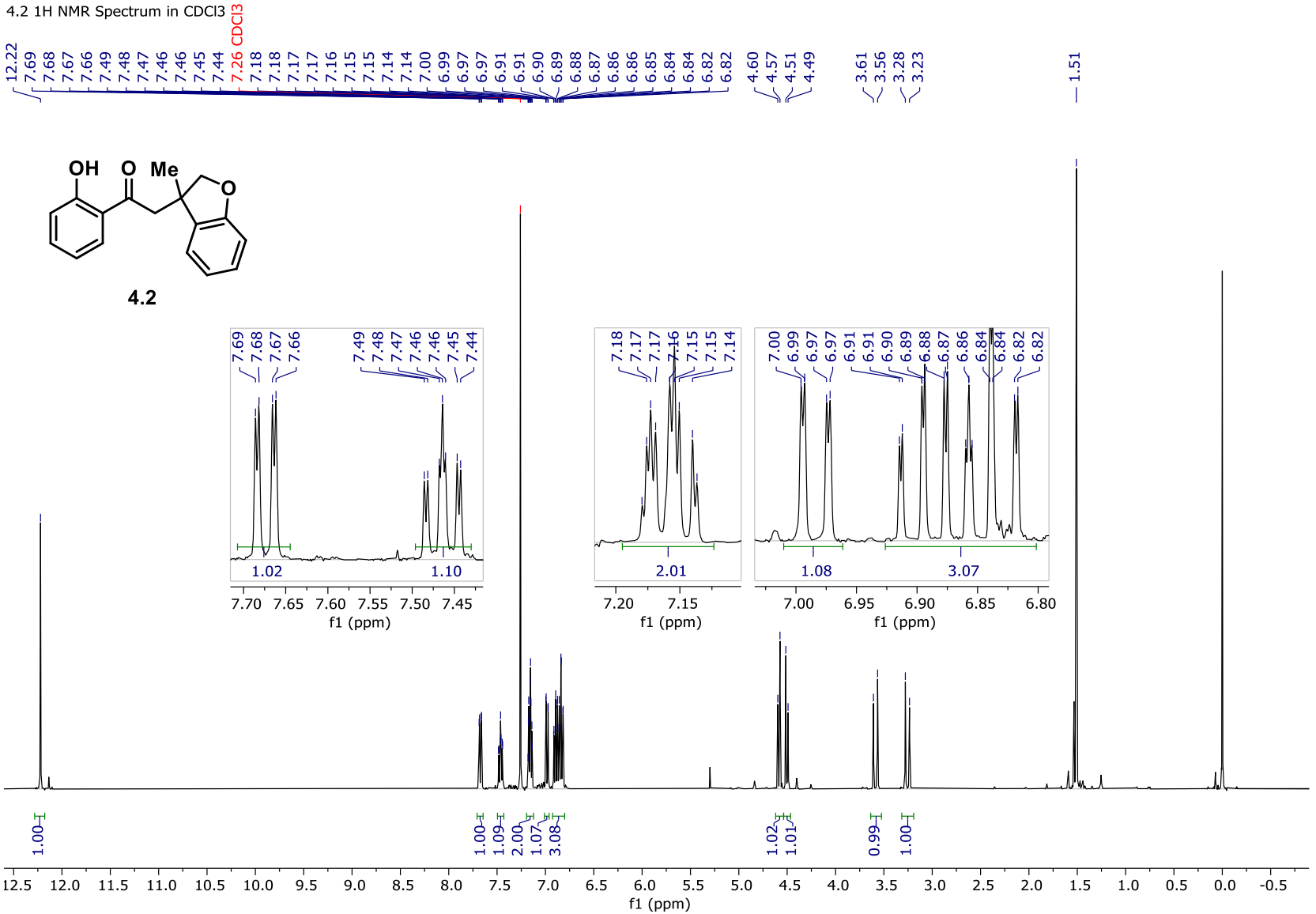
4.2 1H NMR Spectrum in CDCl3
12.22 7.69 7.68 7.67 7.66 7.49 7.48 7.47 7.46 7.46 7.45 7.44 7.26 CDCl3 7.18 7.17 7.17 7.16 7.15 7.15 7.14 7.14 7.00 6.99 6.97 6.97 6.91 6.91 6.90 6.89 6.88 6.87 6.86 6.86 6.85 6.84 6.84 6.82 6.82 4.60 4.57 4.51 4.49 3.61 3.56 3.28 3.23 1.51
OH O Me O
4.2
7.69 7.68 7.67 7.66 7.49 7.48 7.47 7.46 7.45 7.44
1.02 1.10
7.70 7.65 7.60 7.55 7.50 7.45
f1 (ppm)
7.18 7.17 7.17 7.16 7.15 7.15 7.14
2.01
7.20 7.15
f1 (ppm)
7.00 6.99 6.97 6.97 6.91 6.91 6.90 6.89 6.88 6.87 6.86 6.84 6.84 6.82 6.82
1.08 3.07
7.00 6.95 6.90 6.85 6.80
f1 (ppm)
1.00 1.00 1.09 2.00 1.07 3.08 1.02 1.01 0.99 1.00
12.5 12.0 11.5 11.0 10.5 10.0 9.5 9.0 8.5 8.0 7.5 7.0 6.5 6.0 5.5 5.0 4.5 4.0 3.5 3.0 2.5 2.0 1.5 1.0 0.5 0.0 -0.5
f1 (ppm)

4.2 13C NMR Spectrum in CDCl3

204.40
162.69
159.12
136.71
134.95
130.05
128.75
122.93
120.77
119.91
119.07
118.80
110.14
82.72
77.48 CDCl3
77.16 CDCl3
76.84 CDCl3
47.46
44.07
25.37

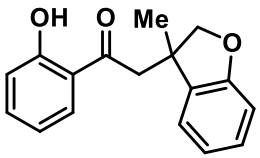

4.2

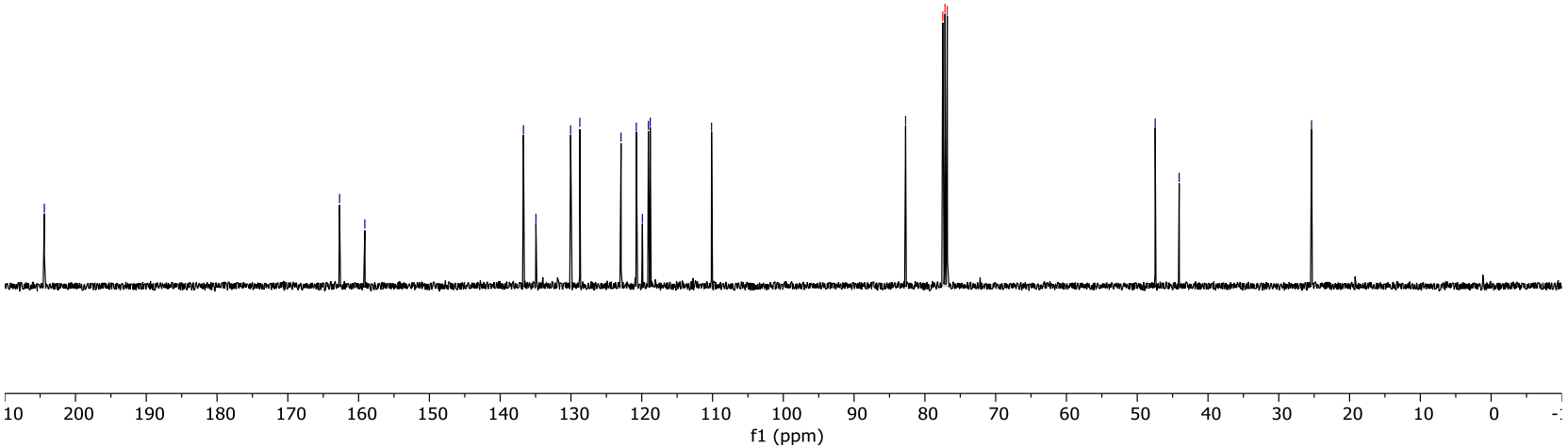

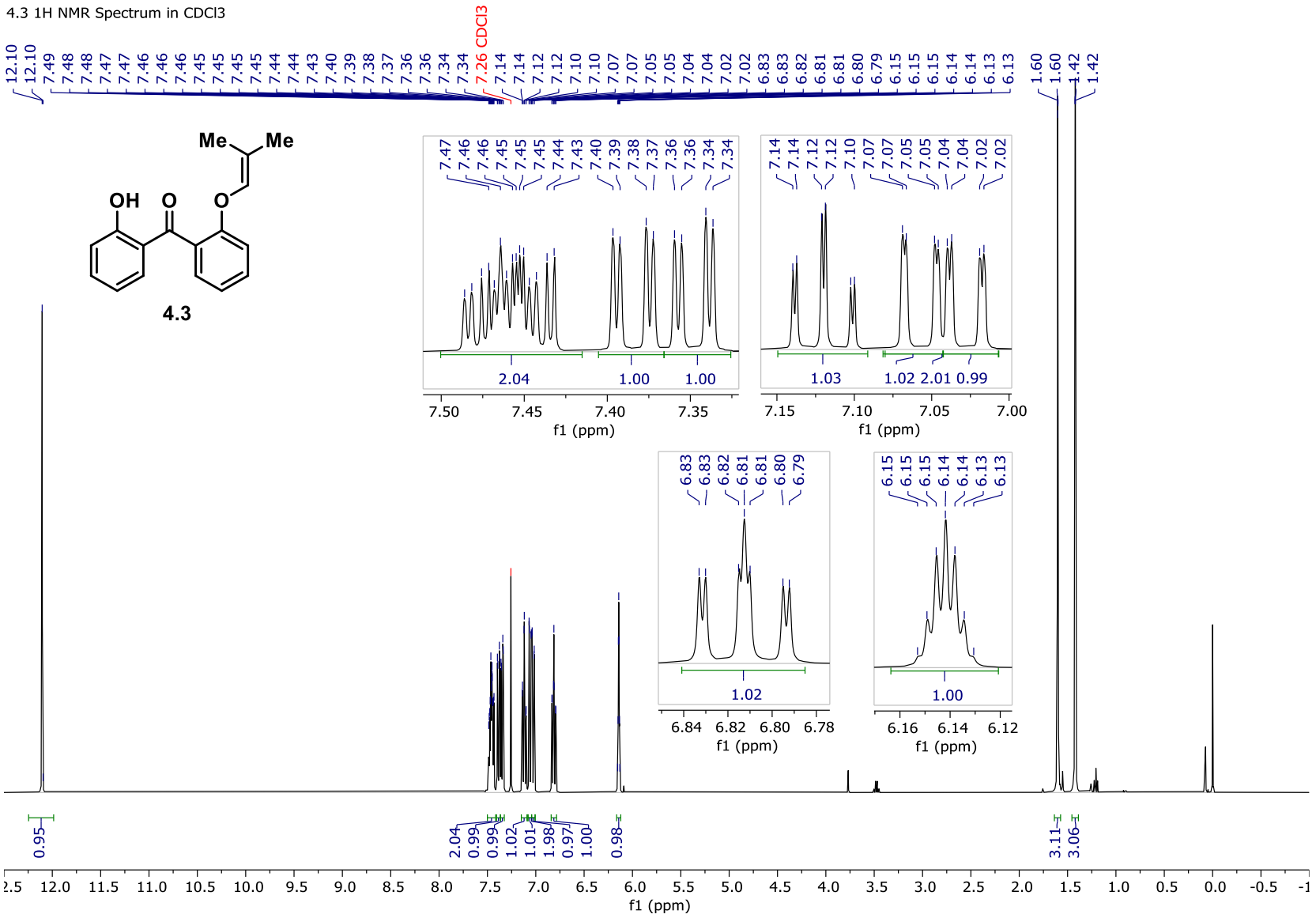
4.3 1H NMR Spectrum in CDCl3
7.26 CDCl3
Me
Me
OH
O
O
4.3
f1 (ppm)

4.3 13C NMR Spectrum in CDCl3